THE EXPERIMENTAL INVESTIGATION OF SOME PROPERTIES OF ENERGETIC CHARGED PARTICLES FOUND ABOVE THE EARTH'S SURFACE.

Thesis Submitted By

NORMAN ARTHUR RIDDLE

For The Degree of Doctor of Philosophy

In The University of London.

MARCH 1967.

ABSTRACT.

A series of 12 latitude surveys of the cosmic ray intensity has been carried out between 1962 and 1965. The scintillation telescope detector has been flown at an atmospheric depth of 145 g cm^{-2}. between 65°N 10°W and Kano, Nigeria.

Two of the surveys were extended into the southern hemisphere to 38°S 38°E. These allowed a comparison to be made of various cut-off rigidity calculations. Cut-offs determined by trajectory computation are demonstrably better than cut-offs obtained from magnetic dipole approximations. Discrepancies found due to the method of interpolation between trajectory-computed cut-offs are discussed. After correcting for these discrepancies, a general lowering of the cut-off rigidities is found over South Africa relative to Western Europe.

The latitude knee in the intensity variation enables an accurate cut-off determination to be made. The cut-off, 1.2 GV, at this position is lower than the value predicted for the Earth's internal magnetic field. Agreement is found with previous observations of reduced cut-offs. It is suggested that the reduction is about 17% between geomagnetic latitudes 55° and 61°. It is shown that reductions of this magnitude do not have their origin in the magnetic field of the quiet-time ring current.

Experimentally corrected cut-off rigidities are derived which are shown to produce an improvement in the rigidity spectrum of the cosmic ray intensity at 145 g cm^{-2}.

The surveys are grouped to represent the mean rigidity spectra at 145 g cm^{-2} for the years: 1962, 1963 and 1964. The rigidity dependence of the modulation is obtained for 1962 and 1963 relative to 1964 and is observed to be similar for these two periods. A comparison is made of the 1963 modulation with that measured by balloon-borne proton/alpha detectors. Good agreement is found, though the data cannot be fitted by the simple form of modulation spectrum as has generally been used. A modulation function is given which provides a close fit to the experimental data between 0.5 GV and 15 GV.

CONTENTS

CHAPTER			PAGE.
		GENERAL INTRODUCTION	7
1.		COSMIC RAYS AND THE GEOMAGNETIC FIELD.	8
	1.1	Dipole Theory.....	8
	1.2.	Non-Dipole Fields.....	13
	1.3	Simulations of the Earth's Field.....	14
	1.4	Threshold Calculations Involving Non-Dipole Fields.	16
	1.5	Integrated Trajectory Cut-offs.....	22
	1.6	Experimental Cut-off Determination.....	30
	1.7	Origin of High Latitude Cut-off Reductions.....	34
	1.8	Summary.....	43
2.		THE LONG TERM MODULATION OF COSMIC RAYS.	
	2.1	Introduction.....	45
	2.2	Basic Modulation Mechanisms.....	52
	2.3	Solar Wind Modulation.....	59
	2.4	Experimental Observations of Interplanetary Conditions.	66
	2.5	Modulation Involving Anisotropic Diffusion.....	75
	2.6	Relative Importance of Energy Loss and Diffusion-Convection.....	80
	2.7	Discussion.....	82

CHAPTER PAGE

3. THE COSMIC RAY RECORDER.

3.1 Recorder Design Requirements..... 83

3.2 Description of the Recorder..... 87

3.3 Environmental Tests..... 91

3.4 Long Term Stability..... 94

4. REDUCTION AND ANALYSIS OF EXPERIMENTAL DATA.

4.1 Survey Routes and Times..... 96

4.2 Data Analysis..... 99

4.3 Reduction of Data to a Common Atmospheric Depth..... 99

4.4 Experimental Errors..... 104

4.5 Effective Cut-off Rigidity..... 112

4.6 Detector Aspect Angle..... 116

4.7 Forbush Decrease Events..... 127

5. A COMPARISON OF VARIOUS CUT-OFF CALCULATIONS.

5.1 Introduction..... 134

5.2 Cosmic Ray Equator..... 135

5.3 Survey Data..... 139

5.4 The L Interpolated Cut-Offs..... 149

5.5 Sources of Cut-off Errors..... 156

5.6 Corrected Cut-off Rigidities..... 170

5.7 Comparison of Cut-off Calculations..... 171

5.8 Conclusions to Cut-off Analysis..... 177

CHAPTER PAGE

6. EXPERIMENTAL OBSERVATION OF THE LONG TERM MODULATION OF COSMIC RAYS.

6.1 Survey Data..... 179

6.2 Rigidity Dependence of the Integral Intensity Changes. 191

6.3 Yield Functions..... 192

6.4 Rigidity Dependence of the Modulation..... 199

6.5 Sun-spot Minimum Modulation..... 207

6.6 Comparison of Results with Balloon Observations..... 206

6.7 Discussion..... 215

ACKNOWLEDGEMENTS..... 227

REFERENCES..... 228

GENERAL INTRODUCTION.

One method of measuring the spectrum of the local cosmic radiation is through the use of the Earth's magnetic field. Particles in the magnetic rigidity range from about 0.5 GV to 60 GV can be measured by the spectrometer effect of the magnetic field. The accuracy of the spectrum determination is directly dependent on the accuracy with which the cut-off rigidities at locations within the field are defined. For this purpose a close definition of the magnetic field is required, involving not only the main core field generated within the Earth but also fields of external origin. The magnetic field at present is described by surface measurements which primarily define the main core field. Cut-off rigidities calculated in this field can be tested by cosmic ray measurements. The accuracy of geomagnetic theory can thereby be observed and the influence of fields of external origin inferred.

Changes in the cosmic ray spectrum with time when measured in an accurate field can provide good definition of the rigidity dependence of these changes. Spectrum changes may then be related to the electro-magnetic state of interplanetary space, thus providing information on its extent and degree of turbulence.

CHAPTER 1. COSMIC RAYS AND THE GEOMAGNETIC FIELD.

The discovery of the cosmic radiation at the beginning of this century was shortly followed by experimental evidence that the radiation was at least partly charged. The latitude dependence of the cosmic ray intensity was first observed by Clay (1927) and later emphasized by Compton (1933). Compton demonstrated that this was a geomagnetic phenomenon, rather than a geographic effect such as caused by atmospheric temperature, by the close correlation of the intensity to the goemagnetic latitude. The calculations of Störmer (1955), originally applied to the motions of electrons in a dipole magnetic field, were applied to the cosmic radiation. Johnson and Street (1933) established that the cosmic ray intensity differed in the east and west directions. This asymmetry in the intensity was explained by an excess of positive particles in the cosmic radiation.

1.1 DIPOLE THEORY.

1.1.1 Störmer Theory.

The Earth's field to a first approximation resembles that of a geocentric point dipole. Analysis of the surface field elements for the 1955 epoch by Finch and Leaton (1957) gave the dipole moment as 8.1×10^{25} gauss cm^{-3}. The dipole axis cut the Earth's surface in the northern hemisphere at $78.5^{\circ}N$, $69.0^{\circ}W$.

In his work on auroras Störmer considered the motion of charged particles in the field of a magnetic dipole. He solved the equation of motion in the meridian plane: the plane containing the particle and

the dipole axis. The solution divides the meridian plane into regions which are allowed or forbidden to the particles. In order to reach a point on the Earth's surface there must be an allowed path between that point and infinity. The dimensions of the allowed and forbidden regions depend upon the particle momentum, charge and its impact parameter when at infinity. A parameter particularly suited to charged particle motion in a magnetic field is the magnetic rigidity P which is given by :

$$P = \frac{pc}{Ze} \qquad 1.1$$

where p is the particle momentum, c the velocity of light and Ze the particle charge. The dimensions of magnetic rigidity are those of voltage. Störmer theory gives the minimum magnetic rigidity a particle coming from infinity requires in order to reach the Earth. This is the condition that the Earth's surface is just connected to infinity by an allowed path. The minimum threshold rigidity or cut-off is given by:

$$P_T = \frac{M}{4\, r_e^{\,2}} \times \frac{\cos^4\lambda}{\left[1 + (1 - \sin\lambda\cos\phi\cos^3\varepsilon)^{\frac{1}{2}}\right]^2} \qquad 1.2$$

where λ is the geomagnetic latitude.

ϕ the azimuth angle of arrival measured from east.

ε the zenith angle of arrival measured from vertical.

r_e the mean radius of the Earth.

M the magnetic moment of the Earth.

The cut-off is thus a function of the direction of arrival at the Earth as well as the latitude. For vertical incidence there is only a latitude dependence :

$$P_v = 14.9 \cos^4 \lambda \qquad 1.3$$

At a given geographic location the cut-off rigidity is commonly typified by the vertical cut-off, henceforth referred to simply as 'cut-off' (P).

The intensity of particles arriving at a point with magnetic rigidity greater than the cut-off can be related to the intensity which would have been recorded had there been no magnetic field to influence the particle motion. It is first assumed that the cosmic radiation is isotropic at infinity. Liouville's theorem is then applied. This states that at a given momentum, the directional intensity of charged particles $\left(cm^{-2}\ sec^{-1}\ ster^{-1}\right)$ is the same in all allowed regions and directions along a particle trajectory whether or not the magnetic field is present.

1.1.2. Modifications to Störmer Theory.

Integration of individual particle trajectories in a dipole field by Lemaitre and Vallarta (1936) showed that in general there was not a sharp threshold in the Störmer sense. Certain rigidities just above the Störmer threshold were found to be forbidden. Trajectories in these regions would have intercepted the solid earth before arriving at the point considered. These additional forbidden trajectories were found to be of two general types:

a) Simple trajectories intercepting the Earth to form an opaque cone (shadow cone) near the horizon. This shadow cone is important only for large zenith angles of arrival.

b) Complex trajectories with many loops turning towards and away from the Earth which produce a region of alternate allowed and forbidden bands (penumbra).

Thus for any location on the Earth the sky may be divided into four regions :

a) Störmer cone - within which particles of a given rigidity are not allowed.

b) Main cone - within which all particles of a given rigidity are allowed.

c) Penumbral region between the Störmer and main cones.

d) Shadow cone.

Schwartz (1959) calculated the penumbral corrections to the dipole threshold rigidities for latitudes up to 50°. The penumbral region was found to be completely opaque near the geomagnetic equator, becoming increasingly transparent towards higher latitudes. The transparency is about 50% at a latitude of 40° geomagnetic.

1.1.3. Experimental Observations.

A variation of the cosmic ray intensity with geomagnetic longitude was observed by Millikan and Neher (1936). By making a partial correction for the eccentricity of the dipole field Johnson (1938) demonstrated that a longitude variation would be produced. The small

latitude effect at sea level, combined with a large temperature effect, led to interpretative difficulties in early surveys. These difficulties were largely resolved with the advent of the neutron monitor. This responds to the nucleonic component of the sea level cosmic radiation produced by primary particles of lower mean energy. The neutron monitor combines a negligible temperature coefficient with a latitude effect five times that of a counter telescope or ionisation chamber at sea level. A sea level neutron monitor survey by Rose et al (1956) clearly revealed discrepancies between the observed intensities and the predictions of the centre dipole theory. At about the same time Waddington (1956) compared high altitude balloon measurements of alpha particles at a similar geomagnetic latitude over England and North America. The measured intensities were compatible with geomagnetic latitudes over North America being about 3° higher and $4\text{-}6^{\circ}$ lower over England than the conventional centre dipole latitudes. Simpson et al (1956) considered that the experimental observations could be reconciled by rotating the geomagnetic equator through 40° to the west. The suggested mechanism producing this effect was the interaction of the dipole field and the highly conducting interplanetary plasma within which it rotated. Kodama and Miyazaki (1957) found that the neutron monitor intensity measured between Japan and the Antarctic was in better agreement with the rotated centre dipole coordinates than with the eccentric dipole coordinates.

An accurate determination of the locus of the cosmic ray intensity minimum was made by Katz et al (1958) with a neutron monitor during

a series of aircraft flights. The results were in disagreement with the almost identical predicted cosmic ray equators of the centre dipole and eccentric dipole theories.

1.2. NON-DIPOLE FIELDS.

Rothwell and Quenby (1958) proposed that the discrepancies between experiment and theory were due to the non-dipole part of the Earth's field. During a sea level neutron monitor survey between England and South Africa they observed a close correlation between the measured intensity and the dip angle of the local magnetic field.

By modifying the Störmer equation to include the surface horizontal field and the magnetic dip angle, Rothwell (1958) was able to improve upon the current geomagnetic theories. Discrepancies with dipole theory were therefore largely attributable to the local magnetic field rather than the effects of a distorted outer magnetosphere. Aeroplane surveys by Sandström (1958) and Storey et al (1958) correlated better with dip latitude than geomagnetic latitude.

A sensitive test of geomagnetic theory was made by Marsden and Wilson (1958) who compared intensity increases recorded by the Leeds and Chicago neutron monitors during the isotropic phase of the solar flare event of 23 February 1956. The Chicago increase was about 30% greater than that at Leeds while the Chicago cut-off is higher than that at Leeds by both centre and eccentric dipole calculations. The accuracy of this method of cut-off comparison is due to the steepness of the solar particle spectrum coupled with the possibility of a comparison being made

over a period of hours during which time variations affecting the 'background' galactic cosmic ray intensity can have little effect. Pfotzer (1958), considering the same solar flare increase at several cosmic ray stations, concluded that the rotated cut-offs of Simpson were inadequate.

1.3 SIMULATIONS OF THE EARTH'S MAIN FIELD.

The correlation of the cosmic ray intensity data with the local surface field emphasises the requirement of an accurate definition of the surface field elements.

The main field representation has generally been obtained by the construction of isomagnetic charts from the available magnetic data. These were usually hand-contoured from data which had been reduced to the epoch of the map by interpolation of the secular changes measured at magnetic observatories. A spherical harmonic analysis could then be carried out using equally spaced grid points. The fundamental analysis was thus in the map-making process. The field simulation was therefore limited by the poor world coverage of survey data, the limited coverage of fixed magnetic stations (mainly in the northern hemisphere) giving the secular changes, as well as the errors involved in the preparation of the magnetic charts.

Such a technique was employed by Finch and Leaton (1957) in their evaluation of the Earth's main field for the epoch 1955 which gave the first 48 terms in the spherical harmonic expansion of the magnetic potential V.

$$V = \sum_{n=1}^{\infty} r_e \left(\frac{r_e}{r}\right)^{n+1} T_n \qquad 1.4$$

where $T_n = \sum_{m=o}^{n} (g_n^m \cos mw + h_n^m \sin mw) P_n^m (\vartheta)$

(r, ϑ, ω) are the spherical coordinates: geocentric distance, colatitude and longitude respectively.

g_n^m, h_n^m, are the gauss coefficients and $P_n^m(\vartheta)$ are the normalized Schmidt coefficients.

The coefficients g_n^m, h_n^m are chosen so that the field $\underline{F} = -\nabla V$ gives the best fit to the surface field data.

The 48 terms of the Finch and Leaton field were obtained by considering fields up to the sixth order: n = 1 to n = 6 .

Jensen and Cain (1962) developed a method in which the harmonic analysis was made to fit the magnetic data directly. This assumed the Finch and Leaton field as a first approximation from which a set of 48 coefficients were derived for the epoch 1960. A more comprehensive quantity of data was used in the main field analysis of Cain et al (1965). Time derivatives of the main coefficients were also evaluated in their field of the epoch 1960. Cain (1966) observed that the data were still characterised more by their heterogeneity than their uniformity : notably there was little data available from Asia. This will be a source of error in any spherical harmonic analysis. A comparison of these three fields by Cain et al (1965) in table 1.1 gives the root mean square deviations from the measured field data.

TABLE 1.1. R.M.S. Field Deviations in γ's [10^{-5} gauss].

Year	Cain et. al.	Jensen & Cain	Finch and Leaton.
1962	280	430	500
1963	250	420	520

The data used in this comparison are essentially those used in the simulation of the field and do not therefore represent the goodness of fit over the whole of the earth's surface. Cain (1966) estimated that the field of Cain et. al. (1965) was probably good to about 0.1 - 1% falling to about 10% at a few Earth radii.

1.4. THRESHOLD CALCULATIONS INVOLVING NON-DIPOLE FIELDS.

No simple analytic integral of the equations of motion of charged particles in the Earth's magnetic field exists when higher order terms are included. The most rigorous method of threshold computation involves the integration of a large number of trajectories from each location at the Earth's surface. Even using present day computer techniques a large amount of computing time is required especially in following the trajectories of particles just above the threshold at high latitudes. As an alternative to this costly and time consuming method there have been a number of approximate calculations.

1.4.1. Quenby and Webber Cut-Offs.

A world grid of cut-offs was produced by Quenby and Webber (1959) in which no account of the penumberal region was taken. The particle motion was treated as being in the field of a dipole to the first approximation, higher order field terms acting as a perturbation on this motion. Terms up to and including the 6th order in the magnetic field potential of Finch and Leaton were considered.

Above 40° latitude the trajectories of particles with rigidity just above the cut-off were assumed to be in close contact with the magnetic field lines. Calculation of the distortion of the dipole field line by the higher order field terms allowed the real field line to be approximated by the field line of a hypothetical tilted dipole with the same moment as that of the Earth's dipole. The latitude in this field $\bar{\lambda}$ could then be used in the Störmer formula to determine the cut-off. The effective latitude $\bar{\lambda}$ was determined to be :

$$\bar{\lambda} = \tan^{-1} \frac{1}{2} \left[\frac{V_d + 0.52\,\Delta V}{H_d + 0.52\,\Delta H} \right] \qquad 1.5$$

The weighting factor (0.52) of the differences ΔV and ΔH between the measured vertical and horizontal field strengths V and H from the dipole values V_d and H_d respectively, was determined from the world-averaged contributions of the higher order field terms.

At the equator the Störmer equation of motion was modified to include the magnetic potentials of the higher order field terms, considering

only their radial dependence. The solution was identical to the Störmer expression with the dipole moment M replaced by M' where M' is given by :

$$M' = M \left[1 + 0.6 \frac{\Delta H}{H_d} \right] \qquad 1.6$$

The weighting factor 0.6 of the difference ΔH of the horizontal field strength H from that due to the dipole moment H_d was again found from the average contribution of the higher order terms.

For low latitudes less than 20° the particle motion was considered essentially perpendicular to the field lines. Correcting the radial dependence of the dipole field to the real field dependence led to a relationship involving the effective latitude $\bar{\lambda}$ which was identical to the high latitude expression.

The cut-offs were given by :

$$\lambda \leqslant 20^\circ : \quad P_v = \frac{M}{4r_e^2} \left[1 + 0.6 \frac{\Delta H}{H_d} \right] \cos^4 \bar{\lambda}$$

$$\lambda \leqslant 40^\circ : \quad P_v = \frac{M}{4r_e^2} \cos^4 \bar{\lambda} \qquad 1.7$$

Cut-offs in the mid-latitude region between 20° and 40° were given as the mean of the values calculated by the high and low latitude approximations.

Quenby and Webber showed that these cut-offs defined the cosmic ray equator more successfully than the dipole theory and improved the observed

rigidity distribution of intensity increases for the solar flare increase of 23 February 1956. Pomerantz et al (1960) observed that the cosmic ray equator measured with a sea level neutron monitor survey at 60°E differed by 4° from the position predicted by Quenby and Webber. The first clear evidence of an area of discrepancy in the Quenby and Webber cut-offs was given by Freon and McCracken (1962). Analysis of the solar flare events of 12 and 15 November 1961 revealed that the cut-off assigned to Port aux Francais in the Kerguelen Islands was too high. Trajectory computations to determine the cut-off produced a value about 20% lower than the Quenby and Webber cut-off and in much better agreement with the flare data.

1.4.2. Quenby and Wenk Cut-offs.

Quenby and Wenk (1962) modified the method of Quenby and Webber to include the effects of the penumbra.

Above 40° latitude, effective latitudes $\bar{\lambda}$ were calculated using the results of field line calculations of Hultqvist (1958). The dipole penumbral corrections of Schwartz (1959) were applied in this high latitude region.

In the low latitude region less than 20°, the penumbral corrections were empirically derived from the neutron monitor surveys of Katz et al (1958) together with the low latitude cut-off approximation of Quenby and Webber. The intensities recorded around the geomagnetic equator where the penumbral effect should be zero were plotted against the Quenby and Webber cut-offs. Locations away from the equator where the

intensity recorded was the same as that at a point on the geomagnetic equator were then assumed to have the same cut-off. The cut-off differences between the Quenby and Webber values and the values derived in this way were the penumbral corrections.

Mid-latitude cut-offs were found from the arithmetic mean of the high and low latitude approximations.

The cut-off assigned at Port aux Francais was in close agreement with the value calculated by Freon and McCracken (1962). In addition, the cut-offs were shown by Quenby and Wenk to be more consistent with the intensity increases observed during three solar flare events than previous cut-off calculations.

1.4.3. Makino Cut-Offs.

Makino (1963) modified the Quenby and Webber cut-offs to include a penumbral correction and a longitude correction. The penumbral corrections at all latitudes were taken to be the dipole values determined by Schwartz. Cosmic rays incident vertically at a given location arrive from a direction to the east. The longitude factor was introduced to represent the influence of fields to the east of the point of observation. Makino considered that the Quenby and Webber cut-offs would give a best fit to the cosmic ray equator if the cut-offs were rotated through 16°. The longitude correction factor was then assumed to fall off with latitude λ as $16\ (\cos^{n}\lambda)^{\circ}$. The empirically determined value of n was 3.

1.4.4. L Parameter Derived Cut-Offs.

Ray (1963) introduced the L parameter of McIlwain (1961) in an attempt to restore dipole symmetry to the ordering of cosmic ray data. This parameter, constant to ~ 1% along lines of force, provides a good demographic description of the trapped particle population [for example McIlwain (1961)] . It has also been demonstrated by Lin et al (1963) to be capable of organising the cosmic ray data obtained from the Explorer VII satellite. Ray found that the threshold rigidity could be approximated by :

$$P = 14.9\ L^{-2} \quad \text{for} \quad L > 2\ Re. \qquad 1.8$$

This is a Störmer threshold as no allowance was made for the penumbra. The inherent identity of this approach and the high latitude approximation of Quenby and Webber was demonstrated by Quenby (1964) . At low latitudes where the first adiabatic invariant of motion is violated, thresholds based upon the L parameter have no real significance.

1.4.5. Experimental Results.

The extensive Project Magnet neutron monitor surveys of Pomerantz and Agarwal (1962) at an atmospheric depth of 680 g cm^{-2} demonstrated the superiority of the Quenby and Wenk cut-offs over those of Quenby and Webber and the eccentric dipole theory. Threshold discrepancies were noted in a region of the North Atlantic as well as an area to the west of the Iberian Peninsular. In the latter region the Quenby and Wenk cut-offs can be as much as 2 GV low. The discrepancies in

the region of the Iberian Peninsula were confirmed by Pomerantz et al (1963) during ship-borne neutron monitor surveys between Scandinavia and Australia via South Africa. The latitude extent of the region was observed to be about 22°N to 40°N.

The absorption of low energy cosmic rays in the atmosphere produces a knee in the spectrum measured within the atmosphere. The position of the knee is subject to a small degree of solar control as evidenced by the aircraft-borne neutron monitor surveys of Meyer and Simpson (1957). The knee position moves to slightly lower latitudes during solar maximum when the primary intensity of low rigidity particles is considerably reduced. The position of the knee in the Capetown area measured by Kodama and Miyazaki (1957) on the survey ship Soya was at a Störmer threshold of 6.4 GV. These data recorded near to solar maximum were corrected for Forbush decrease events occurring during the surveys. This is to be compared with the average value of 2-3 GV observed in other regions by surveys such as Project Magnet. When plotted against Quenby and Wenk cut-offs the position of the Soya knee was 5.6 GV as determined by Shea et al (1965).

1.5 INTEGRATED TRAJECTORY CUT-OFFS.

The technique used is to trace the path of a negatively charged particle from a point at the Earth's surface through the magnetic field. The trajectory is then identical to that of an incoming positive particle moving along the same trajectory.

The Störmer threshold is found by increasing the rigidity until the particle can just escape to infinity.

1.5.1. Calculation of the Penumbral Correction.

The counting rate N(P) of a detector at a fixed atmospheric depth and cut-off rigidity P, ignoring time variations is given by :

$$N(P) = \int_{P_S}^{P_m} j(P)\, S(P)\, dP + \int_{P_m}^{\infty} j(P)\, S(P)\, dP \qquad 1.9$$

where $j(P)$ is the primary differential rigidity spectrum and $j(P)\, S(P)\, \Delta P$ is the number of secondary particles at the atmospheric depth considered, in the rigidity interval ΔP at a rigidity P. The first term is the counting rate due to the transparency of the penumbral region between the Störmer threshold P_S and the main cone threshold P_m. The penumbral region is investigated by making calculations at small rigidity intervals ΔP. This is thus the limit to which the penumbral detail may be observed. A band structure of alternate forbidden and allowed rigidities will result :

$$N(P) = \int_{P_S}^{P_1} j(P)\, S(P)\, dP + \int_{P_2}^{P_3} j(P)\, S(P)\, dP + \ldots\ldots + \int_{P_m}^{\infty} j(P)\, S(P)\, dP \qquad 1.10$$

One trajectory calculation at a rigidity P is used to represent the

behaviour of a family of particles whose rigidities are within $\pm \frac{\Delta P}{2}$ of the rigidity P.

With the assumption that the slope of the primary spectrum j(P) and the rigidity dependent yield S(P) have little effect on the penumbral contribution to the cut-off:

$$N = \overline{j(P)\ S(P)} \int_{P_s}^{P_m} dP + \int_{P_m}^{\infty} j(P)S(P)dP \qquad 1.11$$

$$= \overline{j(P)\ S(P)} \sum_{P_s}^{P_m} A\ \Delta P + \int_{P_m}^{\infty} j(P)\ S(P)\ dP \qquad 1.12$$

where $A = 1$ for allowed rigidities

$= 0$ for forbidden rigidities 1.13

The cut-off rigidity P is therefore given by :

$$P = P_S + \sum_{P_s}^{P_m} A\ \Delta P \qquad 1.14$$

Shea et al (1965) investigated the detail existing in the penumbral regions. Calculations at intervals $\Delta P = 0.01$ GV at 39.8°S, 22.5°E, yielded a cut-off of 3.72 GV. With $\Delta P = 0.02$ GV there was no significant difference in the two possible cut-offs. With $\Delta P = 0.1$ GV, the 10 possible values varied from 3.60 GV to 4.03 GV, the latter differing by $\sim 8\%$ from the value obtained using the more detailed penumbral calculations

with $\Delta P = 0.01$ GV. A significant improvement at this location is obtained with 0.01 GV rigidity steps in the penumbral region.

1.5.2. Threshold Dependence on the Primary Spectrum.

The effect of varying the spectrum index of the primary radiation has been investigated by Kodama (1965) at 85 selected cosmic ray stations.

The integral primary spectrum may be represented by :

$$N(>P) \propto P^{-\gamma} \qquad 1.15$$

Cut-offs were calculated for a galactic spectrum with $\gamma = +1.3$ and for a solar flare spectrum with $\gamma = +5$ at 0.1 GV rigidity intervals.

The greatest spectrum dependences are given in Table 1.2.

TABLE 1.2.

SPECTRUM DEPENDENCE OF CUT-OFFS. (GV)

LOCATION	Finch and Leaton Field.		
	$\gamma = 1.3$	$\gamma = 5$	% reduction
Mexico City	9.42	9.33	1.0
Mr. Norikura	11.47	11.22	2.5
Hafelekar	4.44	4.40	0.9
Irkutsk	3.94	3.39	1.3
Itabashi	11.46	11.21	2.5

The r.m.s. percentage reduction for the 85 stations was + 0.6%.

This difference is not significant as the field is known only to 1%. The error involved in assuming a P^{o} spectrum rather than $P^{-2.5}$ differential rigidity primary cosmic ray spectrum in calculating penumbral contributions will be negligible.

1.5.3. Threshold Dependence on Magnetic Field Simulation.

The r.m.s. differences between the measured surface field and the simulation of Finch and Leaton (1957) and that of Jensen and Cain (1962) are ~400 Y. The surface field, accurate to ~1% at points where the measured data is put into the field model is presumably less accurate in regions where no data is available.

Cut-offs calculated by Shea et al (1965) for the Finch and Leaton and the Jensen and Cain fields have r.m.s. differences ~ 2%. Typical cut-offs are given in Table 1.3.

TABLE 1.3.

CUT-OFF DEPENDENCE ON FIELD SIMULATION (1)

Latitude North	Longitude East	Finch and Leaton	Jensen and Cain	Percentage Difference
59.85	17.92	1.43	1.42	- 0.7
46.10	282.50	1.02	1.04	+ 2.0
36.12	137.56	11.39	11.46	+ 0.6
32.78	263.20	4.35	4.30	- 1.2
-1.00	190.00	15.59	15.53	- 0.4
-12.03	283.12	13.49	13.36	- 1.0
-39.80	22.50	3.72	3.61	- 2.4
-42.92	147.24	1.89	1.85	- 2.1

The more accurate field of Cain et al (1965) was used by Kodama (1965). An overall lowering of the cut-offs resulted from the lowering of the dipole term by 0.4% with respect to the Finch and Leaton field. Several large differences are apparent in the values given in Table 1.4.

TABLE 1.4.

CUT-OFF DEPENDENCE ON FIELD SIMULATION (2)

Latitude North	Longitude East	Finch and Leaton	Cain et al	Percentage Difference
46.10	282.50	1.05	1.15	+ 9.5
-34.42	19.22	5.05	4.64	- 8.0
-12.03	283.12	13.45	13.35	- 0.7
52.27	104.30	3.94	3.74	- 5.0
10.23	77.46	17.45	17.45	0
19.33	260.82	9.42	9.24	- 1.9
36.12	137.56	11.47	11.05	- 3.7
-22.90	316.78	11.85	11.65	- 1.7
41.90	12.52	6.45	6.14	- 4.8
62.02	129.72	1.74	1.75	+ 0.6

1.5.4 Comparison with Experiment.

Kellogg (1960) computed the position of the cosmic ray equator using trajectory computation in the field of Finch and Leaton. The experimental data of Katz et al (1958) showed a root mean square scatter > 0.3 GV from this calculated equator.

After considering the effect of off-vertical incidence, Kellogg concluded that the differences between the observed and the calculated cosmic ray equators were due to the limitations of the geomagnetic field representation.

A computer program developed by McCracken et al (1962) has found wide application in the calculation of cosmic ray cut-off rigidities. A negative particle is followed out from a position 20 km above the Earth's surface and is considered to have escaped when it reaches 25 earth radii. Shea et al (1965) used this program to calculate the cut-offs at the locations of the Project Magnet and the Soya data. An improvement was brought about in the region to the west of the Iberian Peninsula although discrepancies still remained. The Soya knee was found to be at a cut-off of ~ 4 GV with both the Finch and Leaton and the Jensen and Cain field simulations. This value is in better agreement with other observations but is ~1 GV higher. The Soya data were obtained from a neutron monitor which is an omnidirectional detector and so records non-vertically incident particles. The maximum possible reduction of the effective cut-off due to off-vertical incidence was found to be ~0.6 GV. The position of the knee was considered to be in disagreement with the world-averaged value of 2 — 3 GV.

The results of a comparison of the Quenby and Wenk and the Makino cut-offs with trajectory computed cut-offs are given in Table 1.5 from Shea et al.

TABLE 1.5.

R.M.S. DEVIATIONS FROM TRAJECTORY-DERIVED CUT-OFF RIGIDITIES.

REGION	QUENBY & WENK %	MAKINO %
Equatorial $P > 10.0$ GV	3.0	1.1
Mid-latitude $10.0 > P > 1.0$ GV $(P_m - P_s) > 0.5$ GV	9.7	18.6
Mid-latitude $10.0 > P > 1.0$ GV $(P_m - P_s) < 0.5$ GV	12.3	6.5
High latitude $P < 1.0$ GV	16.5	45.8
Soya and Project Magnet Locations	17.8	8.7

From these comparisons the following conclusions were drawn:

a) Makino values superior in equatorial regions.

b) Large differences in mid-latitude regions.

c) Quenby and Wenk values better at high latitudes.

d) Makino values successful in anomalous regions.

1.5.5. Kondo and Kodama Cut-Offs.

Combining the calculations of Kellogg (1960), and Shea et al (1965) with their own, which used a rigidity interval of 0.1 GV, Kondo and Kodama (1966) constructed a grid of cut-offs. Interpolation from this grid to the positions of the basic calculations produced an r.m.s. error of ~ 0.2 GV.

1.5.5. Shea et al Cut-offs.

A more comprehensive grid of cut-off rigidities has been constructed by Shea et al (1966). Rather than constructing grid points by interpolation between more or less randomly distributed points, these authors have calculated the cut-offs at each 15×15 degree grid point over the Earth. Additional calculations have led to large areas being covered with a finer 5×15 degree (latitude $\times$ longitude) mesh of calculated points. From the incomplete 5×15 degree grid an interpolation method based upon the L parameter has been used to produce a 2×2 degree grid. For each adjacent pair of points at the same longitude, values for A and ν were determined from the equation :

$$P = AL^{-\nu} \qquad 1.16$$

These coefficients A and indices ν were then used to interpolate the cut-off at any location.

1.6. EXPERIMENTAL CUT-OFF DETERMINATION.

1.6.1. Neutron Monitor Measurements.

A comparison of cut-offs can be made at the positions of the knee in the latitude intensity curve. As the yield functions for sea level neutrons are not known to a sufficient degree of accuracy an absolute cut-off cannot be given. Neutron monitor surveys by Van der Walt et al (1966) in the Cape Town region indicated that the cosmic ray knee was at a cut-off (Kondo and Kodama) of about 2GV. The discrepancy in this area previously noted in the Soya data is thus doubtful when consideration is given to the Forbush decreases which occurred during the recording of

that data for which inaccurate correction may have been made.

1.6.2. Balloon Measurements.

Cut-offs in the range ~ 1 - 2.5 GV can be measured directly by means of proton and alpha particle observations using detectors high in the atmosphere or above. Because the primary differential rigidity spectrum starts to decrease in this range there has been a degree of ambiguity in cut-offs determined by this means. The majority of such measurements have been made at Minneapolis where the effective vertical cut-off and Störmer threshold are 1.39 GV and 1.32 GV respectively.

A summary of the galactic cosmic ray measurements at balloon altitudes of a few g cm^{-2} has been given by Webber (1962). These suggest that during magnetically quiet times cut-offs $\lesssim$ 2.5 GV are lower than the calculated values. The contributions of the various experimental errors to the apparent spread of particles below the cut-off have been estimated by Webber and McDonald (1964). They found that the effective quiet-time cut-off at Minneapolis was 1.0 - 1.1 GV. This lowering is not explicable in terms of penumbral transparency as the effective cut-off is less than the calculated Störmer cone value. Freier et al (1959) observed a considerable lowering of the cut-off during magnetic storms. Solar protons of 75 MeV were detected showing thatthe cut-off was at some very low value, in disagreement with the calculated Minneapolis cut-off.

Cut-offs can most readily be measured during solar proton events when there are large fluxes of low rigidity particles. Freier (1962) made 6 balloon flights in the period following the solar flare of 10th July 1959. Four were at Minneapolis and two at Fort Churchill. The

geomagnetic cut-off (< 0.21 GV) at Churchill was less than the instrument cut-off and so provided a primary spectrum measurement free from geomagnetic influence.

This allowed details of the cut-off at the lower latitude to be observed. The quiet time main cone cut-off was determined to be 1.20 GV. The intensity below the main cone could be represented by :

$$I = I_o \; e^{-2.30(P_M - P)/0.15} \quad ; \quad P \leqslant P_M \qquad 1.17$$

This represents the effects of the penumbral transparency at cut-offs P below the main cone cut-off P_M.

$$\begin{aligned} I/I_o \quad &\simeq 45\% \quad \text{at} \quad 1.15 \text{ GV} \\ &\simeq 10\% \quad \text{at} \quad 1.05 \text{ GV} \\ &\simeq 1\% \quad \text{at} \quad 0.9 \text{ GV} \end{aligned} \qquad 1.18$$

During the magnetic storm which followed the solar proton event, the cut-off at Minneapolis was observed to fall below 0.7 GV.

1.6.3. Satellite Observations.

An almost uniform flux of 1.5 MeV solar protons was observed by Stone (1964) over the polar region, terminating sharply at a geomagnetic latitude of about 65° at local midnight and about 67° at local noon. The cut-offs over this region must have been less than 0.05 GV. At 65° geomagnetic the Störmer dipole cut-off is 0.48 GV. During the main phase of magnetic storms Pieper et al (1962) observed a marked equatorial shift of the cut-off latitude of 1.15 MeV protons. Particles were observed

down to L values ~ 3.5 corresponding to a geomagnetic latitude of ~ 58°.

The outer boundary of the stably trapped electron population is sharply defined both at low altitudes (for example O'Brien (1963)) and at high altitudes (for example Frank (1965)). Williams and Palmer (1965) measured a pronounced day-night asymmetry of the boundary field lines for electrons of energy $E_e \geqslant 280$ KeV. The latitudes from which the boundary field lines emerged depended upon geomagnetic activity, but at quiet times the night-side boundary was ~68° and the day-side ~70°. An equatorial shift of the outer boundary of trapped electrons of energy $E_e \geqslant 40$ KeV was observed by Maehlum and O'Brien (1963) to occur during magnetic storms.

The high latitude outer boundary of the radiation belts is approximately coincident with the low latitude limit of the low energy solar proton observations. Both are observed to move to lower latitudes during storm times.

1.6.4. Riometer Observations.

The increases in ionisation in the ionosphere caused by solar protons during several polar cap absorption (PCA) events measured by riometers at College (65°N) and Thule (88°N geomagnetic) were found by Leinbach et al (1965) to be very similar. This indicated a more or less uniform flux over the polar cap regions of those solar protons which contribute to the ionisation i.e. probably 1 MeV or less. The absorption at Farwell (61°) was only ~ 10% of that at Thule indicating a cut-off of low energy protons. Riometers situated close to the boundary of PCA events observe a diurnal variation in the ionisation with a decrease at local noon, while those at

higher latitudes show no variation. This was interpreted by Leinbach (1961) as a variation of cut-off rigidity with local time.

1.6.5. Summary.

The experimental evidence for the reduction of high latitude cut-offs is conclusive. Cut-offs above 68° - 70° are probably reduced to a very small value. Reductions at lower latitudes occur up to cut-offs $\sim$ 2.5 GV. Apart from the observations at Minneapolis (1.39 GV) the experimental data is rather sparse. The effective cut-off at Minneapolis during quiet times is probably 1.0 - 1.2 GV.

1.7. THE ORIGIN OF HIGH LATITUDE CUT-OFF REDUCTIONS.

The main theoretical approaches have been via a Westward flowing ring current, the superimposition of an interplanetary magnetic field and the effects of the confinement of the geomagnetic field through interaction with the solar wind.

1.7.1. Ring Current Reductions.

Singer (1957) first suggested that a ring current might have its origin in the drift motions and gyrations of geomagnetically trapped particles. The feasability of geomagnetically trapped particles was discovered by Störmer (1907). Störmer theory showed that particle trapping was possible within a region of limited radial extent $r_1 < r < r_2$ given by :

$$\frac{r_1}{b} = \frac{\cos^2 \lambda}{-\gamma/b + [(\gamma/b)^2 + \cos^3\lambda]^{\frac{1}{2}}} \qquad 1.19$$

$$\frac{r_2}{b} = \frac{\cos^2 \lambda}{-\gamma/b + \left[(\gamma/b)^2 - \cos^3 \lambda \right]^{\frac{1}{2}}} \qquad 1.20$$

where λ is the geomagnetic latitude

$$b = \left[\frac{M}{P} \right]^{\frac{1}{2}} = \left[\frac{\text{Magnetic moment}}{\text{Magnetic rigidity}} \right]^{\frac{1}{2}}$$

γ is an arbitrary constant of integration.

The currents due to a trapped particle population are such as to decrease the overall field close to the Earth and to increase the field external to the trapped particle circulation. The confinement of charged particles by the geomagnetic field was confirmed by Van Allen et al (1959). An approximate calculation by Kellogg and Winckler (1961) gave the threshold P at high latitudes in terms of the internal field threshold P_o as :

$$P = \frac{P_o}{1 + M'/M} \qquad 1.21$$

where M' is the magnetic moment of the ring current and M the magnetic moment of the Earth's field. Akasofu and Lin (1963) calculated the magnetic moments of a number of possible ring currents and concluded that the moment M' is probably never as great as M. The threshold reduction observed by Maehlum and O'Brien (1963) requires $M' \simeq 10M$, while that observed by Pieper et al (1962) requires $M' \simeq 16$ M. The maximum reduction of 50% cannot explain the storm-time threshold reductions although it

could contribute to the quiet-time reductions.

Dessler and Parker (1959) showed that the unperturbed dipole field B_o is increased to $B_o + \Delta B(o)$ at the Earth's centre (and also at the surface) by a particle belt confined to the equatorial plane where :

$$\frac{\Delta B(o)}{B_o} = - \frac{e_D}{} \times \frac{2}{3} \times \frac{\varepsilon}{\varepsilon_D} \qquad 1.22$$

e_D is a north-pointing unit vector, ε is the total kinetic energy of the belt particles and ε_D is the total energy in the dipole field ($= 8.37 \times 10^{24}$ ergs). Hoffman and Bracken (1965) calculated the magnetic effects of the trapped proton population of energy $E > 100$ KeV as measured by Davis and Williamson (1963). The total energy in the belt was estimated to be 5.7×10^{21} ergs. Detailed calculation gave a magnetic moment $M' = 0.029\ M$ and a surface field decrease of 9γ. This 9γ decrease is in good agreement with the value obtained from the approximate equation 1.22. The maximum contribution to the magnetic field is from the lowest energy particles measured, whose directional intensity at $L \simeq 3.5$ was observed to be $\sim 10^7$ $(cm^2\ sec\ ster)^{-1}$. The stability of this population as observed by Davis and Williamson (1963) suggested that only small storm-time enhancements occurred.

The first important evidence of the storm-time enhancement of the ring current has recently been given.

Cahill (1966) observed that during a magnetic storm on 17/18 April 1966 there was a field depression of 217γ near 3 earth radii

simultaneous with the main phase ground decrease of 150 γ. From observations of the asymmetric onset of the decrease, the effect was probably due to enhancement of the proton population. The drift times of protons suggested that the energy of these particles was probably $<$ 60 KeV. At quiet times there was little divergence from the Jensen and Cain main core field.

Direct particle observation has been made by Frank (1966) during two magnetic storms. The detector was a Cd S total energy flux instrument. Large increases of electron flux ($\sim$ 10 x) were recorded at the onset of these storms between L = 2.8 and L = 4.0. By comparing with the response of the other satellite particle detectors, Frank concluded that the increase was due to electrons of energy 100 eV $<$E$<$40 KeV. Omnidirectional fluxes of $\sim$ 1000 ergs cm^{-1} sec^{-1} were observed at L $\sim$ 3.5. Integrating this density over the volume of space between L values $2.8 < L < 4.0$ and latitudes 35°N, 35°S, the estimates of the ground level field decreases in Table 1.6 were obtained from equation 1.21 corresponding to two possible mean electron energies E_e

TABLE 1.6.

SURFACE FIELD REDUCTION BY OUTER RADIATION BELT ELECTRONS.

Field Reduction (γ)	Electron Energy.
- B (o)	E_e
60	500 eV
30	2 KeV.

The large energy densities of electrons observed suggest that they contribute appreciably to the main phase decrease but do not exclude the possibility of a principal contribution from protons.

A surface field analysis by Cain (1965) included three constant orthogonal components. The analysis showed these to be non zero. The main component $\sim 20\gamma$ was parallel to the rotational axis and directed southwards, with a standard error of $\sim 30\gamma$. The direction of this field was the same as would be produced by a ring current.

Although appreciable storm enhanced ring currents do exist, the field due to a quiet-time ring current is still uncertain. The probable limits on this ring current contribution to the surface field are -9γ and -50γ.

1.7.2. Uniform Interplanetary Fields.

Quenby (1964) has calculated that the near-zero cut-offs observed at high latitudes could be explained by the superimposition of a southward pointing interplanetary magnetic field of 50γ. The observed interplanetary field as measured by Ness and Wilcox (1964) has an average magnitude of $3\text{-}6\gamma$ with only a small average component southwards. Following solar flares, large increases in the interplanetary magnetic fields have been observed (for example Fan et al (1960a)). Following a correlation of magnetic bays with southward interplanetary fields by Cahill and Fairfield (1965), Dungey (1966) suggested that the arrival of a field at the Earth whose orientation is different to the steady component would result in a dragging out of the geomagnetic field lines on the night side. The resulting magnetic depression would then affect the storm time arrival

of cosmic rays.

1.7.3. Magnetosheath Currents.

The continuous outflow of the solar wind (section 2.4.1) confines the geomagnetic field to a region extending ~10 Earth radii in the solar direction according to magnetometer measurements of Cahill and Amazeen (1963). The interaction of the highly ionized wind and the magnetic field produces currents in the boundary region of the Earth's field. These cause the magnetic field just inside the interface to be doubled: a condition given by Dungey (1958). From the Earth's surface the measured field increases monotonically over the main field: the magnetosheath currents contributing ~10% at a few Earth radii to 50% near the magnetosheath. Makino and Kodama (1966) computed the effect of the compression of the field. Spherical harmonic terms due to the magnetosheath currents were added to the harmonic expansion of the Earth's internal field. The effect on the computed cut-offs was an increase rather than the observed decrease. This rules out magnetosheath currents alone as a source of threshold reduction.

Akasofu et al (1963) considered the combined effects of a ring current and an azimuthally symmetric field termination. Low energy (~500eV) particles could just penetrate the boundary layer. They were then guided from this position along field lines to the Earth at some high latitude. Threshold reductions at high latitudes similar to those observed were anticipated from a qualitative discussion.

1.7.4. Neutral Sheet.

The passage of the solar wind drags out the geomagnetic field in the anti-solar direction to form a tail to the 'magnetosphere'. The magnetometer measurements of Ness (1965) on the IMP 1 Satellite established the existence of the tail, extending to at least 30 Earth radii (apogee). Field lines in the tail region beyond ~12 Earth radii were observed to be directed in either the solar or anti-solar direction (ignoring a small aberration angle) depending upon whether the measurement was made north or south of the solar ecliptic plane. Between these opposed fields is a region in which the magnetic field is approximately zero. The so-called neutral sheet starts at about 12 earth radii. Just as the compression on the day side increases the field strength in the magnetosphere so the night-side expansion reduces the field strength.

Reid and Sauer (1966) considered the influence of the neutral sheet on cosmic ray cut-offs. Lines of force loaded with trapped particles must be simply reconnected to the Earth. Lines above the outer trapping boundary are probably drawn back into the tail. The lowest latitude field line connected to the neutral sheet is probably just above the stably trapping boundary and likely to be the low latitude boundary of the auroral zone. Cosmic rays with more or less free access into the neutral sheet are injected into the inner magnetosphere from the tail region and therefore have free access to the auroral latitudes and the whole polar cap regions. Figure (1.7.1) shows the assumed variation of the

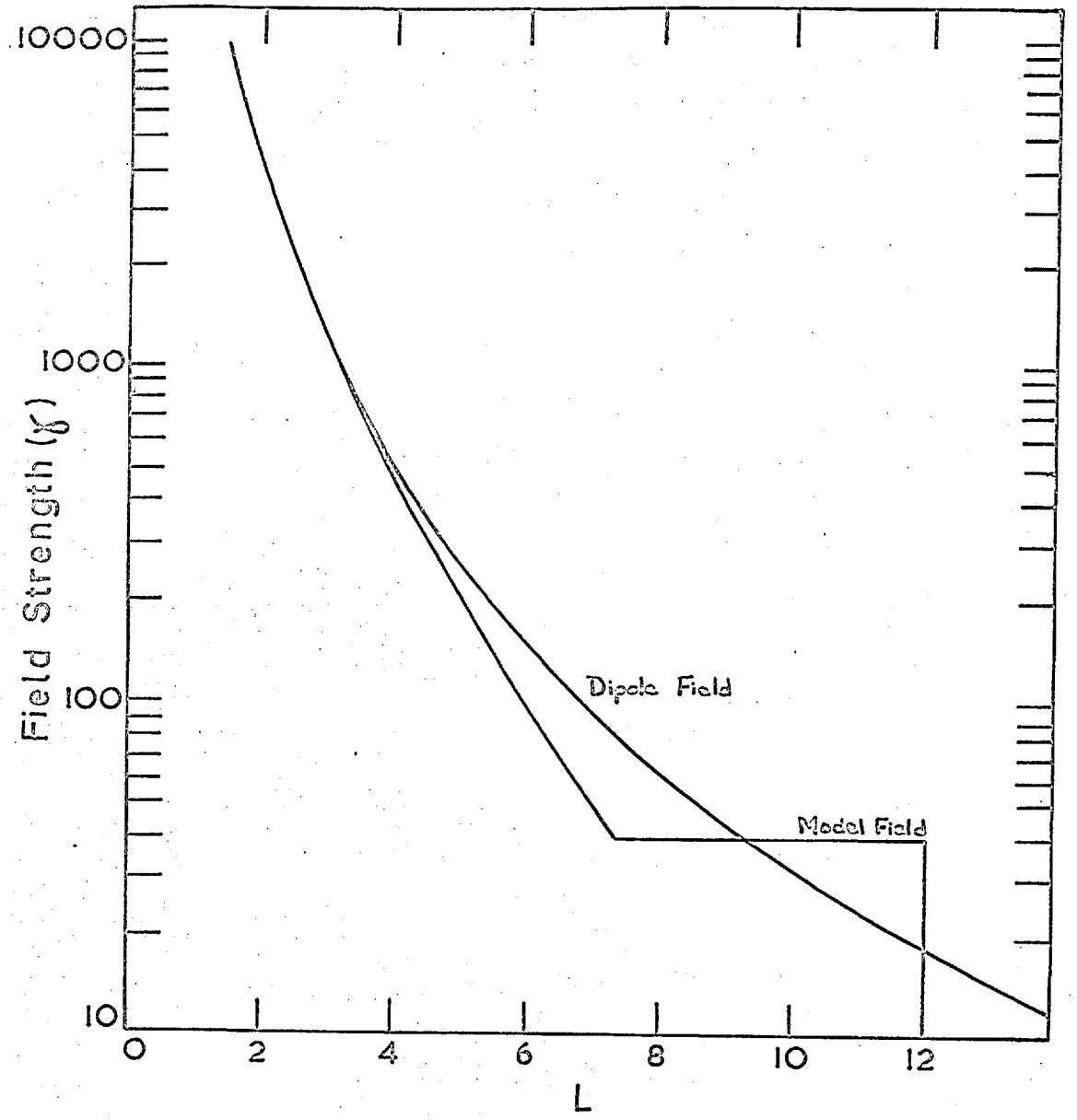


Fig. 1-7.1 The model magnetospheric field with the neutral sheet at 12 R_e: Reid and Sauer (1966).

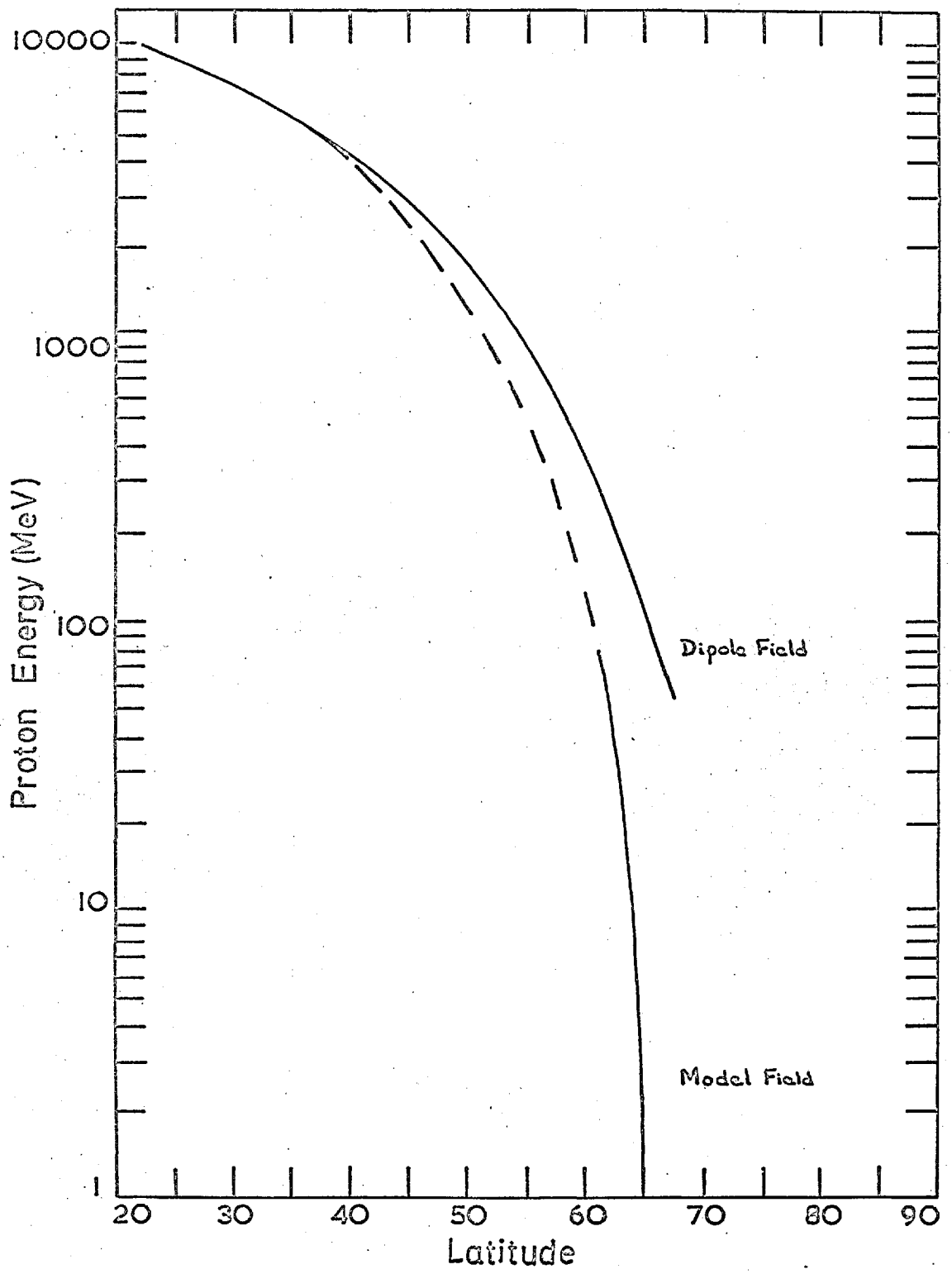


Fig. 1-7.2 Proton threshold energies in the dipole field and in the model field of Reid and Sauer (1966).

field in the anti-solar direction. Particles of a particular rigidity are injected at the neutral sheet termination, then travel in circular orbits in the constant field of 40γ which gives the minimum attainable radial position in the equatorial plane. The particles then attach themselves to the field line at this point and are guided to the Earth. The rigidity of these particles then defines the threshold rigidity at the arrival latitude. Longitude drift in which small angle scattering may produce a continual interchange from free to trapped modes is necessary to remove the anisotropy. The changes of the dipole thresholds calculated by the authors are given in figure (1.7.2).

A model earth experiment by Roberts (1967) in which the cosmic rays are simulated by electrons from an electron gun, has shown that there is a general lowering of high latitude cut-offs when the model dipole field was distorted by a compression on one side and an extension on the opposite side.

1.8. SUMMARY.

a) There is a large amount of data in support of the trajectory integration method of threshold determination.

b) Within the accuracy of the available latitude survey data, the L parameter interpolation method between calculated cut-off locations has proved adequate.

c) Systematic cut-off errors in certain regions could be present due to inaccurate field representation in those areas.

d) High latitude threshold reductions are qualitatively explicable in terms of a combination of ring current and tail current although their relative importance is uncertain.

e) Storm time reductions are due to an enhanced ring current and a dragging out of field lines into the tail region.

CHAPTER 2. THE LONG TERM MODULATION OF COSMIC RAYS.

2.1 INTRODUCTION.

2.1.1 Introductory Experimental Observations.

Cosmic rays of all but the highest energies are thought to be of galactic origin (for example Ginzburg and Syrovatsky (1964)), the Sun emitting energetic particles only during highly disturbed conditions at the solar surface. In addition to this sporadic emission of cosmic rays the Sun exerts a pronounced influence on the cosmic ray intensity observed at the Earth. Variations of atmospheric origin, particularly important in the early methods of measurement, had first of all to be understood and then removed from the data before time variations of external origin could properly be studied. Major contributions to the understanding of the atmospheric influence on the cosmic ray intensity were made by Duperier (1949) and Chasson (1954). Time variations in the cosmic ray intensity were systemetised by Forbush (1954) into the 11 year, 27 day, Forbush decrease and the diurnal variation. All but the last have been shown to be related to solar phenomena. The two most prominent intensity variations are the 11 year and Forbush decrease.

The Forbush decrease is characterised by a sharp intensity decrease occuring generally within a period of hours followed by a slow recovery lasting from a few days to a fortnight. Lockwood and Razdan (1963) analysed a number of Forbush decreases, showing them to be essentially isotropic events. In about half of the events analysed the onsets were isotropic while the remainder were anisotropic. Those stations whose

asymptotic viewing directions were to the west of the Sun-Earth line recorded the decrease about 2 hours in advance of other stations. This was a result of a shift of the maximum of the diurnal variation to the morning hours.

Forbush (1954) first demonstrated the negative correlation between solar activity as measured by the Sun-spot number and the cosmic ray intensity. The world-wide effect of the 11 year variation was observed by Neher and Forbush (1958) for the period 1951 - 1957. They found that the mean annual values of intensity recorded by a shielded ion chamber near the geomagnetic equator correlated well with the intensity measured by an unshielded ion chamber at an atmospheric depth of 15 g cm^{-2} near the geomagnetic pole.

2.1.2. The Rigidity Dependence of the 11 year Modulation.

To specify the modulation, ideally requires comparative measurements of the local interstellar cosmic radiation and the local interplanetary cosmic radiation. The observations have been restricted to changes in the modulation near the Earth rather than the absolute modulation.

The continual observation of the cosmic radiation intensity by a satellite detector through an appreciable fraction of the solar cycle is ruled out by the short mean life of a satellite experiment. Most of the measurements have been observations of the secondary particle intensity within the atmosphere. These observations are related to the primary radiation by the genetic yield functions (section 6.4).

The experimentally observed response for a detector at an atmospheric depth x, and time t, as a function of rigidity is given by the integral of equation 6.2:

$$N(P,x,t) = \int_P^\infty S_G(P,x) \frac{dj(P,t)}{dP} dP \qquad 2.1$$

In the latitude-sensitive region the yield function S_G is practically time independent. The change in counting rate ΔN for a detector at time t is related to the modulation $\Delta J(P,t)$ of the primary spectrum $J(P,t_o)$ by:

$$\frac{\Delta N}{N} = \frac{1}{N(P,x,t_o)} \int_P^\infty \frac{dN}{dP}(P,x,t_o) \frac{\Delta J(P,t)}{J(P,t_o)} dP \qquad 2.2$$

where $J(P,t_o) = \frac{dJ}{dP}(P,t_o)$

and $\Delta J(P,t) = J(P,t_o) - J(P,t)$

Elliot et al (1960) calculated the modulation function ΔJ for the solar maximum period from results at six neutron monitor stations. Using a measured sea level (x_o) differential response curve for a neutron monitor at solar minimum $\frac{dN}{dP}(P,x_o,t_o)$, the modulation function ΔJ was chosen so that the calculated sea level changes ΔN gave a best fit to the measured changes. The ratio of the solar maximum to the solar minimum differential rigidity spectrum found in this way is shown in figure 2.1.1.

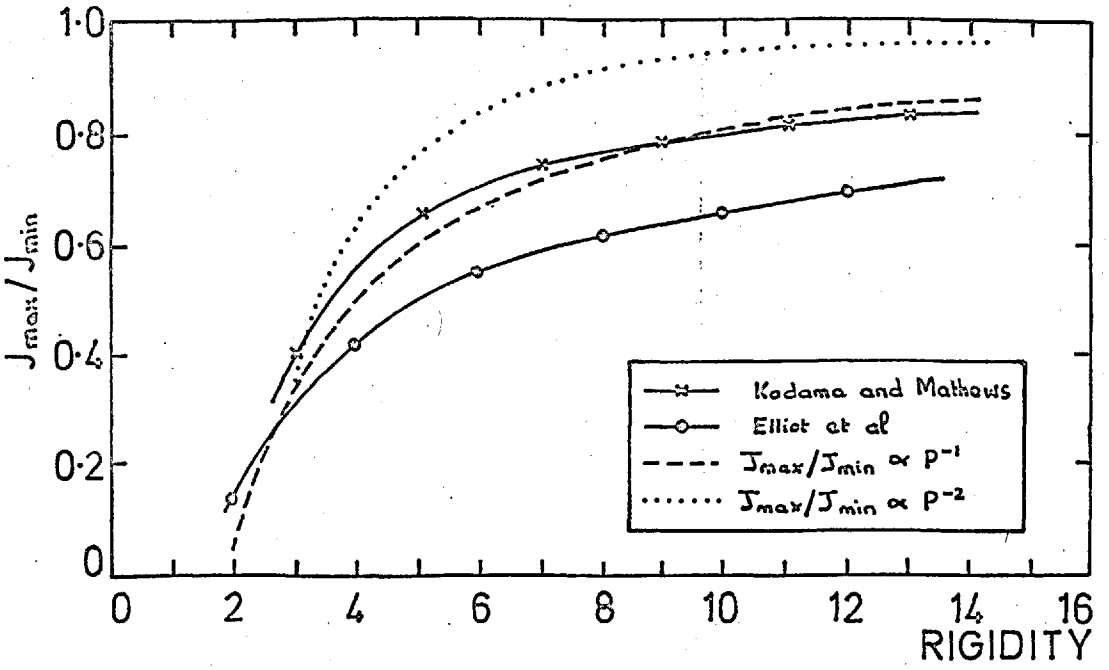


Fig. 2-1.1 Change in the differential rigidity spectrum between solar minimum and solar maximum.

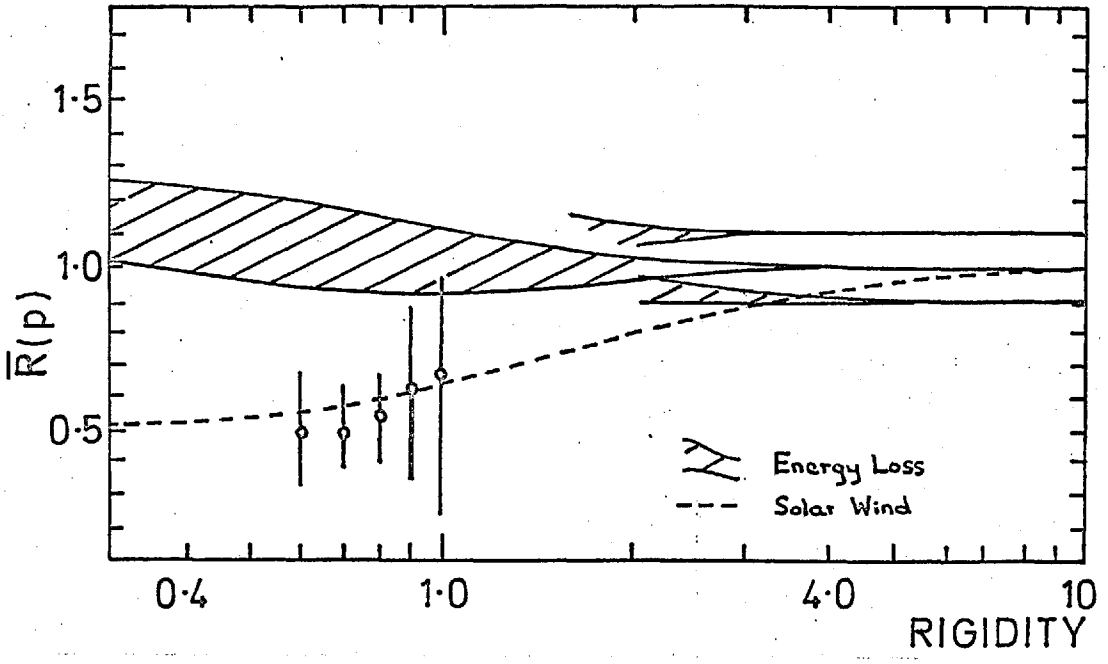


Fig. 2-4.1 Ratio of the logarithms, $\bar{R}(p)$, of the proton and alpha-particle modulation between two epochs as predicted by an electric field deceleration model and the solar wind convection model of Parker. Experimental values between 1963 and 1965 are given. (Diagram from Quenby: 1966).

Assuming that the rigidity dependence of the modulation is of the form :

$$\frac{\Delta J}{J\,(P,\ t_o)} \propto P^{-\gamma} \qquad 2.3$$

then the best fit function required $\gamma < 2$.

From an analysis of data from a number of cosmic ray stations during the period 1956 - 1958 close to solar maximum, McCracken (1960) found that the 11 year modulation was of the form expressed in equation 2.3, with $\gamma = 1.3$. For short term Forbush decrease events, the spectral variation was observed to be flatter with $\gamma = 0.8$.

A simpler and more rigorous method giving the change in the primary spectrum and requiring no 'a priori' knowledge of the modulation has been used by Kodama and Matthews (1964).

$$\frac{J(P)max}{J(P)min} = \frac{(dN/dP)\ max}{(dN/dP)\ min} \qquad 2.4$$

The solar minimum spectrum $\left(\frac{dN}{dP}\right)$ min was obtained from the sea level neutron monitor surveys of Rose et al (1956) completed during 1954-1956. The solar maximum curve $\left(\frac{dN}{dP}\right)$ max was obtained from two of the Soya voyages during 1957-1958 by Kondo et al (1963). The modulation obtained is given in figure (2.1.1).

Cut-offs used in the data of Rose et al (1956) were those of Quenby and Wenk. As the surveys were not conducted in regions where the Quenby and Wenk cut-offs are greatly in error, their use will probably

not introduce significant errors. Trajectory computed cut-offs were used in the analysis of the solar maximum data. These have been shown in Section (1.5.4.) to be more accurate than the Quenby and Wenk cut-offs in the region of South Africa through which the Soya passed. The knee was shown to occur at ~ 4.0 GV so that the modulation function in the rigidity range $\lesssim 4.5$ GV is doubtful.

A different approach has been used by Durney et al (1964) who measured the integral rigidity spectrum for particles of charge $\geqslant 6$. During the period May/June 1962 this was found to be :

$$N(P,t) \propto P^{-1.5} \quad : \quad P > 8.5 \text{ GV} \qquad 2.5$$
$$N(P,t) \propto P^{-1.2} \quad : \quad P < 8.5 \text{ GV}$$

With a primary galactic spectrum of the form $P^{-1.5}$, the modulation is given by :

$$\frac{J_{62}(P)}{J_o(P)} = 1 - 0.8\left[\frac{P}{8.5}\right]^{0.3} ; \quad P < 8.5 \text{ GV} \qquad 2.6$$
$$= 0 ; \quad P > 8.5 \text{ GV}$$

This modulation function has been used by Quenby (1964) to calculate the depression of counting rate below solar minimum level for a number of neutron monitor stations. Within the rather large errors the predicted depressions were in agreement with those measured.

2.1.3. The Charge Dependence of the Long Term Modulation.

A crucial area of investigation is the relative modulation of protons and alpha particles of rigidity $\lesssim 3$ GV. It is in this range of the spectrum that the protons and alpha particles have appreciably different velocities (difference >10%) at the same rigidity. Webber (1962) has summarised the available balloon measurements. He observed no systematic difference in the modulation of protons and alpha particles for $P \gtrsim 1.2$ GV. This suggested that during the period 1955-1959 the modulation was dependent only on rigidity above 1.2 GV. The statistics of this measurement were not good as there were no overlapping differential rigidity data from the two components.

Fichtel et al (1964) and independently Balasubrahmanyan and McDonald (1964) showed that the proton and alpha particle spectra were not identical below ~1.5 GV. The alpha spectrum in this region was observed to be depressed below the proton spectrum if the two were normalised at high rigidities to allow for the relative abundances. These observations did not prove a velocity dependence of the modulation because of the uncertainties of the form of the inter-stellar primary spectra prior to solar modulation.

2.1.4. Solar Flare Data.

While the cosmic rays at the orbit of the Earth have been subject to the modulating conditions beyond the Earth's orbit, solar proton observations essentially yield information on conditions within the Earth's orbit. The flare particles of the event of February 1956 were

observed by Meyer et al (1956) to decay with time as $t^{-3/2}$. This was interpreted as a decay due to isotropic diffusion of particles in an infinite medium. It has subsequently been shown that solar proton events generally can be described by a diffusion process.

2.2. BASIC MODULATION MECHANISMS.

2.2.1. Introduction.

The two methods by which the inter-stellar spectrum may be modulated are through a reduction of the number of cosmic rays or a reduction of their energy. It is probable that modulation occurs by both methods though the dominance of one or the other is not established. The early modulation theories (in this section) were concerned with the fundamental processes, while the more recent theories dealt with in the subsequent sections have been concerned with a sophistication of these ideas.

2.2.2. Energy Loss Mechanisms.

Alfvén (1950) considered the interaction of particles with outward moving solar plasma streams. The high electrical conductivity of these streams resulted in the magnetic field lines being 'frozen' in the plasma. The relativistic transformations of the electric field $\underline{E}'$ and magnetic field $\underline{H}'$ to another frame of reference in which the plasma velocity is $\underline{v}$ are :

$$\underline{E}' = \gamma_L \left[\underline{E} + \tfrac{1}{C}\, \underline{v} \wedge \underline{H} \right] \qquad 2.7$$

$$\underline{H}' = \gamma_L \left[\underline{H} - \tfrac{1}{C}\, \underline{v} \wedge \underline{E} \right] \qquad 2.8$$

The electric field $E' \approx 0$ and the Lorentz factor $\gamma \simeq 1$ for the typical plasma velocity.

$$\therefore \quad \underline{E} \simeq - \frac{1}{c} \left(\underline{v} \Lambda \underline{H} \right) \qquad 2.9$$

and $$\underline{H'} \simeq \underline{H}$$

The electrostatic polarisation field $\underline{E}$ across the plasma stream can produce a deceleration of the particles. Within the frame of reference moving with the wind there is no electric field; the particles move in a static magnetic field. The correct energy loss treatment of Fermi (1949) considered the particle motion within this magnetic field. The maximum energy loss occurs for a tail-on collision with the plasma cloud when the change in energy Δu for relativistic particles is given by :

$$\frac{\Delta u}{u} = - \frac{2v}{c} \qquad 2.10$$

This is an ineffective mechanism as for a typical plasma velocity of 3.10^7 cm sec^{-1} :

$$\frac{\Delta u}{u} \simeq - 2.10^{-3}.$$

A geocentric electric potential was proposed by Nagashima (1953) to account for changes in the cosmic ray intensity. This model is at variance with the observed high degree of correlation between the cosmic ray intensity, which depends on the electro-magnetic fields in interplanetary

space, and solar activity. A modification introduced by Ehmert (1960) considered a heliocentric potential. The electric potential V required at the position of the Earth's orbit was ~1 GV (10^9 volts) at solar minimum and ~ 2 GV at solar maximum. According to Liouville's theorem the density of particles in phase space D is conserved:

$$D = \frac{j}{p^2 \beta} \qquad 2.11$$

where j is the flux $(\text{ster sec})^{-1}$ and β is the particle velocity in units of the velocity of light.

If j is measured as the differential kinetic energy spectrum $j(E)$ then :

$$\frac{j(E)}{p^2} = \text{const.} \qquad 2.12$$

Putting $j_\infty(E)$ as the galactic spectrum of particles of charge z and mass number A, then the spectrum at the Earth $j(E)$ after passing through the potential field V is given by :

$$j(E) = j_\infty(E) \frac{(E-VZ)(E-VZ+2A)}{E(E+2A)} \qquad 2.13.$$

— where the kinetic energy E is in GeV and the potential V in GV. Modulation models requiring a potential field ~1 GV seem implausible in view of the high conductivity of interplanetary space as suggested by the plasma probe observations of Snyder et al (1963). In addition

there has been no evidence of a high energy flux of electrons which presumably should be produced in such a field.

Singer (1958) considered the statistical anti-Fermi mechanism as a modulation source. Solar streams ejected at supersonic speeds formed turbulent vortices at the boundary with the interplanetary medium. As the stream was expanding the net recessional velocity of the scattering centres produced a statistical energy loss for particles random walking through the stream. An additional energy loss mechanism was analysed by Laster et al (1963). The continual expansion of the magnetic field causes a Betatron decleration which cools the cosmic radiation when moving through these fields.

2.2.3. Modulation by Regular Magnetic Fields.

The screening effect of a uniform magnetic field carried by solar plasma to envelop the Earth has been studied by Dorman (1957). This analysis did not complete the field line topology and as observed by Quenby (1964), the screening effect was only considered for particles moving perpendicular to the field lines while the screening for particles moving along the field lines was undetermined.

The solar dipole field was considered by Janossy (1937) to have a shielding effect on cosmic radiation reaching the Earth. The surface polar magnetic field strength on the Sun was thought to be some 10's of gauss. An accurate measurement by Babcock (1959) gave a value of about 1 gauss for the polar field strength. This dipole field is not capable of producing the observed modulation. In addition, the solar dipole moment seems to go through zero near solar maximum according

to the observations of Babcock (1961). This is compatible with the observed maximum modulation at this time only if the dipole moment is not the main modulating influence.

Elliot (1960) suggested that shielding might be effected by a dipole magnetic field generated by an axially symmetric coronal ring current system of radius 5 - 15 solar radii. The current density was such as to produce a field at the Earth's orbit of about 10^{-4} gauss at Sun-spot maximum and 10^{-5} gauss at sun-spot minimum. Superimposed upon this regular field were scattering centres which allowed the entry of low rigidity particles by diffusion. The equilibrium condition was attained with a reduced intensity of these particles depending upon the competition between inward diffusion and a removal process whereby they were guided down field lines to the Sun.

The spectrum observed at the Earth $\frac{dj(P)}{dP}$ was related to the galactic spectrum $\frac{dj_o(P)}{dP}$ by :

$$\frac{dj}{dP}(P) = \frac{dj_o(P)}{dP}\left[\frac{45\ M_s}{r_e\ P^{\frac{1}{2}}}\right]^{\frac{1}{2}\mu} \quad ; \quad \mu = \left[1 - \left(1 + \frac{4k\alpha(P_o+P)}{P^2}\right)\right]^{\frac{1}{2}} \qquad \ldots\ldots\ 2.14$$

where r_e is the Sun - Earth distance, M_s is the solar dipole moment; αk is the probability per collision of being scattered into the loss cone to the Sun; P_o is the magnetic rigidity of a particle whose Larmor radius in the scattering centre is equal to the scale size of the centre; and P is the particle rigidity.

The 11 year intensity variation is produced by the variation of M_s, ak and P_o.

2.2.4. Isotropic Diffusion Models.

Morrison (1956) proposed that variations in cosmic ray intensity might be due to diffusion in tangled magnetic fields carried in clouds of corpusoular radiation ejected from the Sun. The highly ionised clouds, initially devoid of cosmic rays, were sufficiently turbulent to tangle the magnetic field lines. Cosmic rays could then diffuse into the cloud to remove the density gradient. The envelopment of the Earth by such a cloud whose diffusion time was longer than the cloud transit time to the Earth would cause a reduction in the observed cosmic ray intensity.

Random walk of cosmic rays of speed ω and mean free path λ within the cloud produces the isotropic diffusion coefficient K where :

$$K = \frac{1}{3}\omega\lambda \qquad 2.15$$

The flux of particles $\underline{F}$ is proportional to the density gradient :

$$\underline{F} = -K \text{ grad } n \qquad 2.16$$

The increase of cosmic rays at any point is given by:

$$\frac{\partial n}{\partial t} = -\text{div } \underline{F} = \text{div } \left[k \text{ grad } n \right] \qquad 2.17$$

Solving this equation gives the modulation $\Delta J\ (P)$ as :

$$\frac{\Delta J(P)}{J(P)} = - \exp\left[\frac{-\pi^2 \lambda \omega t}{3 r_o^2} \right] \qquad 2.18$$

where r_o is the cloud radius.

Parker (1963) found that the characteristic diffusion times of this equation could not account for Forbush decreases whose recovery times were of the order of a week.

The essentially heliocentric mechanism of Morrison was modified by Parker (1958a). Solar corpuscular clouds, thought to be emitted only in the equatorial region of the Sun would lead to easy access perpendicular to the equatorial plane. To account for the experimentally observed dearth of low energy [$E \lesssim 1$ GeV] cosmic rays required either isotropic cloud emission or a geocentric modulation mechanism . The occasional solar cloud containing tangled magnetic fields was supposed to be captured by the Earth's gravitational field. The cloud, extending to a few Earth radii had a decay time ~ 6 months. Variation of the ejection frequency of the solar clouds with solar activity led to a varying number of captured clouds, thereby producing the 11 year cosmic ray intensity variation.

The values required for the magnetic field strength and mean free path between inhomogeneities were $\sim 3 \times 10^{-2}$ gauss and 2.5×10^{7} cm respectively.

2.3. SOLAR WIND MODULATION.

2.3.1. Introduction.

From observations of luminous comet tails Bierman (1951) considered that the Sun must emit particles continuously, and not just during disturbed solar conditions. This led Parker (1958b) to consider the stability of the solar corona. He found that hydrodynamic equilibrium was not established : that the thermal energy of the coronal gas was greater than the combined restraining forces of the gravitational and magnetic fields. This imbalance of forces in the corona results in the continual outflow of material (completely ionized because of the high coronal temperatures) which constitutes the solar wind. Calculation showed that the flow was supersonic beyond a few solar radii with a quiet day speed V of 300 - 400 km/sec at the Earth's orbit. The solar wind continues to blow outwards, cooling through adiabatic expansion until the outward thermal pressure becomes balanced by the inward pressure of the local galactic magnetic field, the cosmic ray gas, and the interstellar gas.

For a spherically symmetric expansion the wind density N falls off as the square of the distance travelled. If N_e is the density at the Earth's orbit r_e then $N(r)$ is given by :

$$N(r) = N_e \times \left(\frac{r_e}{r}\right)^2 \qquad 2.19$$

The impact pressure $\frac{1}{2} NMV^2$ therefore falls off as $\frac{1}{r^2}$. The thermal pressure at the boundary with the interstellar medium is :

$$P_I = (\tfrac{1}{2} NMV^2) \times \frac{r_e^2}{r_I^2} \qquad 2.20$$

Parker (1963) has equated this pressure to the inward forces on the solar cavity and found the position of the boundary to lie between 45 A.u. and 90 A.u. The general magnetic field over the whole solar surface is ~1 gauss according to the measurements of Babcock and Babcock (1955). Outward convection of the highly conducting solar plasma draws out the magnetic field lines radially. The rotation of the Sun twists the lines into an Archimedean Spiral. The angle between the field line and the Sun-Earth line is given by :

$$\tan\psi = \frac{\Omega r}{V} \qquad 2.21$$

where Ω is the angular velocity of the Sun and V the solar wind speed. This gives a value for ψ of about 45° at the Earth's orbit. The whole of interplanetary space is thus filled with solar magnetic field lines.

Temperature variations in the corona will result in a region of enhanced thermal energy overtaking a slower region at a supersonic speed. Shock waves will result from the interactions of the two streams. These will distort the magnetic field lines producing kinks in the underlying smooth field configuration. These irregularities will become degraded with distance, and consequently less sharp.

The bulk velocity is greater than the random thermal velocities in the plasma and so the expansion is anisotropic. This anisotropic expansion eventually produces plasma instabilities. Hydromagnetic waves are generated by these instabilities. Parker (1963) estimates that their scale size will extend up to $O(10^6)$ Km.

The expanding solar wind therefore carries a general Archimedean Spiral magnetic field upon which are superposed magnetic irregularities and hydromagnetic waves.

2.3.2. Parker's Diffusion-Convection Theory.

It is in the context of the above discussion that Parker (1963) formulated his theory. Magnetic irregularities and waves act as scattering centres which promote the diffusion of charged particles. The principle of the modulation in this model is the competition between the inward diffusion of cosmic rays through the interplanetary magnetic field and the outward convective removal by the solar wind.

The isotropic diffusion equation (2.17) is modified by the addition of a term representing the bulk transport of the solar wind :

$$\frac{dn}{dt} = \underline{V}\, n + \frac{1}{r^2} \frac{\partial}{\partial r} \left(K r^2 \frac{\partial n}{\partial r} \right) \qquad 2.22$$

Steady state conditions are assumed with the diffusion coefficient K and wind velocity $\underline{V}$ independent of radial distance to some value R. Integration of 2.22 gives the particle density at a radial distance r :

$$n(r) = n_{\infty} \times \exp - \int_{r}^{\infty} \frac{V}{K} \, dr \qquad 2.23$$

where n_{∞} is the galactic particle density. Allowing the mean free path to become infinite beyond the radial distance R, the density becomes:

$$n(r) = n_{\infty} \exp - \left[\frac{V\,(R-r)}{K} \right] \qquad 2.24$$

$$= n_{\infty} \exp - \left[\frac{3V\,(R-r)}{\lambda\omega} \right].$$

The mean free path λ between successive scatterings of cosmic rays is in general dependent on the rigidity of the particles and the distribution of scattering centres. In this treatment the centres are assumed to be isotropically distributed through the solar cavity. Parker (1958b) considered the diffusion to be via magnetic field line irregularities. This was done for the two extreme cases : where the gyro-radius in the scattering centre field is bigger than or smaller than the scale size of the centre.

a) 'Thin Centre'

If the scattering centre size ℓ is smaller than the gyroradius Rg there is small angle scattering through angle $\vartheta \simeq \ell/Rg$. Diffusion theory requires scattering through a large angle Θ for a single 'scatter'. This results after ν collisions where ν is given by :

$$\Theta = \nu^{\frac{1}{2}}\vartheta = \frac{\pi}{2} \quad \text{(say)} \qquad 2.25$$

$$\therefore \quad \nu = \left[\frac{\pi}{2\vartheta}\right]^2 \qquad 2.26$$

With the scattering centres closely packed, the mean free path λ is given by:

$$\lambda = \nu\ell = \left(\frac{\pi\, Rg}{2\ell}\right)^2 \ell \qquad 2.27$$

The magnetic rigidity P is related to the gyroradius Rg by:

$$P = 300\ B\ Rg \qquad 2.28$$

where B is the magnetic field.

The particle density becomes:

$$n(r) = n_\infty \exp -\left[\frac{3\ V\ (R-r)}{w} \times \left(\frac{600\ B}{\pi P}\right)^2 \ell\right] \qquad 2.29$$

In this rigidity range the modulation is strongly rigidity dependent, with the scattering mean free path $\lambda \propto P^2$.

b) 'Thick' centres.

A scattering centre of scale size $\ell \geqslant R$ produces large angle scattering. If the scattering centres are again closely packed, the mean free path $\lambda \simeq \ell$ and is independent of rigidity.

The density then becomes:

$$n(r) = n_{\infty} \exp - \left[\frac{3V\,(R-r)}{\omega \ell} \right] \qquad 2.30$$

This depends only on the velocity ω of the particle.

The effectiveness of 'thick' scattering centres depends upon the particle pitch angle. Particles at small pitch angles will follow the field lines through the scattering centre and will suffer no scattering. At larger pitch angles, the particles will be reflected from the scattering centre. Parker (1964), in considering the effectiveness of scattering centres, found that the greatest scattering efficiency occurs when the gyroradius is equal to the scale size of the centre. The efficiency decreases at other rigidities.

The diffusion-convection theory of Parker was modified by Dorman (1963) who introduced a hierachy of scattering centres to give a fit to the observational data. The scale size spectrum was limited so that between rigidities 1.5 GV and 60 GV some centres were smaller and some larger than the gyroradius. This produced a transition region between the low rigidity and high rigidity approximations. The mean free path would then be approximately proportional to rigidity. Below 1.5 GV Parker's 'thick' scattering centre approximation was considered to hold while above 60 GV the 'thin' centre approximation held.

In equation 2.24 the isotropic diffusion coefficient dependence

on velocity and rigidity was given by:

$$\begin{aligned} K &\propto \beta && P < 1.5 \text{ GV} \\ K &\propto \beta P && 1.5 \text{ GV} < P < 60 \text{ GV} \\ K &\propto P^2 \ (\beta \simeq 1) && P > 60 \text{ GV} \end{aligned} \qquad 2.31$$

2.3.2. Electric Field Modulation.

Under the conditions of a continuously flowing solar wind, the electric field model has been re-evaluated by Freier and Waddington (1965). The principal cause of the energy loss is through particle interactions with plasma streams carrying 'frozen-in' magnetic field lines. The energy loss for a particle of charge Ze is given by:

$$\Delta E = - Ze\ V \qquad 2.32$$

where V is the potential difference across the stream boundaries induced by the plasma motion. The modulation produced is therefore mathematically equivalent to the electric potential field modulation obtained without recourse to large static electric fields.

This electric field model was further developed by Nagashima et al (1966) who allowed a rigidity dependent sweeping of the cosmic rays. The energy loss arising from a decelerating potential V was given as:

$$E = \left(\frac{Ze}{A}\right) \times V \times \left(\frac{P_o}{P}\right)^{-\nu} \qquad 2.33$$

where $0 < \nu < 1$.

Defining Rp (P) as the ratio of the differential proton fluxes at times t and t' :

$$Rp\ (P) = \frac{J_p\ (P,t)}{J_p\ (P,t')} \qquad 2.34$$

and similarly for $R_\alpha(P)$; a sensitive test of modulation theory could then be made by experimentally determining the function $\overline{R\ (p)}$ where :

$$\overline{R\ (p)} = \frac{\log R_p\ (P)}{\log R\ \alpha\ (P)} \qquad 2.35$$

With the data available, Nagashima et al could not establish a preference for energy loss or diffusion-convection models.

2.4. EXPERIMENTAL OBSERVATIONS OF INTERPLANETARY CONDITIONS.

Plasma probe and magnetic field observations have been limited in spatial extent to a region near the Earth's orbit. Isolated observations in space are subject to both spatial and temporal variations which lead to uncertainties in interpretation. Complementing these measurements are the studies of solar protons and cosmic rays. The solar protons give information on the inner solar system conditions while the cosmic rays have been subjected to the integrated effects of conditions throughout interplanetary space.

2.4.1. Solar Plasma Velocity.

Plasma probes have established the continued outflow of solar plasma. The measurements of Snyder and Neugebauer (1964) and Bridge et al (1965) establish a quiet-time plasma velocity of ~ 330 $Kmsec^{-1}$. The plasma velocity is variable and Coon (1966) on the basis of Vela satellite electrostatic analyser measurements observed that there was better correlation of the Ap magnetic index with the rate of change of plasma velocity than with the velocity. This suggests that magnetic disturbances are due to transitional effects in the solar wind.

2.4.2. Cosmic Ray Density Gradient.

Early observations of cosmic rays in interplanetary space failed to establish the existence or otherwise of a radial gradient in the cosmic ray intensity (for example Fan et al (1960b)). The Mariner II ionisation chamber of Neher and Anderson (1964) established a gradient of 12 ± 4 %. The uncertainty in this measurement is due to the necessity of removing time variations from the data.

2.4.3. Interplanetary Magnetic Field.

Magnetic field measurements on the IMP 1 satellite out to 30 Earth radii by Ness and Wilcox (1965) established the general spiral form of the interplanetary field lines. The average magnitude of the field in the solar ecliptic plane was found to be 5γ with a direction $\sim 45^{\circ}$ to the Sun-Earth line; thus confirming the theoretical predictions of Parker (1958b).

Parker (1965) produced a synthetic magnetic field line from the IMP 1 magnetometer data. Field line kinks and waves were apparent. The kink separations were of the order of the gyroradius of protons of energy 2 GeV ~ 10 GeV. A harmonic analysis of the field fluctuations from Mariner 11 during late 1962 was given by Gloeckler and Jokipii (1966). The power (P_f) in the fluctuations of the field perpendicular to the wind velocity was found to be :

$$P_f = \frac{\delta}{f} \quad : \quad f \lesssim 5\ 10^{-4} \text{ c.p.s.}$$

$$\frac{\delta}{f^2} \quad : \quad f \gtrsim 5\ 10^{-4} \text{ c.p.s.} \qquad 2.36$$

A similar analysis of the Mariner IV measurements in late 1964 showed the same low frequency distribution. The limit of the f^{-1} variation was reduced to $\sim 10^{-4}$ c.p.s.

2.4.4. Solar Proton Events.

a) Arrival of Solar Protons.

Solar proton events are often characterized by a marked degree of anistropy in their arrival directions at the Earth. Those events in which the anisotropy is most marked are generally correlated with flares on the west limb of the Sun.

McCracken (1962) observed the anisotropic arrival of solar protons from a direction 45° to the west of the Sun-Earth line. This was consistent with their motion along the spiral magnetic field

lines from the Sun. The observed distribution of arrival directions was greater than would occur if the first adiabatic invariant were conserved in the magnetic field. McCracken concluded that scattering centres must be superposed on the spiral field lines. The effect of scattering centres is to partially remove the anisotropy.

Of four solar proton events analysed by Bryant et al (1965), two could be explained by a velocity dependent diffusion. The intensities of protons of a given energy between 1.4 MeV and 500 MeV were plotted against the time elapsed after the visible flare responsible for the event. In two of the events the intensity-time profiles could be normalised to a common curve. The most probable distance travelled by these particles was found to be ~10 A.u., showing that considerable scattering had occurred. At that time in the solar cycle and in this energy range, rigidity independent diffusion was established for the two events. Assuming isotropic diffusion, the scattering mean free paths lay in the range 0.04 - 0.06 A.u. $\left[\sim 10^{12} \text{ cm}\right]$.

Satellite measurements have observed the anisotropic arrival of solar protons following solar flares. Bartley et al. (1966) observed the field line streaming of 13 MeV protons. The field must have been relatively free of scattering centres of scale size $\sim 10^{10}$ cms to preserve the anisotropy.

b) Decay of Solar Proton Event.

The arrival and initial stages of the decay of solar protons are often consistent with isotropic diffusion in an infinite medium. The decay then proceeds as $t^{-3/2}$. In the later stages, the decay is

more rapid and can usually be represented by an exponential time function. This was originally explained by the ad hoc assumption of a boundary to the diffusing region beyond which the particles escaped.

A large number of events have been analysed by Webber (1964). The time dependence of the initial decay was best fitted by :

$$n(t) \propto t^{-\eta} : \frac{3}{2} < \eta < 2 \qquad 2.37$$

The mean position of the boundary was found to be 1 - 3 A.u. while in some events the boundary was within 1 A.u.

In many of these events the diffusion has been observed to be anisotropic at least in the inner solar system. Parker (1965) considered the anisotropic field line diffusion of solar protons. The diffusion coefficient K was allowed to be a function of the radial distance R :

$$K \propto r^{s} \qquad 2.38$$

The density of solar protons was found to decay as

$$n(t) \propto \frac{1}{t^{3/(4-s)}} \qquad 2.39$$

The observed initial decay rates therefore require $2.0 < S < 2.5$ i.e. the diffusion must increase rapidly with distance.

A number of mechanisms exist which can contribute to the decay without recourse to a boundary layer.

Convective removal by scattering centres in the solar wind results in a reduction of the intensity. For a spherically symmetric wind and a diffusion coefficient K independent of radial distance, Parker (1965) calculated a reduction of intensity of a factor 2 with $\frac{RV}{K} \sim 1$. The effect of particle deceleration in the solar wind due to adiabatic deceleration and the Inverse Fermi effect have been treated by Quenby (1964). This contribution to the decay can be large but its magnitude depends greatly on the mode of propagation of the solar protons. Energy loss alone cannot explain the very rapid decrease observed during some solar proton events. An increase of diffusion with radial distance is therefore required but probably not as great as that estimated by Parker (1965).

2.4.5. Modulation of Protons and Alpha Particles.

The results from individual experiments have often been conflicting. A number of attempts have been made to combine the experimental information obtained in particular periods in order to define the velocity and rigidity dependence of the modulation. The most noteable of these have been by Silberberg (1966) and Quenby (1966b).

Silberberg has analysed balloon data from the years 1959, 1961 and 1963.

a) 1959/1963

The modulation over this period could be represented by either of two dependences of the diffusion coefficient K :

$$K \propto \beta P \qquad 2.40$$

$$\text{or} \quad K \propto P$$

The 1959 alpha particle data extended down only to 1.2 GV so that the data was not extensive enough to show a velocity dependence.

b) 1961/1963.

During this period the modulation was fitted by the following dependence of the diffusion coefficient :

$$K \alpha \beta P \quad : \quad P > 1.2 \text{ GV} \qquad 2.41$$

$$K \alpha \beta \quad : \quad P < 1.2 \text{ GV}$$

The accuracy of this result was rather limited and applied to the available proton, alpha overlap region above 0.8 GV.

Figure (2.4.1) from Nagashima et al (1965) gives the variation of $\overline{R(p)}$ (sub-section 2.3.2) with rigidity P for the electric field and solar wind modulation mechanisms. The bounded regions arise because of the uncertain rigidity dependence of the modulation in equation (2.33) together with the uncertain spectrum in local interstellar space.

Representing the local interstellar spectrum by :

$$J_\infty(E) \quad \alpha \quad E^{-\delta} \qquad 2.42$$

the predicted $\overline{R(p)}$ is given for 3 cases :

a) $\delta_p = \delta_\alpha = \delta$; $2 < \delta < 2.45$; $0 < v < 1$; Band A

b) $\delta_p = 2.0$; $\delta_\alpha = 2.45$; $0 < v < 1$; Band B

c) $\delta_\alpha = 2.0$; $\delta_p = 2.45$; $0 < v < 1$; Band C

Also included in the figure are the experimental data from 1963 and 1965 given by Quenby (1966b). These data indicate a clear preference for the solar wind modulation theory.

In the low rigidity region, all modulation models based on diffusion convection theory produce a modulation of the form :

$$\ell n \left[\frac{n_e}{n_\infty}\right] = -\text{const.} \left[\frac{1}{\lambda\beta}\right]$$

This can be written :

$$\log_{10} \frac{J(t_1)}{J(t_2)} = \frac{\text{const}}{\lambda\beta} \qquad 2.43$$

Measurements of the differential rigidity spectrum $J(t)$ at two times t_1 and t_2 in the solar cycle will then give the rigidity dependence of the scattering mean free path λ. The observed modulations for protons and alphas for 1963/1965 were fitted by the functions :

$$\log_{10} \frac{J(65)}{J(63)} = \frac{0.0856}{\beta} \quad ; \quad P < 1\text{GV}$$

$$= \frac{0.0856}{\beta P} \quad ; \quad P > 1\text{GV} \qquad 2.44$$

In the rigidity range above 1 GV a P^{-2} dependence of the modulation was not ruled out because of the data accuracy and the limited rigidity range 1 GV - 4 GV. A similar analysis for the years 1956 and 1959 with rather limited data indicated that a rigidity-independent form of modulation as in 2.43 could not explain the modulation.

In the latitude sensitive region Quenby calculated the modulation at solar maximum from the latitude surveys of Sandström et al (1963) and Rose et al (1954). This was found to be in agreement with that obtained by Kodama and Matthews. The data were not sufficiently accurate to distinguish between a modulation of the form 2.43 with $\lambda \propto P$ or $\lambda \propto P^2$. When these data were combined with the alpha particle data from 1957-1958 and the following solar minimum 1965, the rigidity dependence of the modulation favoured $\lambda \propto P$.

2.4.6. Summary.

a) A continuous flowing solar wind exists, dragging out the solar field lines into a spiral form. The quiet-time plasma velocity and magnetic field strength are ~ 330 km sec^{-1} and 5γ respectively.

b) Superposed on the spiral field lines are kinks and waves which lead to charged particle diffusion.

c) Convective modulation in the solar wind is in better agreement with the observed cosmic ray intensity modulation than the electric field model.

d) The diffusion coefficient for cosmic rays is probably purely velocity dependent for rigidities $\lesssim$ 1 GV near to solar minimum.

e) In the latitude sensitive region 1 GV $< P <$ 15 GV, the data suggest that the diffusion coefficient $K \propto \beta P$ at solar max. although the observations are sparse and of limited accuracy.

f) The diffusion of charged particles in the inner solar system is highly anisotropic with field line diffusion exceeding cross field line diffusion i.e. $K_{\parallel} > K_{\perp}$.

g) The observed decay of particle intensities following a solar proton event requires a combination of increase of diffusion with radial distance (i.e. $K \propto r^s$ with $s > 1$), and outward convection and energy loss in the expanding solar wind.

2.5. MODULATION INVOLVING ANISOTROPIC DIFFUSION.

Observations in local interplanetary space have established anisotropic diffusion of charged particles along the field lines. In other words the cyclotron frequencies of the particles are greater than the collision frequencies. Near the boundary of the solar wind where its velocity becomes subsonic, the shock waves set up will produce highly tangled magnetic field lines. Here the diffusion will be isotropic with scattering frequencies much larger than cyclotron frequencies. Between these two limiting regions of interplanetary space the diffusion will be intermediate between isotropic and anisotropic field line diffusion. Cosmic ray modulation occurs mainly beyond the Earth's orbit, while the parameters available to a theory of cosmic ray modulation apply only to the inner solar system. The early theories considered the simpler case of isotropic diffusion while the more recent theories have considered the diffusion to be primarily along the field lines.

Parker (1965a) solved the equations of motion of the anisotropic diffusion of particles in a spiral magnetic field for the case with motion being entirely restricted to the field lines. The motion was therefore independent of the density of particles on other neighbouring lines. Parker showed that the effect of field line diffusion was analagous to

isotropic diffusion with a diffusion coefficient increasing with radial distance.

An alternative treatment of anisotropic diffusion has been given by Axford (1965). This involved the solution of the Boltzmann equation. The interstellar cosmic rays were treated as a gas diffusing into a region containing a second 'gas', the 'particles' of which were the magnetic field irregularities. Assuming that the mean free path was proportional to the radial distance a large modulation resulted with the interstellar boundary at 30 A.u. The energy density of the cosmic rays in interstellar space was then required to be of similar magnitude to the energy density of the local interstellar magnetic field.

A relativistic solution of Axford's treatment has been given by Quenby (1966a). The diffusion coefficient K_{ij} was found to be :

$$k_{ij} = \frac{1}{3} \beta c \lambda \begin{vmatrix} 1 & 0 & 0 \\ 0 & \frac{\nu^2}{\omega^2+\nu^2} & -\frac{\omega\nu}{\omega^2+\nu^2} \\ 0 & \frac{\omega\nu}{\omega^2+\nu^2} & \frac{\nu^2}{\omega^2+\nu^2} \end{vmatrix} \qquad 2.45$$

where the Larmor angular velocity has been modified by the Lorentz factor :

$$\omega = \frac{eB}{\gamma mc} \qquad 2.46$$

and ν is the collision frequency.

The diffusion equation has been solved for two radial distributions of the mean free path : $\lambda \propto r$ and $\lambda \propto r^2$.

(i) $\lambda \propto r$ (Quenby 1966a) Beyond the Earth's orbit the field is mainly azimuthal. The separation of scattering centres in the form of convected kinks in the field lines will be proportional to the radial distance.

The density of a group of particles n_e in a given energy or rigidity range at the earth is given by :

$$\frac{n_e}{n_\infty} = \left[\frac{\Omega^2 r_e^2 + \omega_e^2 \tau_e^2 V^2}{\Omega^2 r_s^2 + \omega_e^2 \tau_e^2 V^2} \right]^{(1+\omega_e^2 \tau_e^2)\ \frac{\tau_e V}{K_e}} \qquad 2.47$$

where V is the solar wind velocity, Ω the angular velocity of the Sun, ω_e the Larmor frequency of the particles at the Earth, τ_e is the collision period, and n_∞ the particle density at infinity, $K_e = \frac{1}{3} \beta^2 C^2 \tau_e$, r_s is the boundary of the modulating region, r_e the Earth's radial distance from the Sun.

(ii) $\lambda \propto r^2$ (Quenby 1966 b) . This is a form of mean free path distribution which results in less modulation than the $\lambda \propto r$ case. If kinks are the principal scattering centres, this represents a reduction of their effectiveness with distance convectøed.

The reduction in density is given by :

$$\frac{n_e}{n_\infty} = \exp\left[\int - \left(\frac{C}{1+B} \right) \left[\frac{1}{r_e} - \frac{1}{r_s} + A\ (r_s - r_e) \right] \right] \qquad 2.48$$

where $A = \frac{(\omega_e \tau_e)^2}{r_e^2}$, $B = \frac{(\omega_e \tau_e)^2 V^2}{\Omega^2 r_e^2}$

and

$$C = \frac{3V r_e^2}{\beta^2 c^2 \tau_e^2}$$

Applying numerical values to these cases, the best fit to the experimental data with $\lambda \propto r$ was obtained with $r_s \sim 12$ A.u. at solar minimum, ~6 A.u. at solar maximum and a scattering centre mean free path $\lambda \simeq 10^{12}$ cms. Larger values of r_s produced too much modulation so that n_∞ would be larger than is generally thought possible. For the second case with $\lambda = 10^{12} \times P$cm, $r_s = 50$ A.u; then $\frac{n_e}{n_\infty} = 5\%$, a value consistent with that expected.

With $\lambda \propto r$ and the boundary of the modulating region ~ 6-12 A.u. then the modulation is velocity dependent because of the rigidity independence of the scattering mean free path. This is contrary to the experimental observations which indicate a rigidity dependence for rigidities above ~1 GV at solar minimum.

For $\lambda \propto r^2$, the modulation produced with the boundary of the modulating region coincident with the boundary of the interstellar medium, is in agreement with the anticipated modulation.

Using the more realistic mean free path $\lambda \propto r$ or $\lambda \propto r^2$ in the isotropic diffusion equation 2.23, Quenby found that the resulting modulation was insufficient to explain the observed variations at the Earth.

Anisotropic diffusion through waves in the interplanetary magnetic field has been calculated by Gloeckler and Jokipii (1966). In this calculation, the diffusion coefficient along the lines of force K_{11} is related to the observed Fourier spectrum of magnetic field irregularities (Section 2.4.2). Scattering of particles whose cyclotron radius is r_c in the average magnetic field is determined by the power in the field component fluctuations perpendicular to the wind velocity at frequencies :

$$f = \frac{V}{2\pi r_c} \qquad 2.49$$

For the measured power spectrum at frequencies $\lesssim 10^{-4}$ c.p.s. where $P(f) \simeq \frac{\delta}{f}$, the diffusion coefficient parallel to the field lines K_{11} was given by :

$$K_{11} \simeq \left(\frac{c\, B_o}{3\pi\delta} \right) \times P\beta \qquad 2.50$$

If the conditions producing this form of modulation were to persist out to appreciable distances from the Sun then the modulation produced in the cosmic ray intensity would be :

$$J_e(P) \simeq J_\infty(P) \times \exp(-\delta/P\beta) \,. \qquad 2.51$$

This form of the modulation is qualitatively in agreement with experiment in the latitude - sensitive region of the primary spectrum. Near solar minimum the change in the power spectrum at $\sim 10^{-4}$ c.p.s. to $\sim \frac{\delta}{f^2}$ produces pure velocity dependent diffusion for rigidities $\lesssim 1$ GV.

2.6. RELATIVE IMPORTANCE OF ENERGY LOSS AND DIFFUSION-CONVECTION.

Energy loss mechanisms are due to the Betatron deceleration in the expanding interplanetary field and the inverse Fermi effect due to the mutual separation of scattering centres.

The Betatron effect was given by Quenby (1966a) as :

$$\frac{\delta P}{P} = - \frac{V\,dt}{r} \qquad 2.52$$

with V the solar wind velocity and r the radial distance.

The inverse Fermi effect on the cosmic rays random walking in the expanding solar wind scattering centres was given by Laster et al (1963) as :

$$\frac{\delta P}{P} = - \frac{4}{3} V \frac{dt}{r} \qquad 2.53$$

For a power law primary spectrum $J(p)$ given by :

$$J(P) = P^{-\gamma} \qquad 2.54$$

$$\frac{\Delta J(P)}{J(P)} = -\gamma \frac{\delta P}{P} \qquad 2.55$$

The total flux change is therefore

$$\frac{\Delta J}{J} \propto - \int \frac{V\,dt}{r} \qquad 2.56$$

Quenby (1966 b) has suggested that the right hand side of equation 2.56 $\propto \frac{1}{\beta \lambda}$.

The modulation produced by the energy loss is then :

$$\mathrm{Ln}\left[\frac{J_e}{J_\infty}\right] \propto \frac{1}{\beta P} \qquad 2.56$$

Parker (1965b) has calculated the combined solar modulation effects of convection and energy loss for two cases where the diffusion is isotropic and the diffusion constant is not a function of radial distance:

a) Large moductions acting on the interstellar cosmic ray spectrum in kinetic energy per nucleon and an energy independent diffusion coefficient K.

b) Small modulations with $K \propto T^s$, where T is the kinetic energy, and a primary spectrum of arbitrary shape.

Both Parker (1965b) and Quenby (1966b) have shown that the magnitude of the modulation produced by energy loss is comparable to that produced by convection. In the rigidity range <1 GV where the primary spectrum decreases towards lower rigidities, an energy loss dominance in the modulation would produce an increase in the differential counting rate. Such an increase with increasing solar activity has not been observed. The energy loss contribution to the modulation in this rigidity range must therefore be less than that due to convection.

Quenby has shown that all the energy loss models have a similar dependence on the diffusion coefficient which to the first approximation is the same as that given by equation 2.43 for the diffusion-convection models. It is therefore not possible to distinguish easily between the convection and energy loss mechanisms in the solar wind.

2.7. DISCUSSION

With realistic radial variations of the scattering mean free path rather than a constant value right out to the interstellar boundary, the modulation predicted by isotropic diffusion is too small. Anisotropic diffusion along the field lines must be invoked to lengthen the diffusing paths and so increase the modulation. Models with diffusion taking place entirely along the field lines are probably good approximations only in the inner solar system. Solar proton events for which this approximation holds require the diffusion to increase with radial distance to explain the observed decay rates. Energy loss in the solar wind is an important contribution to the modulation but at low rigidities at least it is smaller than the contribution from convection. The gross features of the modulation can be explained by anisotropic diffusion with the mean free path increasing as $\lambda \propto r^2$. The dependence of the mean free path on the rigidity of the incoming particles in the latitude sensitive region is not established with certainty. At solar minimum the mean free path is probably rigidity independent for rigidities $\lesssim$ 1.0 GV. The modulation is probably due to diffusion through magnetic field line kinks as well as through waves in the field lines.

CHAPTER 3. THE COSMIC RAY RECORDER.

3.1 RECORDER DESIGN REQUIREMENTS.

3.1.1. Introduction to Design Requirements.

The recorder, designed, constructed and environmentally tested by A. Bewick, will be described to bring out its salient features.

The principal factors determining the choice of the aircraft detector were the requirements of compactness coupled with maximum response to the secondary particle population at the flight altitude. The large intensity variations which occur at low magnetic rigidities make it desirable to extend the measurements to the lowest possible rigidity. The air above the detector acts as an absorber in which the cosmic ray energy is degraded through interactions with atmospheric atoms. The absorbed energy takes the form of atmospheric heating, electromagnetic radiation and the production of secondary particles. At low rigidities the primary particle energy becomes completely degraded at small atmospheric depths : the lower the rigidity the smaller the atmospheric depth to which the primary particle effects can be measured. The low rigidity limit of observation is thus dependent on the operational ceiling of the aircraft available. A Canberra jet bomber was to be used for which a suitable target altitude close to its operational ceiling was 45,000 ft. (atmospheric depth of 145 g cm^{-2}).

The geometric factor of the detector should be such that enough counts can be accummulated in a short time interval. While air-borne, the detector integrates the cosmic ray intensity over about 8' arc for each

minute of the basic counting interval. A short counting interval will reduce the uncertainty in the cut-off applicable to a particular count.

3.1.2. Relative Intensities of Particles at 145 g cm^{-2}.

The Pfotzer maximum of the secondary particle altitude distribution is located near an atmospheric depth of 145 g cm^{-2}, and is latitude dependent. In this region particle production, absorption and decay are equally important in determining the particle population. A small number of primary protons (attenuation length = 120 g cm^{-2}) reach this depth. Heavier primary particles with much larger interaction cross-sections are reduced in intensity to correspondingly negligible proportions. The kinetic energy per nucleon being much larger than the nucleon binding energy, the heavy nuclei probably separate into individual nucleons at their first interaction with an atmospheric atom. $\mu^{\pm}$mesons are predominantly the decay products of $\pi^{\pm}$ mesons [2.6×10^{-8} secs half-life] with a smaller contribution from $K^{\pm}$ meson decay [1.2×10^{-8}secs]. The major constituents in the upper atmosphere (50 g cm^{-2} - 600 g cm^{-2}) are the electron and photon components. Most are included in the non-equilibrium cascade component which originates in the decay of the short lived π^{o} mesons [1.9×10^{-16} secs] . There are also the equilibrium contributions from ionising collisions, bremmstrahlung and μ meson decay [2.2×10^{-6} secs]. Small numbers of secondary protons and neutrons, the products of nuclear collisions, are also present.

The approximate relative omnidirectional intensities at 150 g cm^{-2} are given in Table (3.1).

TABLE 3.1.

RELATIVE OMBIDIRECTIONAL INTENSITIES AT 150 g cm^{-2}.

Particle	Relative Intensity	Energy
Photon	460	
Electron	230	10 MeV
Fast μ's	60	220 MeV
Fast p's	50	$\geqslant$ 3 BeV
Slow p's	25	$0.4 \leqslant E \leqslant 3$ Bev
Fast n's	20	$\geqslant 3$ BeV
Slow μ's	17	$0.27 \leqslant E \leqslant 220$ MeV
Heavies	1.5	

The figures may be obtained from Puppi (1956).

At a given atmospheric depth, the intensities depend upon the cut-off rigidity and the incident primary spectrum. To a lesser degree the density structure of the overlying atmosphere determined by the temperature profile will influence the intensities. The temperature effect is discussed in sub-section (4.4.9).

3.1.3. Type of Detector.

The choice of detector lay between a neutron monitor and a charged particle detector. The surveys were to be carried out at a constant pressure altitude and consequently at a fixed depth within the atmosphere. The intensity would not therefore be subject to variations

due to the amount of mass above the level of measurement. The remaining atmospheric effect is due to redistributions of mass caused by variations in temperature. The number of neutrons produced in nuclear interactions depends essentially on the mass of air and not upon its distribution. A neutron monitor therefore has the advantage of being practically independent of variations of atmospheric origin when flown at a constant pressure altitude. An additional advantage of the neutron monitor is its greater sensitivity to low energy primary particles than a detector responding to charged particles or photons. Against these advantages are the following disadvantages :

a) The small nucleon flux coupled with the insensitivity of the counter requires a large counter for good statistics. The consequent large mass of lead is incompatible with the objective of high altitude surveys.

b) The omnidirectional sensitivity of the neutron monitor adds complications to the study of cut-off rigidity through integrating the secondary particle contributions from the whole sky. This effect becomes increasingly important at high altitudes where the off-vertical contribution is much enhanced. Difficulty is then introduced in ascribing a cut-off rigidity to an intensity measurement.

c) The omnidirectional nature of the detector leads to the possibility of contamination of the counting rates through the moderation of neutrons in the hydrogenous aviation fuel.

A charged particle detector was chosen and of the various types it was decided upon a scintillation telescope.

3.2. DESCRIPTION OF THE RECORDER.

3.2.1. General Features.

The detector consisted of two scintillator elements viewed in coincidence by two photomultiplier tubes. Each scintillator was a circular disc of plastic NE102 supplied by Nuclear Enterprises Ltd. The response of this phosphor is about 60% that of **anthracene**, with a decay constant of 3.5×10^{-9} sec. Both scintillators were coated with a diffuse white paint to aid uniformity of response. The photomultiplier tubes, manufactured by E.M.I., were 5" tubes of type 9530 with a photo-efficiency of 87 μA/lumen.

The geometry of the detector was designed to obtain the maximum counting rate while retaining compactness of the overall dimensions. A block diagram of the detector is given in figure (3.2.1). Each scintillator was 1" thick and 2' in diameter with a separation of 2'. The geometric factor for the telescope was 1575 cm^2 ster. The photomultipliers were held firmly in optical contact with the scintillators. A basic counting interval of 4 minutes was chosen during which the position of the detector when air-borne would move through ~ 32' arc.

Passage of a charged particle through the scintillators produced an electrical pulse in both photomultiplier head units. These pulses, having amplitudes greater than the threshold level of the discriminators, triggered an output from the coincidence unit. Coincidence pulses were

Block Diagram of Scintillation Telescope

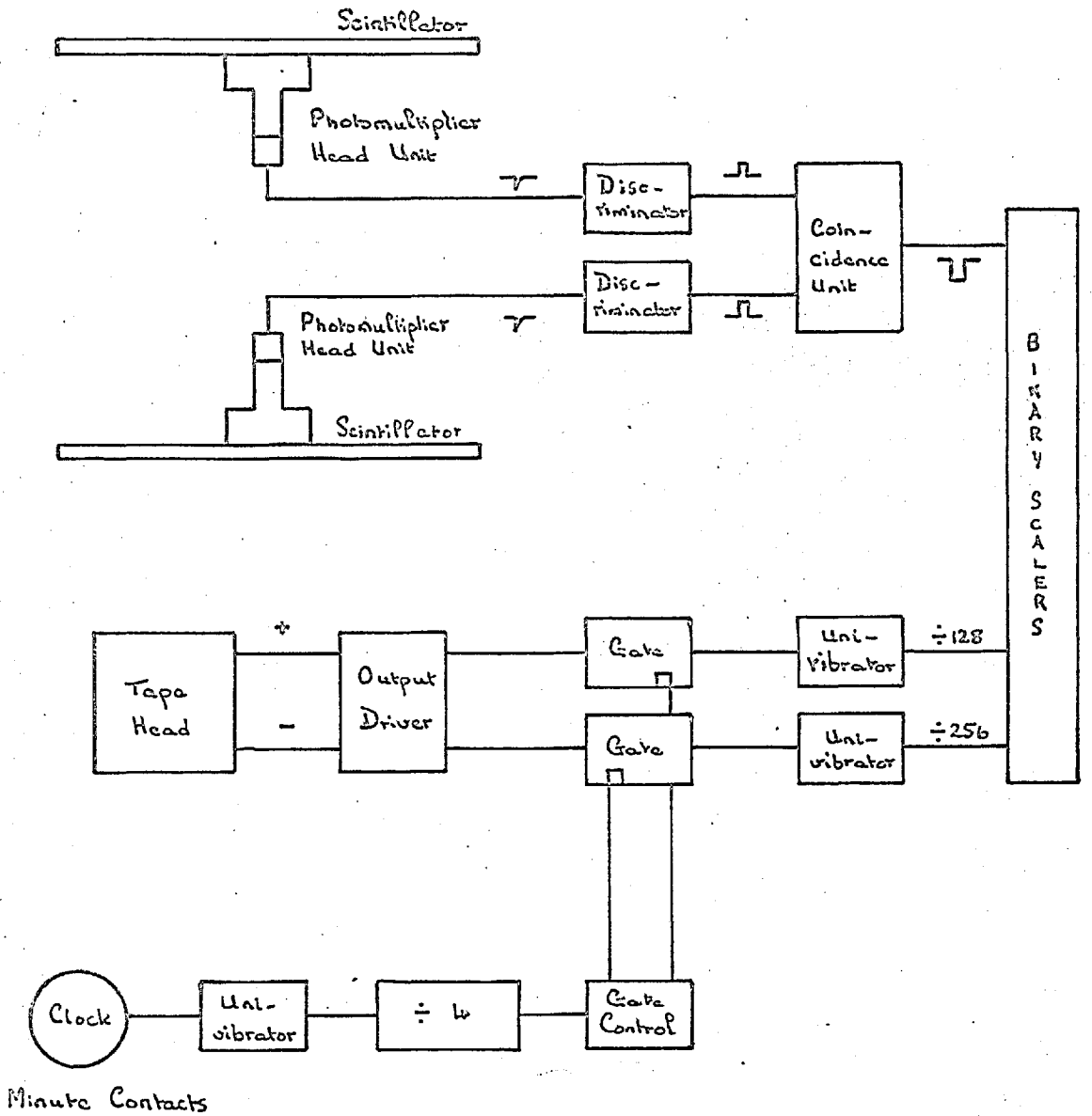


Fig. 3-2.I

scaled by a factor of 128 or 256 depending upon the state of a binary gate control whose polarity was reversed every 4 minutes. The scaled coincidence pulses triggered an output circuit into driving 0.5 m sec pulses to the recording head of a magnetic tape recorder. The polarity of the output pulses depended upon the scaling factor introduced : either 'positive' pulses scaled by 128 or 'negative' pulses scaled by 256 were recorded. A slow speed tape drive of 0.4"/sec ensured adequate storage capacity for the complete survey data.

The stored 'positive' and 'negative' pulses were separated by a playback amplifier sensitive to the polarity of the tape output. Pulses were routed to one of two pulse counters depending upon their polarity.

3.2.2. Electronic Circuitry.

The circuitry was fully transistorised and was powered by a stabilized 9 volt supply. The total current required for the electronics and tape drive of 90 milliamps was provided by Ever Ready Bell 126 batteries.

a) E.H.T. Supply

The 1560 volt E.H.T. supply to the photomultiplier tubes was originally provided by a 2,400 volt battery which fed into a 1600 volt corona discharge tube. The supply was changed in 1963 between surveys 6 and 7 to a D.C./D.C. converter. The peak to peak ripple on the converter output was 0.05 volts. The E.H.T. battery was not removed from its housing in the recorder as it was positioned in the opening

angle of the telescope and its removal would have resulted in a change of sensitivity.

b) Head Unit.

The pulses from the photo-multiplier were negative with a length of about 1 μ sec. These were fed by means of an emitter follower along coaxial cable to the discriminator unit. The voltage divider and emitter follower were potted into the head unit by means of Glocel, forming a cellular structure of expanded polyurethane. This low density structure has good thermal insulation properties and so protects the sensitive head units from thermal changes.

c) Discriminator Unit.

The level of the pulse height discriminator was adjusted to eliminate part of the background noise from the photomultiplier proffered to the coincidence unit. The operating characteristics of the telescope were chosen to minimise the effect of a drift in discrimination level. The discrimination level was set at 140 mV, the output being positive with an amplitude of 0.4 V and a length of 0.1 μsec. These pulses were square-formed to give a well-defined resolving time in the coincidence circuit.

d) Coincidence Unit.

The coincidence resolving time was about 10^{-7} sec. Coincident input signals triggered negative square-formed output pulses of 3.5V amplitude and 0.7 μsec length.

3.2.3. Overall Characteristics.

The variation of singles rates and coincidences with E.H.T. voltage in the laboratory are plotted in figure (3.2.2.). The counting rate coincidence plateau is due mainly to sea level minimum ionising μ mesons. The plateau slope is 5.5 % per 100 volts.

Each circuit board was potted in Silastomer synthetic rubber for mechanical, thermal and electrical reliability. Heavy thermal insulation was provided by plastic foam which produced a thermal time constant of about one day. The telescope was enclosed in a metal box, providing a screen against external fields. The overall dimensions of the recorder were 62.5 x 62.5 x 69 cm^3, and the weight was 71 K gm.

High latitude Counting rate at 45,000 ft: 30,000/min .

Counting rate at sea level: 900/min .

3.3. ENVIRONMENTAL TESTS.

The positioning of the detector in the fuselage of the Canberra meant that it was subjected to the ambient temperatures at altitudes. The temperature at 45,000 ft. is generally - 50°C to - 60°C. Bench testing of the recorder showed the counting rate to increase with temperature: 0.4 % per 10°C. This was done by observing the change of counting rate of γ rays from a radioactive source as a function of the temperature. The increased slope of the coincidences counting rate plateau for γ rays as compared to charged particles amplified the changes of sensitivity of the detector.

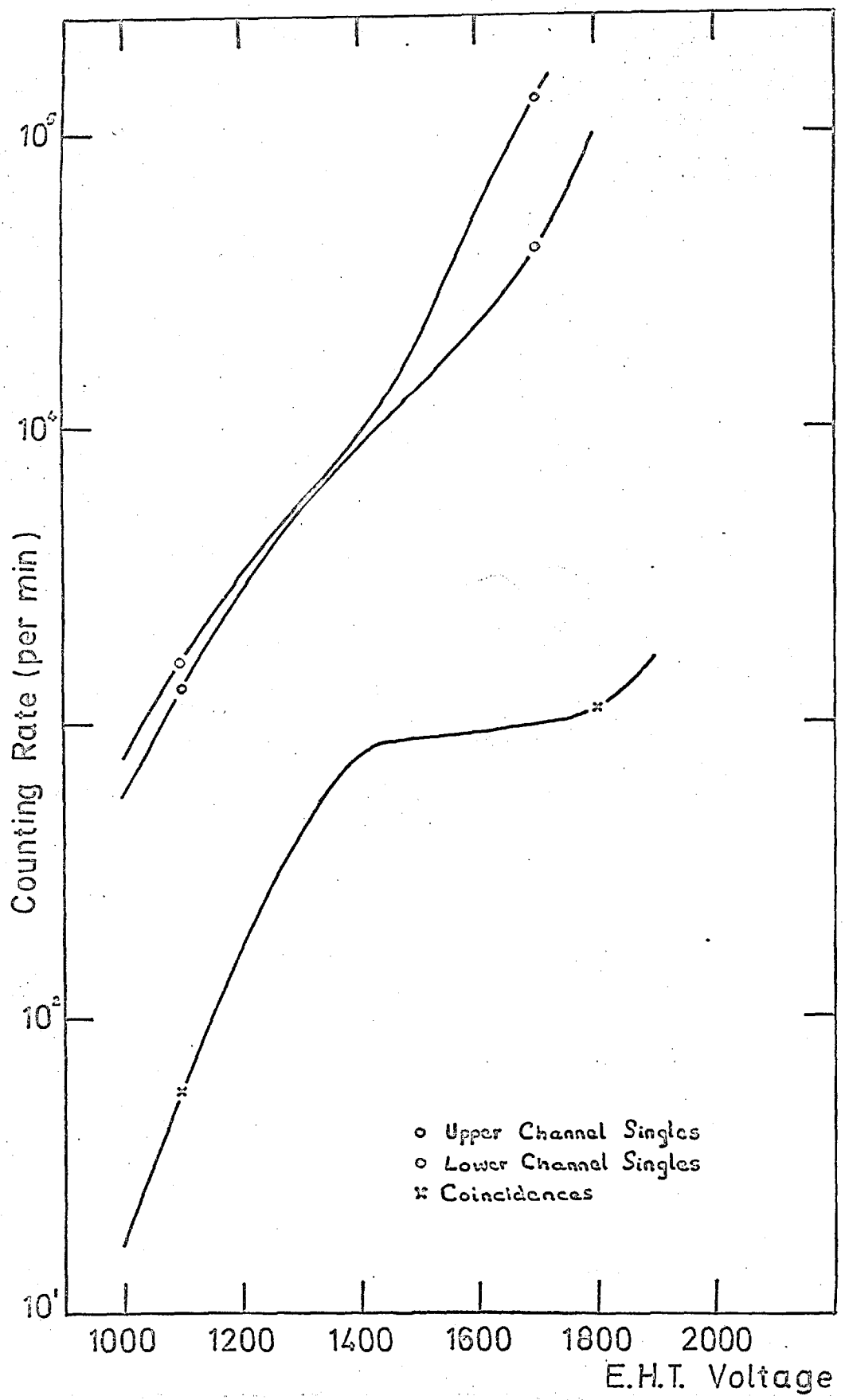


Fig. 3-2.2 The variation of singles and coincidence counting rates with E.H.T. voltage.

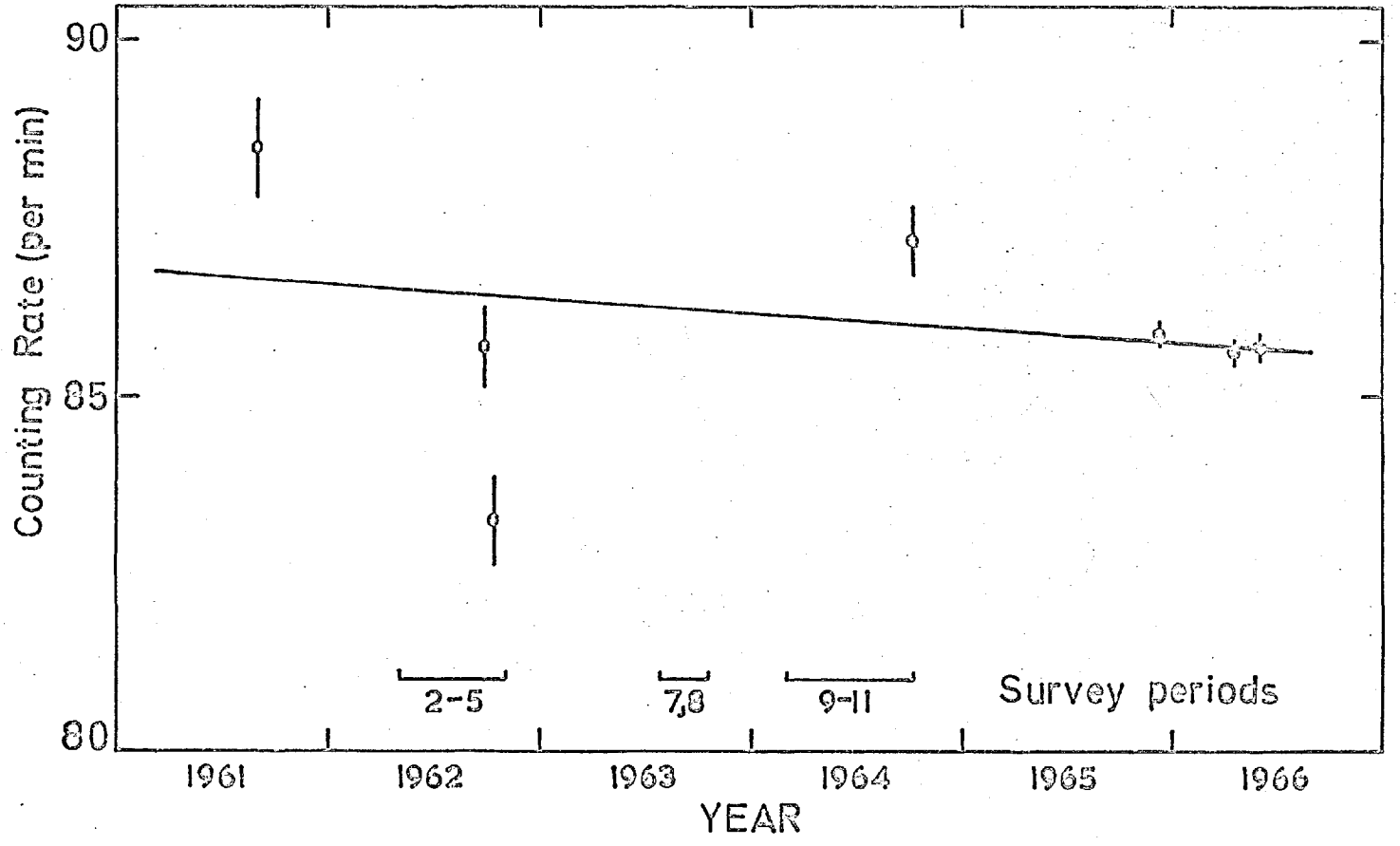


Fig. 3-4.1 Counting rate of the cosmic ray recorder at an underground depth of 60 metres water equivalent during the period 1961 - 1966.

During a test flight the counting rate plateau slope was monitored. This was done by observing the coincidence outputs produced by scintillator outputs of between ~ 90 mV and ~140 mV. This provided a measure of the slope of the coincidence plateau at altitude. The slope as measured was similar to that at sea level. The observed sensitivity change in the laboratory will therefore be representative of the temperature effects at altitude.

3.4. LONG TERM STABILITY.

The overall system has been checked at regular intervals by monitoring the counting rate of cosmic rays at a depth underground of 60 metres water equivalent in Holborn underground station. The secondary particles at this depth have their origin in primary cosmic rays of several hundred GeV. Solar cycle modulation of these energies and fluctuations of atmospheric origin are small. The greatest intensity variations at this depth are due to the very occasional large Forbush decrease. One such event recorded by Mathews (1963) at Holborn depressed the cosmic ray intensity by 0.5 %. The cosmic ray flux at this depth thus provides a check on the entire recorder sensitivity: optics, e.h.t. supply, pre-amplifier gain, discrimination levels and coincidence resolving time. The pressure coefficient, - 0.037% per millibar, used to correct the data is that obtained for scintillation telescopes in Holborn by Dutt and Thambyahpillai (1965).

Measurement of the plateau slope underground revealed that it was a factor 10 times that at ground level and consequently 10 times that at

altitude. This is due to the high proportion of counts produced by the natural background ratio-activity. Changes in sensitivity are therefore amplified by a factor ~ 10.

The calibration data are plotted against time in figure 3.4.1. together with the times of the aircraft surveys. A least squares fit gives a slope of - 0.02 % per year. The error bars are the r.m.s. counting rates. The data are not inconsistent with a gain change in the range - 2% to + 1.5% over the 5 year period from 1961 to 1966. Between the years 1962 and 1964 during which surveys 1 - 11 were made the gain change was probably within - 0.8% to + 0.6%. The maximum fluctuation from the mean curve is 3.8%.

The sensitivity changes at altitude must therefore be small. The long term drift is ~ 0.04 % per year with a possible short term change ~ 0.4 %.

CHAPTER 4. REDUCTION AND ANALYSIS OF EXPERIMENTAL DATA.

The series of aircraft surveys has been carried out in a Canberra jet bomber of the Royal Aircraft Establishment, Farnborough. The detector was secured by brackets in the rear of the fuselage just aft of the camera hatch. This position was well removed from fuel tanks and the possible influence of the fuel levels on the recorded intensities.

4.1. Survey Routes and Times.

A total of 12 latitudes surveys have been made between 1962 and 1965. Whenever possible the aircraft has followed the same route. At the same Störmer threshold there can be considerable variations in the complexity of the penumbral region at different locations. Consequently the penumbral contribution to the effective threshold will vary. By following the same flight path it is possible to remove a contribution from the cut-off uncertainties in the study of time variations. The routes followed during the surveys are plotted in figure 4.1.1. and detailed in Table 4.1. together with the times of the surveys. Apart from survey 1 which followed path 6 via 60°N and Wildenrath to Idris, each survey followed a common course, path 2, to Idris. From Idris, all surveys with the exceptions of surveys 6 and 8 followed path 4 to Kano. Surveys 6 and 8 were extended surveys following path 7 to 38° South. The routes north of Farnborough show the greatest variability, but this is probably of little consequence. Penumbral corrections to the cut-off rigidities in this region are small and any

---

Footnote.

Cut-offs referred to in this chapter are due to Shea et al.

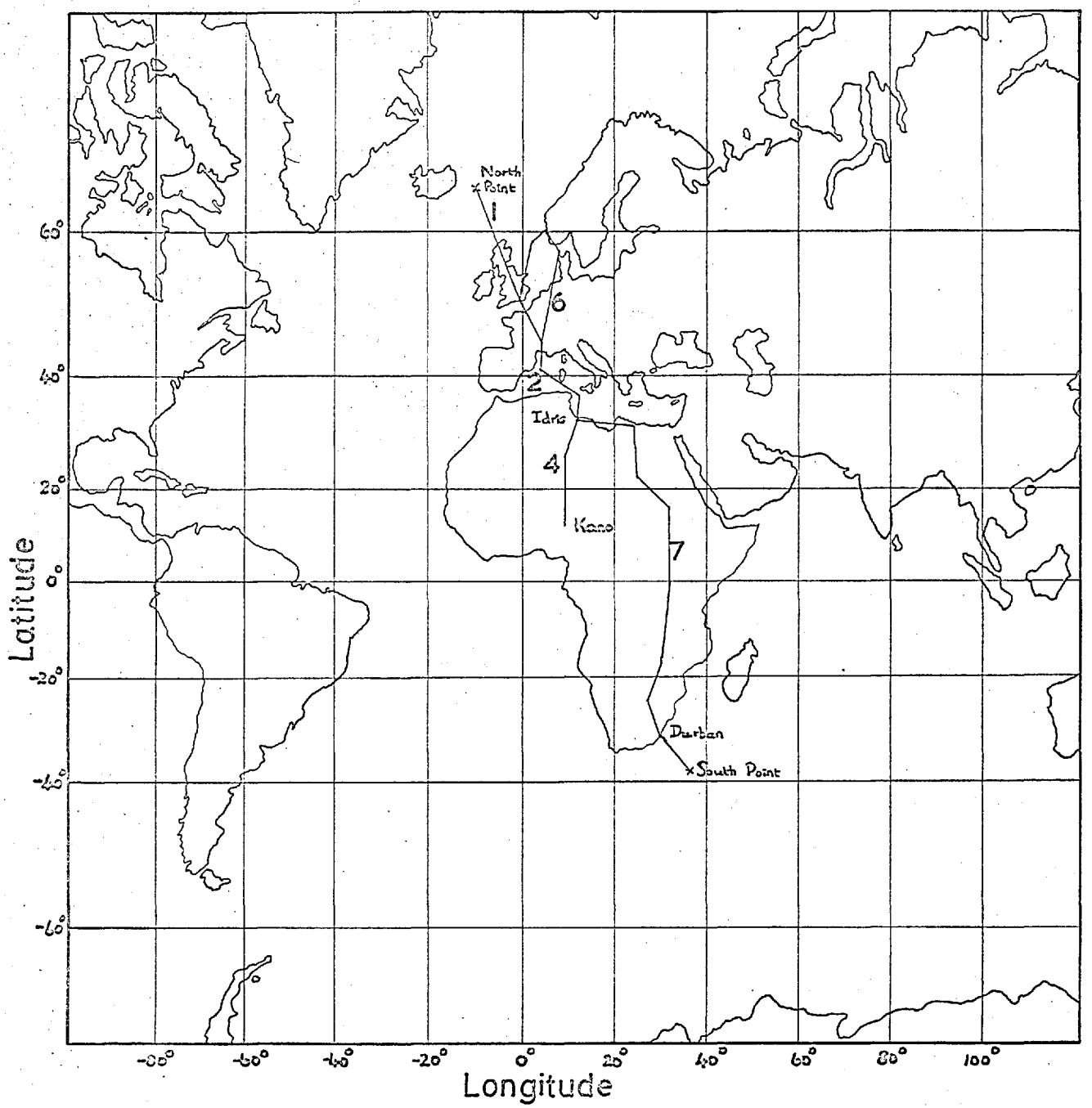


Fig. 4-1.1 Survey routes.

TABLE 4.1

SURVEY ROUTES

SURVEY		PATH						
No.	Period of Survey	1	2	3	4	5	6	7
1	26/2/62 – 5/3/62				x		x	
2	2/5/62 – 11/5/62	x	x		x	x		
3	3/7/62 – 8/11/62	x	x		x	x		
4	9/10/62 – 11/10/62	x	x					
5	1/11/62 – 6/11/62	x	x		x			
6	1/3/63 – 18/3/63	x	x					x
7	23/7/63 – 8/8/63	x	a					
8	7/10/63 – 18/10/63	x	x					x
9	2/3/64 – 6/3/64	b	x		x			
10	3/6/64 – 8/6/64	c	x	x				
11	2/10/64 – 5/10/64	x	x		x			
12	23/12/65- 23/12/65	a						

Key

Path		Route
1	x	Farnborough to North Point: 65°N 10°W
	a	: 65°N 6°W
	b	: 59°N 1°W
	c	: 60°N 4°50'W
2	x	Farnborough to: Idris
	a	: Malta
3	x	Idris to 25°N to Idris
4	x	Idris to Kano
5	x	Kano to 5°N to Kano
6	x	Farnborough to Wildenrath to Idris
7	x	El Adem to 38°S via Khartoum, Entebbe, Salisbury and Durban.

external contributions to the high latitude cut-offs are likely to be unique functions of the main field cut-off rigidity at a particular time over the limited longitude range covered by the surveys.

4.2. DATA ANALYSIS

Analysis of the survey data is based upon the navigator's flight log together with the times at which the cosmic ray recorder is switched on and off. The flight log includes altitude, times of reaching and leaving a specified altitude, and position fixes and times for each heading change. The data which are collected over 4 minute periods are considered to represent the counting rates for the aircraft positions at the mid-points of the time periods. These positions are determined by assuming that the aircraft flies at constant velocity between the successive positions given in the flight log. The flight path is plotted on a cartesian coordinate map. Also plotted on this map are lines of constant cut-off rigidity constructed from the available threshold grids. Cut-off rigidities can thus be assigned to the 4-minute averaged data.

4.3. REDUCTION OF DATA TO A COMMON ATMOSPHERIC DEPTH.

Air traffic regulations do not always permit the use of the target pressure altitude of 45,000 ft. The variation of the secondary particle intensity with atmospheric depth requires that all data be reduced to a common atmospheric depth. The intensity depth variation depends upon the energy per nucleon of the primary particles and is therefore dependent upon the cut-off at the point of measurement. An empirically determined correction factor was obtained from the altitude

dependence of the recorder counting rate near Farnborough (at 3.1 GV), Idris (at 10.45 GV) and Kano (at 15.1 GV). The intensity versus altitude profiles were constructed from a combination of survey data recorded at various levels together with special altitude surveys at these positions. These special surveys seemed preferable as navigation errors would be ~ zero. Flights were made at different altitude levels, each of about 16 minutes duration. The flights were made along the same path in the east-west directions so as to be approximately along isorigidity contours. As will be pointed out in section (4.6) large errors due to the non-vertical alignment of the cosmic ray telescope are expected in the east-west directions. Considerable smoothing of these results was required at 10.45 GV and 15.1 GV and great weight was placed on the altitude dependence deduced from the essentially north-south survey data upon which the detector attitude has little effect.

Figure (4.3.1) from Bewick (1963) shows the smoothed intensity-altitude curves at 3.1 GV, 10.45 GV and 15.1 GV. In figure (4.3.2) the results of the altitude intensity surveys at 10.45 GV and 15.1 GV are compared with the smoothed curves. The dashed curves are the probable variations drawn after correcting data for the attitude error. For altitudes close to 45,000 feet, the differences in relative counting rates given by the two curves are small. This is therefore a second order correction and is not considered in the analysis.

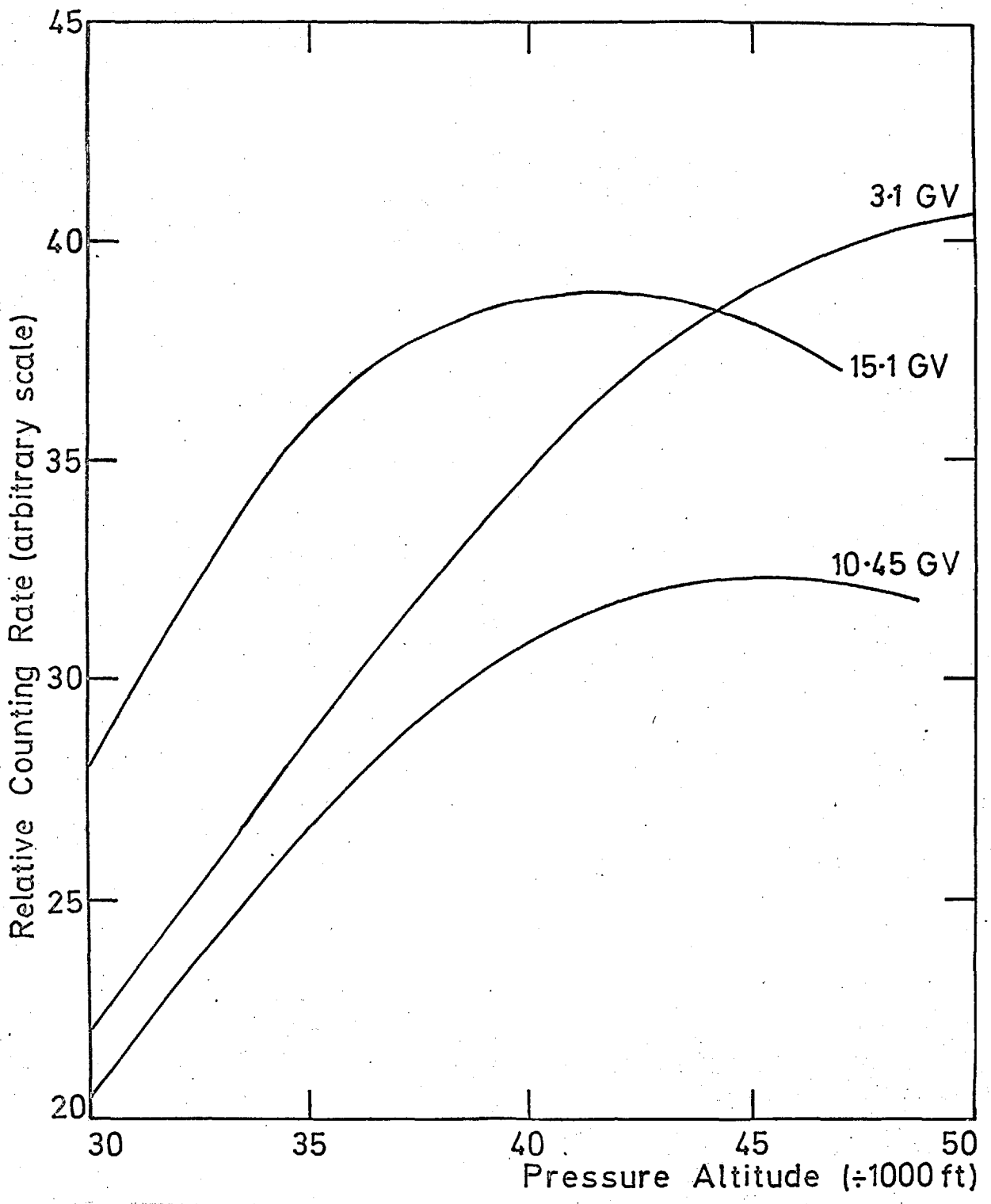


Fig. 4-3.I Altitude variation of the detector counting rate at 3.I GV, I0.45 GV and I5.I GV. (from Bewick: I963).

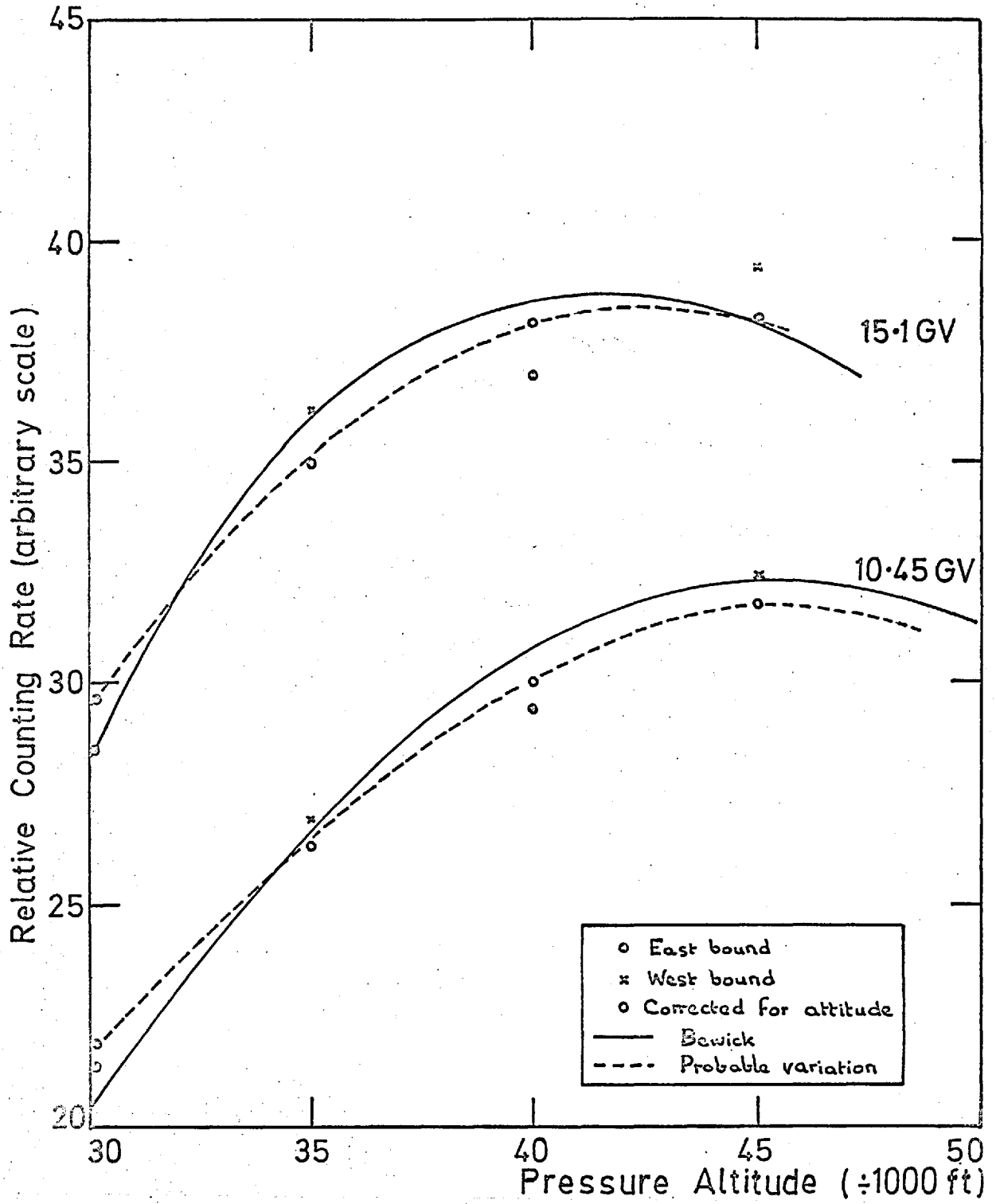


Fig. 4-3.2 Altitude survey data collected during east-bound and west-bound runs at 10.45 GV and 15.1 GV. The smooth lines are the same as in fig. 4-3.1. The dashed lines are drawn through the data after correcting for the attitude of the detector.

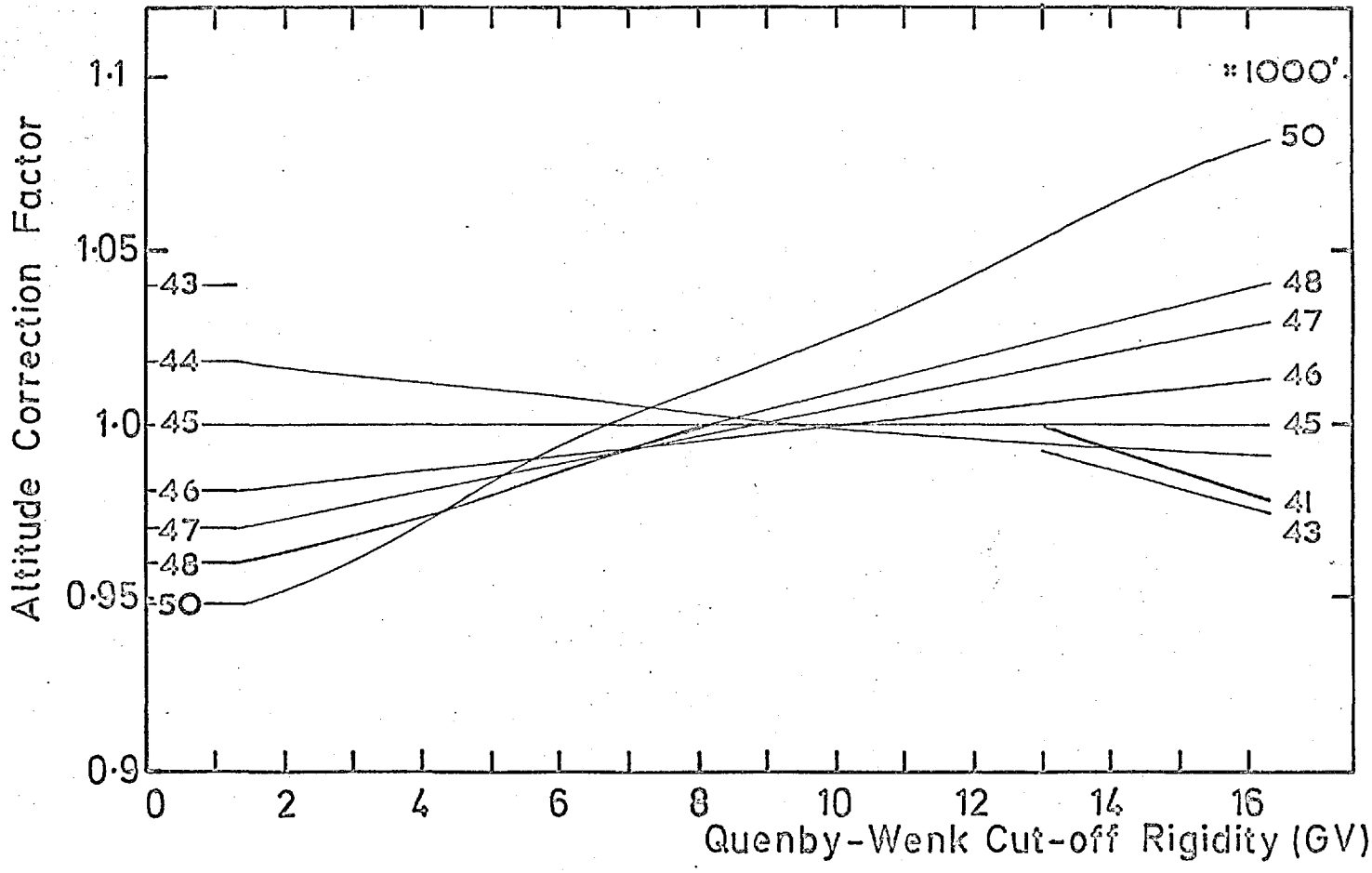


Fig. 4-3.3 Altitude correction factors constructed from fig. 4-3.1 (from Bewick: 1963).

The altitude correction factor required (the inverse of the counting rate relative to 45,000 ft) can be determined at other cut-offs by interpolation. The variation of the altitude correction factor with altitude and cut-off as given by Bewick (1963) is shown in figure (4.3.3).

The accuracy of the altitude correction factor is demonstrated through its ability to reduce the survey data obtained from different altitudes to a single-valued function of the cut-off rigidity.

The Pfotzer maximum is located at ~50,000 ft. at 3 GV and ~41,000 ft. at 15 GV. The target altitude of 45,000 ft. therefore closely follows the maximum in the secondary particle altitude - intensity distribution. This will minimise any errors that might arise due to altitude inaccuracies.

4.4. EXPERIMENTAL ERRORS.

The various sources of error are considered and estimates made of their magnitudes.

4.4.1. Statistical Errors.

These are due to the finite counting intervals in which a Poissonian frequency distribution is assumed:

Latitudes above knee ~ 0.3 %

Equatorial latitudes ~ 0.5 %

4.4.2. Navigation Errors

There have been three methods of navigation employed on the Canberra: radio compass, magnetic compass and optical sighting. Navigation errors depend upon the method used to fix the position and additionally upon the position where that method is used. The flight path is divided into 6 areas where these errors are considered. The magnitudes of the errors in these regions have been estimated by Farnborough navigators.

(i) Atlantic Ocean north of Scotland.

The magnetic compass alone can be used but is least accurate at high latitudes where the horizontal component of the Earth's magnetic field is small.

Errors ~ 25 n miles $\simeq$ 23' arc

(ii) Over Europe.

Both radio compass and optical sighting can be used.

Errors ~ 10 n miles $\simeq$ 10' arc

(iii) Mediterranean area.

The flight path passes a point about (35°N 13°E) which is about 130 n. miles from the coasts of Tunisia and Lybia. The accuracy of radio beacon fixes will be a minimum at this position.

Errors ~ 25 n. miles $\simeq$ 23' arc.

(iv) Sahara desert.

The radio coverage along the flight route is good.

Errors ~ 10 - 15 n. miles $\simeq$ 12' arc.

(v) South Africa.

The errors will be similar to those in (iv).

(vi) Indian Ocean.

Large navigation errors are likely near the south point:

38°S 38°E.

Errors ~ 23' arc.

4.4.3. Timing Errors.

Times are given to the nearest minute. Errors in each reading = $\pm \frac{1}{2}$ min; therefore the error in the difference is $\pm$ 1 min. $\simeq$ 8' arc. An additional source is in the reading of the switch on and off times. This will produce a systematic error in each data point.

Error ~ $\pm \frac{1}{2}$ min $\simeq$ 4' arc.

4.4.4. Altitude Variation.

Both systematic and random errors can result from altitude inaccuracies.

(i) While flying a level course, the altimeter reading can be maintained to ~ 50'. On banking the height can change by ~ 500'.

The effect of 50' variation is negligible while a sudden loss of altitude in a turn is immediately noticeable in the data. Data recorded during turns are therefore removed from the analysis.

(ii) The recorder was flown in the same Canberra during surveys 1-11 but during the short survey 12 another Canberra was used. The same altimeter was used during the first 11 surveys and so each survey should have been similarly affected by any systematic errors. The comparison of surveys 1-11 should not be affected by altimeter inaccuracy. A more accurate altimeter was used for survey 12.

Altimeter Accuracy (feet).

	Altitude (x 1000 ft.)		
	42	45	48
Surveys 1-11	± 600	± 670	± 675
Survey 12	± 140	± 150	± 160

There is a possibility of a difference ~ ± 600 feet when comparing altitudes given during survey 12 with surveys 1-11. This will produce the largest intensity changes for altitudes well away from the Pfotzer maximum:

Cut-off	1.5 GV	8 GV	15 GV
Approx. Error	1%	0	0.8 %

4.4.5. Variation of Wind Speed.

With a wind speed variation of 100 m.p.h. between nagivation check points separated by 4° the errors introduced will vary from zero at position fixes to a maximum of ~12' arc .

4.4.6. Cosmic Ray Anisotropy.

The amplitude of the diurnal variation determined by Rao et al (1963) from neutron monitor analysis was:

$\sim 0.4 \cos \lambda \%$ where λ is the geographic latitude.

The maximum occurs at about 1800 hours local time. This variation is of the same order as the statistical uncertainty at all latitudes.

4.4.7. Interpolation of Cut-off Rigidities.

The error due to the interpolation will depend upon the coarseness of the cut-off grid from which the cut-offs are being derived. Estimates of the interpolation errors are given in Table 4.1.

TABLE 4.1.

ESTIMATED INTERPOLATION ERRORS

Cut-offs.	Grid	Maximum Error
Quenby and Wenk	$2\frac{1}{2} \times 5$ degrees	5' arc.
Makino	10×15	10'
Kodama	5×10	8'
Shea et al	2×2	5'

Graphical interpolation by construction of smooth curves through the grid cut-offs was used for the first three cut-off calculations. In the fine 2×2 degree grid of Shea et al., linear interpolation was used.

4.4.8. Change in Detector Sensitivity.

The sensitivity of the detector may change due to :

(i) Mechanical shock.

(ii) Long term drift in characteristics of the electronics or scintillator.

(iii) Temperature changes during flight.

The first two possibilities can be observed from the long term calibration runs carried out underground. The fall in temperature inside the recorder is $\sim 10^{\circ}C$ per 3 hours. From the discussion of chapter 3:

Error ~ 0.4 %

4.4.9. Atmospheric Temperature Effect on the Secondary Cosmic Radiation.

Changing temperatures in the stratosphere lead to redistributions of the atmosphere above the detector and so might influence the secondary particle intensities. Dorman (1963) has emphasised that there is a statistical correlation between temperatures at different atmospheric levels but that no direct functional relationship exists. The mass redistribution cannot therefore be represented by the temperature at a particular isobaric level, but requires information on the complete temperature structure in the stratosphere above the detector. The ambient air temperatures are recorded during flights but the intensity and temperature data are not sufficiently numerous to make a quantitative study of their statistical relationship. The

qualitative effects of temperate changes can be found by considering the effects on the individual particles.

(i) μ mesons.

Varying the path length of low energy μ mesons from their mean generation level to the detector level will lead to a variation in their intensity because of their short life-time (2.15 μsecs).

(ii) Decay electrons.

The decay products of μ mesons will show similar variations to the parent μ's.

(iii) δ electrons.

The δ electrons knocked out of atmospheric atoms by collisions with μ mesons will have a similar temperature effect to the μ mesons.

(iv) Non-equilibrium soft component.

The intensity of electrons and photons making up this component is determined predominantly by the amount of absorber and not by its distribution. Temperature effects will be negligible.

(v) Nucleons.

The absorption of nucleons shows negligible temperature effects. Dorman (1957) has given the following proportions of electrons at various atmospheric depth:

	Decay	δ	N.E.	(%)
sea level	50	40	10	
650 cm^{-2}	29	14	57	
300 $g\ cm^{-2}$	18	4	78	

The proportion of non-equilibrium electrons will be a maximum near the Pfotzer maximum. The temperature effect will be due to variations of decay electrons, δ electrons and μ mesons which together probably contribute $\sim$10% of the total charged particle intensity at the Pfotzer maximum. It seems likely that the effect of atmospheric changes will be $\lesssim$0.3 %, the statistical errors of the counting rates.

4.4.10. Magnitudes of the Experimental Errors.

The sums of the errors from 4.4.1. to 4.4.9 are given in Table 4.2.

TABLE 4.2

ESTIMATED ERRORS DUE TO SOURCE 1-9

	Area.	Equivalent Position Error	Equivalent Counting rate error.
(i)	Latitudes above the knee.	24' arc.	0.45%
(ii)	Europe	13'	0.5
(iii)	Mediterranean	24'	0.55
(iv)	Sahara	14'	0.6
(v)	Southern hemisphere over Afria.	13'	0.5
(vi)	South of Durban	24'	0.5

In most regions the errors are largely navigational.

4.5. EFFECTIVE CUT-OFF RIGIDITY.

4.5.1. Approximate Calculations.

An additional error source especially in equatorial regions might result from a difference between the effective cut-off and the vertical cut-off. The cosmic ray recorder integrates the intensity of secondary particles arriving with zenith angles up to 45°. Assuming that the mass absorption law holds and the absorption curves for off-vertical zenith angles are identical to the vertical curves, the effect of the finite opening angle of the telescope may be calculated.

From simple Stőrmer theory, the zenith and azimuth dependence of the cut-off is a maximum at the geomagnetic equator. A calculation is made of the effective cut-off for the cosmic ray recorder at the equator for a simple dipolar magnetic field.

The cut-off rigidity at the equator as obtained from equation (1.2) is given by :

$$P = \frac{59.6}{[\,1 + (1 - \sin\varepsilon\cos\phi)^{\frac{1}{2}}\,]^{2}} \text{ GV.} \qquad 4.1$$

The increase of atmospheric depth with increasing zenith angle ε is approximated by :

$$\text{depth} \propto \sec\varepsilon$$

From the altitude-intensity curves of figure (4.3.3) a graph of counting rate at different altitudes relative to the Pfotzer maximum

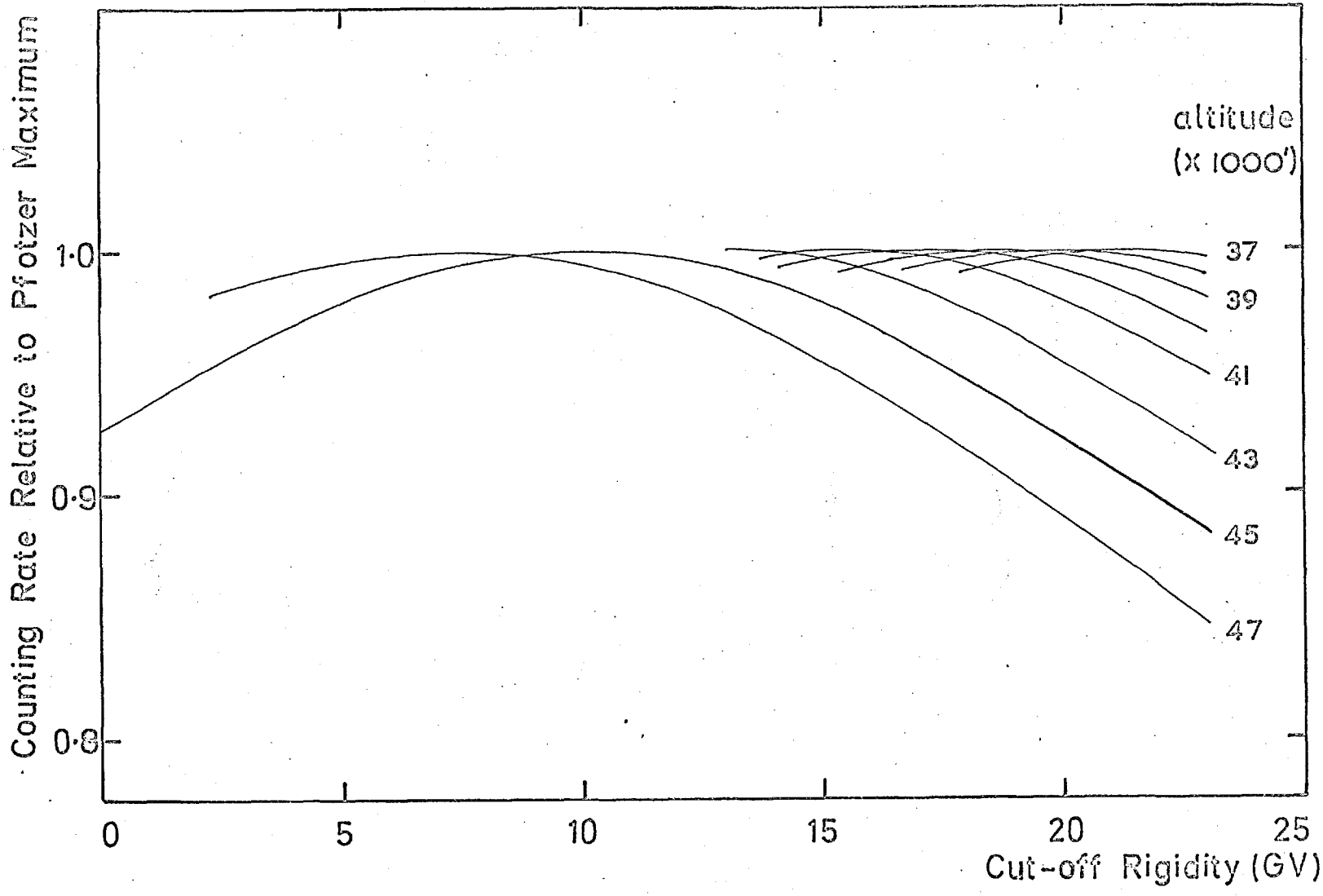
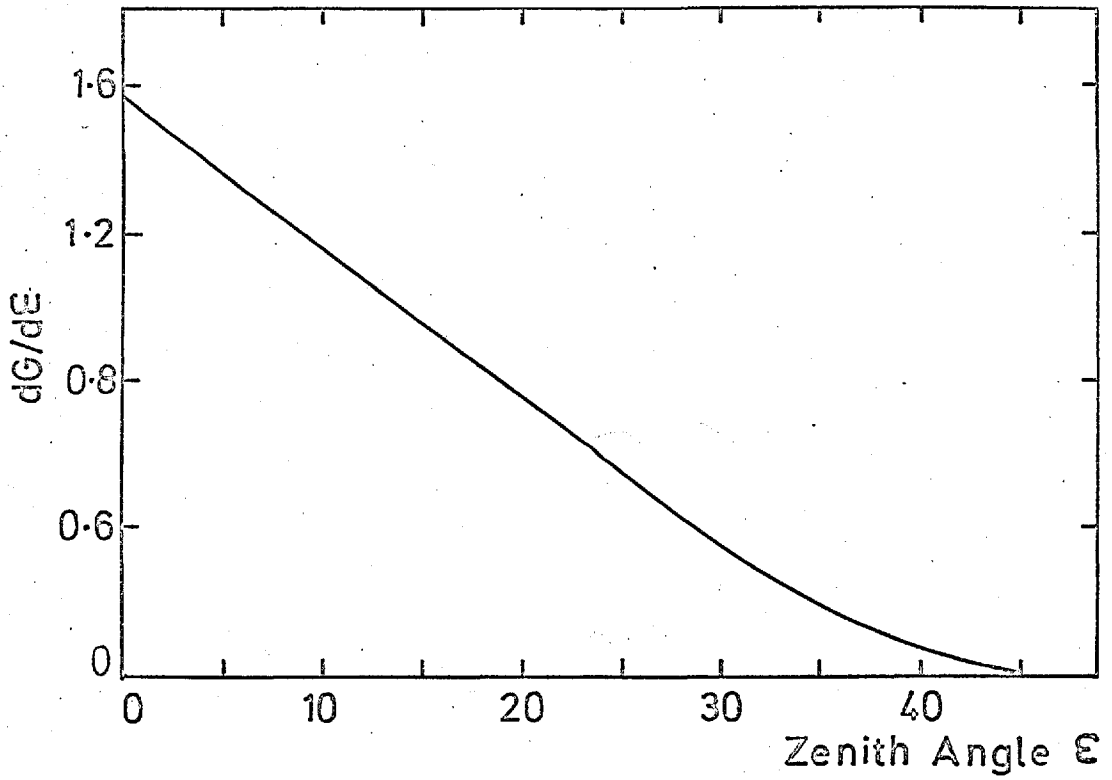


Fig. 4-5.1 The rigidity dependence of the counting rate of the detector at various altitudes relative to the counting rate at the Pfotzer maximum.



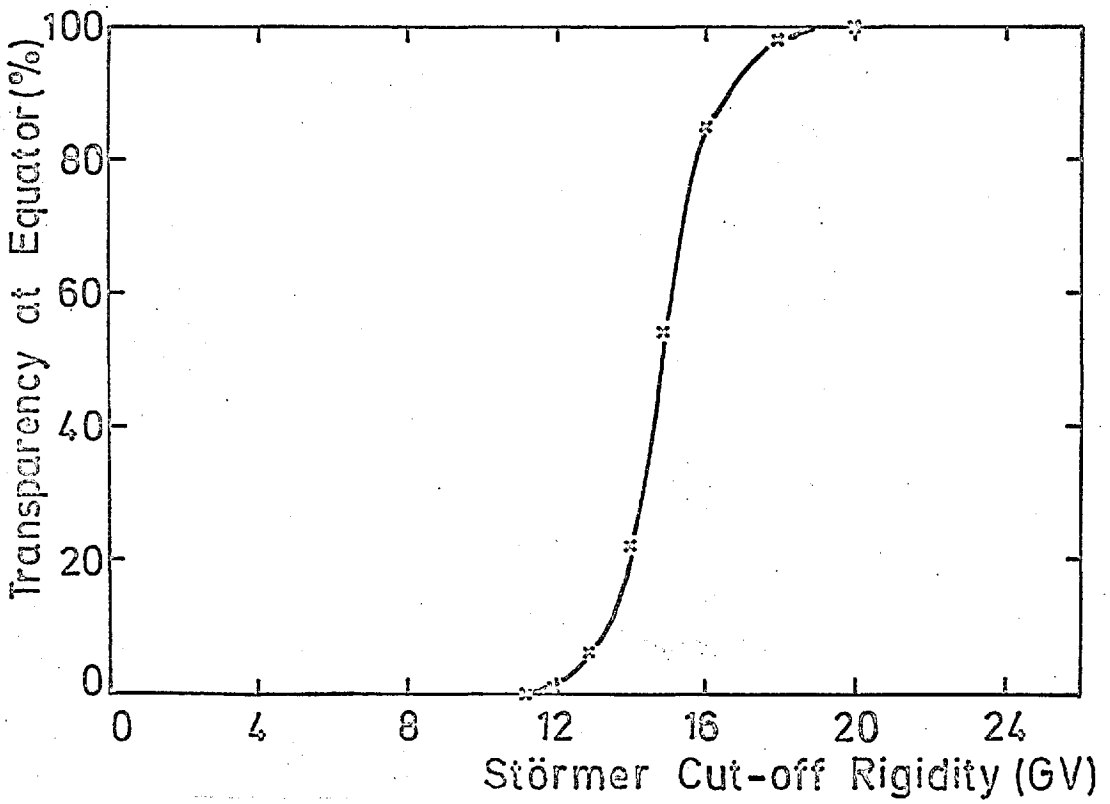


Fig. 4-5.2 The differential geometric factor, $\frac{dG}{d\varepsilon}$, of the detector as a function of zenith angle.

Fig. 4-5.3 The transparency of the geomagnetic field (dipole) at 14.9 GV for the detector at the Pfotzer maximum.

counting rate (for convenience) can be constructed as in figure (4.5.1). The depth of the Pfotzer maximum is approximately proportional to rigidity in the latitude-sensitive region. From this observation, the data has been extrapolated to 23 GV, the maximum cut-off rigidity within a zenith angle of 45° at the equator.

The calculated derivative of the telescope geometric factor (G.F.) with respect to the zenith angle $\left(\text{i.e. } \frac{d(G.F.)}{d\varepsilon}\right)$ is plotted in figure (4.5.2).

Numerical integration was then performed over the allowed solid angle, constructed graphically from equation (4.1), at 1 GV intervals from 11 GV to 23 GV.

The resulting percentage transparency as a function of cut-off is plotted in figure (4.5.3).

Assuming the primary spectrum (11 GV to 23 GV) to be represented by :

$$\frac{dN}{dP} \propto P^{-2.5}$$

the calculated effective threshold rigidity is equal to 14.9 GV. This is identical to the vertical cut-off rigidity.

It is therefore concluded that the vertical cut-off rigidity is a good parameter for organising the recorder data.

4.5.2. Trajectory Integration.

This problem is difficult to analyse by computing individual particle orbits within the allowed solid angle. A compromise solution is to calculate the cut-off for a particular zenith angle in the north,

south, east and west directions and to compare the mean value with the vertical cut-off. Two such calculations made by Hynds (1965) at a 15° zenith angle at locations on the flight path are given in Table 4.3.

TABLE 4.3.

EFFECT OF OFF-VERTICAL INCIDENCE ON CUT-OFF RIGIDITY

Location		Azimuth				Mean	Vertical
Lat.	Long.	N	E	S	W	Cut-off	Cut-Off.
16 S	32 E	11.15	13.15	11.55	11.30	11.48	11.35
33 N	13 E	9.35	10.65	10.75	10.15	10.23	10.35

The differences here are ~ 1% which is the limit of the accuracy of the threshold using 0.1 GV rigidity intervals.

4.6. DETECTOR ASPECT ANGLE.

The consideration of the experimental errors when applied to surveys 6 and 8 showed that the data for both flights separately could not be reduced to a single-valued function of the cut-off rigidity. The following sections are a treatment of the errors in surveys 6 and 8, and the correction needed to produce the required ordering of the data.

4.6.1. Introduction

The data obtained in the northern hemisphere from surveys 6 and 8 are plotted against Shea et al cut-off rigidities in figures(4.6.1) and

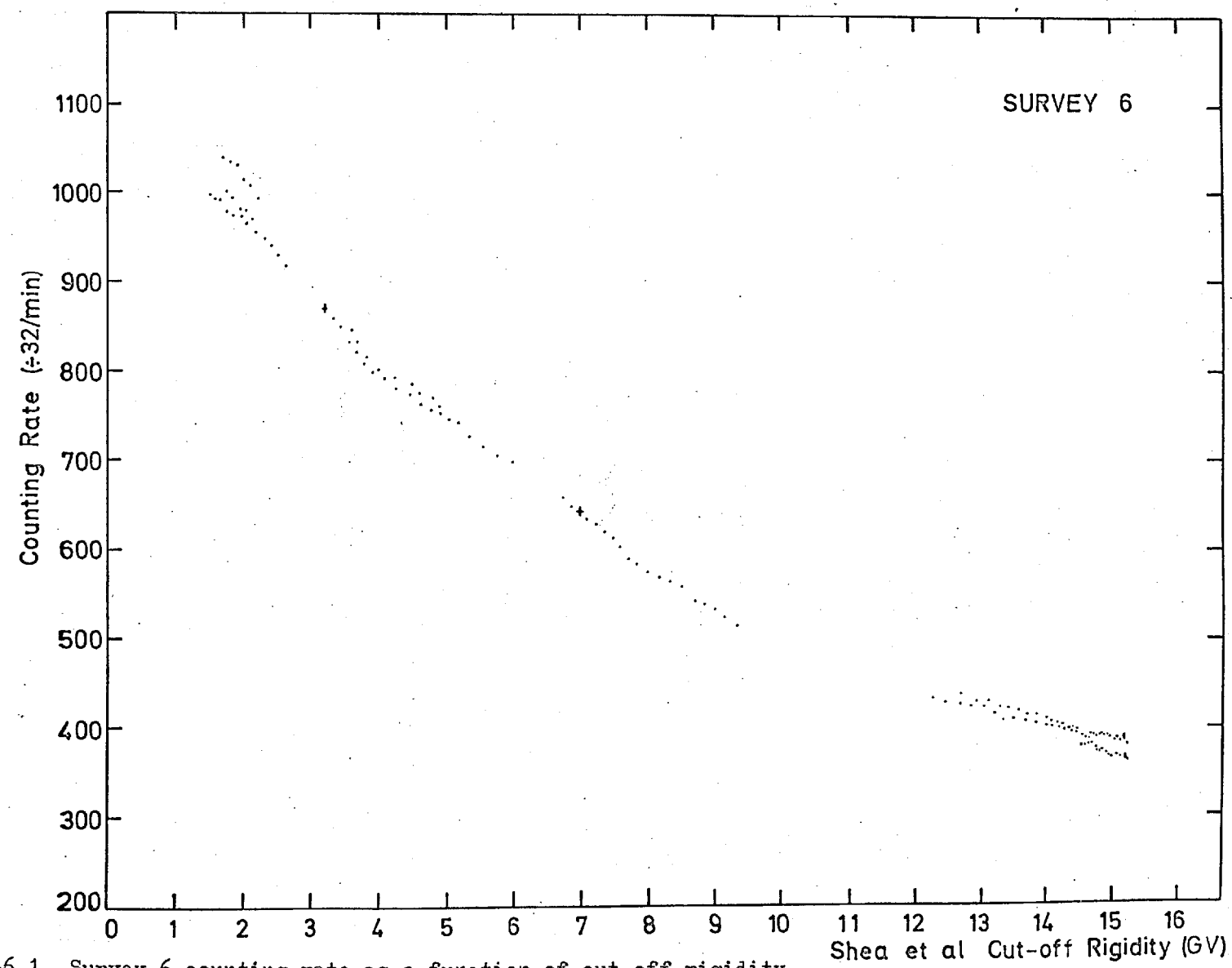


Fig. 4-6.1 Survey 6 counting rate as a function of cut-off rigidity.

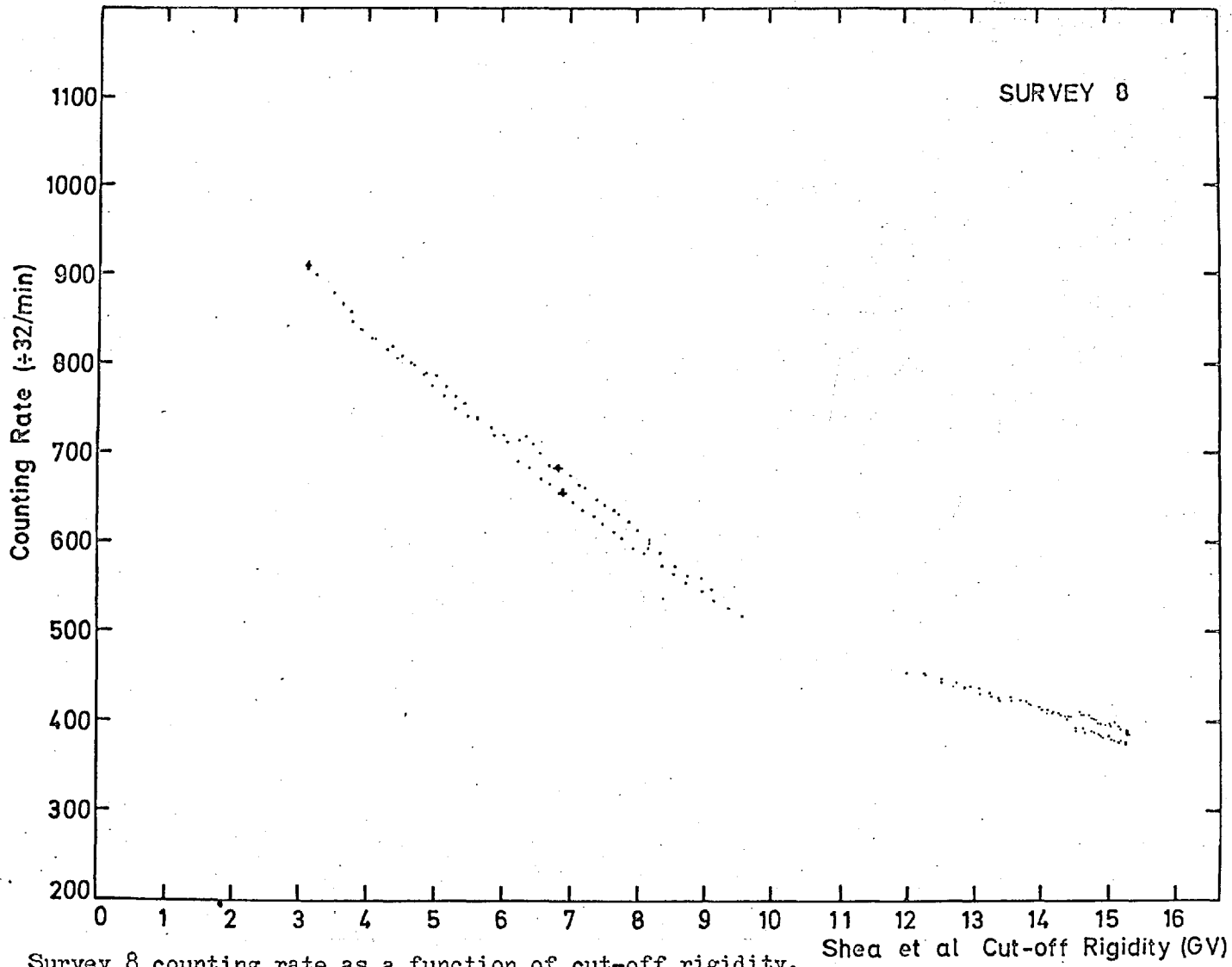


Fig. 4-6.2 Survey 8 counting rate as a function of cut-off rigidity.

(4.6.2). The data from each survey are obtained while travelling northwards and southwards over the same route. The spread of data points should indicate the magnitude of the errors involved. Most of the data points on the south-bound Farnborough to Idris leg of survey 6 were lost due to the occurrence of spurious pulses. In the mid-latitude region and in the equatorial region there is a splitting of the counting rate against cut-off rigidity. The possibility of this splitting being due to navigation errors is explored in a discussion of errors applied to the whole survey region.

(i) The flight path crosses the north coast of Scotland at about (58.6°N, 5°W) where the cut-off is 1.24 GV. The large navigation errors which can occur in the North Atlantic are in the region above the intensity knee and therefore unimportant. The knee occurs overland where the errors will be minimal.

(ii) Durban (30°S ,30.9°E) has a cut-off of 6.09 GV. From Durban the flight path is approximately south-east over the Indian Ocean to a position (38°S ,38°E) where the cut-off is 3.84 GV. Navigation errors will be large for the southern hemisphere cut-offs < 6.09 GV with a maximum error at 3.84 GV of $\pm$ 0.12 GV.

(iii) Navigation errors over Africa are small. This will apply to data obtained between Idris (32.7°N , 13.2°E) where the cut-off is 10.51 GV and Durban (6.09 GV).

The errors are therefore small for :

N. hemisphere $P > 10.5$ GV

S. hemisphere $P < 6.09$ GV

(iv) The route through the Mediterranean area is shown in figure (4.6.3). The position fixes detailed in Table 4.4 for surveys 6 and 8 are usually made close to coast-lines. During all surveys a change of course occurs 100 - 150 miles to the north of the Lybian coast and 100 - 150 miles to the east of the Tunisian coast. Examination of table 4.4. shows that the most accurate position fixes will be at the coasts of Sardinia and France in addition to the coast of Libya (at take-off and landing). Position errors are likely to be greatest in the cut-off range 9.0 GV to 9.7 GV.

Figure (4.6.4) shows a plot of the latitude gradient of the Shea et al cut-off rigidities $\frac{dP}{d\lambda}$ against latitude along the $13^{o}E$ meridian. The threshold gradient has a maximum value of 0.46 GV per degree latitude at latitude $35^{o}N$ which corresponds to the cut-off of 9.5 GV. Navigation errors in this region are therefore particularly important.

4.6.2. Aspect Angle Correction.

The large spread of data in the equatorial regions cannot be explained by the error sources which have been discussed, due to the small differential rigidity response $\frac{dN}{dP}$ and the small latitude derivative of the rigidity $dP/d\lambda$. The data were obtained near Khartoum and represent a splitting of the north-bound and south-bound data. A more detailed plot is given in figure (4.6.5). The splitting, ~ 4% in intensity, cannot be statistical or due to change of sensitivity of the recorder. It must therefore be due to change of threshold rigidity.

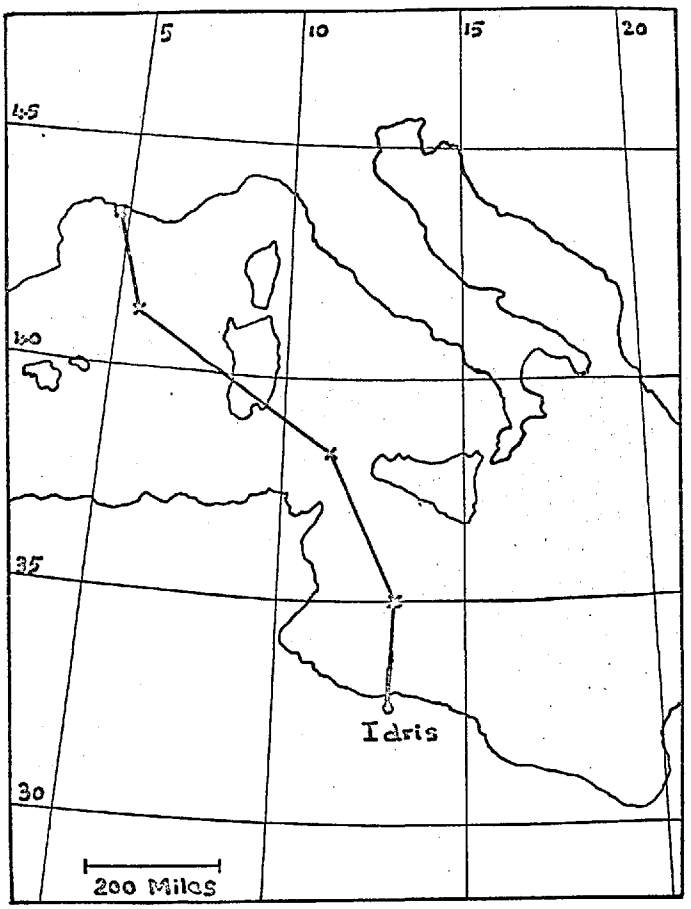


Fig. 4-6.3 Typical flight path across the Mediterranean.

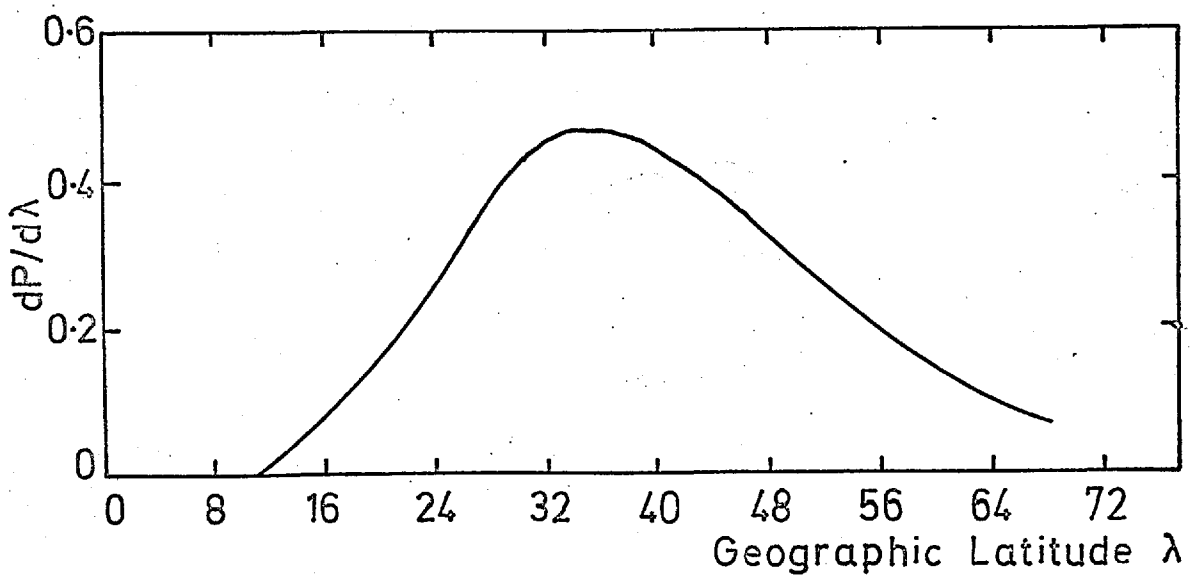


Fig. 4-6.4 The latitude derivative of the cut-off rigidity, $dP/d\lambda$, as a function of geographic latitude. The cut-off rigidities are due to Shea et al.

TABLE 4.4.

POSITION FIXES OVER THE MEDITERRANEAN

SURVEY	ROUTE	DESCRIPTION (approximate)	POSITION		APPROXIMATE CUT-OFF
			°N	°E	
6	*	South coast of France	43°20'	4°55'	5.60
	Farnborough	150 miles from French coast	41°30'	5°	6.30
	to	Sardinian coast	39°05'	9°35'	7.45
	Idris	150 miles from Tunisia	35°50'	12°50'	9.15
		150 miles from Lybian coast	34°50'	13°00'	9.55
	Idris	70 miles from Tunisia and Sicily	36°45'	12°00'	8.65
	to	40 miles from Sardinia	38°40'	09°55'	7.65
	Farnborough	Sardinian coast	39°10'	09°30'	7.45
		French coast	43°45'	04°50'	5.50
8		South coast of France	43°29'	04°56'	5.50
	Farnborough	30 miles from Sardinia	40°10'	07°40'	7.0
	to	40 miles from Tunisia and Sicily	38°15'	11°25'	7.90
	Idris	100 miles from Lybian coast	34°22'	13°20'	9.75
		100 miles from Lybian coast	35°23'	12°41'	9.30
	Idris	70 miles from N.E.Tunisia	38°00'	11°30'	8.05
	to	Coast of Sardinia	39°06'	09°31'	7.45
	Farnborough	Coast of France	43°36'	04°49'	5.50

* No data available for this leg.

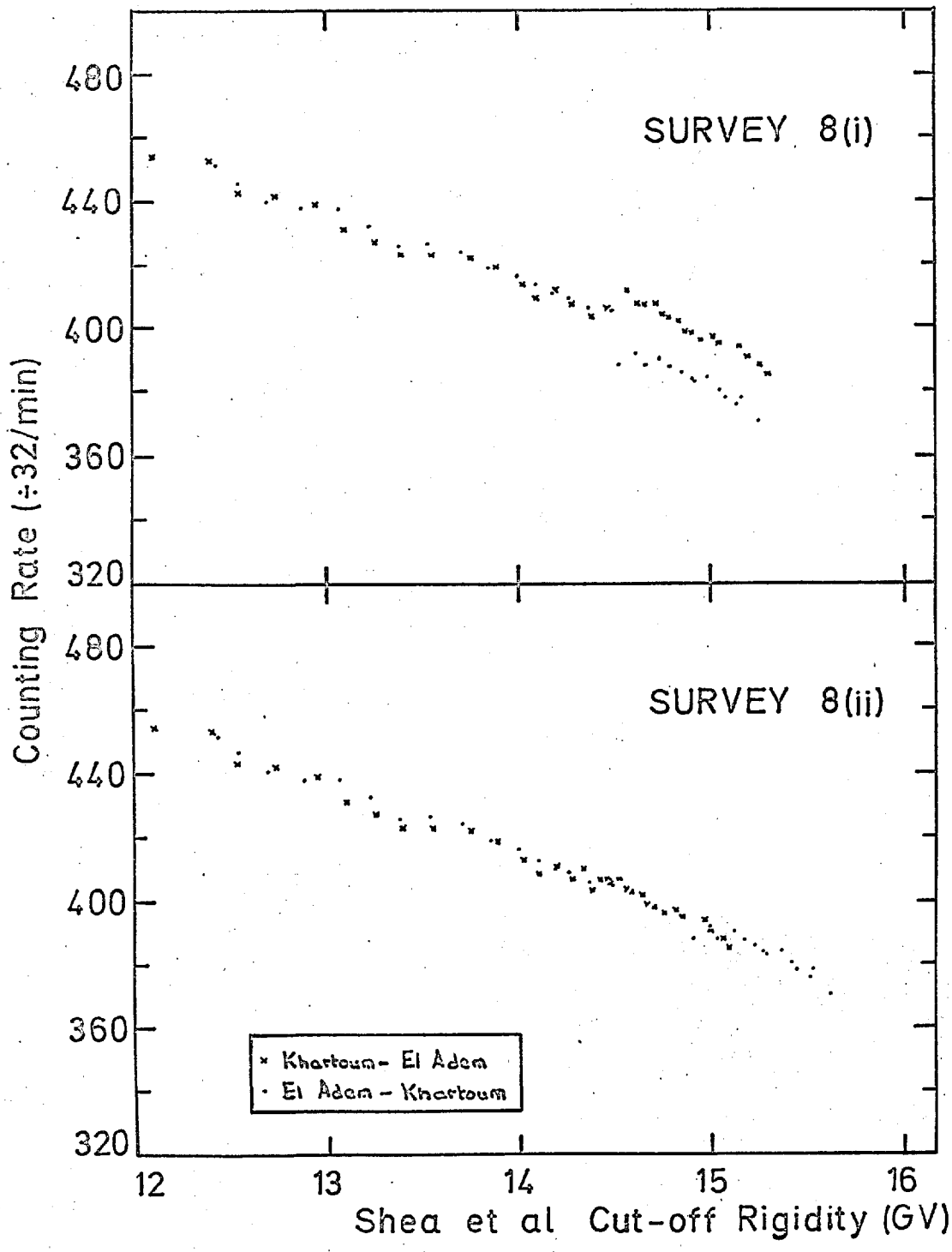


Fig. 4-6.5 Survey 8 data recorded between Khartoum and El Adem. Correction is made for the aspect angle of the detector.

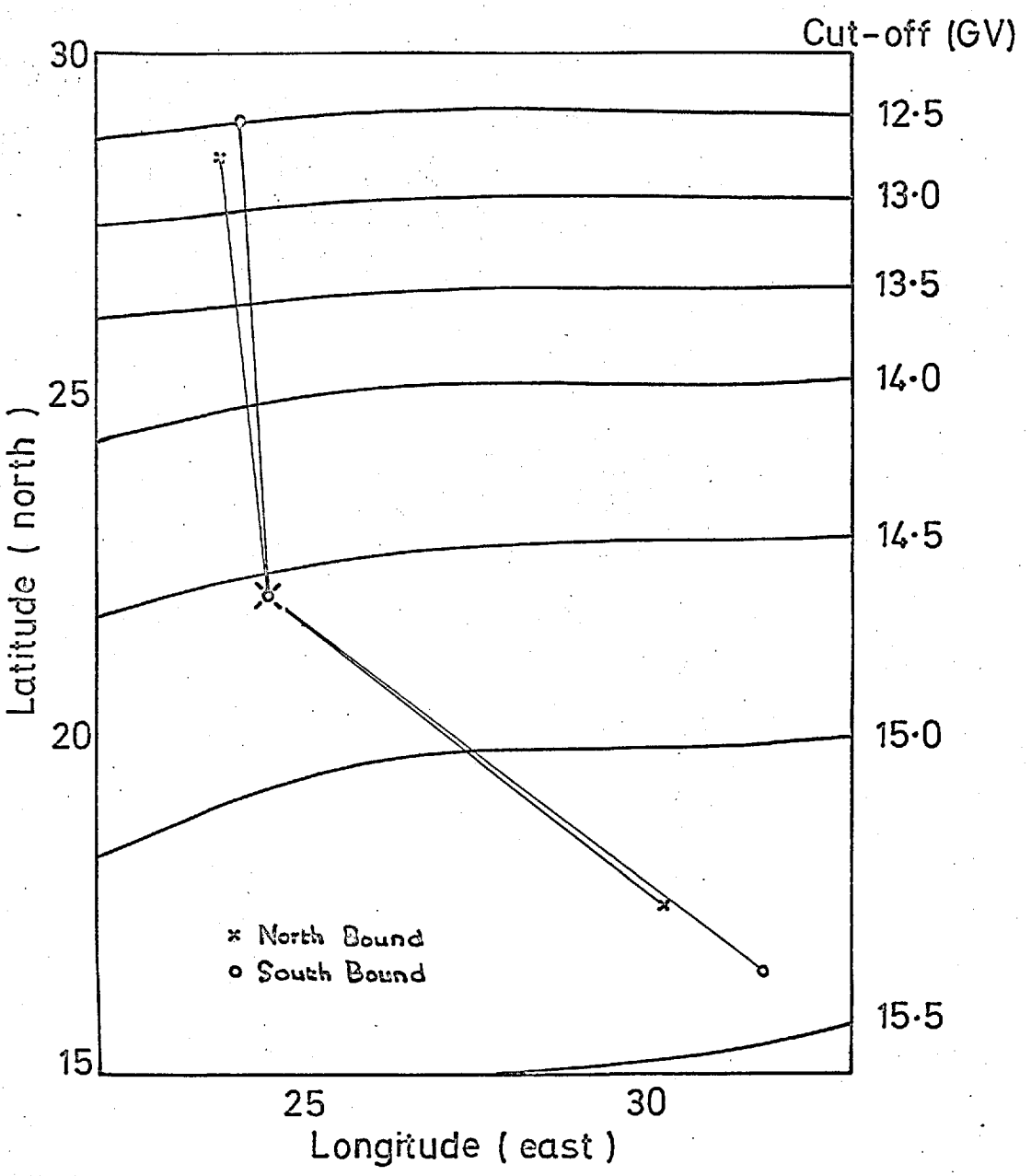


Fig. 4-6.6 Section of the route followed during survey 8. Contours of constant Shea et al cut-off rigidity are also shown.

The difference corresponds to about 0.6 GV near 15.3 GV. This would require a navigation error of approximately 200 nautical miles.

Inspection of the data revealed the existence of a course change at the precise position where the latitude intensity curve becomes double-valued. This was particularly noticeable when the data was plotted against the cut-offs of Shea et al. Over the section of the route covering the threshold range 14.6 GV - 15.6 GV the thresholds seemed to be lowered by a discreet amount when recorded in one direction and raised a similar amount when travelling in the opposite direction. The heading change at 14.6 GV was almost identical for both stages of the two surveys. Figure (4.6.6) indicates that the route changed from a N-S direction north of 14.6 GV (i.e. for $P < 14.6$ GV) to a NW - SE direction south of 14.6 GV ($P > 14.6$ GV).

At small zenith angles in the N-S plane, Störmer theory predicts that the cut-off varies little from the vertical value. The variation becomes marked in the E-W plane particularly at equatorial latitudes. The solution then appeared to be that the recorder was not truly vertical but was inclined so as to observe the E-W asymmetry. The direction of inclination had to be forward so that the effective threshold was raised when travelling eastwards and lowered when travelling westwards. Calculation indicated that the threshold would change ~0.15 GV for each degree off vertical in the NW - SE plane. A 2° forward inclination would then explain the observed splitting. The normal flying attitude of an aircraft would be expected to produce a backward tilt. It was therefore anticipated that the attitude of the recorder

must be far enough forward to obviate the effect of a backward tilt in flight. It was confirmed that with the wing horizontal in flight the recorder was inclined forward through an angle of 6°. During a 3 hour flight, typical of most legs, the inclination of the wing to the horizontal varies from $+4\frac{1}{2}^{\circ}$ with full fuel complement to $+3\frac{1}{2}^{\circ}$ at the end of the flight. The recorder therefore looks forward through $1\frac{1}{2}^{\circ}$ at the beginning and $2\frac{1}{2}^{\circ}$ near the end of a flight. This is then the explanation of the splitting: the observed effect agreeing with that predicted for the recorder aspect angle. The effect away from the equator at higher latitudes cannot be analysed simply because of the penumbra. All that can be said is that the Störmer threshold changes, due to the aspect of the recorder, will fall off with increasing latitude as obtained from equation (4.1). There is only one other important region in which there is an appreciable E-W component in the flight direction and that is over the Mediterranean. The sudden splitting apparent in figure 4.9 for $P > 6.2$ GV coincides with a course change from N-S ($P < 6.2$ GV) to NW-SE ($P > 6.2$ GV) and again the intensity changes are in the direction predicted by the simple Störmer theory. In the absence of information on the penumbral correction variation with latitude, the correction applied has been that predicted by equation 4.1 for the change of vertical Störmer cut-off. Inspection of figure 4.6.2 shows that the splitting from the mean curve at 6.2 GV is approximately symmetrical, as the change in Störmer cut-off would be.

Because of the symmetry of the aspect angle correction, the mean latitude curve will not be affected: the effect is to increase the confidence limit of the mean value. This correction has therefore been applied to all flight paths which have an east-west component.

Additional evidence of the correction needed for the attitude of the detector was given in Section 4.3.

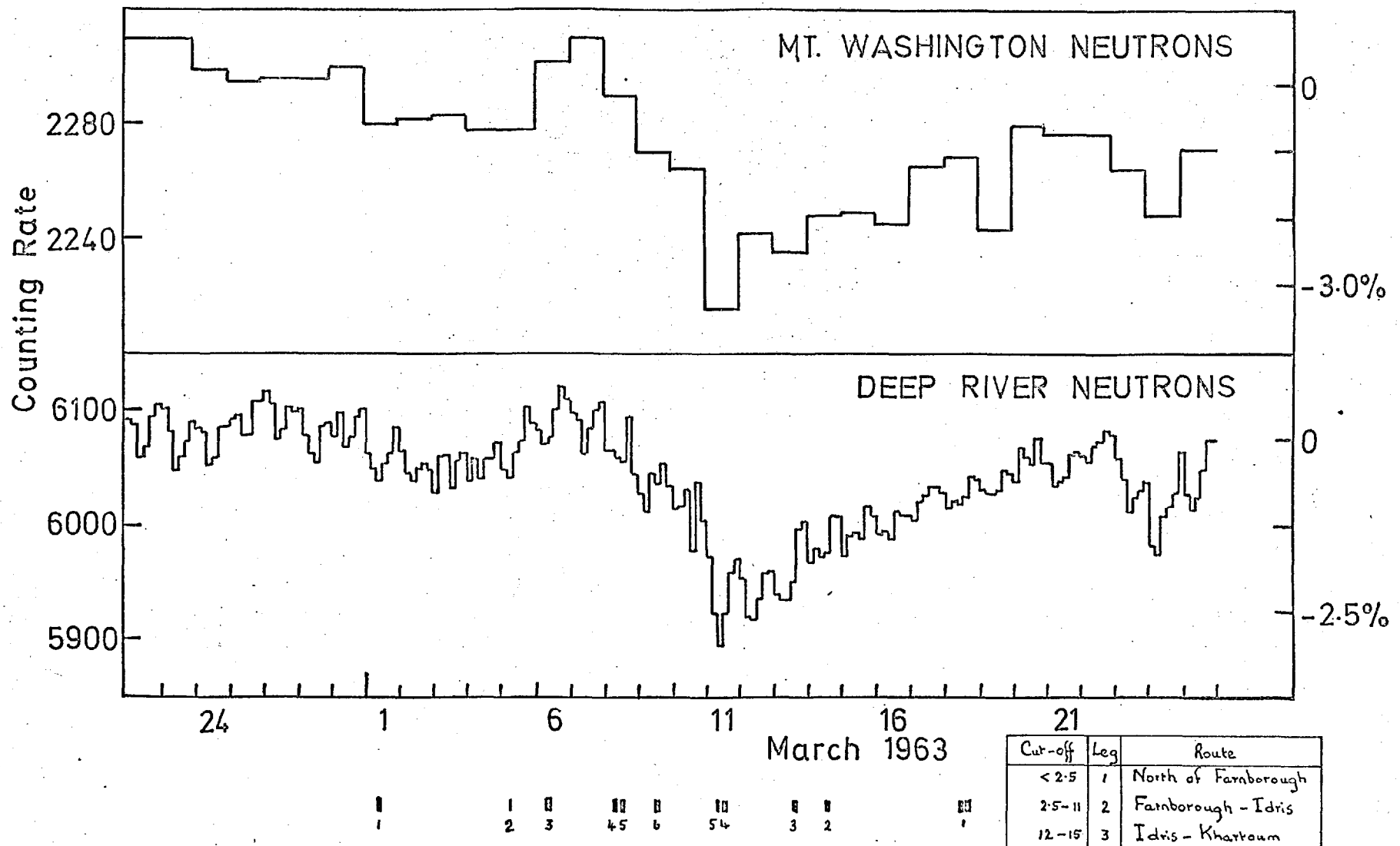
The magnitude of the correction applied to the survey data and the altitude - intensity data in section 4.3. were the same apart from a factor $\cos^2\theta$ required in the survey data due to the angle θ between the flight path and the E-W direction when plotted on a cartesian world map.

4.7. FORBUSH DECREASE EVENTS.

4.7.1. Forbush Decrease of March 1963.

A small Forbush decrease occurred during survey 6. The decreases recorded by the Deep River and Mount Washington neutron monitors are plotted in figure (4.7.1). The decrease phase lasted ~ $2\frac{1}{2}$ days, the intensity reaching a maximum depression of about $2\frac{1}{2}\%$ below the pre-decrease level. The time constant of the recovery phase was ~ 6 days. During the recovery phase the Deep River neutron monitor shows the presence of an enhanced daily variation.

The onset occurred on 8 March. Data recorded subsequently would be subject to the superimposition of the Forbush decrease modulation mechanism and the pre-decrease long term modulation mechanism. Magnetic records showed only small disturbances implying



Cut-off	Leg	Route
< 2·5	1	North of Farnborough
2·5 – 11	2	Farnborough – Idris
12 – 15	3	Idris – Khartoum
15 – 11	4	Entebbe – Salisbury
11 – 6	5	Salisbury – Durban
6 – 4	6	South of Durban

Fig. 4-7.I The Forbush decrease event of March 1963 recorded by the Deep River and Mt. Washington neutron monitors. The days of data recording are also shown.

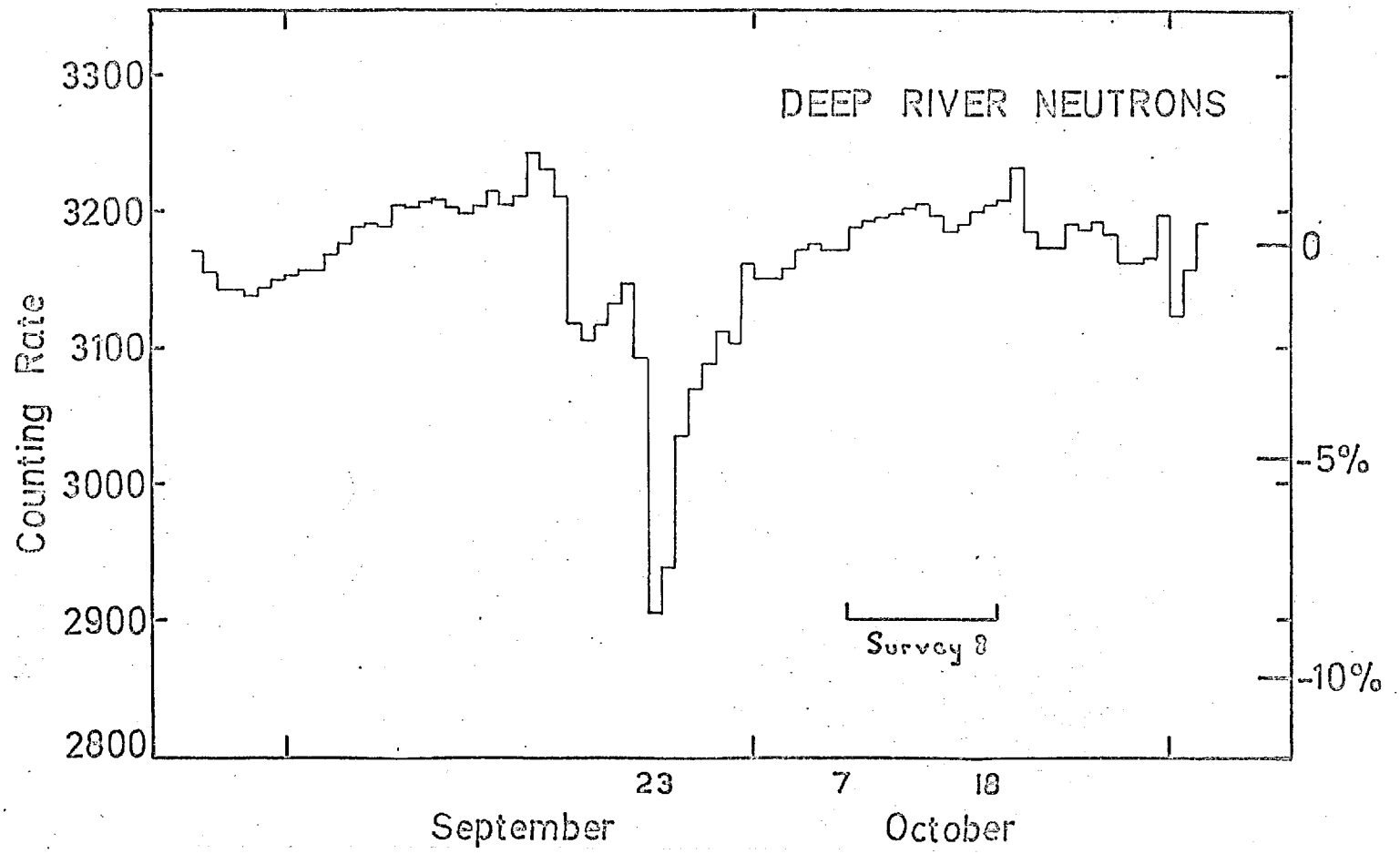


Fig. 4-7.2 The Forbush decrease event of September 1963 recorded by the Deep River neutron monitor. The period of survey 8 is also shown.

that there was little enhancement of the ring current at this time.

The flight periods during this survey are also given in figure (4.7.1) together with the cut-off ranges observed. The effect of the Forbush decrease is considered in convenient rigidity intervals.

(i) 4-10 GV

Northern Hemisphere.

Pre-decrease south-bound data from Farnborough to Idris is available only from ~3.5 GV to 5 GV and is ~1.2% higher than the north-bound data of 14th. March when Deep River was depressed 1.5%.

Southern Hemisphere.

Data south of Durban from ~ 4-6 GV were obtained just after the initial decrease when Deep River was depressed 0.7 GV.

8-10 GV data obtained on 8th. March before the decrease and 11th. March (maximum depression) show no evidence of the decrease within the experimental uncertainties (~0.5%).

(ii) 11-15 GV

Northern hemisphere pre-decrease data of 5th. March and 14th. March (1.6% Deep River depression) show no evidence of the Forbush event.

Southern hemisphere data obtained on 11th. March (2.5% depression) were consistent with the pre-decrease data of 8th. March.

(iii) 16 GV.

The Khartoum-Entebbe and Nairobi-Khartoum legs lie within 0.5 GV of 16 GV and so the observation at 16 GV has good statistical accuracy together with negligible navigation errors. The routes are both

approximately north-south requiring no attitude correction.

Deep River	Date	Intensity
Predecreases	6th. March	362 ± 2
2% decrease	13th. March	366.7 ± 3

The errors are due to altitude uncertainties primarily.

(iv) $P < 2.5$ GV

Relative Cosmic Ray Recorder Intensity at 2 GV	Date	Time (GMT) during which low rigidity results obtained	Relative Deep River Intensity.
1	1st. March	1030-1100	1
- 3.3% ± 0.5%	18th. March	1030-1100	- 0.7%
- 4.5% ± 0.5%	18th. March	1400-1600	

The results obtained on 18th. March are not in agreement. This must be due to the cosmic ray anisotropy although the neutron records examined show the daily variation maximum to have been ~ 1800 hrs. local time. A more complete study of neutron monitor records of greater world coverage might reveal the maximum to be displaced to the morning hours on this day.

Summary.

a) The decrease was not observed at cut-offs greater than 8 GV.

b) In the region 4-8 GV the maximum effect was ~1.2% at 4 GV when Deep River was depressed 1.5%. The modulation effect on the southern hemisphere data in this range, obtained during the decreasing phase with Deep River ~0.7% depressed, will probably be <1.2%.

c) The steep rigidity dependence of the modulation on 18th. March noted in (iv) above indicates that the high rigidity particles recovered more quickly than the low rigidity particles.

Survey 6 has not been used in the study of the long term modulation. It has been used only in the study of cut-off rigidities which is restricted to $P > 4.2$ GV. The large variations observed for $P < 2.5$ GV will not affect this study.

A correction is needed only for the Farnborough to Idris leg of ~ 1% at 4 GV to ~ zero at 8 GV. Without knowing the precise rigidity dependence of the modulation little error will result by assuming it to be linear.

4.7.2. Forbush Decrease of September 1963.

A Forbush decrease occurred on 17th. September 1963 prior to survey 8(which began on 7th. November with the northern leg measurement of the low rigidity ($P < 2.5$ GV) end of the spectrum). The maximum depression recorded by the Deep River neutron monitor in figure 4.7.3. was ~ 8% on 23rd. September. The recovery time constant was ~3 days and the intensity reached the pre-decrease level on

4th. October. Evidence is given in Section (6.1) that the intensities at rigidities down to 1.2 GV had recovered to their pre-decrease level by 7th. October.

The rigidity characteristics of the recovery phase of this decrease are quite different to the March event where the recovery times were strongly rigidity dependent.

CHAPTER 5. A COMPARISON OF VARIOUS CUT-OFF CALCULATIONS.

5.1 Introduction.

Surveys 6 and 8, extended into the southern hemisphere, provide a particularly exacting test of geomagnetic theory because of the proximity of the South African magnetic anomaly. Given an accurate definition of the magnetic field, it should be possible to order the cosmic ray data measured at a particular time as a single-valued function of the cut-off rigidity. The determination of cut-offs by the numerical integration of the cosmic ray trajectories attempts to define the behaviour of a family of trajectories by a single calculation.

This can only be an approximation, as the penumbral regions at mid-latitudes have been shown to exhibit fine structure on the scale of the most detailed calculations. The errors involved in this method can be made small, however, and the experimental evidence for the validity of the method is undoubted.

The limits to the accuracy of these cut-offs are the knowledge of the magnetic field (of both internal and external origin) and the uncertain penumbral corrections for detectors of finite solid angle. Because of the large amount of computer time required and the consequent expense involved in trajectory computations only limited regions have, until recently, been investigated by this technique. There still remain areas with few trajectory calculations and it is in these areas that the limitations of cut-offs found by interpolation should become apparent. Latitude surveys of cosmic ray

intensity provide a means of assessing the relative merits of these interpolated cut-offs and other methods of cut-off calculation.

Previously, surveys obtained over long periods of months or years have been compared and have necessitated uncertain corrections for both short term and long term intensity variations. The present analysis compares the consistency of threshold calculations in individual surveys each lasting about two weeks. The comparisons have been carried out close to solar minimum when there has been a marked absence of Forbush decrease events to complicate the analysis. The magnetic field simulations used in these calculations have been shown to be accurate to about 1%. This is therefore the limit to which the cut-off calculations can be compared. The cut-off calculations to be compared are those of Quenby and Wenk (1962), Makino (1963), Kondo and Kodama (1966) and Shea et al (1966).

5.2. COSMIC RAY EQUATOR.

The counting rates for the two surveys are plotted in figure (5.2.1) as a function of the geographic latitude. Following the method of Pomerantz et al (1960) the counting rate (y) may be represented by the power series expansion in the latitude (x) thus :

$$y = \sum_{o}^{n} a_n x^n \qquad 5.1.$$

Little difference in the position of the minimum was observed with $n = 2$ or $n = 3$. It was concluded that $n=2$ was a sufficiently good representation.

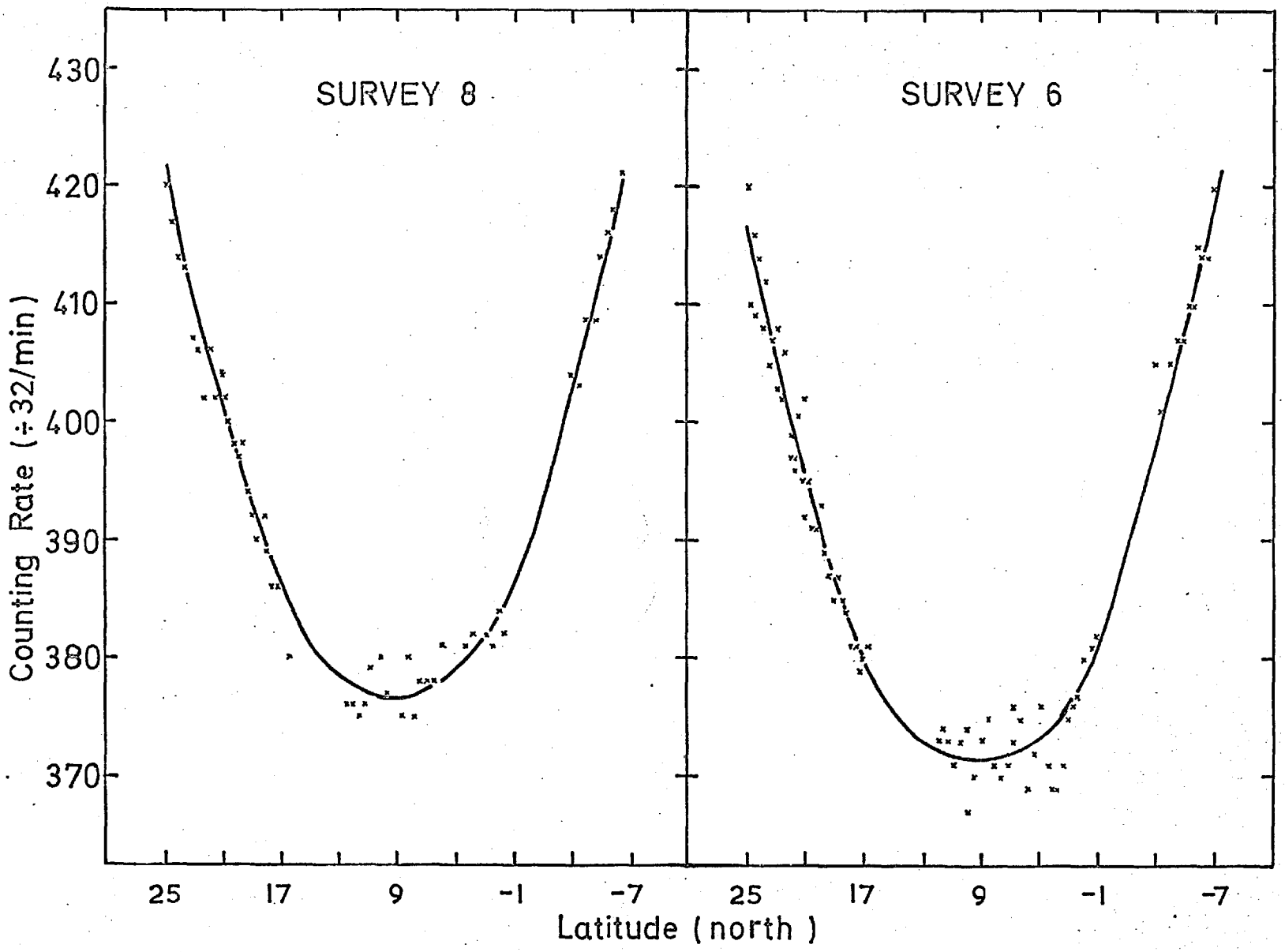


Fig. 5-2.I The cosmic ray equator determined during surveys 6 and 8.

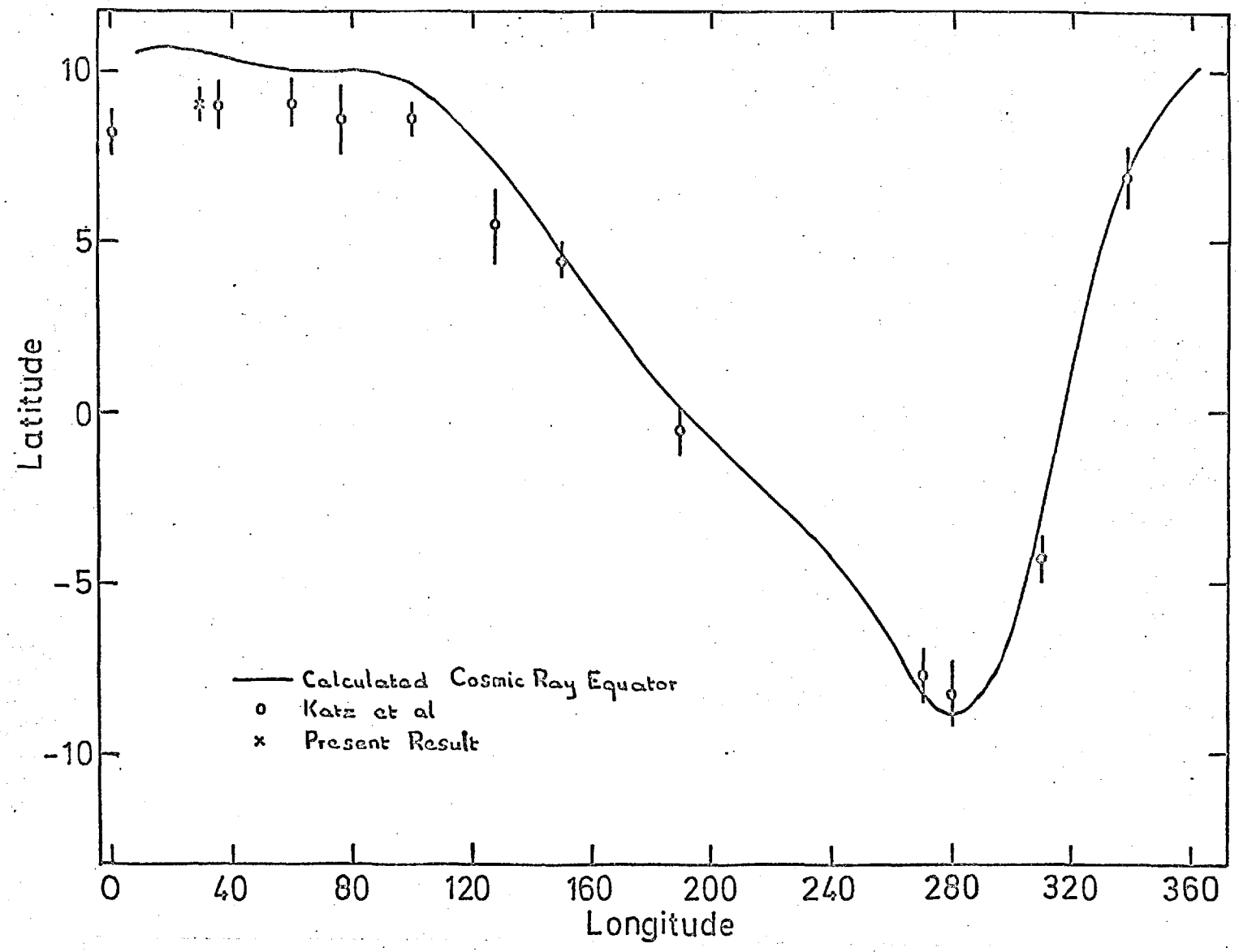


Fig. 5-2.2 The cosmic ray equator calculated by trajectory computation in the field simulation of Finch and Leaton (after Shea and Smart: 1966). The present observation of the minimum is shown together with the positions found by Katz et al: 1958).

Using this as a basis the data was fitted by the simple parabolic form :

$$y = a_o + a_2 x^2 \qquad 5.2.$$

i.e. eliminating the asymmetric term $a_1 x$.

The positions of the cosmic ray minimum determined from the two surveys are given in Table (5.1.) .

TABLE (5.1)

POSITION OF COSMIC RAY EQUATOR

Survey	Latitude	Longitude
6	9.1 ± 0.5	31.6
8	9.1 ± 0.4	31.7

The present result is in good agreement with the data of Katz et al (1957) shown in figure (5.2.2).

Shea et al (1966) have calculated the position of the cosmic ray equator using both the Finch and Leaton (1957) and the Jensen and Cain (1962) field simulations.

TABLE (5.2)

CALCULATED POSITION OF COSMIC RAY EQUATOR

Field Model	Latitude	Longitude
Finch-Leaton	10.7°N	31.6°E
Jensen-Cain	11.6°N	31.6°E

The position of the equator given in Table (5.2) for the Finch and Leaton field is in better agreement with the experimental data in this region, the error being 1.6°.

5.3. SURVEY DATA.

The data from surveys 6 and 8 are plotted against the Quenby and Wenk cut-offs in figures (5.3.1) and (5.3.2) respectively. The gaps in the data are due to take-off and landing at Farnborough, Idris and Durban. Large differences in intensity occur at locations with the same cut-off in the northern and southern hemispheres. The maximum difference is observed at 9.0 GV where the intensity is 18.6% higher in the southern hemisphere than in the nothern. The differences in cut-off for locations where the same cosmic ray intensity is recorded are plotted against the northern hemisphere cut-offs in figure (5.3.3). The good agreement between the cut-off differences for the two surveys supports the conclusion reached in 4.7: the effect of the Forbush decrease during survey 6 was shown to depress the northern hemisphere intensity by ~1% at 4 GV and ~ 0 at 8 GV. This is equivalent to ~0.07 GV

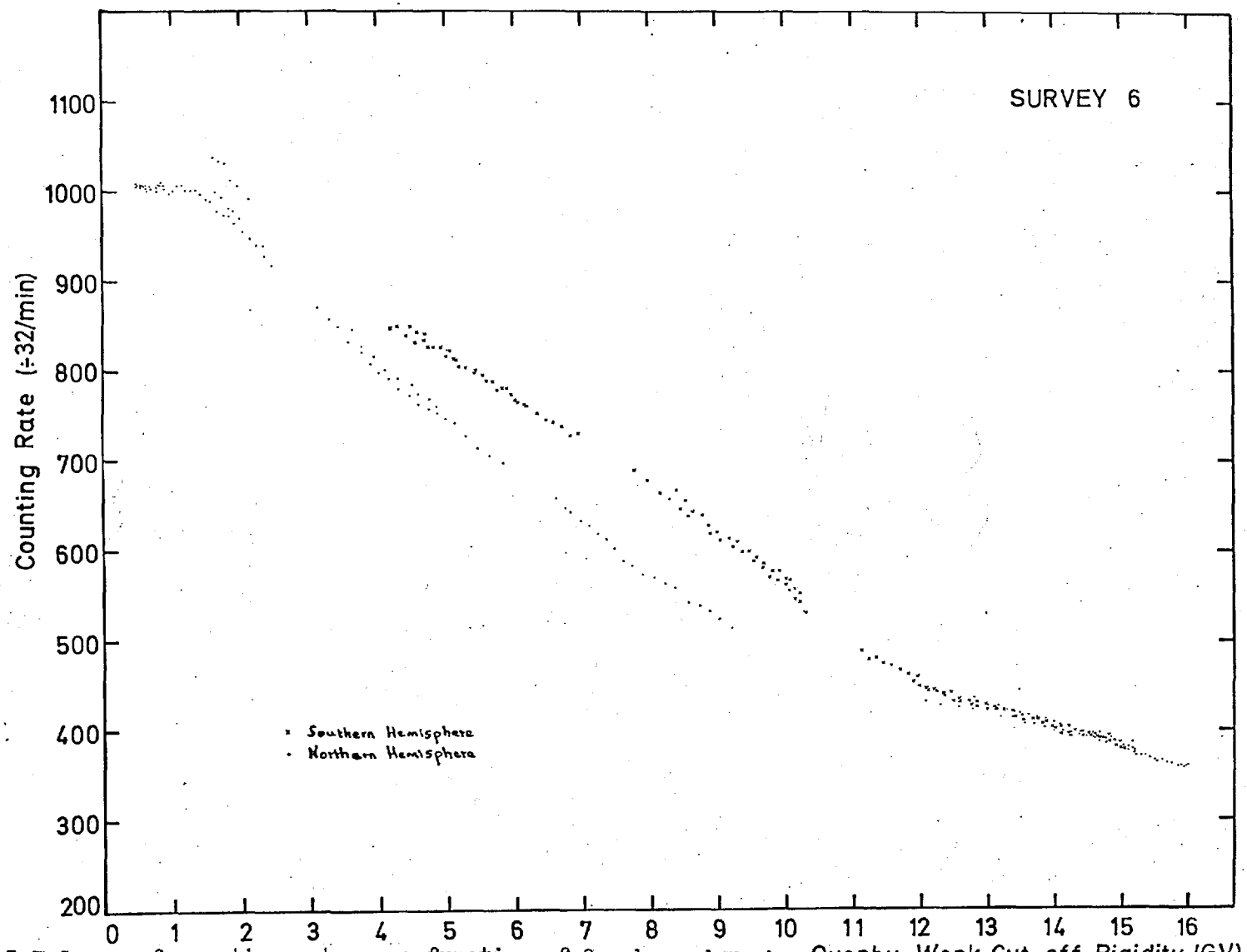


Fig. 5-3.I Survey 6 counting rate as a function of Quenby and Wenk cut-off rigidity.

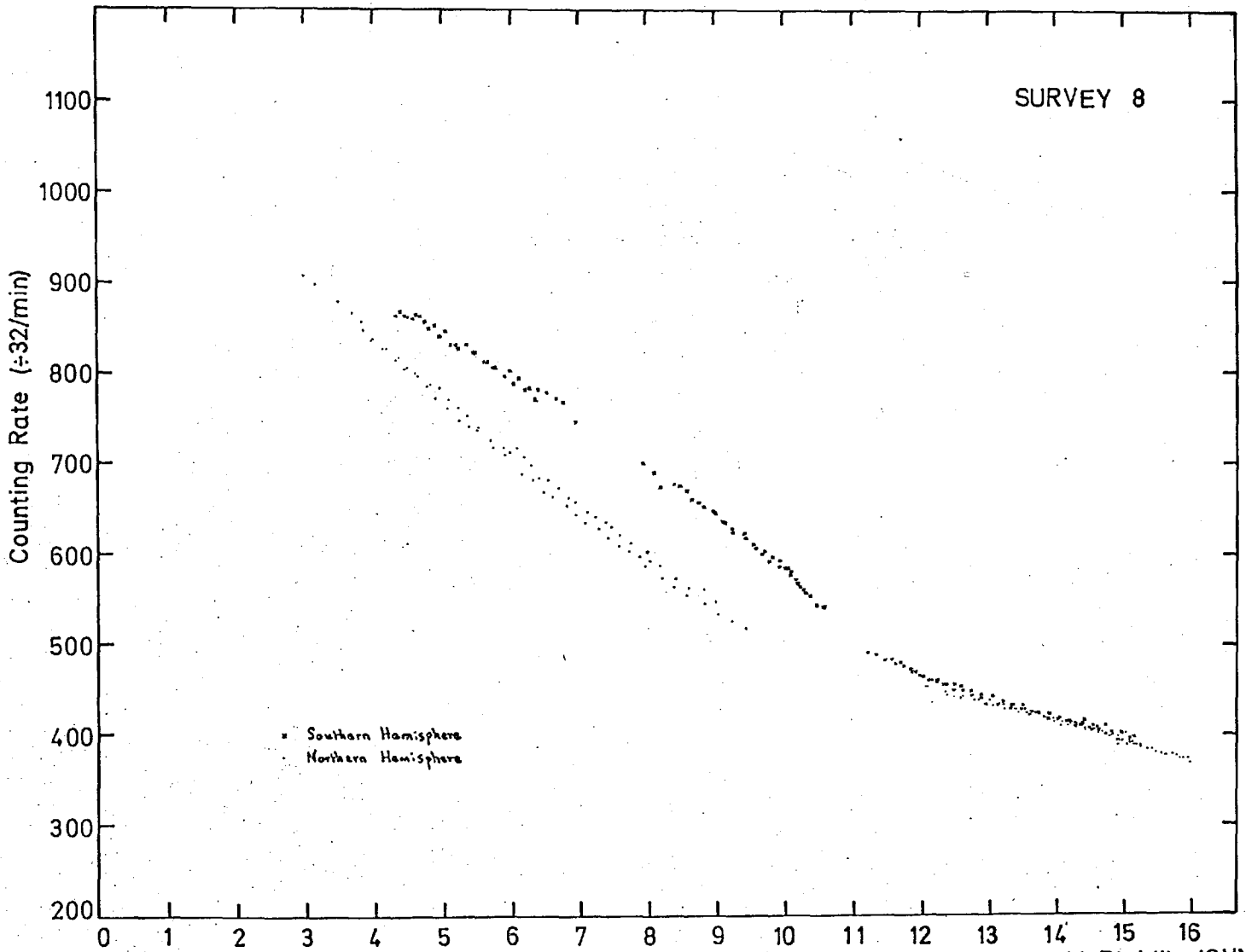
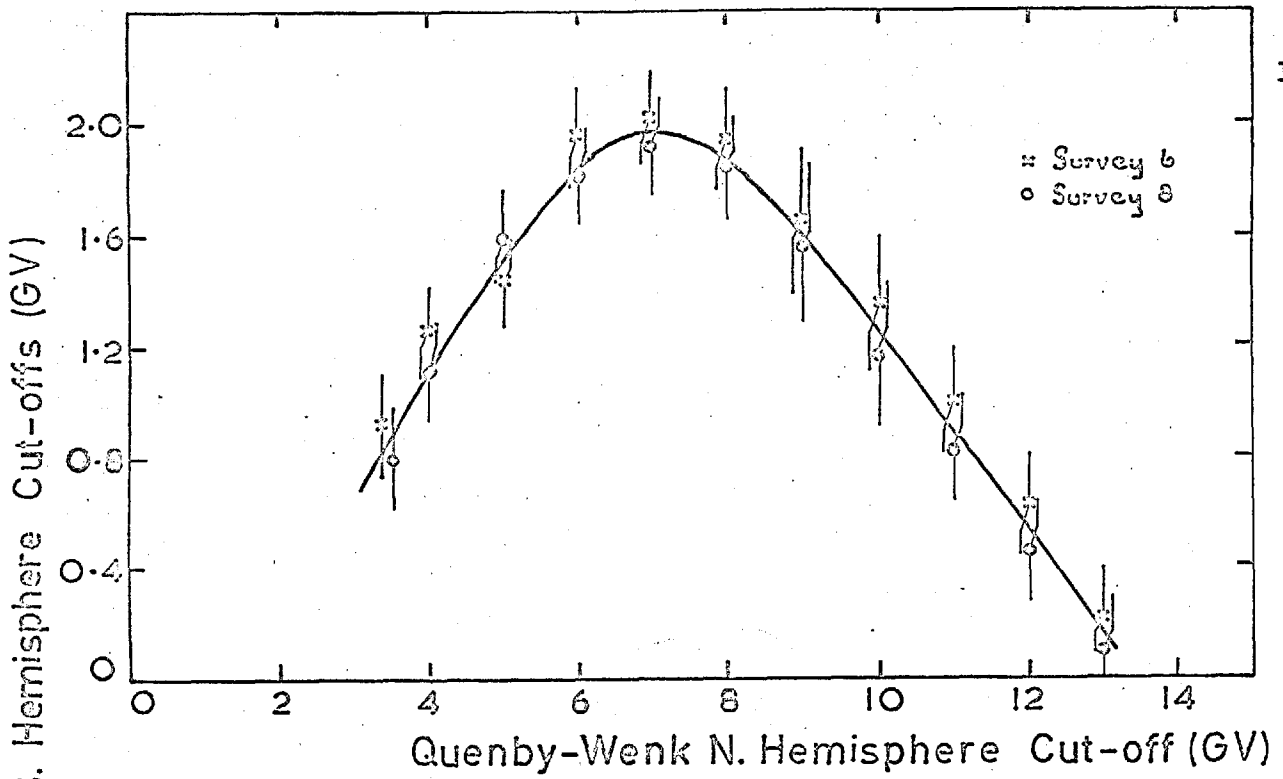


Fig. 5-3.2 Survey 8 counting rate as a function of Quenby and Wenk cut-off rigidity.



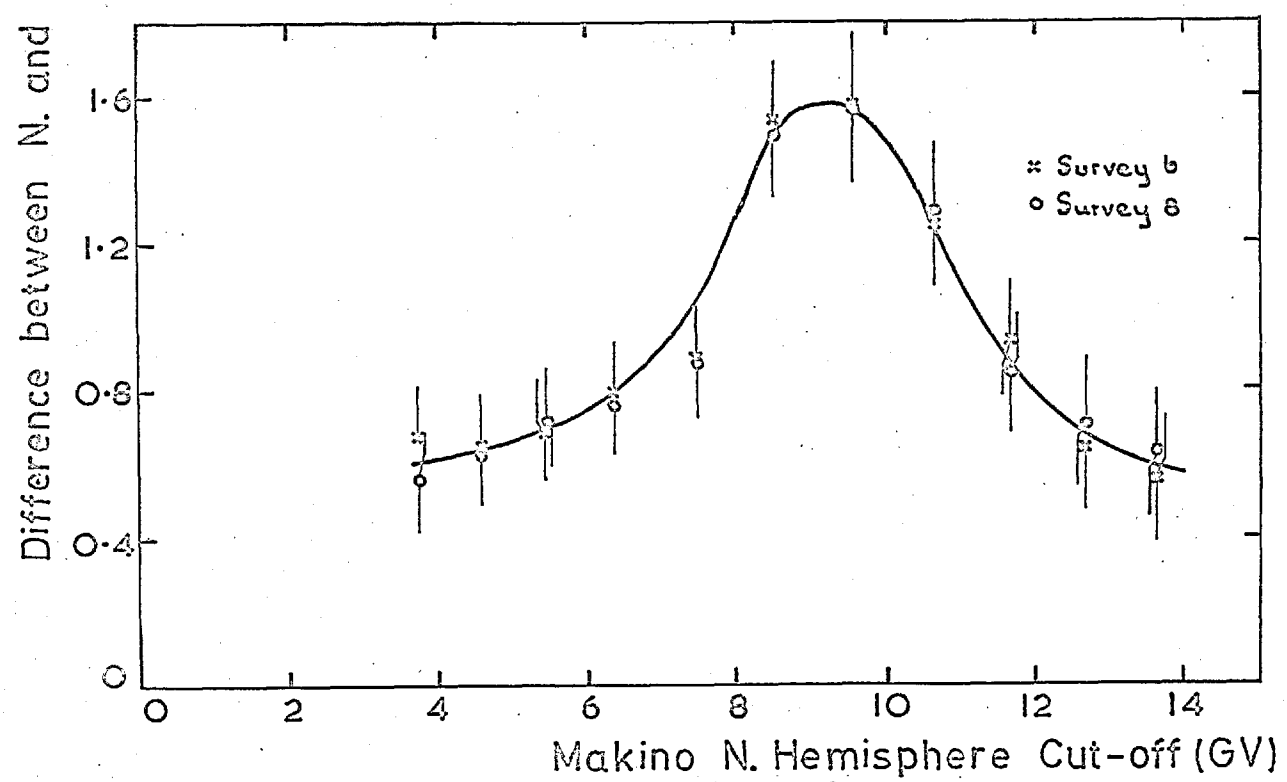


Fig. 5-3.3 Discrepancies between the northern and southern hemishere Quenby-Wenk cut-offs as a function of the northern hemisphere cut-off.

Fig. 5-3.10 Discrepancies between the northern and southern hemisphere Makino cut-offs as a function of the northern hemisphere cut-off.

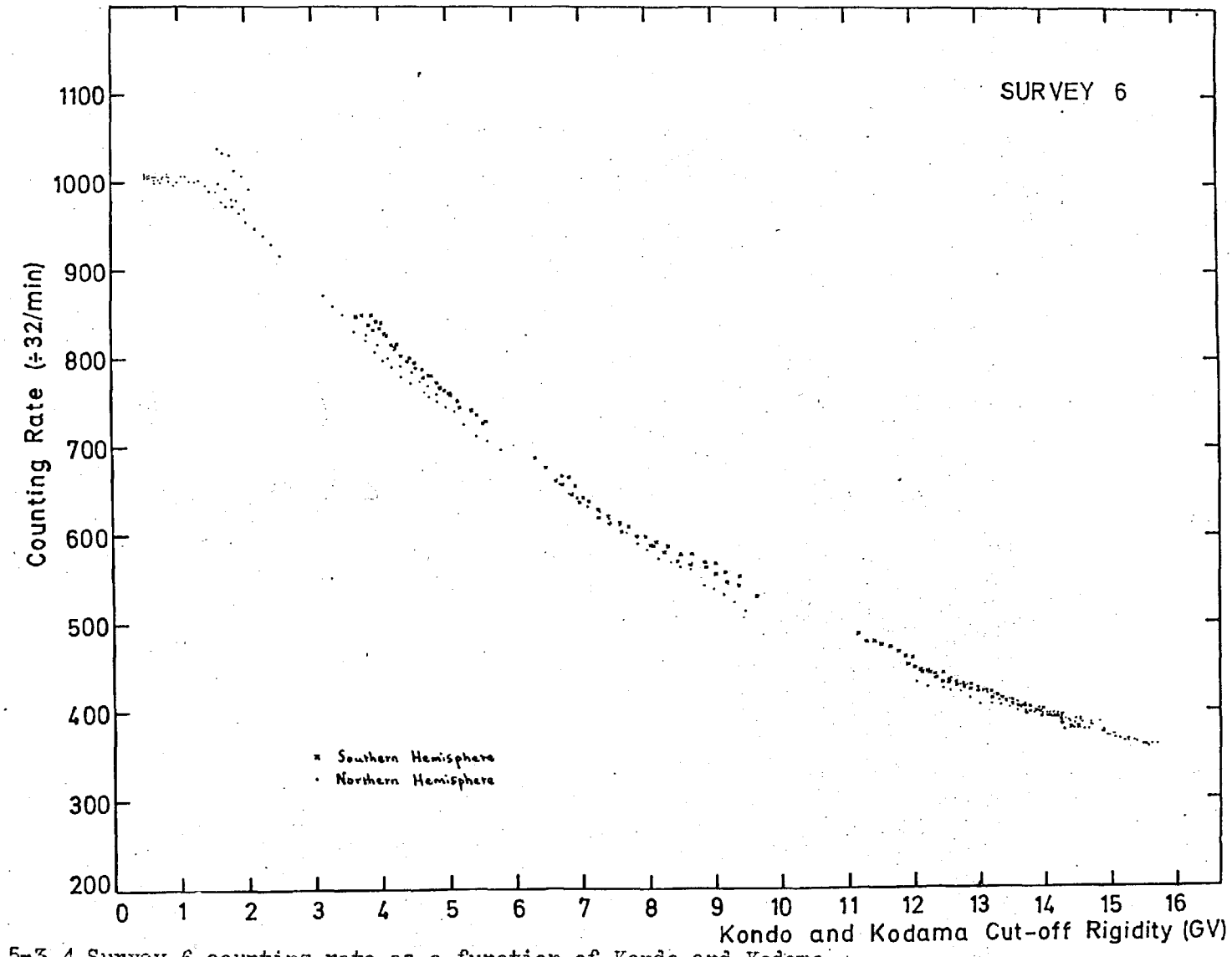


Fig. 5-3.4 Survey 6 counting rate as a function of Kondo and Kodama cut-off rigidity.

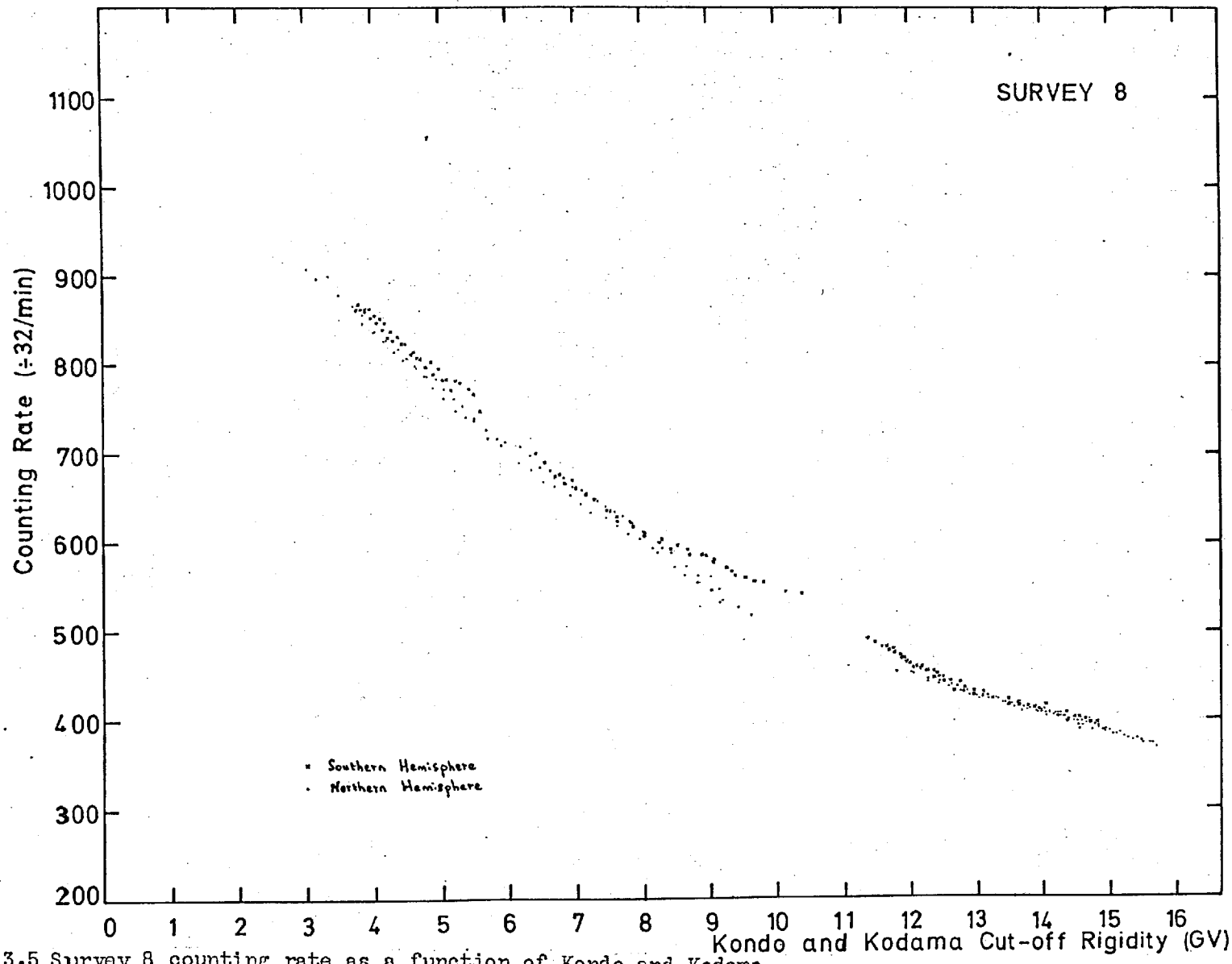


Fig. 5-3.5 Survey 8 counting rate as a function of Kondo and Kodama cut-off rigidity.

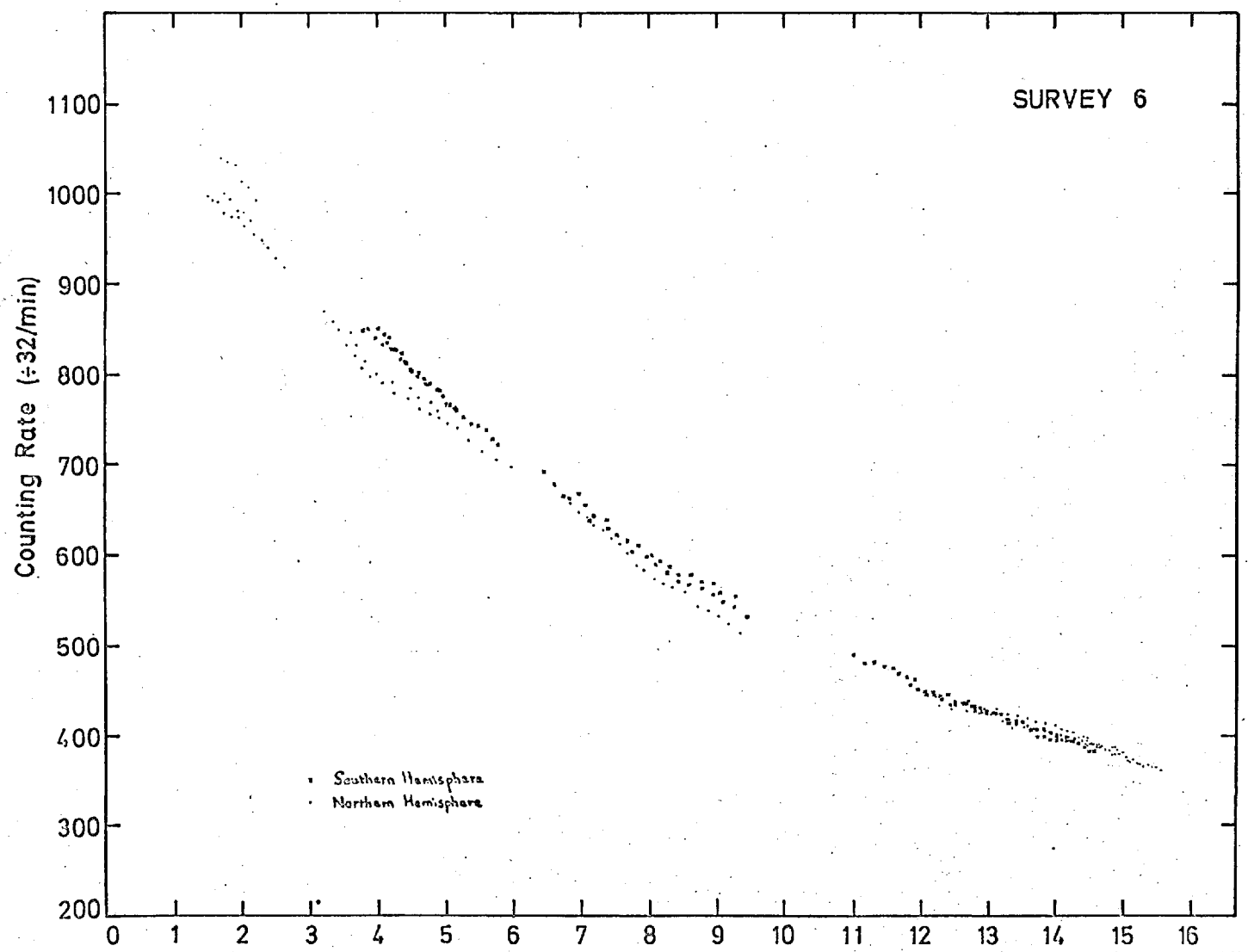


Fig. 5-3.6 Survey 6 counting rate as a function of Shea et al cut-off rigidity.

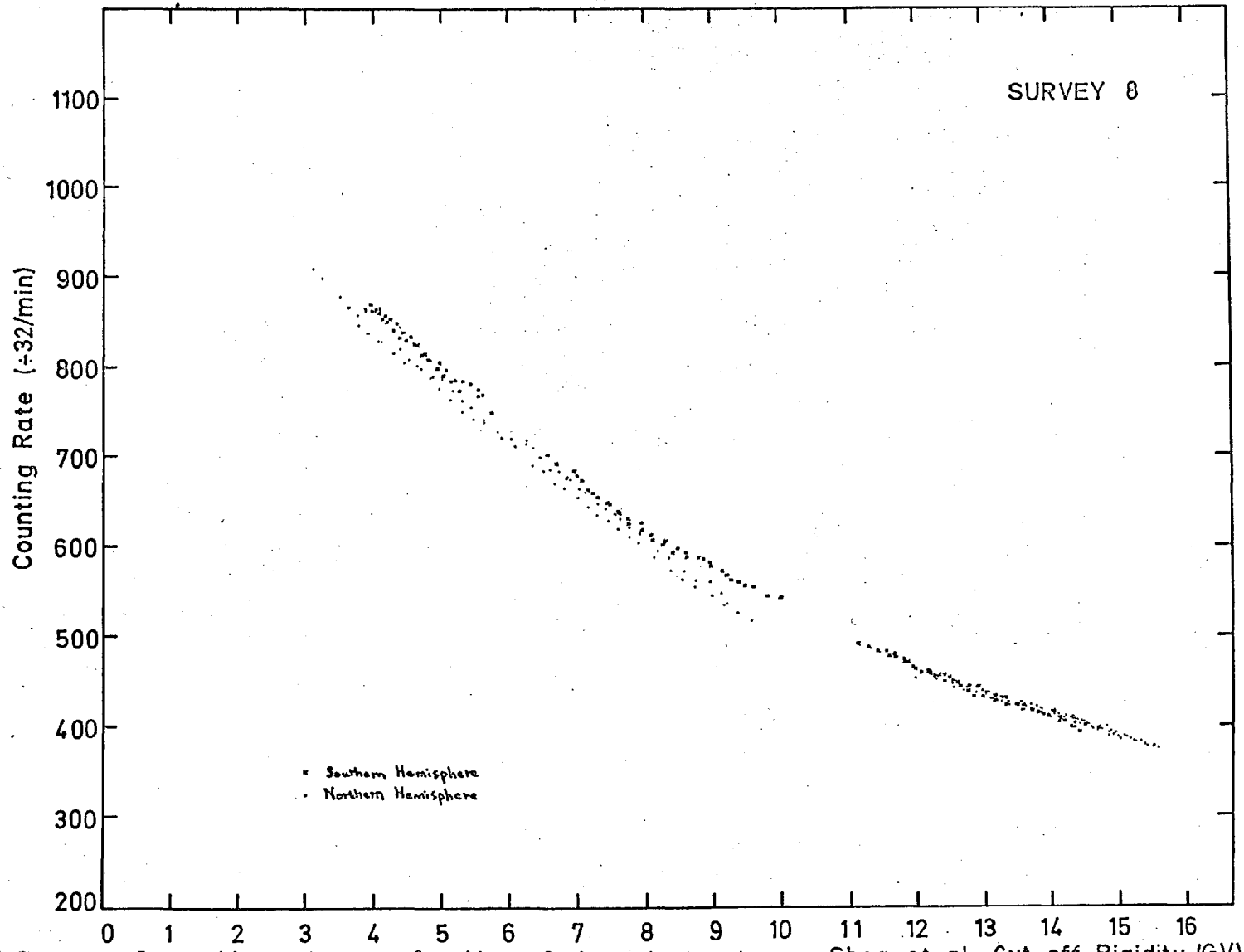
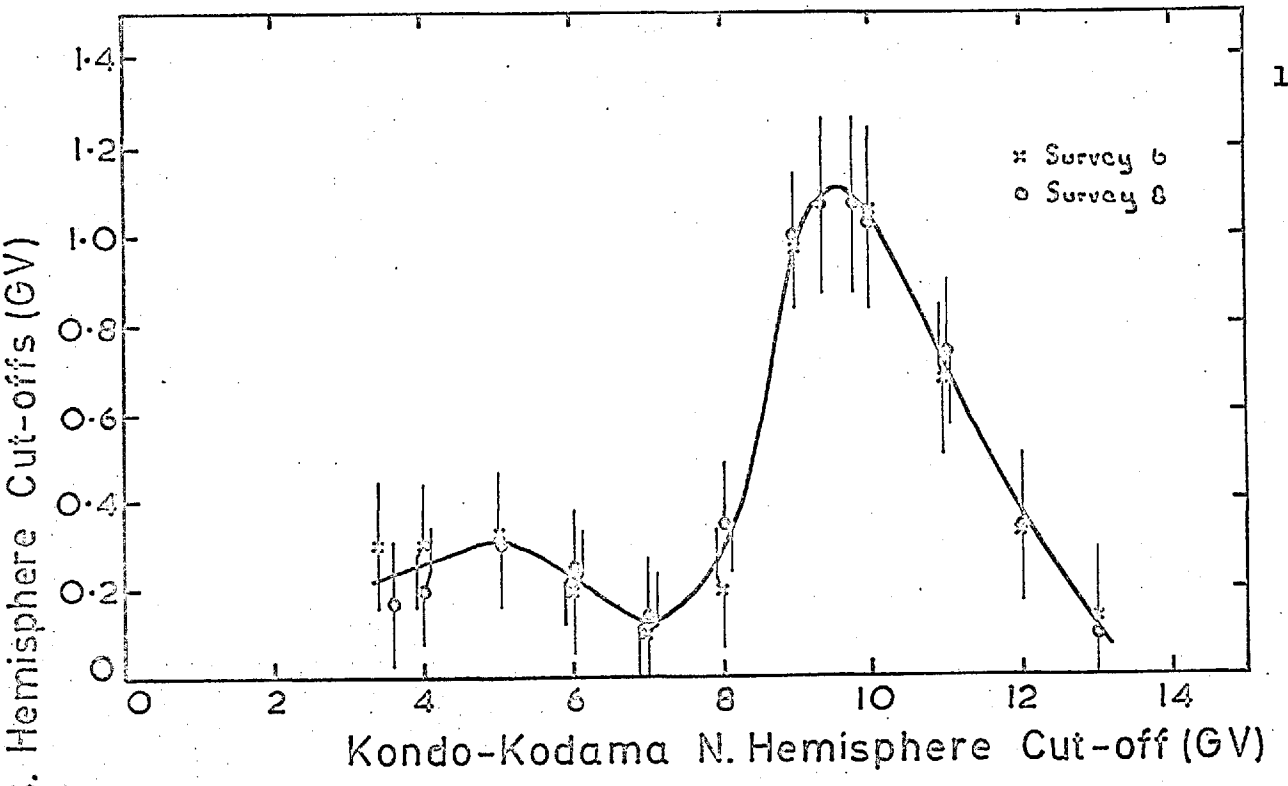


Fig. 5-3.7 Survey 8 counting rate as a function of Shea et al cut-off rigidity.



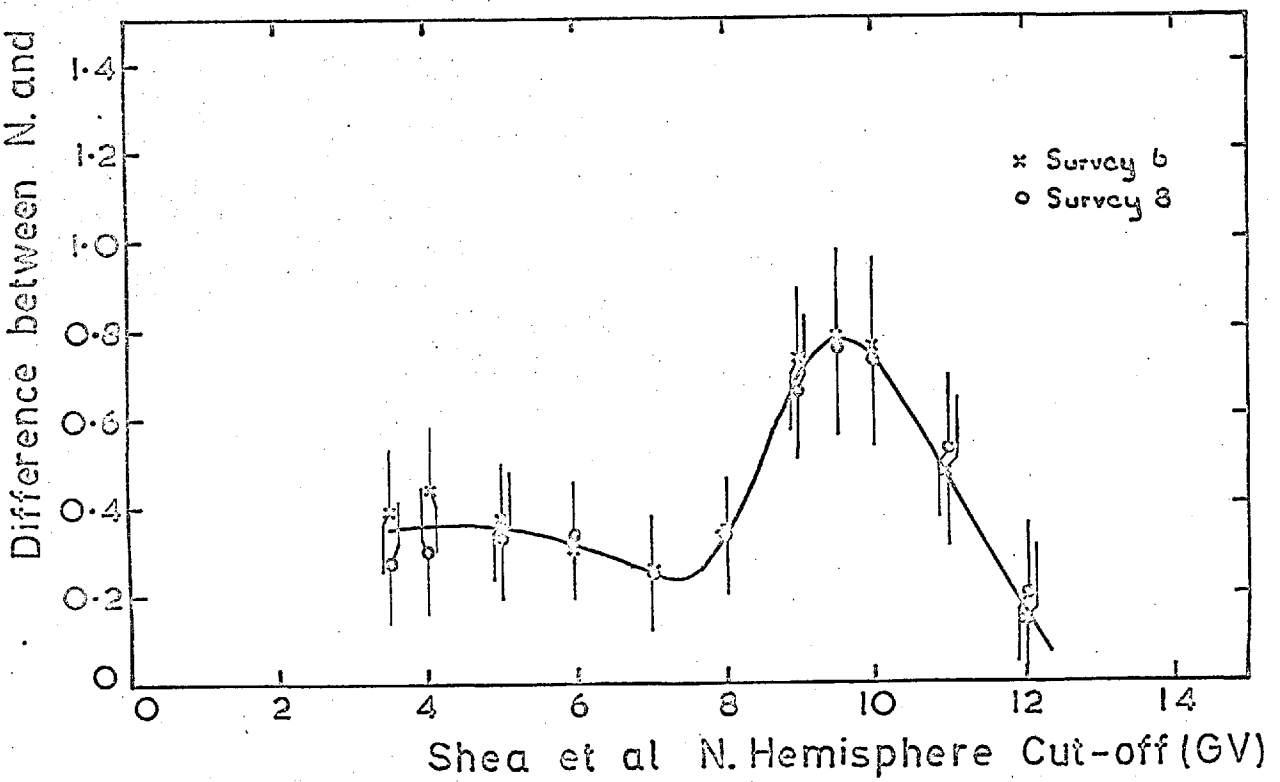


Fig. 5-3.8 Discrepancies between the northern and southern hemisphere Kondo-Kodama cut-offs as a function of the northern hemisphere cut-off.

Fig. 5-3.9 Discrepancies between the northern and southern hemisphere Shea et al cut-offs as a function of the northern hemisphere cut-off.

at 4 GV and ~0 at 8 GV. The data are shown plotted against Kodama (1964) and Shea et al (1966) cut-offs in figures 5.3.4. to 5.3.7. A comparison of the cut-offs of Kodama (1964) and Kondo and Kodama (1966) has shown them to be almost identical in the survey regions. The analysis of the Kodama cut-offs is therefore also applicable to the Kondo and Kodama cut-offs. The Kodama cut-offs are subsequently referred to as Kondo and Kodama cut-offs. Differences in the cut-off rigidities of Kondo and Kodama, and Shea et al are plotted in figures 5.3.8. and 5.3.9. The equatorial cut-off differences, not plotted in these figures, are all zero within the experimental error of $\pm$ 0.2 GV.

A more simplified and less rigorous approach was used for the cut-offs of Makino. Graphically interpolated cut-offs were compared with the cut-offs of Shea et al along the flight route. From this comparison, the cut-off differences curve in figure 5.3.10. was constructed with the aid of figure 5.3.9. This should not differ significantly from the curve given by a more detailed data analysis as used in the first three cut-off models.

The cut-off rigidity models involving trajectory integration are much more successful than the modified dipole calculations. Large differences still remain in the region of 9.5 GV.

A measure of the self-consistency of the cut-off calculations in these regions is given in Table 5.3. by the root mean square of the percentage deviation of the cut-offs from the mean curve.

TABLE 5.3.

R.M.S. DEVIATION OF CUT-OFF RIGIDITIES

Cut-off Calculation	Shea et al	Kondo and Kodama	Quenby and Wenk	Makino
R.M.S. % Deviation	2.8	3.1	11.2	6.5

This is not a good comparative test when used in a region of limited extent as it gives no information as to where the errors occur.

The cut-off rigidities of Shea et al are to be used in preference to those of Kondo and Kodama for the following reasons :

(i) Improved ordering of the data.

(ii) Convenience of the fine mesh 2×2 degree L interpolated grid.

(iii) More detailed cut-off calculations using rigidity steps of 0.01 GV against 0.1 GV of Kondo and Kodama.

5.4. L INTERPOLATED CUT-OFFS

The availability of the locations of the trajectory computed cut-offs used as the basis for the 2×2 degree L interpolated grid allows a more detailed investigation.

The 2×2 degree grid is being continuously up-dated through the introduction of a greater number of trajectory computed cut-offs as the basis for the interpolation. Figure (5.4.1) shows plots of 2 × 2 degree cut-off grid points against latitude for several longitudes near the Greenwich meridian. These curves constructed from a grid dated July 1, 1966 are compared to those from a previous 2×2 grid of March 1st, 1966 . The later grid points are affected in this region only through the introduction of a machine computation at the location (35°N 0°E). The effect has been to produce a hump in the curves of $\pm 5^{\circ}$ latitude extent. Figure (5.4.2) shows a plot through latitude 35°N of the differences in cut-off between the July 1st and March 1st grid points against geographic longitude. This reveals the longitude effect of the introduction of 3 trajectory calculations into the July 1st grid at longitudes 330°, 345° and 0° east. Similar longitude plots along the latitude parallels 30°N and 40°N do not show the effects of these three calculations. The threshold rigidity humps extend over $\pm 5^{\circ}$ latitude, $\pm 15^{\circ}$ longitude. The introduction of smoothing over such a limited region seems rather arbitrary with the result that the L interpolated points around trajectory computed cut-offs in this area would appear to be in error.

The aircraft survey flight path passes close to the region represented in figure (5.4.1), crossing the 35°N latitude parallel at 12.5°E. This point can be seen to be unaffected by the inclusion of the neighbouring calculation at (35°N 0°E). Because of the arbitrary smoothing over $\pm 15^{\circ}$ longitude it might be expected that the

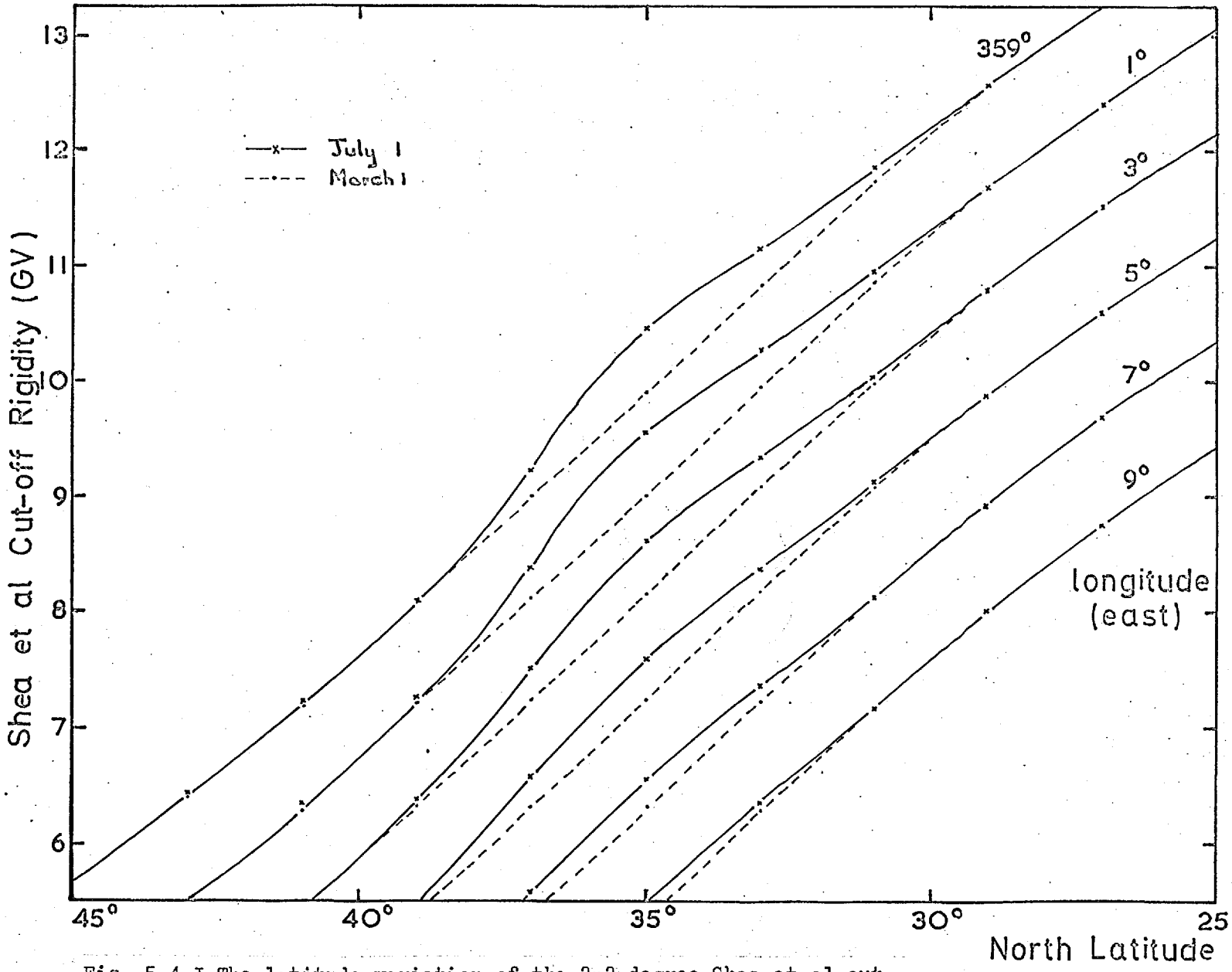


Fig. 5-4.I The latitude variation of the 2x2 degree Shea et al cut-off grid values at several longitudes near the position 35°N, 0°E. The solid line is from an up-dated cut-off grid.

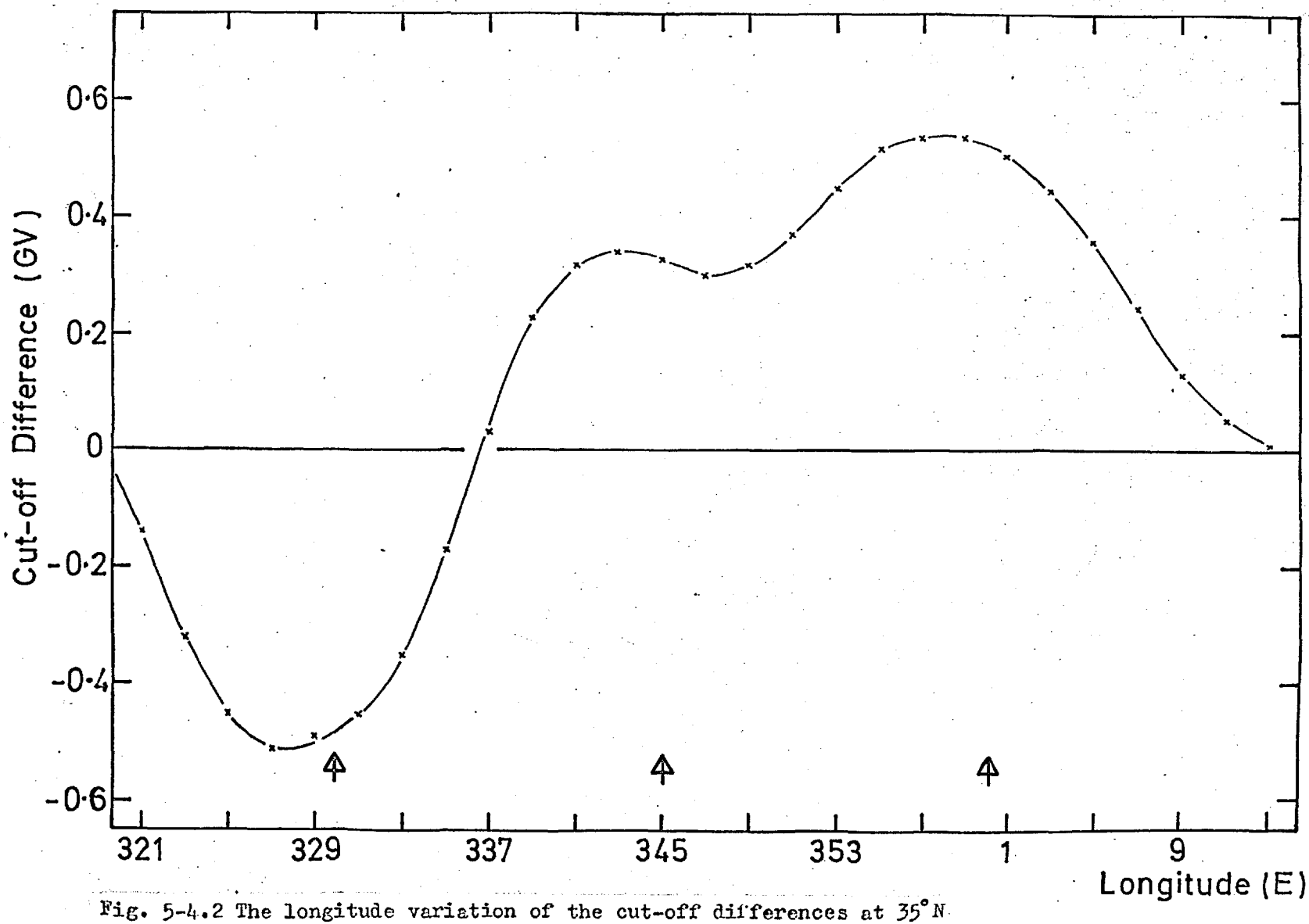
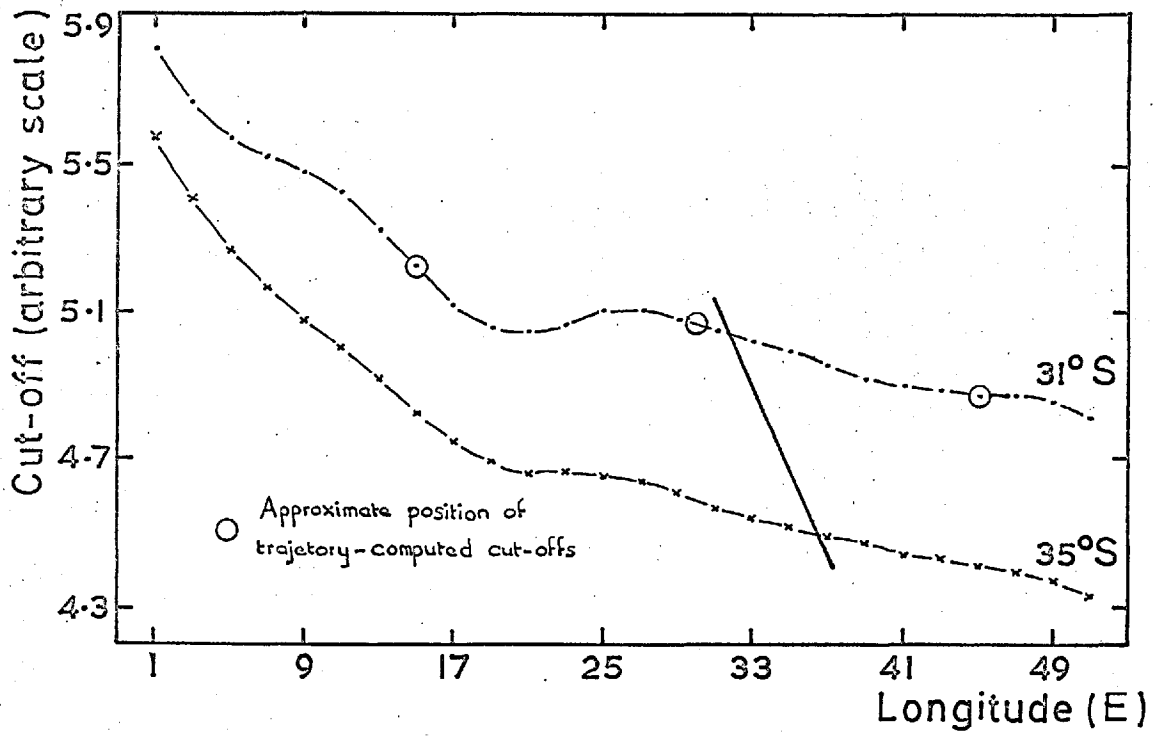


Fig. 5-4.2 The longitude variation of the cut-off differences at 35°N between the Shea et al 2 × 2 degree grid values of 1 March 1966 and the up-dated grid values of 1 June 1966. The positions of three trajectory-computed cut-offs introduced into the later grid are shown.



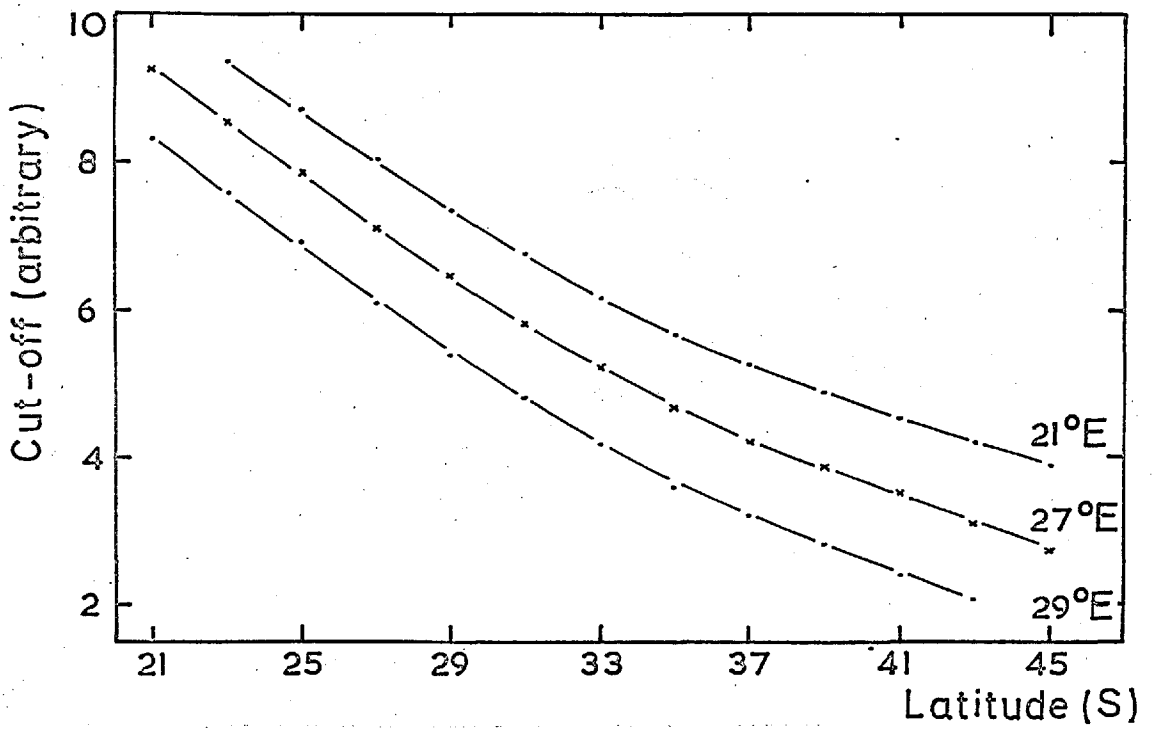


Fig. 5-4.3 The longitude variation of the Shea et al cut-off grid values at 31 S and 35 S in the region of the flight path. Locations close to the trajectory-computed cut--ffs in this region are shown.

Fig. 5-4.4 The latitude variation of the Shea et al cut-off grid values in the same region covered by fig. 5-4.3.

L interpolated cut-off at (35°N 12.5°E) is low. In addition the cut-off differences in figure (5.3.9) are a maximum at the northern hemisphere cut-off of 9.5 GV (34.9°N 12.5°E) . Two cut-off computations were performed by Shea (1966) at the positions (34.9°N 12.5°E) and (20.5°S 30.0°E) both of which have a threshold of 9.50 GV as obtained from the 2×2 degree grid of July 1st 1966. The results of these calculations are given in Table (5.3).

TABLE (5.3)

COMPARISON OF L INTERPOLATED AND TRAJECTORY CALCULATED CUT-OFFS.

Lat.	Long.	P_M	P_S	P_C	P_L
34.9	12.5	10.43	8.39	9.82	9.50
-20.5	30.0	10.03	8.39	9.46	9.50

The L interpolation would be expected to be more successful as an interpolation for the Störmer cone threshold (P_S) than for the effective cut-off (P_C) . As these two points have the same Störmer cone threshold 8.39 GV and the same L interpolated cut-off (P_L) 9.50 GV, then the error must lie in the inaccurate interpolation of the penumbral contribution.

The northern hemisphere calculation shows that the L interpolated value is low by 0.32 GV. From the previous discussion, the closer the L interpolated points are to trajectory computed points the less they will

be in error.

Errors are likely to be larger in the northern hemisphere where the trajectory calculated points form a coarse 15 x 15 degree grid in comparison to the finer 5 x 15 degree grid in the southern hemisphere.

A longitude variation in figure (5.4.3) of the cut-off was noticed at 31° S in the region of 20°E. The grid points circled are close to the basic trajectory integrated grid points. This is to be compared with the variation along the 35° S latitude parallel. This effect will probably be a product of the interpolation. The positions of the flight path are also indicated in the figure. The smooth latitude variation in this area obtained in figure (5.4.4) indicates that the ± 5° latitude separation of the computed cut-offs is close enough for successful interpolation by the L parameter. The large variation of cut-off rigidity with longitude in this region is probably the reason for the longitude variation in figure (5.4.3).

SUMMARY.

(i) L interpolated cut-offs in the region of (35°N 12.5°E) have been shown to be in error by ~ 0.3 GV. The magnitude of the error depends upon the proximity to a computed cut-off grid point. Greater accuracy in the cut-offs will result from a finer 5 x 15 degree computed threshold grid in the northern hemisphere area.

(ii) The 15 degree longitude interval in the basic computed cut-off grid is too coarse in regions such as the South African area where there is a large longitude gradient in the cut-off rigidity.

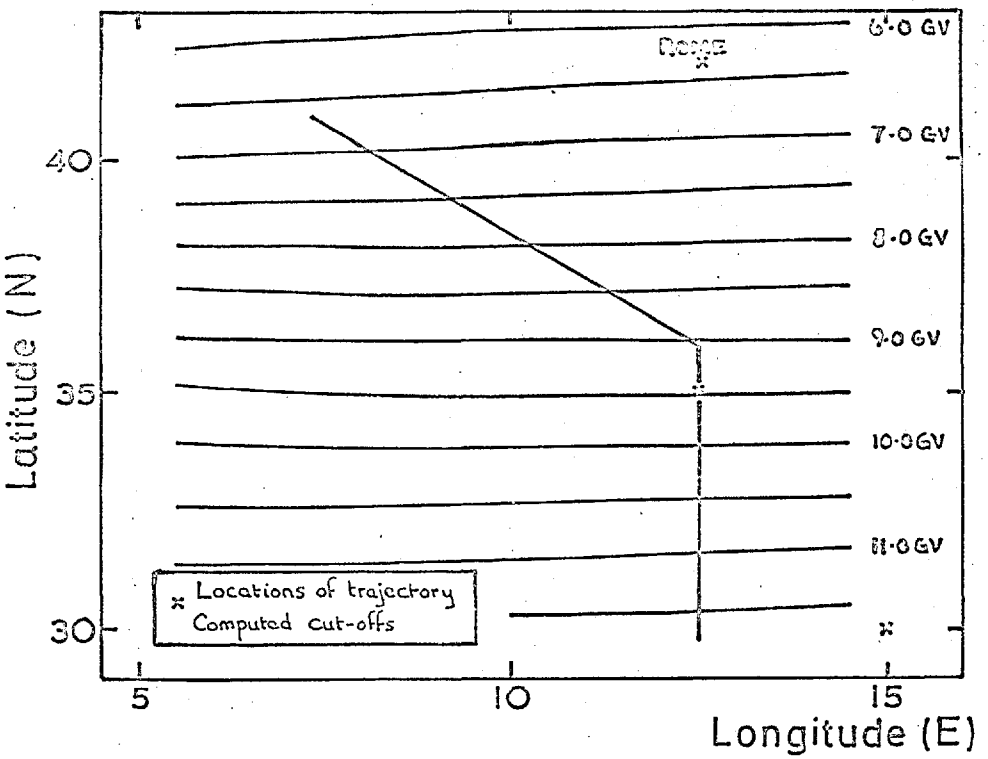
Application of an interpolation based upon the L parameter will probably lead to inaccuracies.

5.5. SOURCES OF CUT-OFF ERRORS.

5.5.1. Correction for L Interpolation errors.

Figure (5.5.1) shows the flight route in the neighbourhood of (35°N 12.5°E). The route passes close to a trajectory computed point at (30°N 15°E) where the cut-off rigidity is ~ 11.8 GV. The error due to interpolation near 11.8 GV in the northern hemisphere will therefore be small. From the observed variation of the north-south cut-off differences and the error in the northern cut-off at 9.5 GV, the probable variation of these differences after allowing for the N.hemisphere L interpolation errors near 9.5 GV is given in figure (5.5.2).

The symmetry of the threshold differences curve caused by the sag in the L interpolated cut-offs in the northern hemisphere suggests that the cut-off error is small at 7.1 GV. This corresponds to the position where the flight path crosses the 40°N latitude parallel as can be seen in figure 5.5.1. The corrections required for the flight path cut-offs therefore add a 'hump' of approximately $\pm 5^{\circ}$ latitude extent to the cut-off versus latitude curve. This is similar to the effect of the addition of the calculation at (35°N 0°E) in figure 5.4.1. The experimental evidence suggests that the 'hump' noted in figure 5.4.1. is probably a real effect in this region and that it extends to at least 12.5°E. A machine computation of Shea et al (1965) at Rome (41.9°N, 12.52°E) gave the cut-off as 6.31 GV. This is precisely



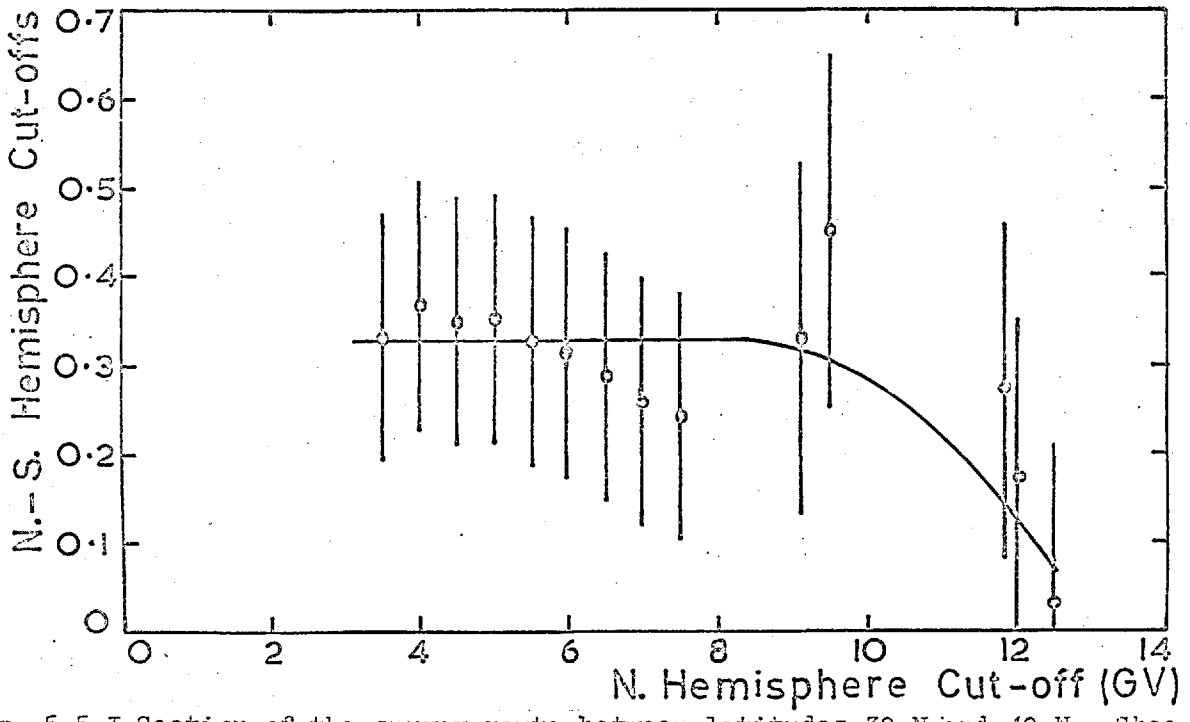


Fig. 5-5.I Section of the survey route between latitudes 30 N and 40 N. Shea et al contours of constant cut-off rigidity are drawn. The locations of trajectory-computed cut-offs in this region are marked.

Fig. 5-5.2 The discrepancies remaining between the northern and southern hemisphere cut-offs after correcting for the cut-off errors near 34 9 N, I2 5 E plotted against the northern hemisphere cut-offs.

the value obtained by interpolation from the 2 × 2 degree grid. The L interpolation errors in that area do not therefore extend to 41.9°N.

A 'hump' in the latitude variation of the cut-off rigidity in the northern hemisphere at 12.5°E has been observed experimentally. This is in qualitative agreement with the 'humps' apparent in the 2 × 2 degree cut-offs at 35°N as calculated by Shea et al. The 'hump' peaks in the July 1st. 2 × 2 degree L interpolated cut-off grid coincide with the additional trajectory computed cut-offs at the three locations along 35°N (figure (5.4.2)). This could mean that the 'humps' are even larger and that the peaks appear at 35°N because of the use of the L interpolation at surrounding positions. This would appear to be more plausible than the occurance of 'humps' in the cut-offs, all coinciding with the 35°N latitude parallel. Qualitatively this is supported by two facts:

a) The 'hump' region should extend eastwards to 12.5°E whereas the L interpolated cut-offs have smoothed it out at this longitude.

b) The 'hump' as mentioned in section 5.4. is probably a penumbral effect in which case the L interpolation would not reproduce the true shape.

The actual shape of the 'hump' can only be measured by the use of trajectory integration to determine the cut-offs at points between 30°N and 45°N. The completion of the 5 × 15 degree grid of trajectory computed cut-offs in this region will probably define the 'hump' more

accurately.

The differences remaining in the north-south cut-offs are partly attributable to L interpolation errors in both the northern and southern hemispheres. That the differences cannot be wholly explained by the L interpolation is illustrated by the intensities recorded at the two locations given in Table 5.4.

TABLE 5.4.

COSMIC RAY INTENSITY AT POINTS WITH THE SAME L INTERPOLATED CUT-OFF.

Survey 8 Intensity.	Lat.	Long.	L interpolated cut-off.
808 counts (÷ 128)	45.8°N	2.3°E	4.48 GV
828	35.1°S	34.75°E	4.49 GV

These locations are close to the locations (45°N 0°E) and (35°S 35°E) where trajectory integrated cut-offs have been calculated. The interpolation errors should be small, yet the intensity recorded at the southern point is 2½% greater than that at the northern point.

The remaining systematic difference must be due to the inaccurate definition of the magnetic field in the region of the surveys. If the magnetic field as defined by a field simulation is in error in a particular area then cut-off rigidities in this region will be affected.

If the representation is low (say) then the predicted thresholds in the immediate vicinity will be low. Penumbral particles oscillate from hemisphere to hemisphere before arriving at a particular point. The 'low' region will therefore influence the trajectories of these particles, having the greatest influence on those which will arrive at the opposite hemisphere just to the west of the 'low' region. The computed trajectory of such a particle passes through the 'low' field then travels to the west and to the opposite hemisphere. The trajectory intersects the Earth at a higher latitude than it would in the real field. The effect is therefore to increase the rigidity required of a particle to penetrate the 'low' field region to reach the opposite hemisphere location.

An inaccurate field definition will thus result in a systematic lowering of cut-offs in one hemisphere and a raising in the other.

5.5.2. Neutron Monitor Survey

An overland neutron monitor survey by Carmichael et al (1966) revealed several cut-off discrepancies over North America. It was observed that a smooth curve of intensity against cut-off rigidity could not be fitted to the data. The cut-offs were calculated using trajectory integration at steps of 0.1 GV. A smooth curve was drawn through the data and from this the corrected cut-offs were estimated. Several of the experimentally corrected cut-offs are given in Table 5.5. Added to these cut-offs are the L interpolated values. The latitude curve using the latter cut-offs is drawn in figure 5.5. These cut-offs provide a satisfactory fit to the experimental data.

TABLE 5.5

A COMPARISON OF EXPERIMENTALLY SMOOTHED CUT-OFFS (CARMICHAEL et al : 1966) AND L INTERPOLATED CUT-OFFS.

Location	Relative Neutrons	Trajectory Integration (Carmichael et al)	Experimentally Smoothed	L Interpolated Cut-offs.
Acapulco	0.659	10.55	10.58	10.97
Mexico City	0.697	9.45	9.48	9.87
San Luis Potosi	0.731	9.15	8.50	9.0
Saltillo	0.792	7.25	7.15	7.52
Climax	0.961	3.15	3.08	3.11
Denver	0.966	3.15	2.93	2.97
Mt.Washington	1.0	1.24	1.24	1.24

TABLE 5.6

LATITUDE KNEE CUT-OFF RIGIDITY

SURVEY	KNEE CUT-OFF (GV)
1	1.46 ± 0.1
2	1.30 ± 0.1
3	1.45 ± 0.05
4	1.43 ± 0.05
5	1.45 ± 0.08
6	1.40 ± 0.01
7	1.38 ± 0.07
8	1.40 ± 0.08
9	1.38 ± 0.1
11	1.43 ± 0.1
12	1.35 ± 0.08

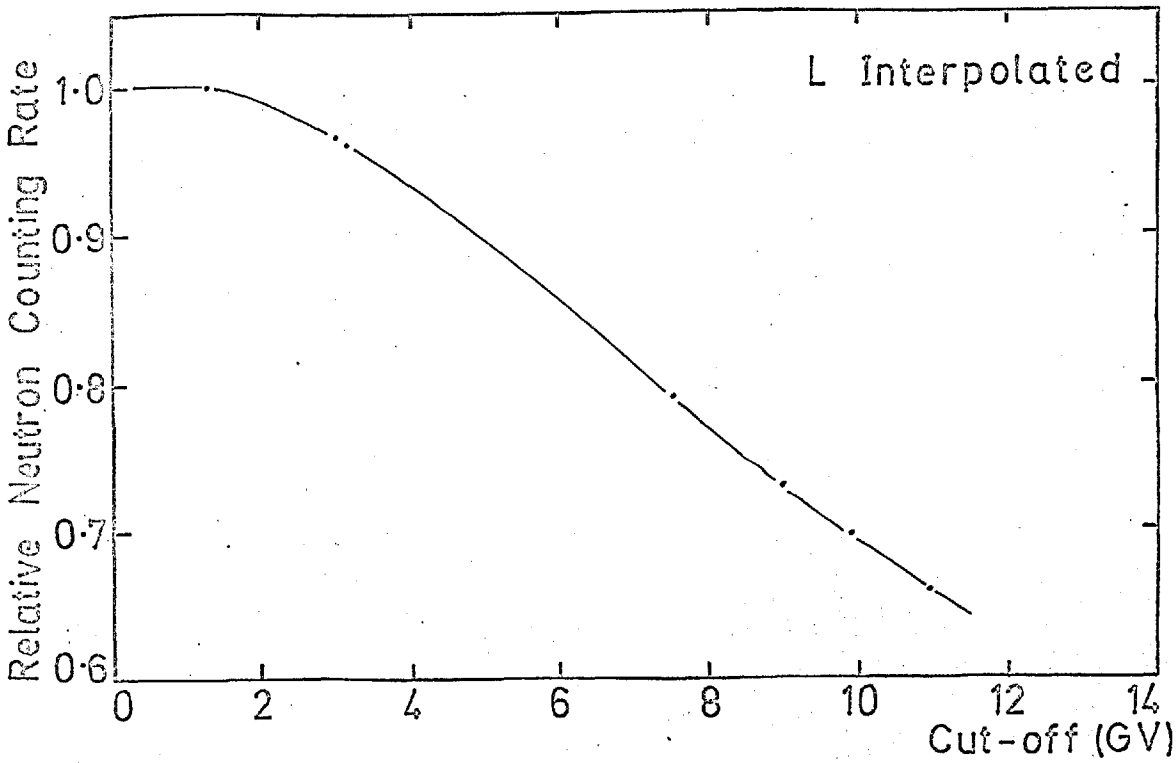


Fig. 5-5.3 The neutron monitor data of Carmichael et al (1966) plotted against the cut-offs of Shea et al.

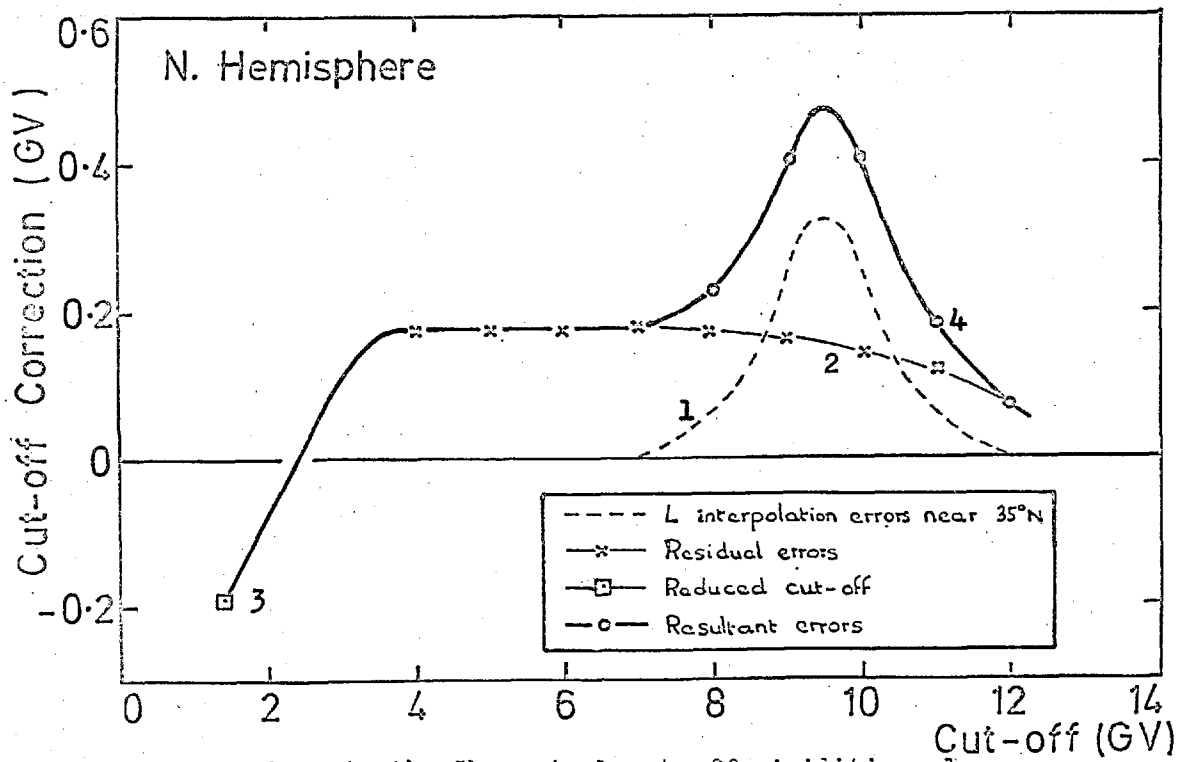


Fig. 5-6.I Corrections to the Shea et al cut-off rigidities along the flight path in the northern hemisphere. The solid curve represents the sum of corrections due to the high latitude theshold reduction by external fields, L interpolation errors near 34 9 N, I2 5 E, and the mean of the residual differences from fig. 5-5.2.

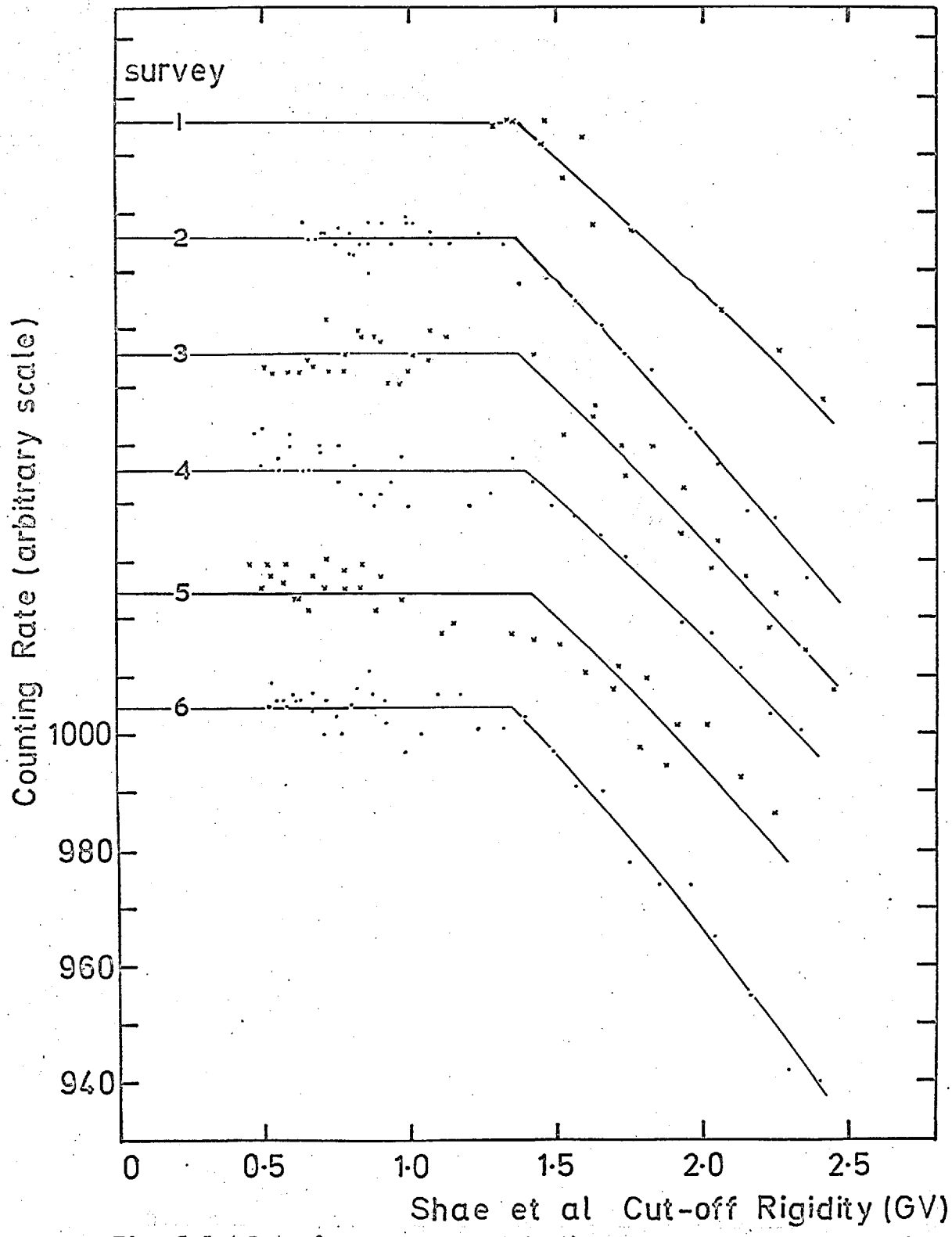


Fig. 5-5.4 Data from surveys I-6 in the region of the intensity knee as a function of the Shea et al cut-offs.

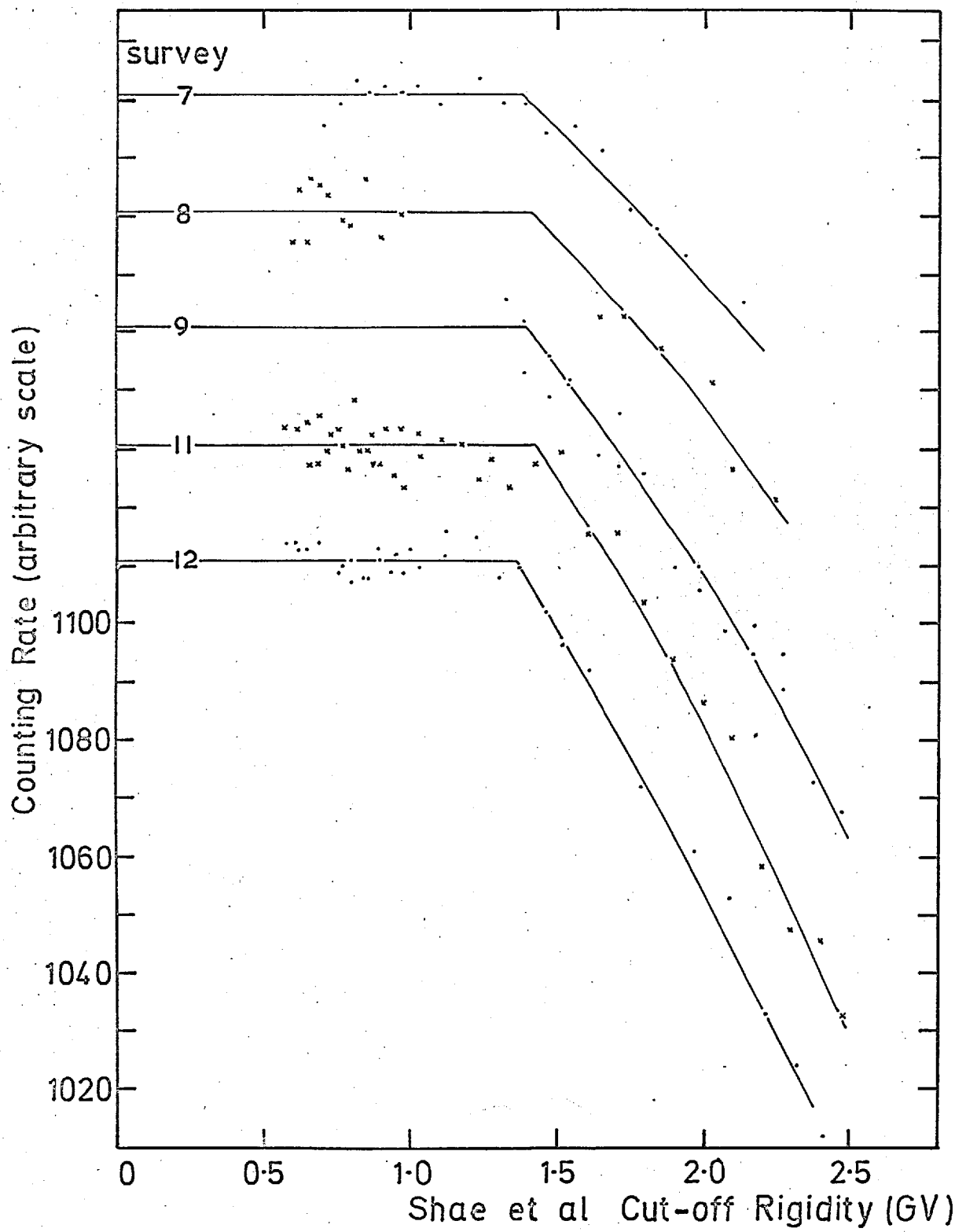


Fig. 5-5.5 Data from surveys 7-9, II and I2 in the region of the latitude knee as a function of the Shea et al cut-offs.

The cut-off rigidity for Mexico City, one of the locations for the survey data, was calculated by Shea et al (1965) to be 9.53 GV while the L interpolated value is 9.90 GV. This does not produce a significant difference in the neutron intensity curve as the statistical accuracy of the data is 1%. Although the Mexico City L interpolated cut-off is in error by 5% the data used are not sufficiently accurate or numerous to observe the error.

5.5.3. The Latitude Knee.

In figures 5.5.4 and 5.5.5, the high latitude data from 11 surveys are plotted against the cut-offs of Shea et al. The knee in the intensity distribution is sharply defined and its position did not vary during the period of the surveys. The positions of the cosmic ray knee determined from these surveys are given in Table 5.6. The mean position of the latitude knee is $(1.39 \pm .05)$ GV. The geographic coordinates of this position are (57.7°N 5°W) which corresponds to a geomagnetic latitude of $\sim 61^{\circ}$.

The presence of low energy primary particles with rigidities below 1.4 GV during the periods of these surveys has been established by balloon observations [for example Courtier and Linney (1966)]. The knee must therefore be due to atmospheric absorption of the primary particles of rigidity 1.39 GV and less. The differential number spectrum of the secondaries at low rigidities is shown in section 6.3 to be almost entirely due to the incident proton flux. Protons in a given absorber have a definite range-energy relationship. The momentum of a proton which will penetrate 145 g cm^{-2} atmosphere and the recorder

to just record a coincidence is 1.2 GeV/c. Heavier primaries at this rigidity split up into separate nucleons after about their first collision. These nucleons, because of their slower velocity, are absorbed before reaching the recorder scintillators. The experimental spread of .05 GV in the mean cut-off at the position of the knee is probably greater than the inaccuracy of the Shea et al L interpolated cut-off for the following reasons :

(i) The L interpolation becomes a better approximation at high latitudes.

(ii) The penumbral contribution to the cut-off is small ($\sim$ 0.05 - 0.1 GV).

(iii) The longitude variation of cut-off is small ($\sim$0.02 GV per degree) coupled with the fact that the knee location is only 1.3° of latitude from 60°N along which the basic integrated trajectory cut-off grid points are located.

The cut-off at this point is thus (86%) $\pm$ 4% that due to the Earth's main core magnetic field. The penumbral width in this region is $\sim$0.15 GV, opacity $\sim$50% and the Störmer threshold $\sim$1.32 GV.

5.5.4. Comparison of Threshold Reduction with Balloon Observations.

The cut-off rigidity calculated by Shea et al (1965) for Minneapolis ($\lambda = 55.5^{\circ}$ geomagnetic) is 1.39 GV. Experimentally, the main cone quiet time threshold has been observed to be 1.20 GV by Freier (1962) during solar events. Webber and McDonald (1964) consider from observations of cosmic rays that the cut-off is 1.0 - 1.1 GV.

This implies a quiet time reduction of ~ 30%.

Both the ring current and geomagnetic tail models of threshold reduction would predict a smaller reduction at the lower geomagnetic latitude. The statistical accuracy of the present result is greater than the balloon cosmic ray observations of Webber and McDonald. It seems unlikely that the reduction at Minneapolis should exceed that at 61° geomagnetic. Accepting the accuracy limit of the present measurement the reduction at Minneapolis is probably ~ 17%. This would imply a quiet time cut-off at 1.15 GV. This cut-off is in good agreement with the penumbral transparencies given by 1.18.

5.5.5. Comparison of Threshold Reductions with Theory.

(a) The Magnetic Tail.

The effect of the magnetic tail model at latitudes much below the auroral latitudes is uncertain although qualitatively there will be a lowering of the cut-offs.

The cut-off rigidity reduction given by Sauer and Reid in figure 1.7.2. at $\lambda = 61^{\circ}$ geomagnetic is ~30%. This is in the extrapolated region beyond their auroral latitude calculations. However, from the magnitude of the estimated reduction this would appear to be a promising source of threshold reduction.

(b) The Quiet-Time Ring Current.

The threshold reduction at high latitudes is given by equation 1.21. Assuming that this equation is applicable at a geomagnetic latitude of 61°, the ring current magnetic moment required to explain

the observed thresholds is :

$$M' \simeq 0.3\ M \qquad 5.1$$

The average contribution to the magnetic moment from a particle of energy ε in the mean magnetic field B at the ring current position was given by Kellogg and Winckler (1961) as :

$$M' = \frac{2\varepsilon}{B} \qquad 5.2$$

If the total number of particles of mean energy $\bar{\varepsilon}$ contributing to the moment is N then :

$$M' = \frac{2N\bar{\varepsilon}}{B}$$

$$= \frac{2\omega}{B} \qquad 5.3$$

where ω is the total energy in the belt. For a ring current at L = 3.5 earth radii, the field B is related to the surface field B_o (= 0.32 gauss at the equator) by :

$$\frac{B}{B_o} = \frac{1}{L^3} \qquad 5.4.$$

$$\therefore \quad B = 7.4 \times 10^{-3} \text{ gauss.}$$

The energy ω required is :

$$\omega = \frac{BM'}{2} = 3.7 \times 10^{-3} \times .3 \times 8.1 \times 10^{25}$$

$$= 9.0 \times 10^{22} \text{ ergs.} \qquad 5.5.$$

The magnetic effect at the ground is given by equation (1.22)

$$B(o) = \frac{2}{3} \times \frac{9 \times 10^{22}}{8.4 \times 10^{24}} \times 0.32 \text{ gauss}$$

$$= 230\ \gamma \qquad 5.6$$

If the ring current moment is due primarily to protons of energy $E_p \simeq$ 10 KeV and these are approximately isotropically distributed in the volume of the ring, then their omnidirectional intensity may be calculated.

If the ring occupies a volume (V) from L = 2.8 to L=4 and λ = 35°S to 35°N , then the number density is given by :

$$N = \frac{\omega}{V E_p}$$

$$= \frac{9.0 \times 10^{22}}{V \times 10^{4} \times 1.6 \times 10^{-12}} \quad \text{cm}^{-3}$$

$$= \frac{9 \times 10^{22}}{2.10^{20} \times 1.6} \quad \text{cm}^{-3}$$

$$\simeq 300 \quad \text{cm}^{-3} \qquad 5.7$$

The omnidirectional flux Nv is

$$\sim 300 \times 1.3 \times 10^{8} \quad (\text{cm}^2 \text{sec})^{-1}$$

$$\simeq 4 \times 10^{10} \quad (\text{cm}^2 \text{sec})^{-1} \qquad 5.8$$

From equations 1.21 and 1.22

$$\frac{M'}{B(o)} \quad \alpha \quad \frac{1}{B} \qquad 5.5$$

Magnetometer observation has shown the enhanced ring current to be near L = 3.5 earth radii. In addition, the greatest particle intensities have been observed near this L value. The quiet-time ring current must therefore lie at L ~ 3.5 Re. The value of B in 5.5 cannot therefore be varied very much. A ring current of moment 0.3× M at L = 3.5 earth radii is incompatible with limitations on the surface field effects as discussed in section 1.7.1.

The observed cut-off reductions are probably not due entirely to the quiet time ring current. A complete theory should involve a detailed magnetic mapping of the magnetosphere. This information could then be used in the trajectory integration computer program.

5.6. CORRECTED CUT-OFF RIGIDITIES.

In figure (5.6.1) are shown the three probable error sources in the Shea et al northern hemisphere cut-offs. Curve 1 is the probable variation of the error due to the L interpolation near 35 N 12.5 E. Curve 2 is the mean of the residual cut-off differences between the northern and southern hemispheres after removing the error of curve 1. The third source is the reduced cut-off at 1.39 GV due to magnetic fields having sources external to the earth. The experimental evidence suggests that the reduction in cut-offs occurs only at high latitudes. The curve 3 is drawn to join smoothly to curve 2 at 3-4 GV. The sum of these three error

sources, curve 4, represents the errors in the northern hemisphere cut-offs.

The removal of these errors brings about a notable improvement to the northern hemisphere latitude curve of survey 6 plotted in figure (5.6.2). The resulting curve varies more smoothly than the curve obtained by plotting the data against the cut-offs of Shea et al.

5.7 COMPARISON OF CUT-OFF CALCULATIONS.

Figures (5.7.1) to (5.7.3) have been constructed by comparing the various calculated cut-offs in the areas of the flight path with the experimentally corrected cut-offs. The root mean square percentage deviations from the corrected cut-offs are given in Table (5.7) for cut-offs above 4.0 GV so as to exclude the effects of fields of external origin.

TABLE (5.7)

R.M.S. DEVIATIONS FROM EXPERIMENTALLY CORRECTED CUT-OFFS.

REGION	Quenby and Wenk	Makino	Kondo and Kodama	Shea et al.
Anomalous Magnetic Region (corrected cut-offs < 10 GV).	17.4	3.4	3.5	2.4
Non-anomalous region	4.09	7.04		

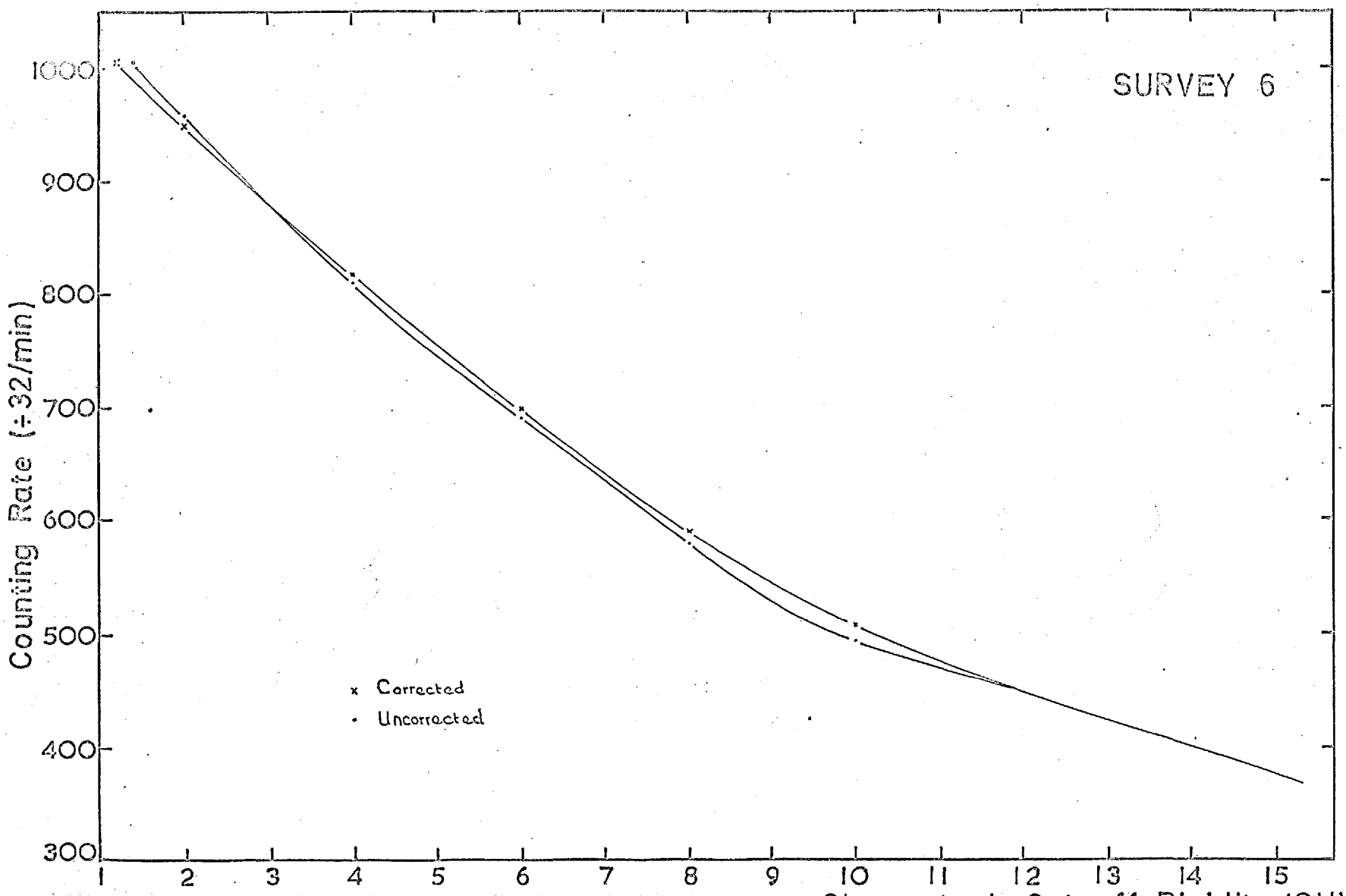


Fig. 5-6.2 The northern hemisphere data of survey 6 plotted against the Shea et al cut-offs and the experimentally corrected cut-offs.

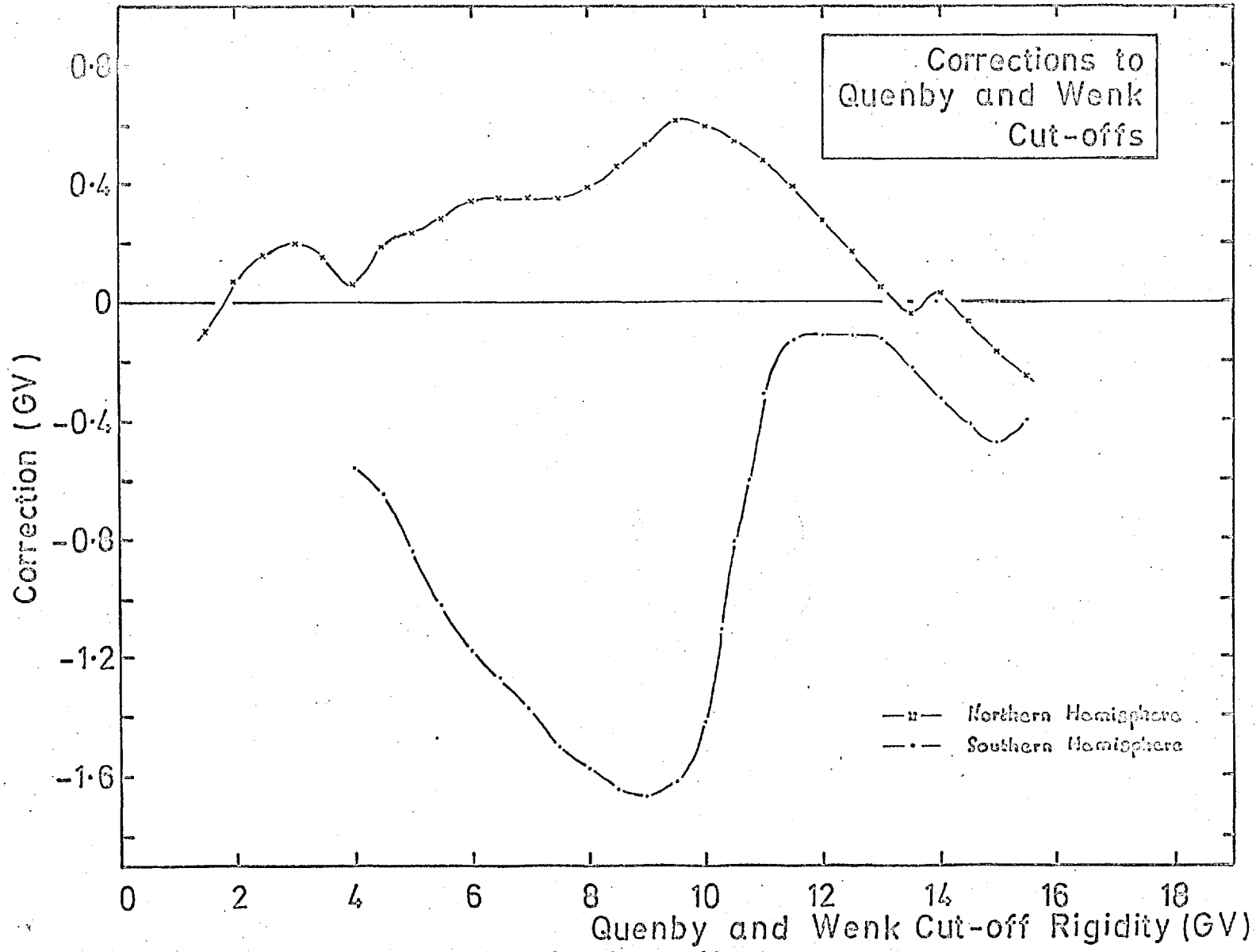


Fig. 5-7.I Corrections to the Quenby and Wenk cut-offs along the survey route obtained from the experimentally corrected cut-offs.

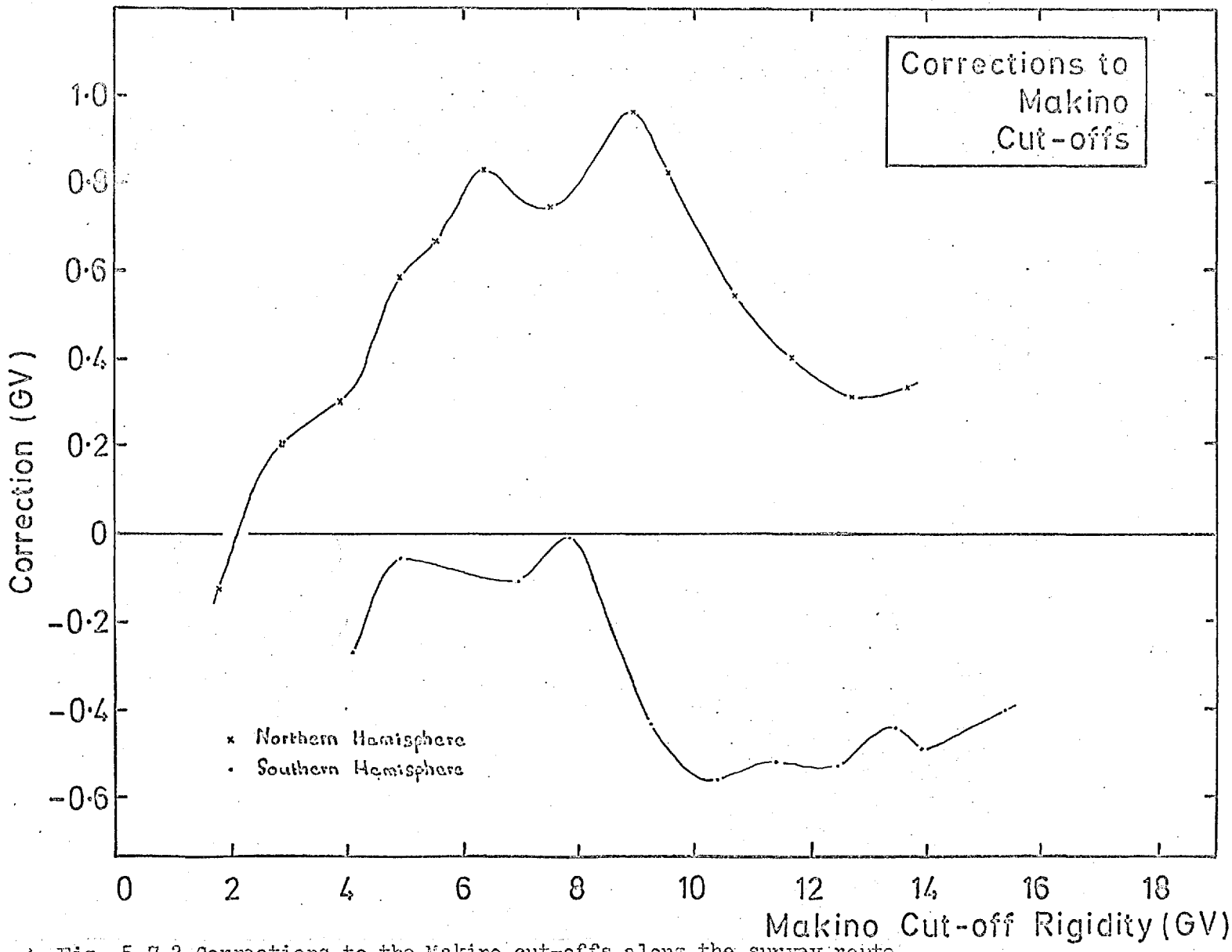


Fig. 5-7.2 Corrections to the Makino cut-offs along the survey route obtained from the experimentally corrected cut-offs.

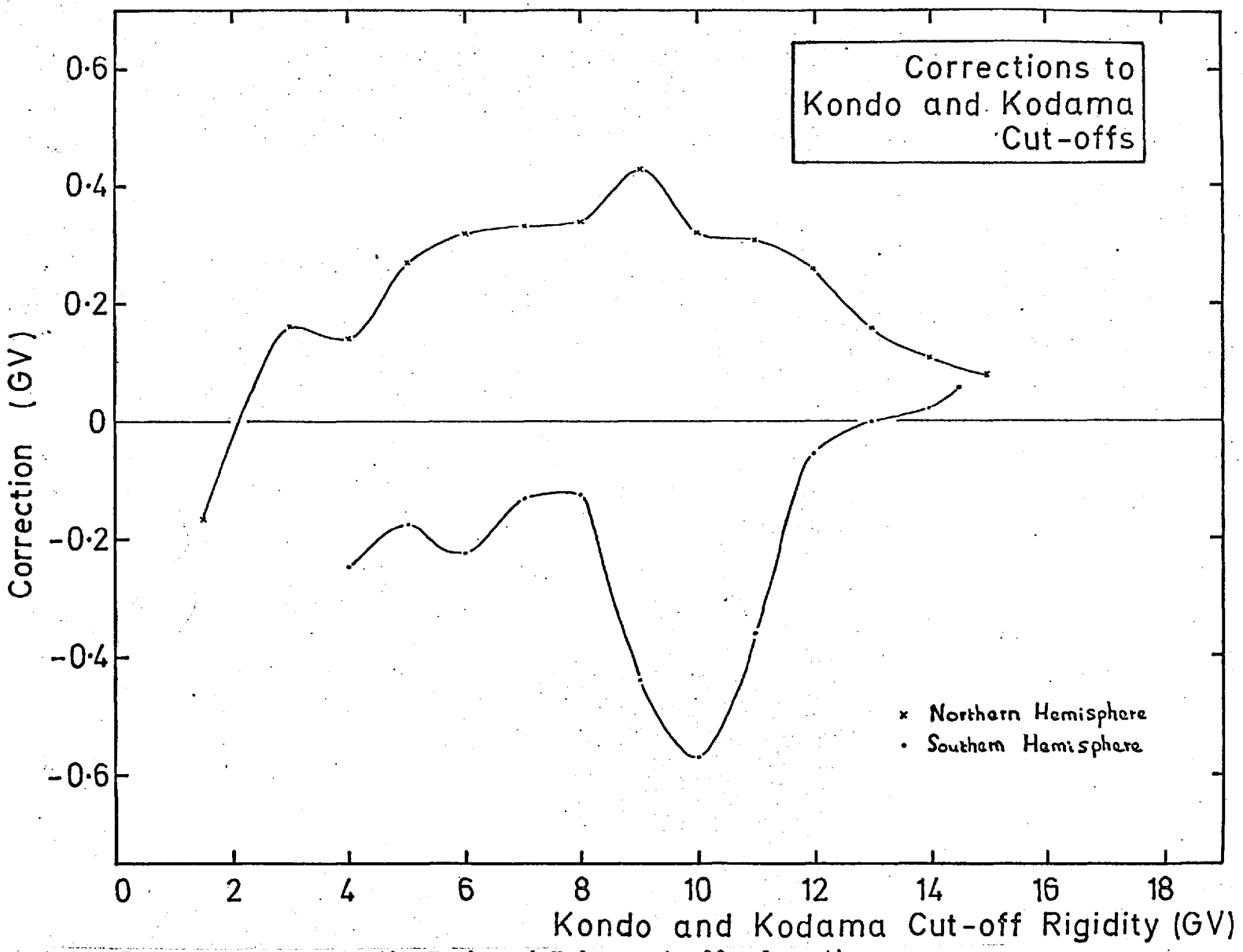


Fig. 5-7.3 Corrections to the Kondo and Kodama cut-offs along the survey route obtained from the experimentally corrected cut-offs.

(i) Kondo and Kodama.

These cut-offs order the experimental data as well as those of Shea et al for cut-offs below ~7 GV. The cut-off errors are increased above 7 GV with a maximum error in the southern hemisphere near the grid point (20°S 30°E). The cut-off at this point is given as 10.05 GV while that interpolated from the Shea et al 2 × 2 degree grid is 9.67 GV. The error in this region must be due to an insufficient number of cut-off calculations in the South African area resulting in interpolation errors.

The Kondo and Kodama value for the cut-off calculated by Shea (1966) at (34.9°N 12.5°E) is 9.55 GV. The error here is therefore 0.27 GV.

(ii) Quenby and Wenk.

The Quenby and Wenk cut-offs are seen to be accurate to ~4% along the survey route in the areas unaffected by the South African anomalous field. In the anomalous region, the deviations of the Quenby and Wenk cut-offs from the experimentally corrected cut-offs are large. This area of discrepancy is in the mid-latitude region where the Quenby and Wenk cut-offs were not well-defined. In addition, the anomalous field would be expected to produce errors in calculations in which the world average of higher order field effects was considered.

(iii) Makino.

These cut-offs apply well in the anomalous region where their deviations are similar to those of the trajectory computed cut-offs. In the remaining region the cut-offs are systematically low in the northern

hemisphere and high in the southern hemisphere. The deviations in these areas are about twice those of the Quenby and Wenk cut-offs. The large equatorial errors apparent in these cut-offs are at first sight surprising in view of the fact that the equatorial cut-offs were adjusted to fit the observed cosmic ray minimum. However it was shown in section 5.2 that the experimental results differ most from the predicted minimum in the South African region. The differences in the equatorial regions will therefore be partly due to errors in the integrated trajectory cut-offs (and consequently in the experimentally smoothed cut-offs).

5.8. CONCLUSIONS TO CUT-OFF ANALYSIS.

a) The 2 x 2 degree cut-off grid of Shea et al (1966) provides the best fit to the experimental data. The r.m.s. percentage deviation of these cut-offs from the experimentally corrected values is 2.4%.

b) The coarse 15 x 15 degree grid of computed cut-offs in the northern hemisphere leads to errors when an interpolation based upon the L parameter is used. The interpolation error at (34.9°N 12.5°E) was found to be 0.32 GV.

c) The 15 degree longitude interval in the 5 x 15 degree computed cut-off coverage of South Africa is probably too big due to the large longitude variation of the cut-off rigidity near the magnetically anomalous region.

d) Apart from a limited region in the southern hemisphere near (20°S 30°E) the differences in the cut-offs of Kondo and Kodama, and Shea et al are small.

e) Quenby and Wenk cut-offs in non-anomalous regions are accurate to $\sim 4\%$, but are greatly in error in the region of the South African magnetic anomaly.

f) Makino cut-offs are accurate in the anomalous region to $\sim 3\frac{1}{2}\%$ but elsewhere they are less accurate than the cut-offs of Quenby and Wenk.

g) A reduction of the high latitude cut-offs has been observed which is consistent with previous observations if the percentage reduction at geomagnetic latitudes $56^{\circ} - 61^{\circ}$ is 17%. A ring current alone cannot produce this reduction. It is likely that magnetic fields from magnetosheath and magnetic tail currents as well as a trapped particle ring current contribute to the observed cut-offs.

CHAPTER 6. EXPERIMENTAL OBSERVATION OF THE LONG TERM MODULATION OF COSMIC RAYS.

6.1. SURVEY DATA

The data obtained from the 12 surveys are given in figures (6.1.1) to (6.1.12) using the experimentally corrected cut-off rigidities (the diagrams are given in an appendix to this chapter). Corrections to the data have been applied for altitude and recorder attitude. The period of the 11 year solar cycle covered by these surveys is shown in figure (6.1.13). relative to the Mount Washington neutron monitor. During the survey periods the neutron intensity recovered from a mean 1962 level ~11% below the maximum of 1954 to a mean 1964 level ~4% below the 1954 maximum. All the surveys have been made during the slow recovery of the cosmic ray intensity towards its maximum level. This phase of the solar cycle is particularly suited to the study of the long term modulation because of the relative inactivity of the Sun. The decrease phase on the other hand is a more rapid variation of intensity characterised by the occurrence of large short term Forbush decrease events. A more detailed plot of the neutron intensity during the period of the surveys is given in figure (6.1.14). The high latitude intensity recorded above the cosmic ray knee during survey 8 is at a similar level to the previous survey. Together with the neutron monitor data given in Section 4.7.2., this is evidence of the recovery of the cosmic ray intensity at this time after the September 1963 Forbush decrease.

In figures 6.1.15 and 6.1.16 the intensities recorded above the latitude knee are plotted as a function of the mean daily counting rates

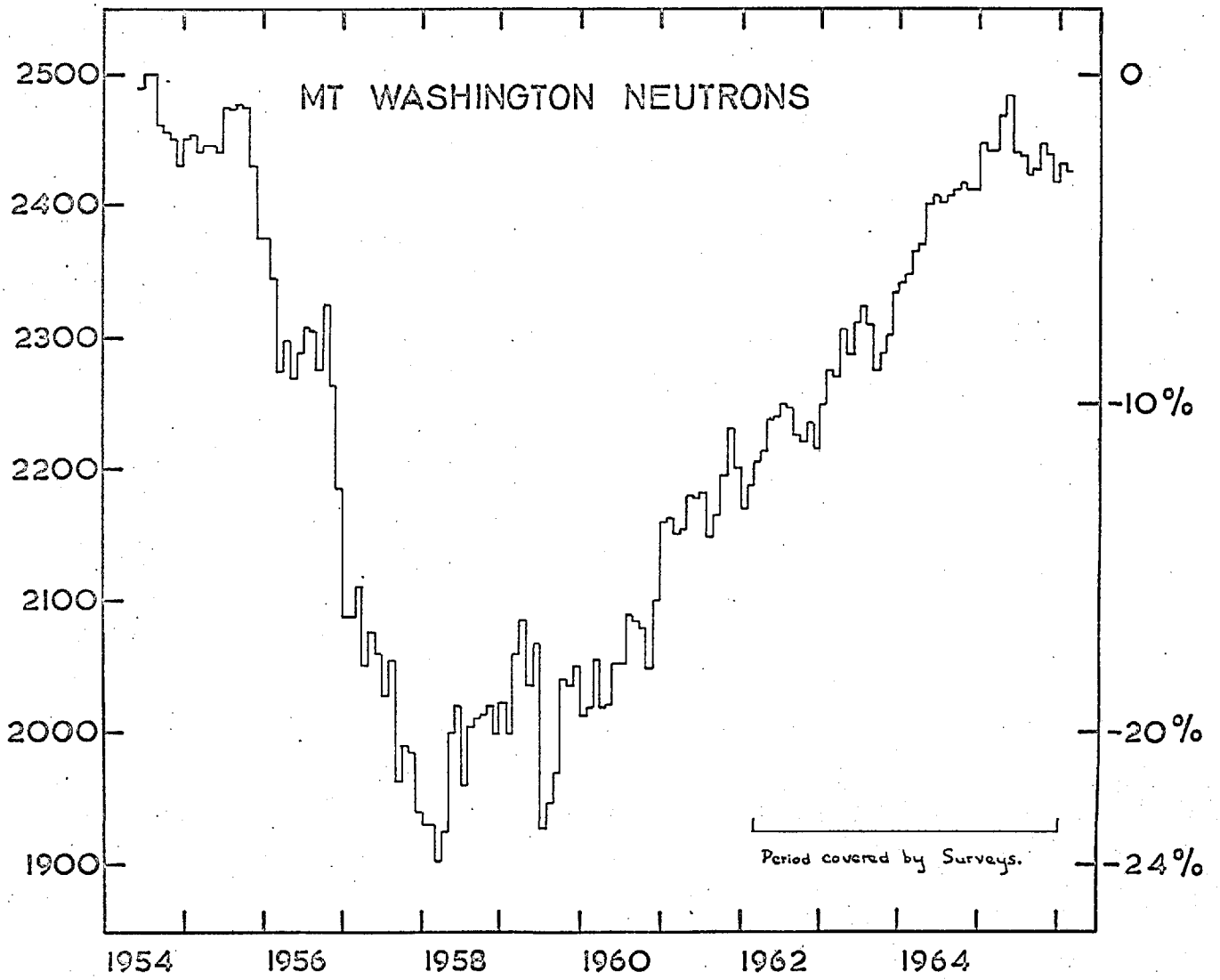


Fig. 6-I.I3 The Mount Washington neutron monitor counting rate during the solar cycle: I954-I965. The period of the cycle covered by the surveys is shown.

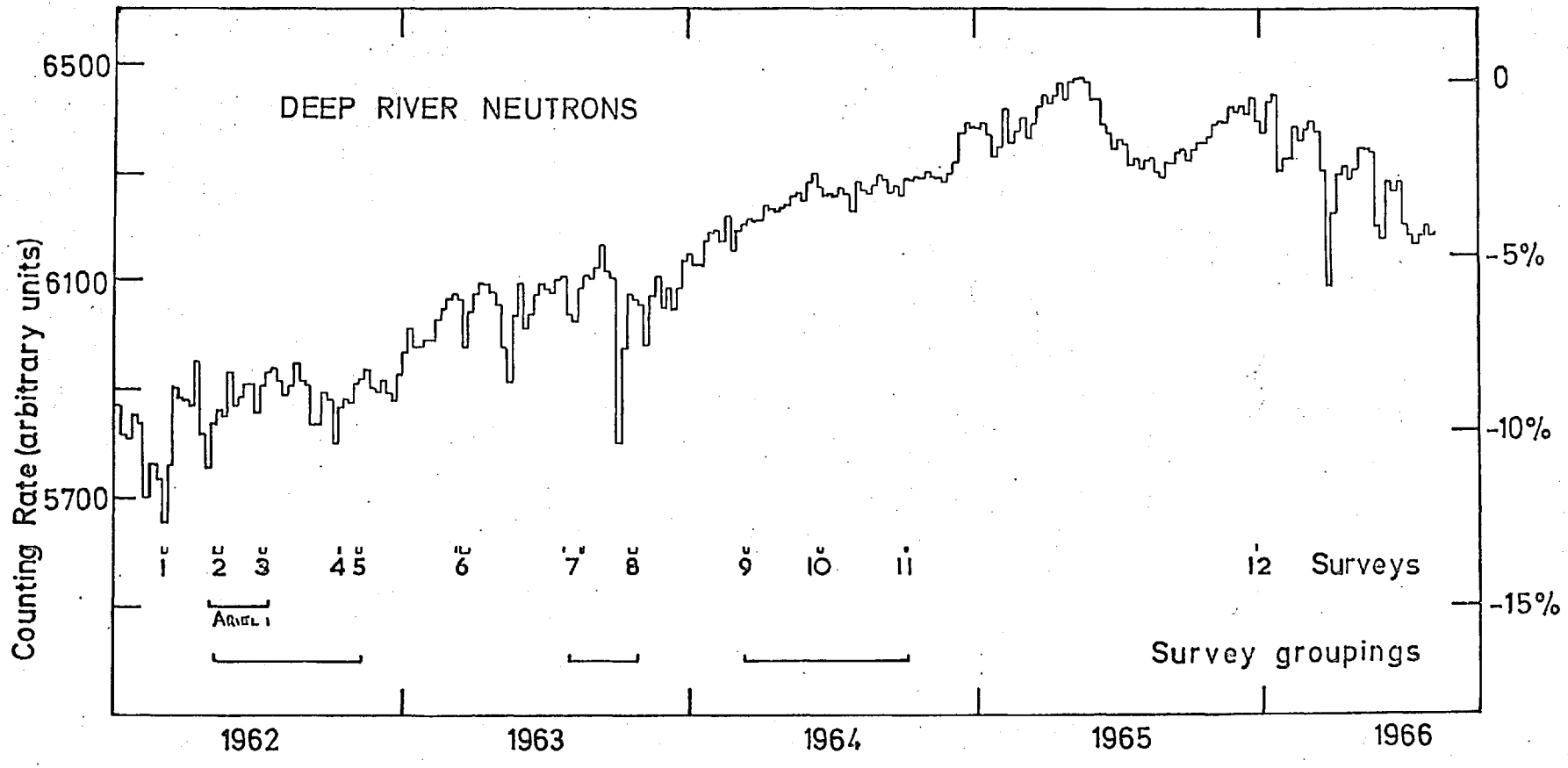
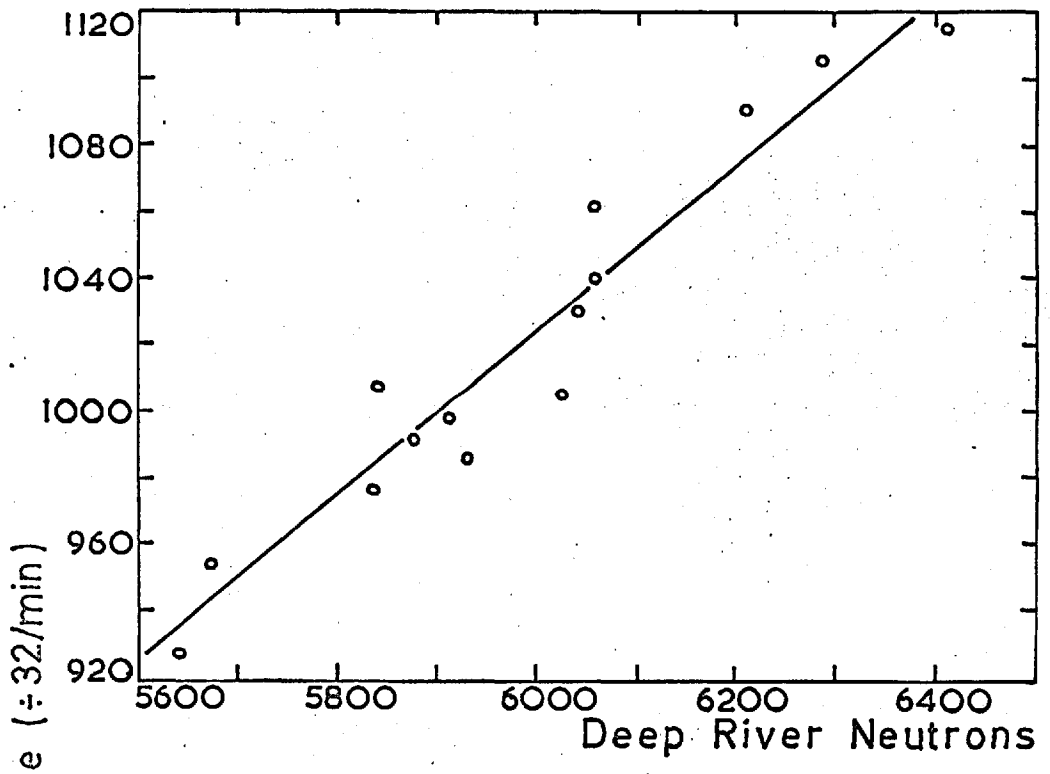


Fig. 6-I.I4 The Deep River neutron monitor counting rate 1962-1966. The times of the surveys are marked together with the period of operation of the satellite Ariel I.

TABLE (6.1)

DATES OF THE COSMIC RAY SURVEYS

Survey	Period of Survey Year.		Date of high Latitude Log		High lat. Intensity	Daily 2 hr.mean counting rate Deep River	Mt.Wash.
1	12/2 - 5/3		26/2		927	5643	2157
1			5/2		953	5675	2155
2	2/5 - 11/5		2/5		1008	5843	2234
2		1962	11/5	1962	990	5875	2239
3	3/7 - 8/7		3/7		998	5911	2249
4	9/10 - 11/10		9/10		976	5832	2213
5	1/11 - 6/11		6/11		986	5929	2251
6	1/3 - 18/3		1/3		1042	6057	2280
6		1963	18/3	1963	1005	6026	2268
7	23/7,6/8-8/8		23/7		1030	6042	2313
8	7/10 - 18/10		7/10		1040	6061	2323
9	2/3 - 6/3		2/3		1090	6212	2358
11	2/10 -5/10	1964	30/9	1964	1105	6287	2430
12	23/12	1965	23/12	1965	1115	6412	2397



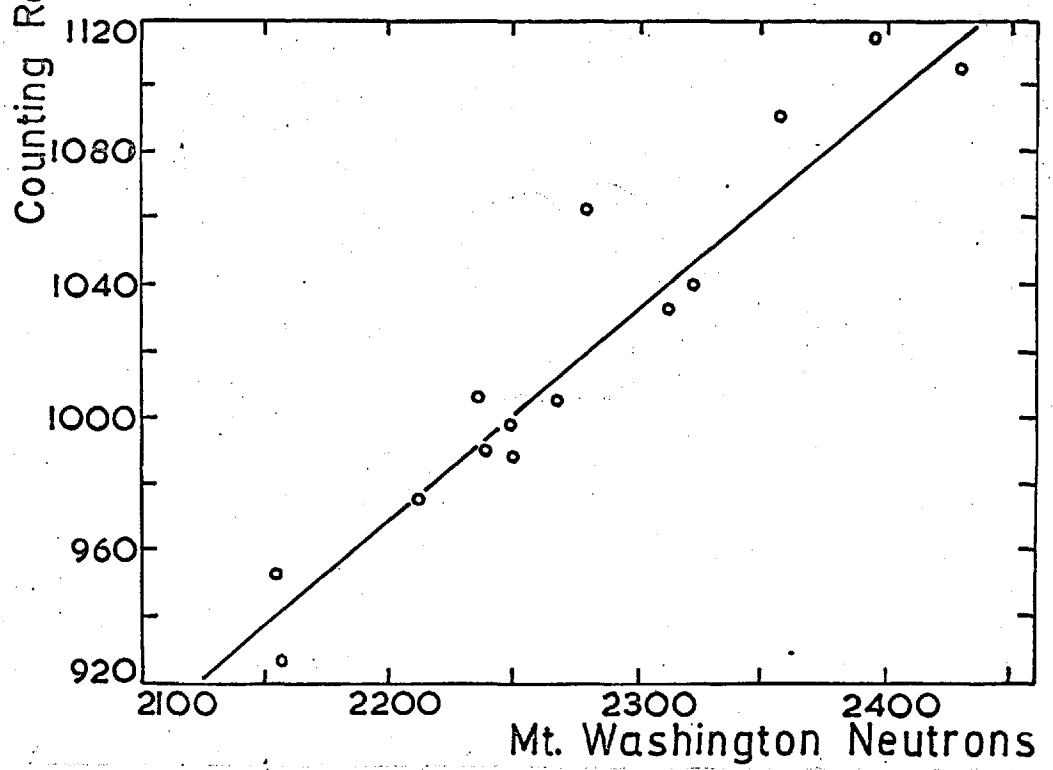
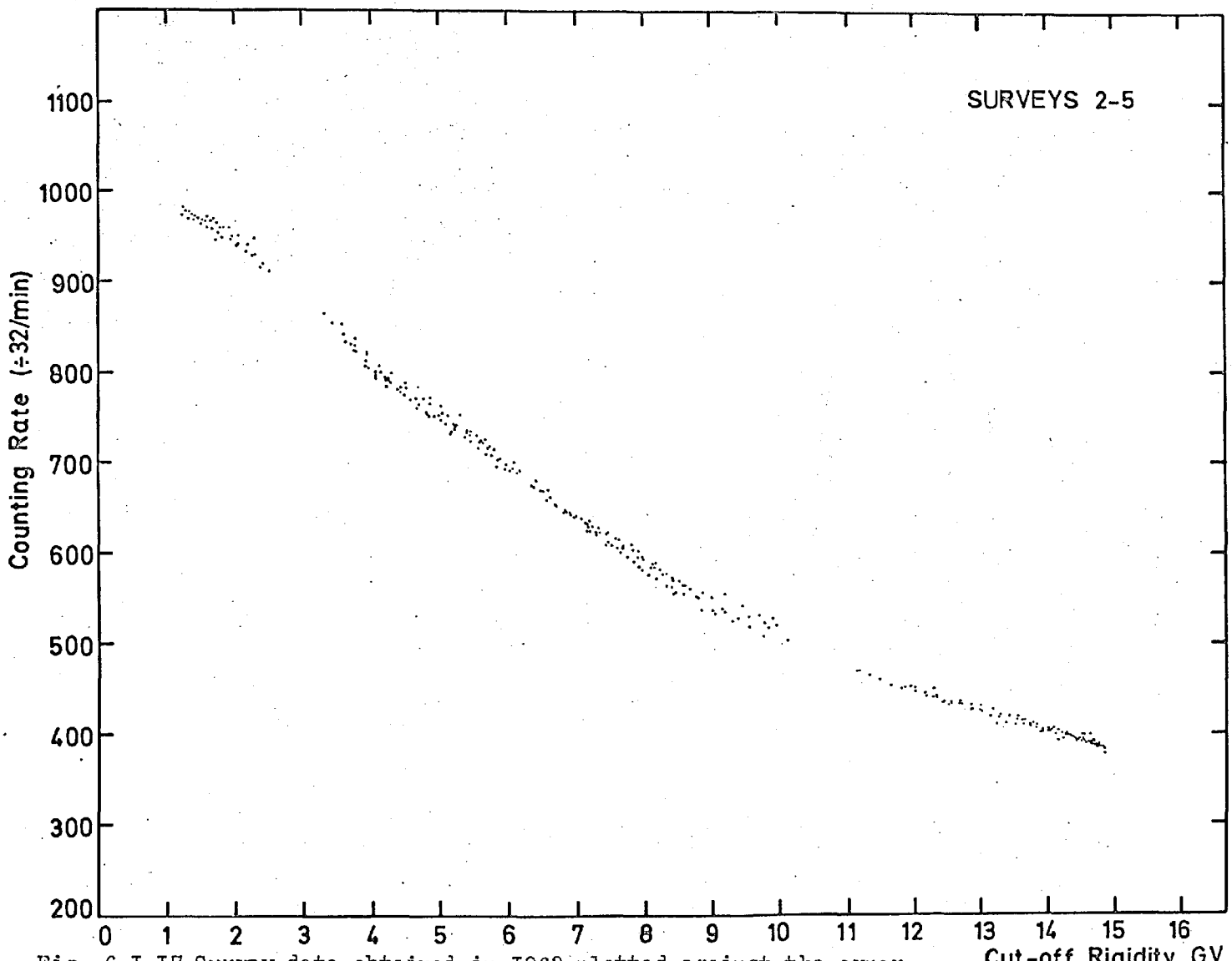


Fig. 6-I.I5 Counting rate above the knee at 45,000' plotted against the Deep River neutron monitor counting rate.

Fig. 6-I.I6 Counting rate above the knee at 45,000' plotted against the Mount Washington neutron monitor counting rate.



Fig, 6-I.I7 Survey data obtained in I962 plotted against the experimentally corrected cut-offs.

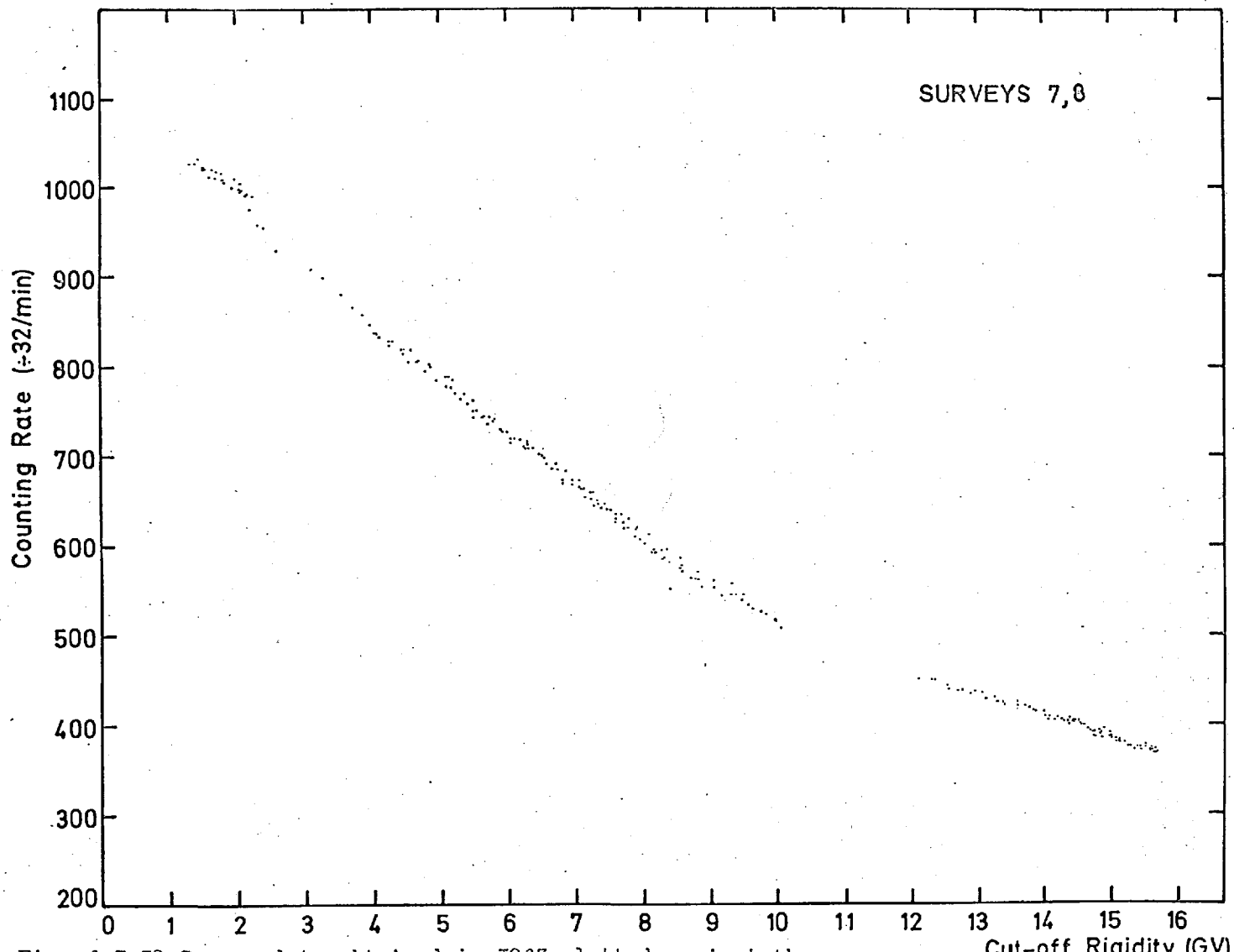


Fig. 6-I.I8 Survey data obtained in I963 plotted against the experimentally corrected cut-offs.

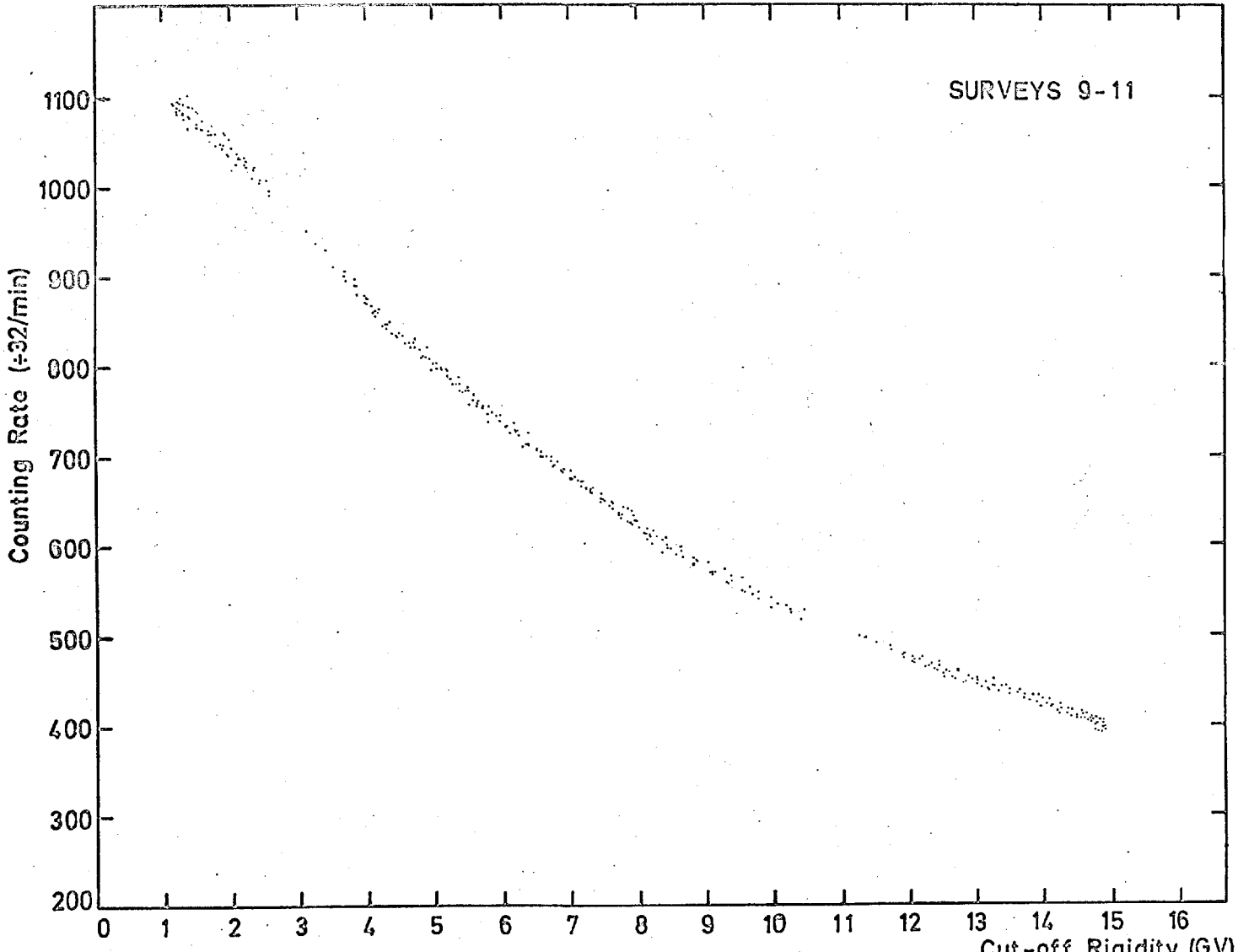


Fig. 6-I.19 Survey data obtained in 1964 plotted against the experimentally corrected cut-offs.

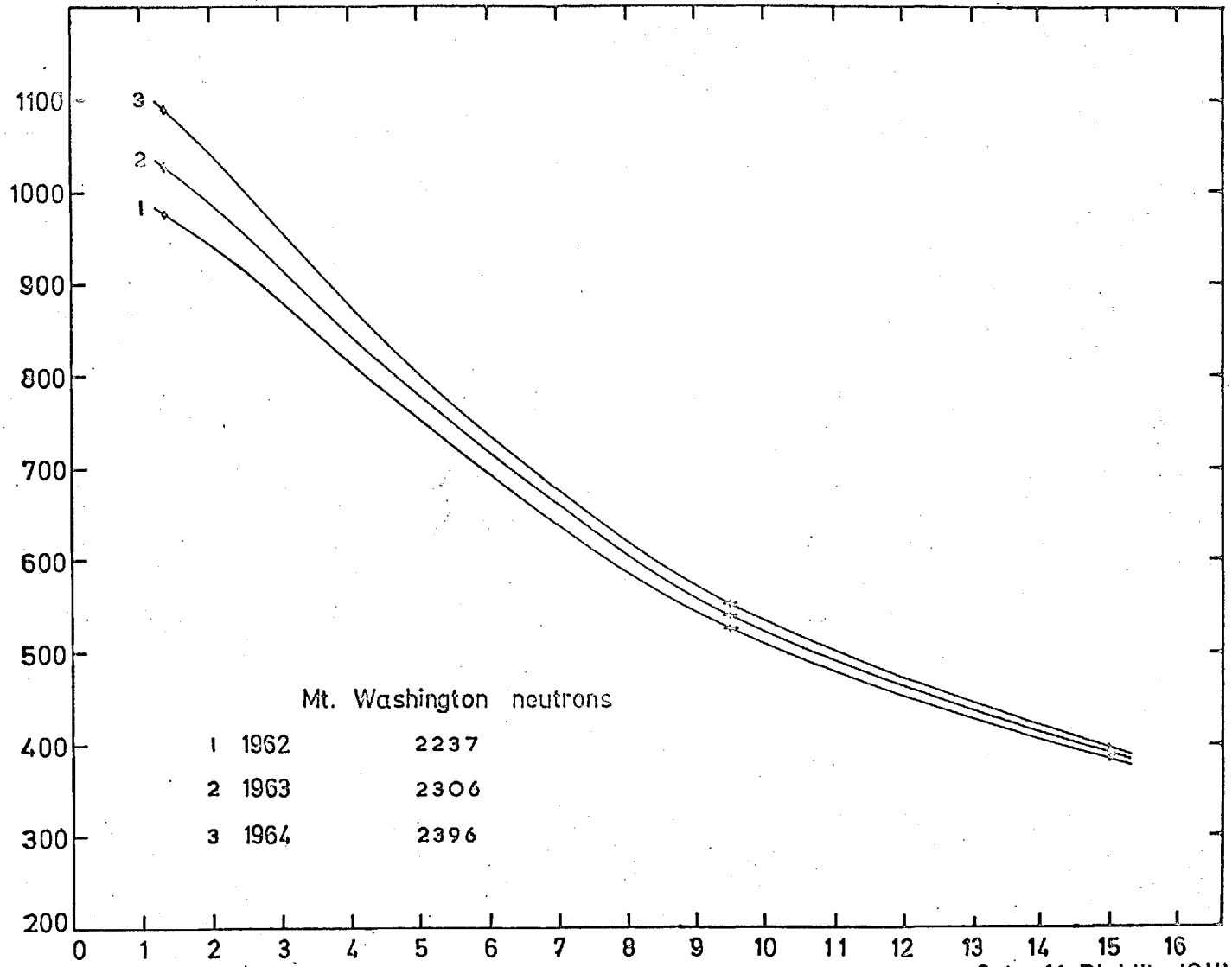


Fig. 6-I.20 The mean integral response functions at 45,000' for the years 1962, 1963, and 1964.

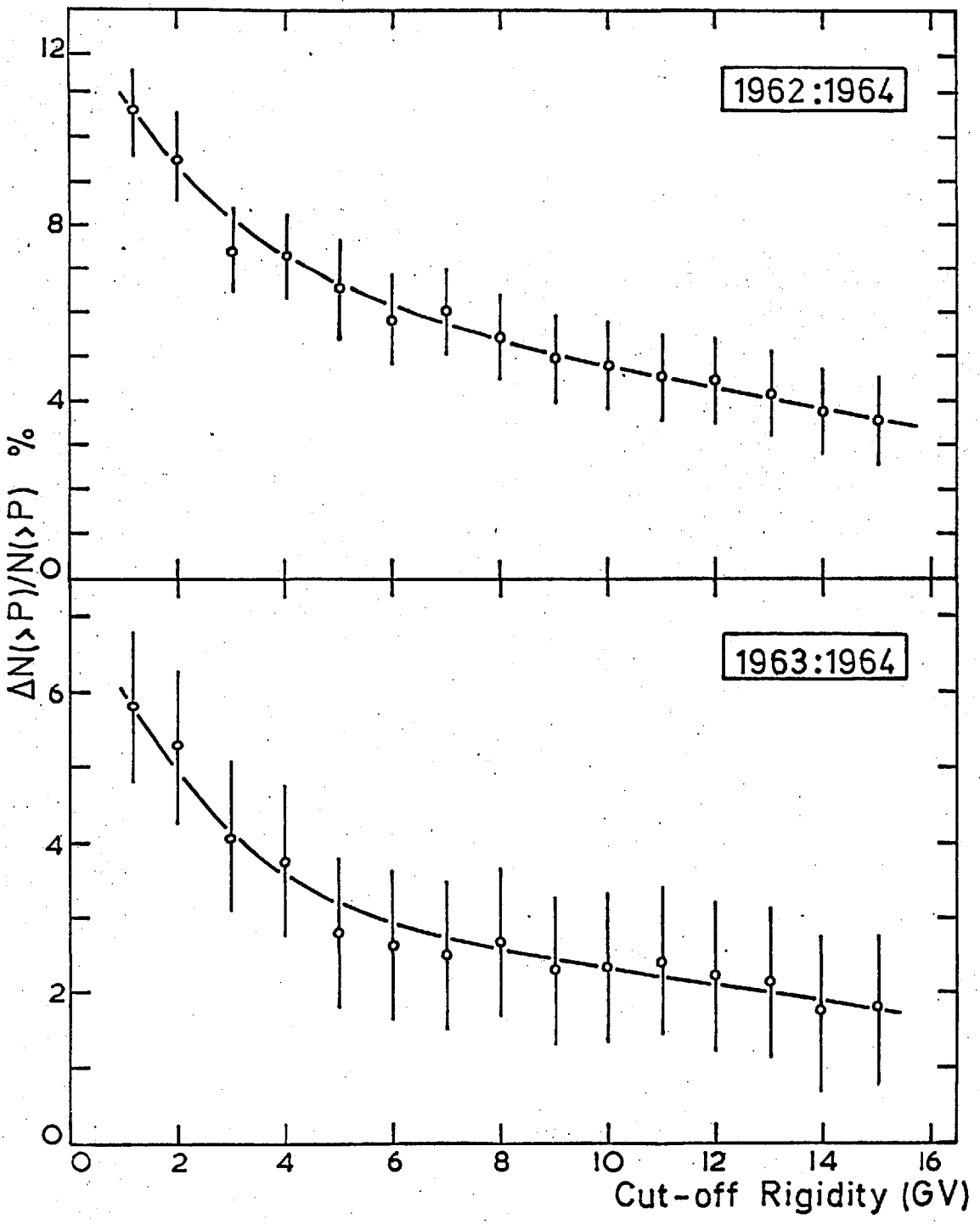


Fig. 6-2.I The integral modulation in the years I962 and I963 as a function of rigidity.

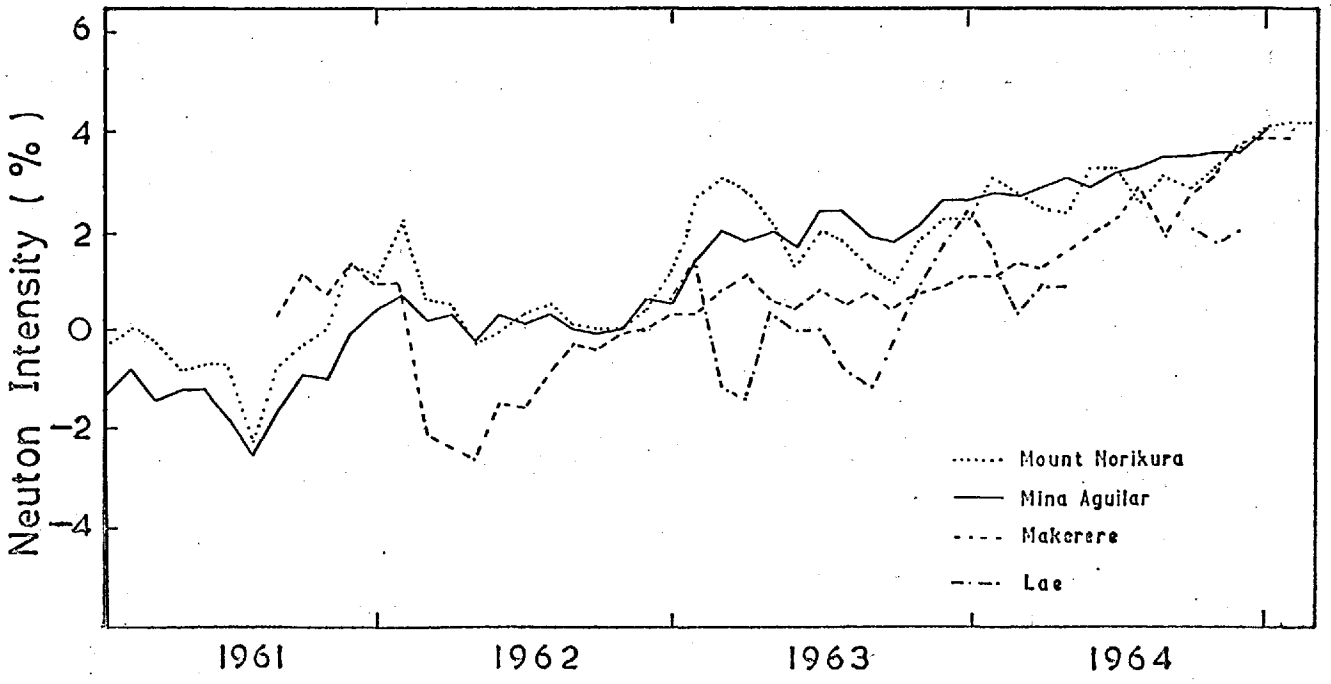


Fig. 6-2.2 High latitude neutron monitor intensities: 1961 – 1964.

of the Deep River (1.08 GV) and Mount Washington (1.24 GV) neutron monitors respectively. These data together with the survey dates are given in Table 6.1.

The slopes of the regression lines obtained by least squares analysis are :

Deep River	:	1.40 ± 0.07
Mount Washington	:	1.38 ± 0.09

As the sea level yield function for neutron monitors is approximately zero for rigidities less than about 2 GV, the two regression slopes should be the same (providing there is no long term drift in one of the recorders). The regression curves are therefore mutually consistent.

The surveys fall conveniently into three time periods during which the intensity changes were small :

Surveys 2-5	March – November	1962
Surveys 7,8	July – october	1963
Surveys 9-11	March – October	1964

The high latitude intensities recorded during survey 3 at rigidities < 2.5 GV were increased above those recorded during surveys 2,4 and 5. In this rigidity range, the mean intensities of surveys 2, 4 and 5 were taken as representative of the 1962 period while at lower latitudes all four surveys are considered.

The data grouped into these time periods are given in figures 6.1.17 to 6.1.19.

To construct the mean curves, the data were divided into rigidity intervals of $\frac{1}{3}$ GV and the centroid of each group was calculated. Curves constructed through these positions are given in figure 6.1.20.

A possibility of a systematic difference between survey 12 and the other surveys due to a change of altimeter was introduced in section 4.4.4.

	Relative Intensity at 45,000 ft recorded above knee	Relative Neutrons	
		Mt. Washington	Deep River
Survey 12	1115	2425	6400
Surveys 9-11	1100	2396	6260
Intensity increase	1.4%	1.2%	2.2%

The possibility of a 1% systematic difference is not ruled out, but the observed change is not inconsistent with the Mt. Washington and Deep River neutron monitors.

6.2. RIGIDITY DEPENDENCE OF THE INTEGRAL INTENSITY CHANGES.

The percentage reductions in the integral intensities during 1962 and 1963 relative to the 1964 level are plotted in figure 6.2.1.

The consistency of the intensity changes is considered by comparing the observed changes to those recorded by ground level detectors at high and low latitudes. The high latitude integral intensity changes

recorded at 45,000 ft. have been shown to be consistent with high latitude neutron monitors through the regression curves of figures 6.1.15 and 6.1.16. Figure 6.2.2. is taken from Quenby (1966a). The mean level of the Mt. Norikura (11.39 GV) and Mina Aguilar (12.51 GV) neutron monitor intensities was depressed ~3% in 1962 relative to 1964. This is in agreement with the observed intensity changes at 45,000 ft. of $3\frac{1}{2}$ - 4% between 12 GV and 15 GV. The neutron monitors at Lae (15.50 GV) and Makerere (14.95 GV), while not showing such good agreement, confirm that intensity increases occurred throughout the latitude sensitive region of the cosmic ray spectrum for the years 1962-1964. The integral intensity variations are thus consistent with ground level detectors.

6.3. YIELD FUNCTIONS.

6.3.1. Gross Yield Function.

The observed intensities of secondary particles inside the atmosphere must be related to the primary cosmic rays in order to make use of the Earth's magnetic field as a charged particle spectrometer. This relationship depends primarily upon the energy and charge of the primary particles as well as the atmospheric depth of measurement and detector response. Knowing this relationship, the primary spectrum may be determined at any time from data recorded within the atmosphere.

The differential counting rate of a detector at atmospheric depth x, time t and a vertical cut-off P, due to primaries of charge z is $\frac{dN}{dP}_z(P,x,t)$. This may be related to the primary differential rigidity spectrum $\frac{dj_z}{dP}(P,t)$ for that charge z by the specific yield function

$S_z\ (P,x)$.

The response due to contributions from all charged particles z is :

$$\frac{dN}{dP}\ (P,x,t) = \sum_z S_z\ (P,x)\ \frac{dj_z}{dP}\ (P,t) \qquad 6.1$$

Webber (1962) observed that the spectra $\frac{dj_z}{dP}$ are similar above ~1.2 GV for all z at solar minimum. In addition the differential rigidity spectra were observed to change in a similar manner throughout the solar cycle.

The spectrum $\frac{dj_z}{dP}\ (P,t)$ can thus be written as $\frac{dj}{dP}\ (P,t)$.

$$\therefore\ \frac{dN}{dP}\ (P,x,t) = \frac{dj}{dP}\ (P,t)\ \sum_z S_z\ (P,x)$$

$$= S_G(P,x)\ \frac{dj}{dP}\ (P,t) \qquad 6.2$$

where $S_G(P,x)$ is the gross yield function and N(P,x,t) is the experimentally measured integral spectrum at depth x in the atmosphere. From a simultaneous measurement of the primary spectrum $\frac{dj}{dP}\ (P,t)$ and the secondary integral spectrum the gross yield function may be determined. Simultaneous measurements of the primary and secondary spectra were possible during the period of operation of the satellite Ariel 1. Durney et al (1964) measured the integral rigidity spectrum of cosmic rays of charge $z \geqslant 6$. The differential rigidity spectrum calculated from this is approximately $\frac{dj}{dP}\ (P,t)$ because of the similarity

of all $\frac{dj}{dP}$ z (P,t) in this rigidity range (3.5 GV - 15 GV). The data was accummulated during the period 26th. April 1962 to 9th July 1962. In this period two latitude surveys, numbers 2 and 3, were made. There was little change in the average level of the cosmic ray intensity in the period March-November 1962. The secondary particle spectrum during this period can therefore be represented by the mean of surveys 2-5.

The primary differential rigidity spectrum derived from the Ariel data and the differential counting rate at 145 g cm^{-2} are compared in figure (6.3.1). The gross yield function obtained from these spectra is given in figure (6.3.2).

6.3.2. Cut-off Rigidities used in Yield Function Calculation.

Ariel 1 was launched on 26th. April 1962 into a 54° inclination orbit with perigee 390 km and apogee 1215 km. The data used in the analysis were collected between 390 km and 800 km altitude and were organised by the Quenby and Wenk cut-offs. These cut-offs show large errors in certain regions. A complete world collection of data over the 54° latitude range would probably have smoothed out these areal inaccuracies. This is evidenced by the observation that the mean curve through the extensive latitude surveys of Project Magnet is similar for both Quenby and Wenk cut-offs and the more accurate L interpolated cut-offs. Figure (6.3.3) is taken from the data of Shea et al (1966). Because of the altitude limitation on the acceptance of data there was not a uniform coverage of the world. Data obtained in areas where there are large errors in the Quenby and Wenk cut-offs were omitted.

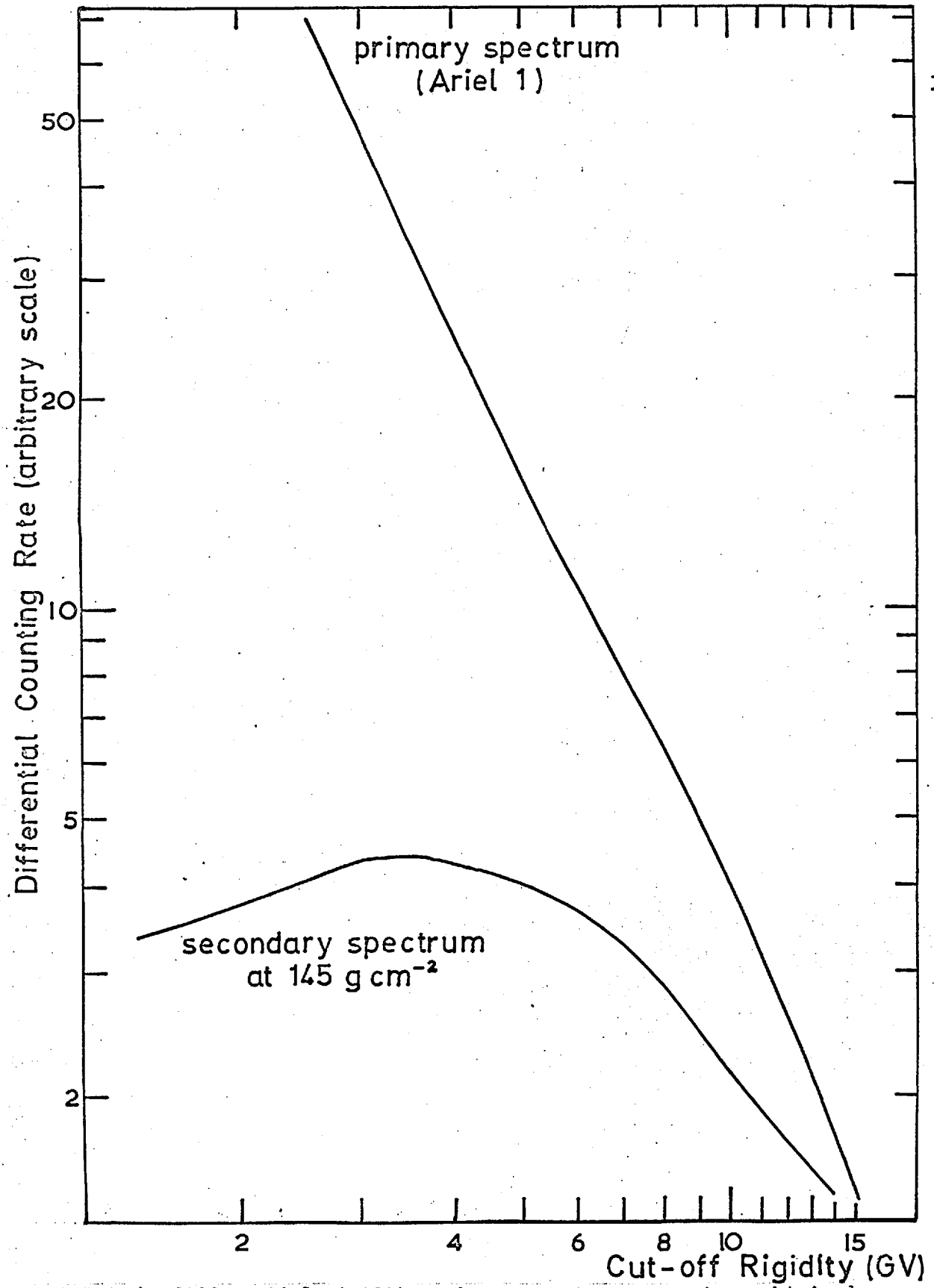


Fig. 6-3.I The differential rigidity primary cosmic ray spectrum obtained from the Ariel I measurements of Durney et al (1964). Also shown is the differential response of the detecter at 45,000' measured during the operation of Ariel I.

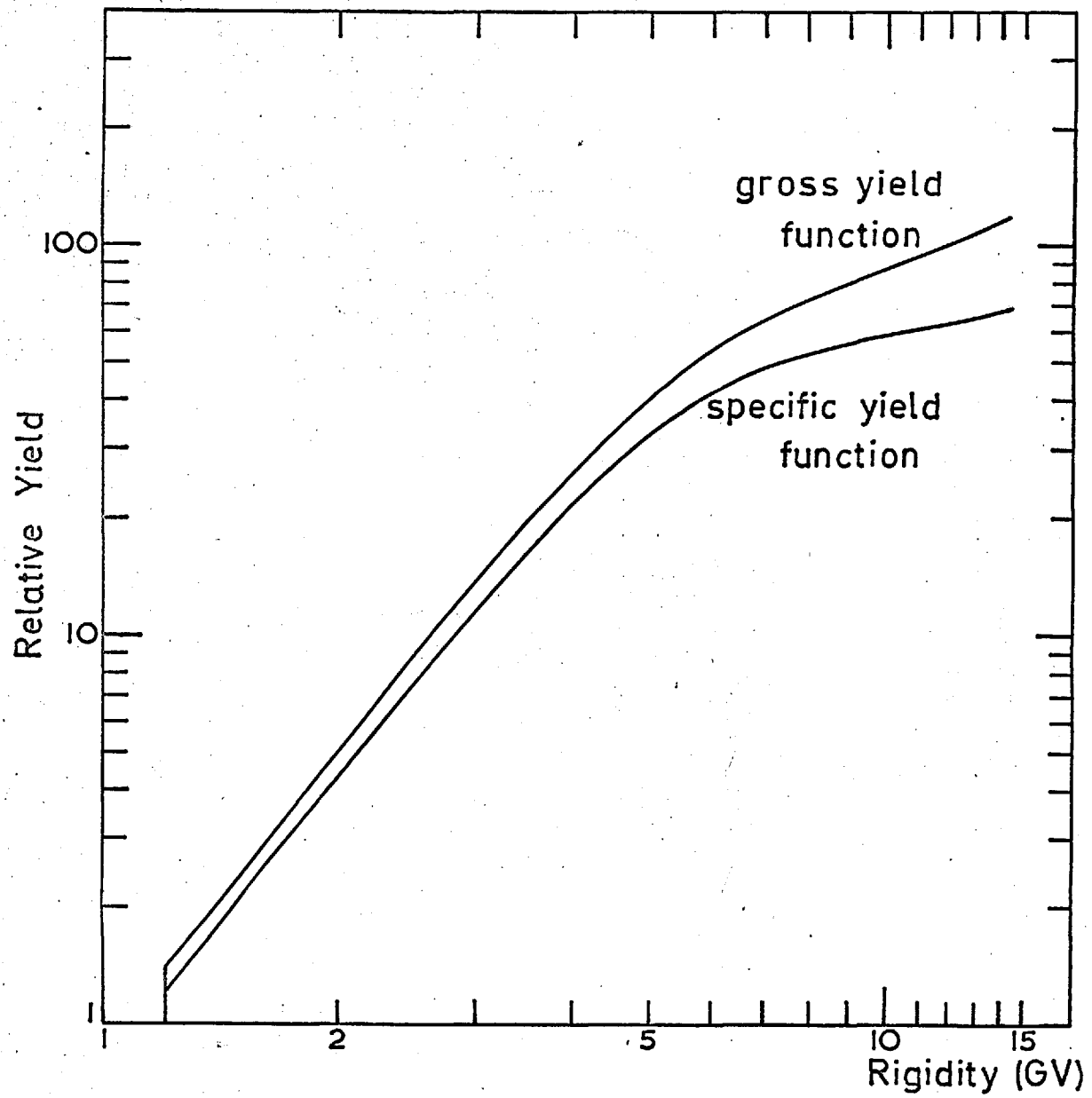


Fig. 6-3.2 The gross yield function for the detector at 45,000' and the specific yield function for primary protons.

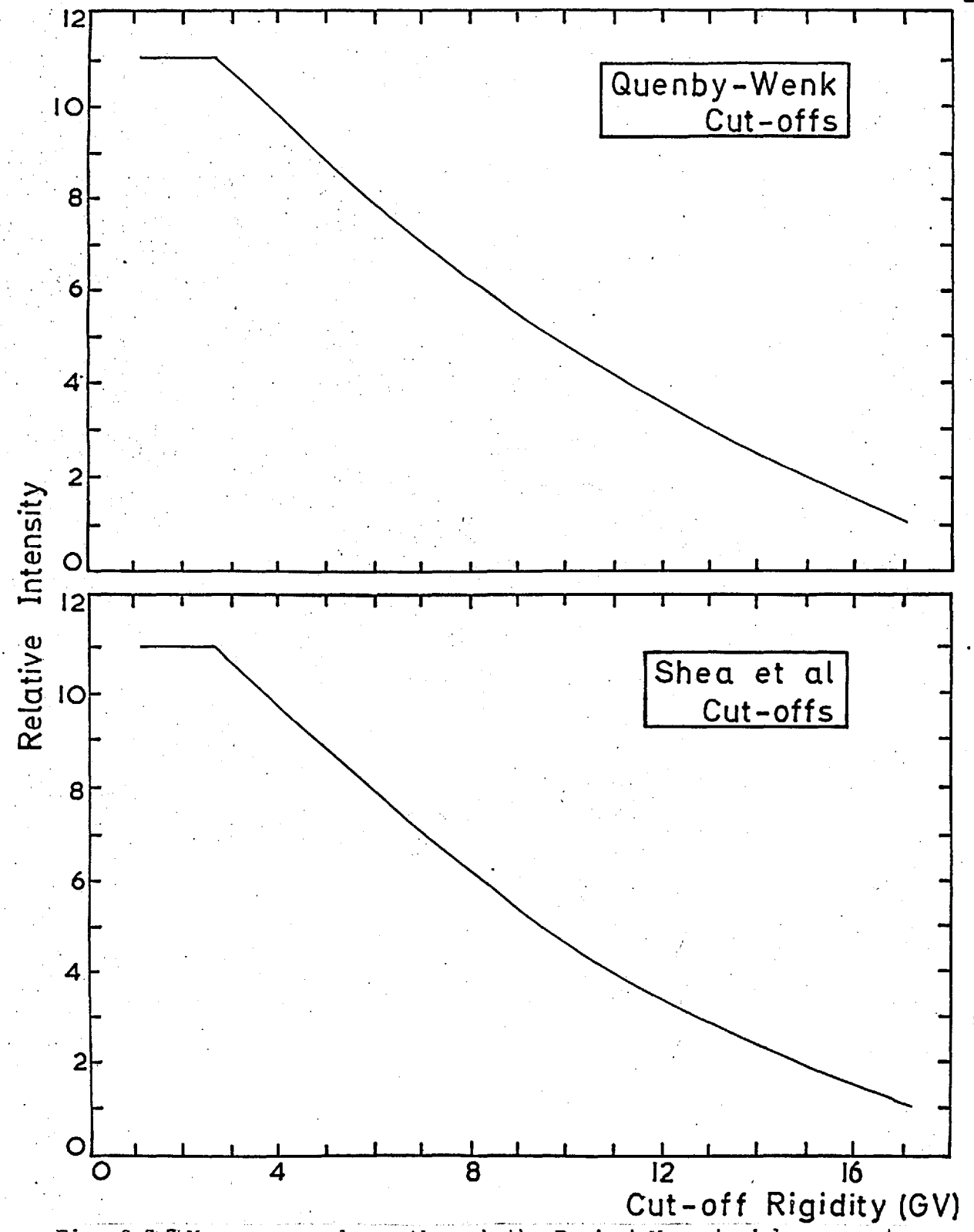


Fig. 6-3.3 Mean curves drawn through the Project Magnet airborne neutron monitor surveys. (Data from Shea and Smart: 1966)

The error involved in the spectrum measured against Quenby and Wenk cut-offs is probably small.

6.3.3. Specific Yield Function.

Following the method of Webber and Quenby (1959) we can derive the specific yield function due to the primary protons from the measurement of the gross yield function. About 50% of the incident nucleons are protons and the rest make up the heavier ($z>1$) cosmic ray nuclei. The average charge to mass ratio $\frac{z}{A}$ of the heavy particles is $\frac{1}{2}$. At the same velocity the rigidity of a proton ($\frac{z}{A} = 1$) will be half that of a heavy nucleus. Once inside the atmosphere it is assumed that the nucleons act independently. The specific yield function $S_z(P,x)$ will be equal to that due to a proton with rigidity P/2.

From equation 6.2. : $S_G = \sum_z S_z(P,x)$

$$= K_p S_p(P) + \Sigma_z K_z A_z S_p(\tfrac{P}{2})$$

Where K_z is the isotopic abundance of charge z, and A_z the mass number of the nucleus.

$$\therefore \quad S_G = S_p + S_p\,(P/2, x) \qquad 6.4$$

The specific yield function is found by an iterative process in which the first trial solution is :

$$S'_p \quad (P,x) \quad = \quad S_G \quad (P,x)$$

then: $$S_p{}^2 \quad (P,x) \quad = \quad S_G \quad (P,x) \quad - \quad S'_p \quad (\frac{P}{2},x)$$

6.5.

Successive iterations gave S_p^3 (P,x) as a close fit to equation (6.4). The specific yield function is plotted in figure (6.3.2) It is apparent that the yield at low rigidities is due mainly to the proton contribution.

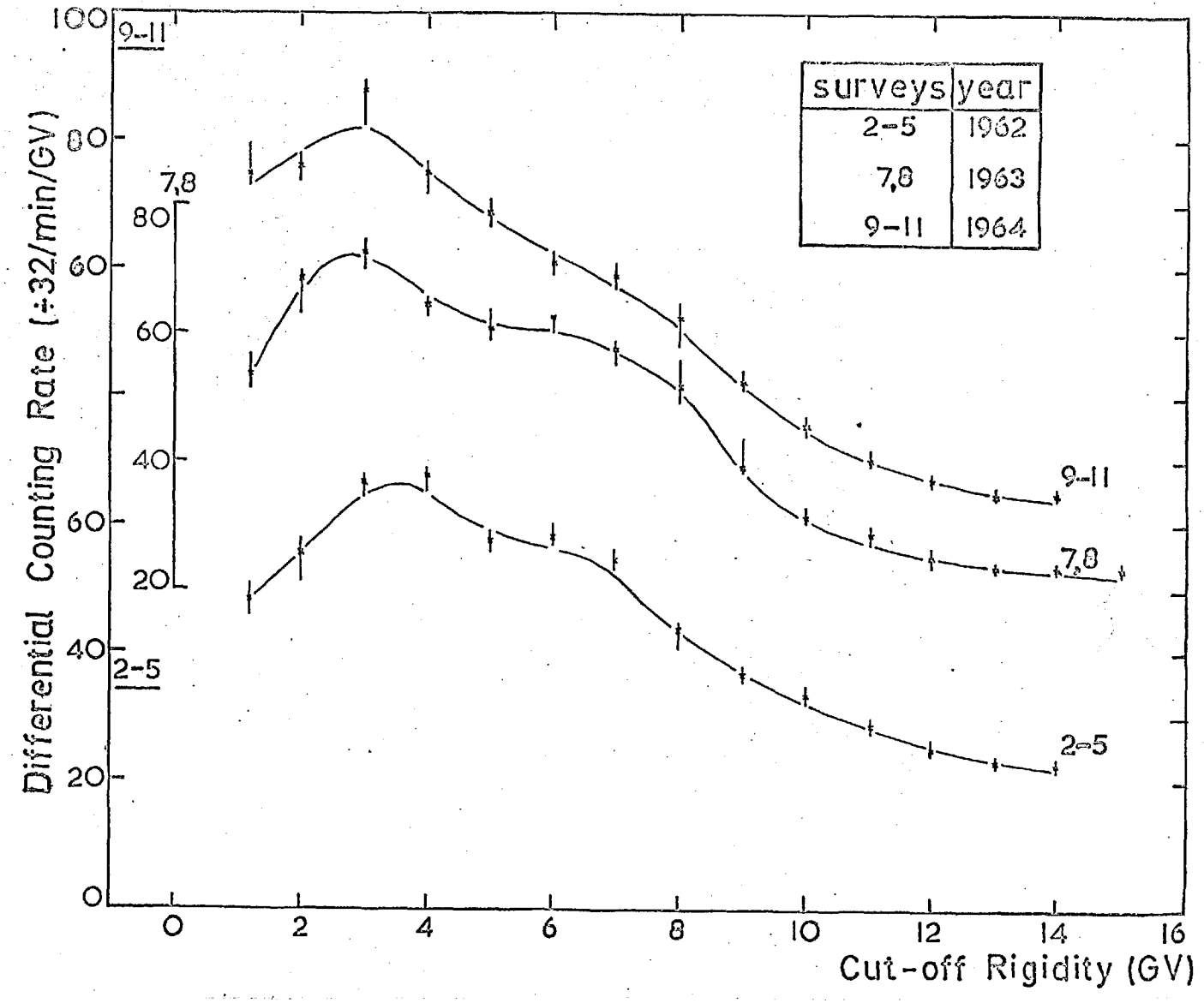
6.3.3. Concluding Remark.

Subsequent measurements $\frac{dN}{dP}$ (P,x,t') at different times t' in the solar cycle may be used to determine the form of the incident cosmic ray spectrum. A measurement during the sun-spot minimum period is particularly useful as this might lead to information on the modulation existing at that time.

6.4. RIGIDITY DEPENDENCE OF THE MODULATION.

The differential rigidity spectra from the 3 data periods are given in figures (6.4.1), (6.4.2) and (6.4.3) for 1962, 1963 and 1964 respectively. The superimposition of these spectra in figure (6.4.4) shows the variation with time of the differential response.

The gross yield function is not needed explicitly to determine the rigidity dependence of the modulation. This can be obtained from the ratio of the differential counting rates at two times t_1 and t_2.



Figs. 6-4.I - 6-4.3 The differential response curves for the detecter at 45,000' for the years I962, I963 and I964 respectively.

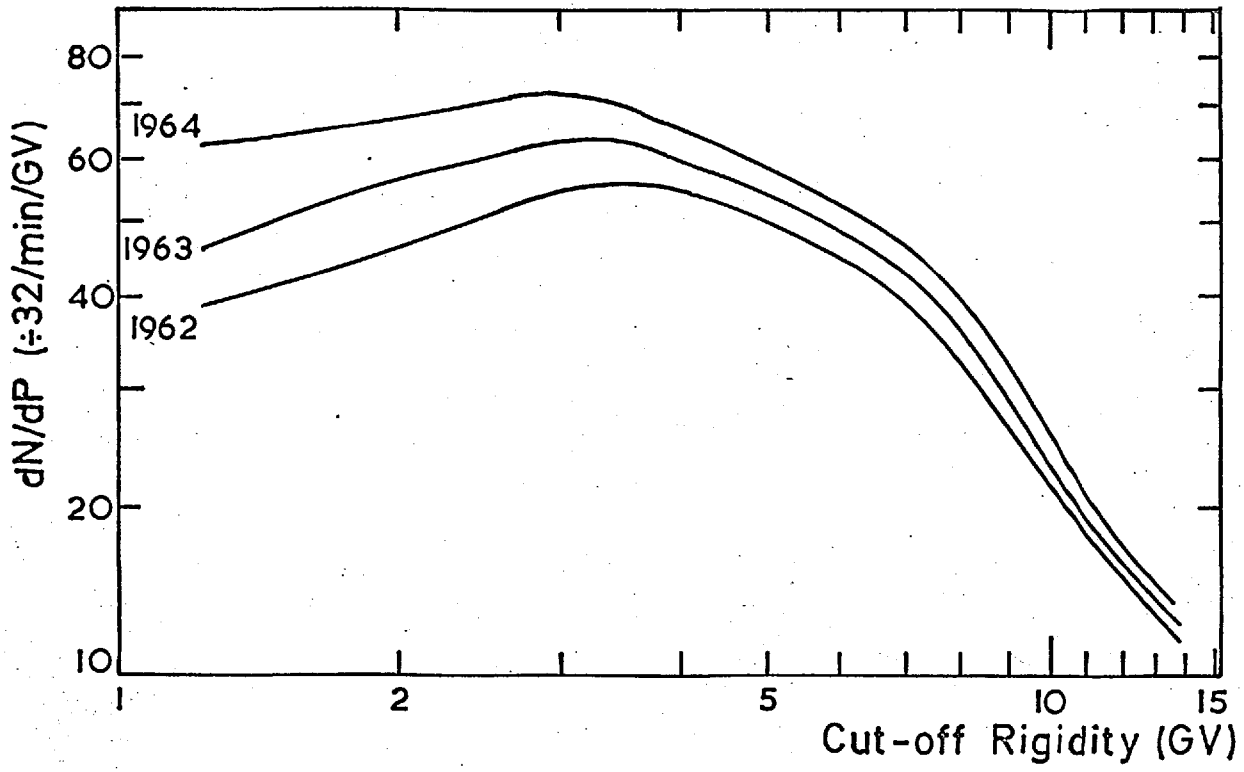


Fig. 6-4.4 Differential response curves I962 - I964.

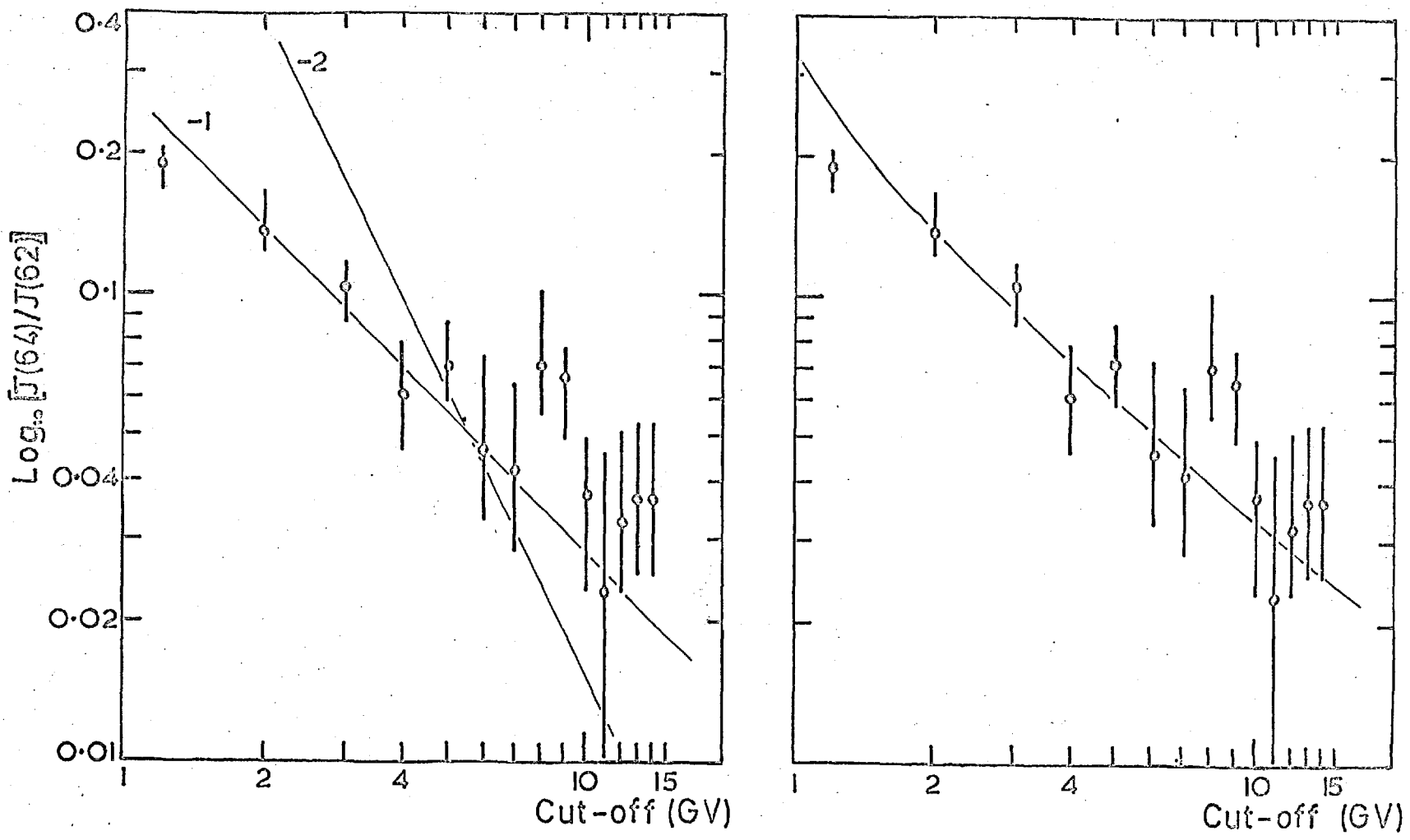


Fig. 6-4.5 The logarithm of the ratio of the differential response functions for I964 and I962 is plotted. Straight lines of slope -1 and -2 are constructed through the data.

Fig. 6-6.4 The logarithm of the ratio of the differential response functions for I964 and I962 is plotted. The solid curve has the form:

$$J(64)/J(62) = 1{\cdot}9\beta^{-1}P^{-0{\cdot}75}$$

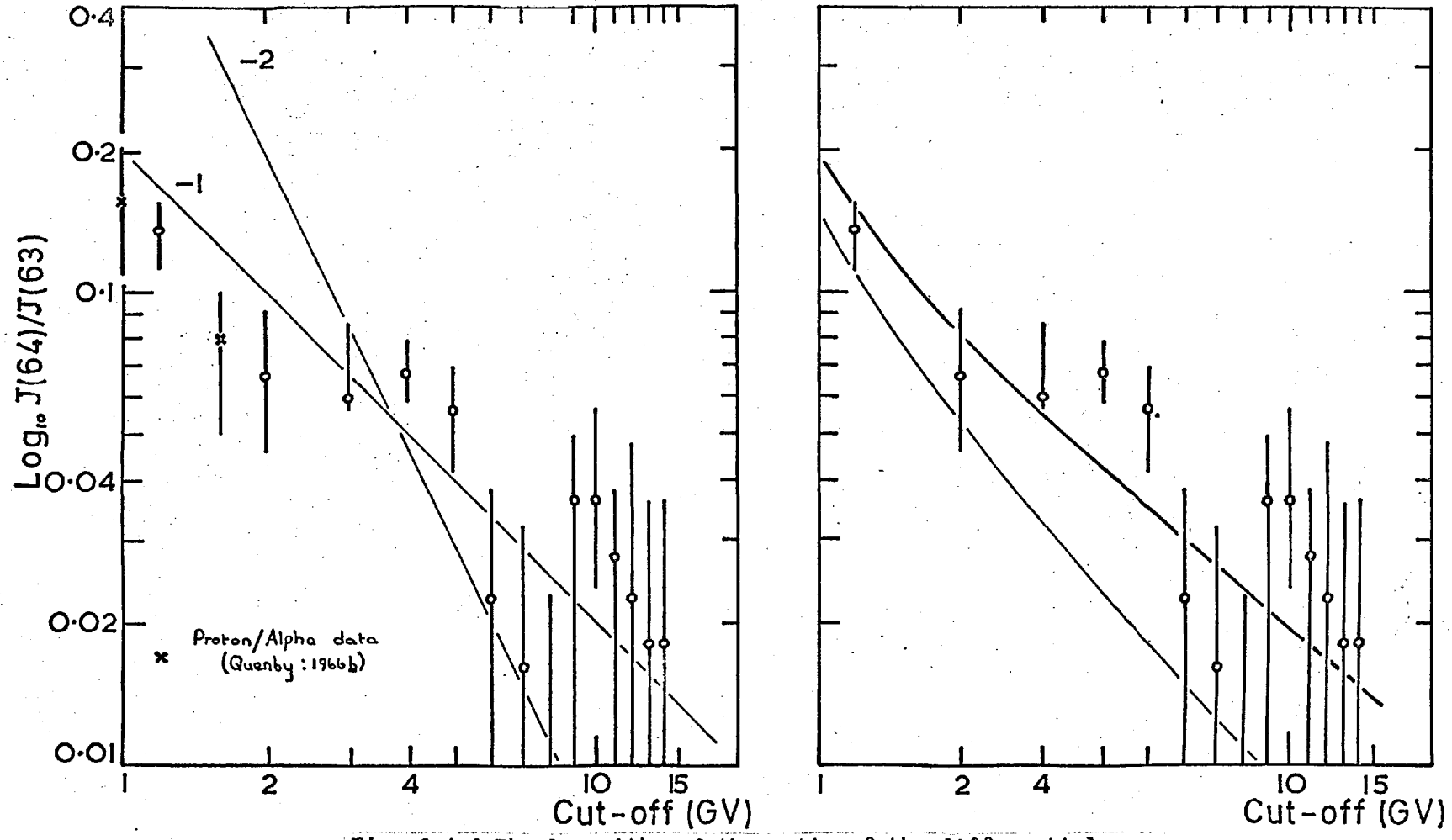


Fig. 6-4.6 The logarithm of the ratio of the differential response functions for I964 and I963 is plotted. Straight lines of slope -1 and -2 are constructed through the data.

Fig. 6-6.2 The modulation function fitted to the proton/alpha data in fig. 6-6.I is plotted (light curve) together with the present results for I963 relative to I964. Also plotted is an empirical modulation function (heavy curve):

$$J(64)/J(63) = 1{\cdot}1\beta^{-1}P^{-0{\cdot}75}$$

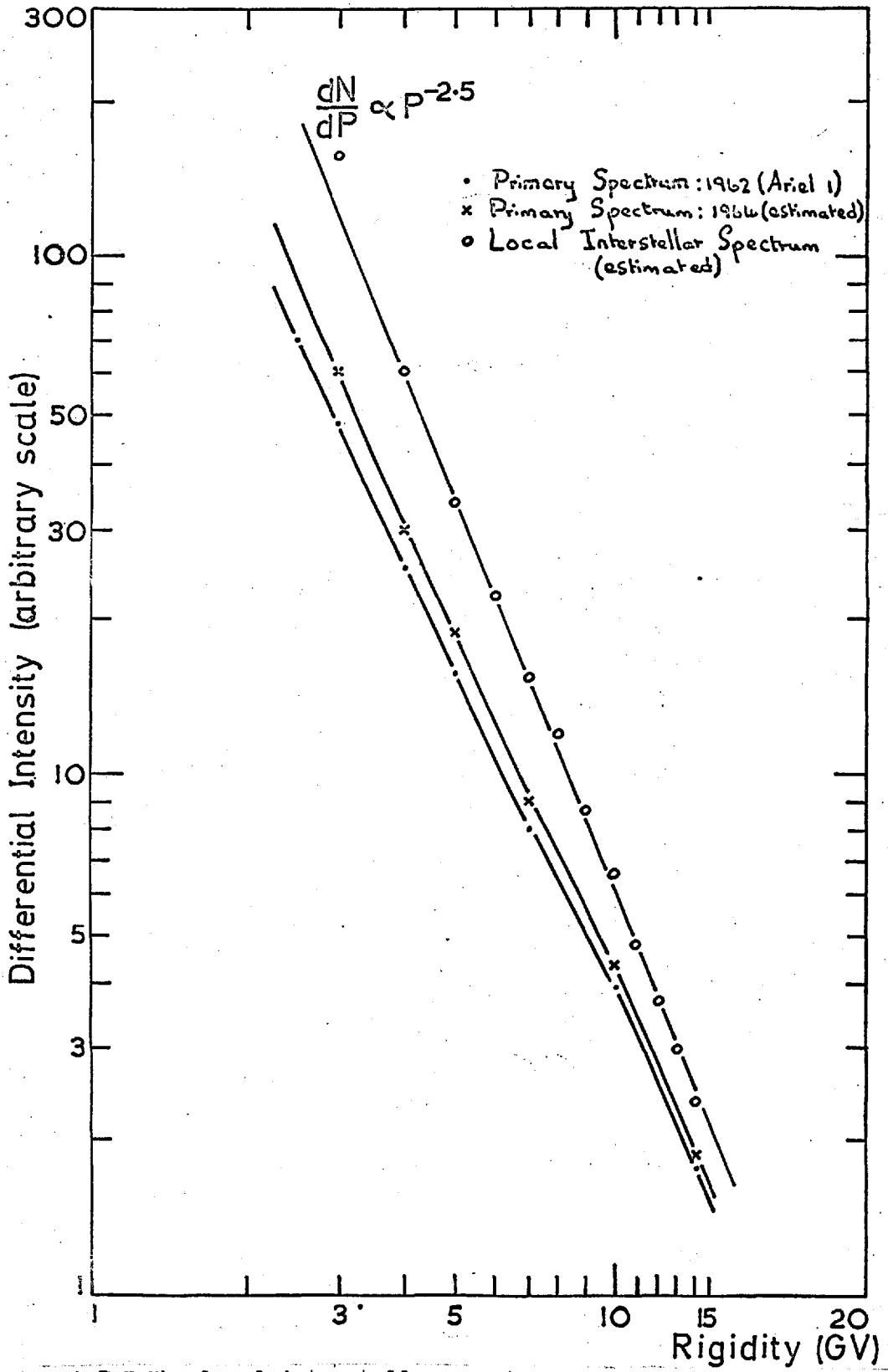


Fig. 6-5.I The local interstellar spectrum is constructed from the Ariel I spectrum and the modulation function of fig. 6-4.5. Also drawn are the Ariel I spectrum and the estimated 1964 primary spectrum at the position of the Earth's orbit.

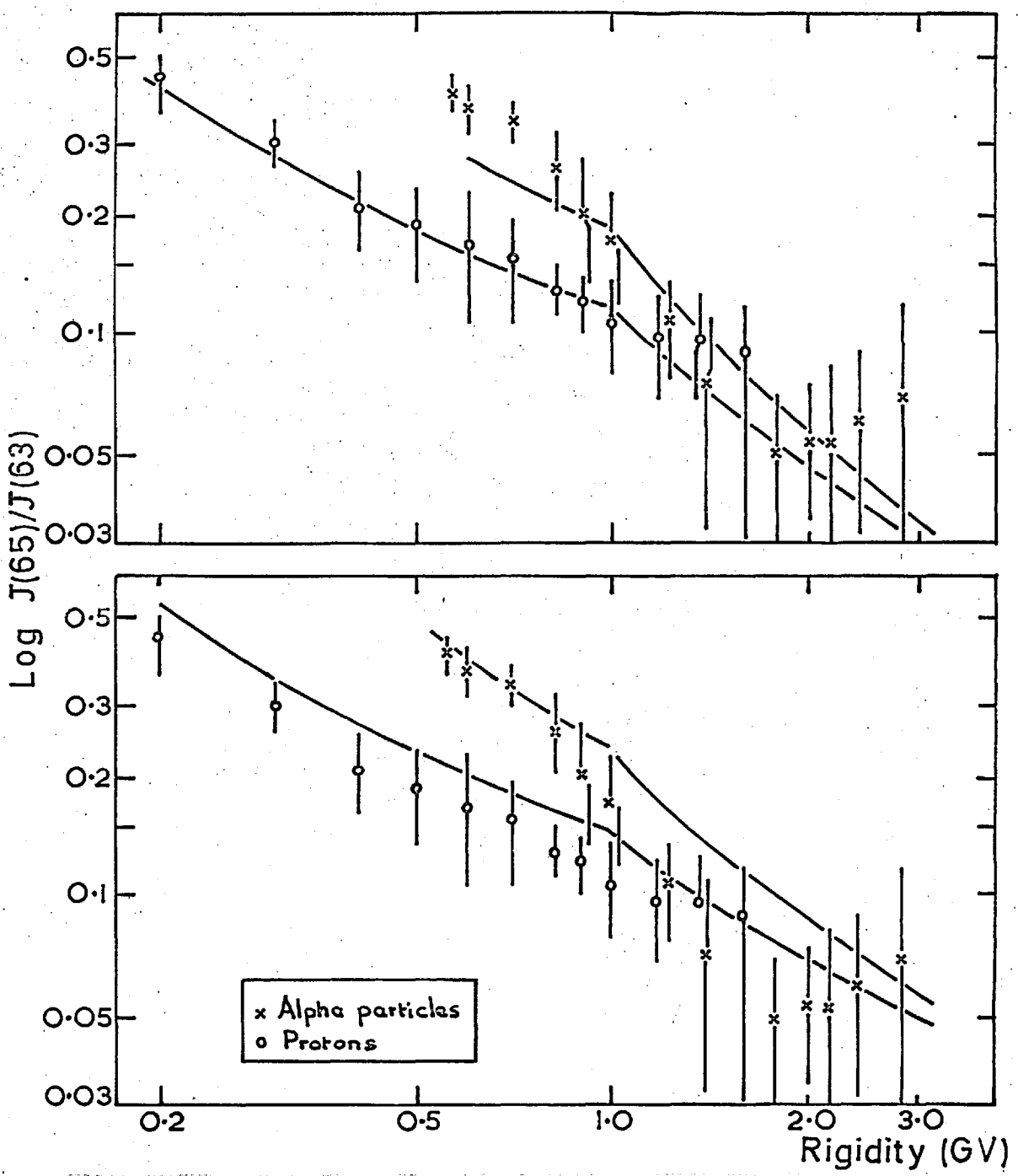


Fig. 6-6.1 Modulation of the differential proton and alpha particle spectra between 1963 and 1965. Curves are based on a diffusion-convection modulation model with the mean free path rigidity independent below 1 GV, and directly proportional to rigidity above 1 GV. (Quenby: 1966b)

Fig. 6-6.2 The proton/alpha data given by Quenby (1966b) is fitted by the empirical modulation function:

$$J(64)/J(63) = 1{\cdot}1\beta^{-1} \qquad P < 1 \text{ GV}$$
$$= 1{\cdot}1\beta^{-1}P^{-0{\cdot}75} \qquad P > 1 \text{ GV}$$

From equation (6.2) :

$$\left.\frac{dN}{dP}\right|_{t_1} = \left.\frac{dJ}{dP}\right|_{t_1} \sum_z S_z(P,x) \qquad 6.6$$

Similarly at t_2 :

$$\therefore \quad \frac{\left.\frac{dN}{dP}\right|_{t_1}}{\left.\frac{dN}{dP}\right|_{t_2}} = \frac{\left.\frac{dJ}{dP}\right|_{t_1}}{\left.\frac{dJ}{dP}\right|_{t_2}} = \frac{J_1(P)}{J_2(P)} \qquad 6.7$$

It has been shown in Section 2 that the modulation produced by all the convective models is of the form :

$$\ell_n \frac{n_e}{n} \propto \frac{1}{\lambda \beta}$$

From this we can write :

$$\log_{10} \frac{J(t_1)}{J(t_2)} \propto \frac{1}{\lambda\beta} \qquad 6.8$$

Expressing the rigidity dependence of λ as $\lambda \propto P^n$ a log x log plot of $\log_{10}\left[\frac{J(t_1)}{J(t_2)}\right]$ against rigidity P will reveal the rigidity dependence of the mean free path.

Plots of $\log_{10} \frac{J(64)}{J(62)}$ and $\log_{10} \frac{J(64)}{J(63)}$ are given in figures 6.4.5 and 6.4.6. together with the best fit to the data for the index n = 1 and n = 2. In both periods there is a clear preference for n = 1. The agreement is good though it is more significant statistically for $\frac{J(64)}{J(62)}$.

This implies that the diffusion mean free path is directly proportional to rigidity in the range 1.2 GV $<$ P $<$ 15 GV during the period of measurement 1962-1964.

6.5. SUN-SPOT MINIMUM MODULATION.

The observed modulation function 1962 - 1964 has been used to determine the 1964 primary spectrum by means of equation 6.7. This spectrum is plotted in figure 6.5.1. together with the 1962 spectrum obtained from the Ariel 1 measurements. This procedure is justified by the analysis of Webber (1966) of the relative behaviour of the various charged particles. Above 2-3 GV the ratios of the differential rigidity spectra of the various components were found to be approximately constant. These results suggested that the galactic spectra were similar rigidity spectra rather than energy per nucleon spectra. From the observed modulation function 1962-1964 and the Ariel 1 spectrum, it is possible to obtain an estimate of the modulation existing at solar minimum. This involves the following assumptions:

a) The modulation at sun-spot minimum has the same rigidity dependence between 3 GV and 15 GV as that determined for 1962 relative to 1964.

b) All components of the galactic spectrum have the same rigidity power low spectrum between 3 GV and 15 GV.

The normalization factor is then found for the 1962: 1964 modulation function so as to generate a simple power law primary

galactic spectrum from the 1962 spectrum. The best fit spectrum for a normalization factor of 5 is also plotted in figure 6.5.1. The modulation existing in 1964 is therefore ~ 4 times the modulation 1962-1964. Comparing this figure with the variation of the modulation over a complete solar cycle: the sun-spot minimum modulation is about 1.5 times the modulation at solar maximum relative to solar minimum. This is a reasonable figure in view of the balance of energy between the galactic magnetic field and the cosmic ray energy density. To produce isotropy of the cosmic radiation , it is probable that the galactic magnetic energy density will be $\sim$ the galactic cosmic ray energy density. Using the observed cosmic ray density as given by Komori (1962) and the factor 1.5 for the ratio of galactic cosmic ray energy density to observed energy density, then the galactic magnetic field must be $\gtrsim 6 \times 10^{-6}$ gauss. This is to be compared with the estimate of the mean galactic disc magnetic field of $\sim 10^{-5}$ gauss. The slope of the galactic spectrum found in this way is 2.5.

6.6 COMPARISON OF RESULTS WITH BALLOON OBSERVATIONS.

The observed modulation function $\frac{J(64)}{J(63)}$ can be compared to the proton and alpha particle balloon data given by Quenby (1966 b) for 1963 and 1965. These results are plotted in figure 6.6.1. The solid lines are given by equation 2.43. The mean bihourly counting rates of the Mt. Washington neutron monitor are given in Table (6.1) for the various data used in the analysis.

TABLE (6.1)

1963/1965 PROTON AND ALPHA MEASUREMENTS.

	Mt. Washington neutrons.	
Alpha Particles	1963	1965
Ormes and Webber (1966)	2320	2420
Balasubrahmanyan et al	-	2420
Freier and Waddington (1964)	2323	-
Protons		
Ormes and Webber (1966)	2320	2420
Balasubrahmanyan et al (1966)	-	2420

The mean Mt. Washington counting rates during the measurement of J(63)/J(64) from the aircraft surveys are :

1963 : 2306 6.9

1964 : 2396

The mean Mt. Washington levels in the analysis of Quenby [table (6.1)] are :

1963 : 2320 6.10

1965 : 2420

The two analyses are thus directly comparable. If the 1965 integral spectrum is N(P), then $\frac{1}{2}\ \frac{\partial N}{\partial P}$

is due to protons and $\frac{1}{2}\frac{\partial N}{\partial P}$ to heavies. The fractional change at 145 gcm^{-2} $f_{145}(P)$, is related to the proton change $f_p(P)$ and the heavies change, $f_h(P)$ $(= f_\alpha(P))$ by :

$$\frac{1}{2}\frac{\partial N}{\partial P} f_p(P) + \frac{1}{2}\frac{\partial N}{\partial P} f_H(P) = f_{145}(P)\frac{\partial N}{\partial P} \quad . \qquad 6.11$$

this becomes :

$$\frac{1}{2} f_p(P) + \frac{1}{2} f_\alpha(P) = f_{145}(P) \qquad 6.12.$$

From figure (6.6.1) the predicted modulations at 145 g cm^{-2} at two points where the proton and alpha particle spectra overlap are plotted in figure (6.4.6). These points are in good agreement with the modulation obtained from the surveys.

A good fit cannot be obtained with equation (2.43) as this modulation function falls off too quickly at the high rigidities. The function is compared to the experimental results in figure 6.6.2.

A possible way of reconciling the two sets of data can be found with the following conditions :

$$\log_{10}\frac{J(65)}{J(63)} = 0.11\,\beta^{-1} : P < 1.0 \text{ GV} \qquad 6.13$$
$$= 0.11\,P^{-1} : P > 1.0 \text{ GV}$$

In view of the fact that diffusion theories introduce the particle velocity it seems implausible that above 1.0 GV the velocity should not influence the modulation.

A good fit can be obtained by allowing the modulation in the rigidity range above 1.0 GV to be represented by :

$$\log_{10} \frac{J(t_1)}{J(t_2)} = A\,\beta^{-1}\,P^{-\alpha} \qquad 6.14$$

This function is drawn in figure (6.6.2) for the best fit values of $\alpha = 0.75$ and $A = 0.11$. The modulation is thus best represented by :

$$\log_{10} \frac{J(65)}{J(63)} = 0.11\,\beta^{-1} \qquad P < 1.0 \text{ GV} \qquad 6.15$$

$$= 0.11\,\beta^{-1}\,P^{-0.75} \qquad P > 1.0 \text{ GV}$$

The proton/alpha measurements fitted to these conditions are plotted in figure (6.6.3).

Introducing the velocity dependence of the modulation to the 1962 spectrum, it is found that the data in figure 6.6.4 is well fitted by :

$$\log_{10} \frac{J(1964)}{J(1962)} = 1.9 \times \beta^{-1} \times P^{-0.75} \times 10^{-1}$$

$$\text{for} \qquad P > 1.0 \text{ GV} \qquad 6.16$$

6.7 DISCUSSION

It is to be stressed that a number of rigidity functions can be fitted to these data above 1.0 GV by varying the upper rigidity limit to the rigidity range where the modulation is purely velocity dependent. The 1.0 GV limit in 6.15 for 1963 is based on proton/alpha measurements which are able to separate the effects of velocity and rigidity. Experimental evidence has suggested that the limit of pure velocity dependence is reduced towards solar maximum. The modulation in 1962 in the region measured ($P > 1.2$ GV) must then be represented by a function such as (6.16).

It is possible that the rigidity dependence of the modulation changes gradually from a rigidity independent form to a P^{-1} dependence. This dependence of the modulation could be made to fit the data but would not result in simple expressions such as 6.15 and 6.16. The data above a few GV rigidity could then be represented by the form :

$$\frac{J(t_1)}{J(t_2)} \propto \exp - \frac{1}{\beta P} \qquad 6.17$$

In view of the complicated 'meteorological' conditions in interplanetary space it is not surprising that the modulation should not have a simple integer index for the rigidity dependence but rather it would be surprising if it were so. If the diffusion is mainly via hydromagnetic waves then the generation spectrum of waves

can probably be defined analytically, but the spatial density of sources of hydromagnetic waves and consequently the radial dependence of the power spectrum is not known. Similarly, if the scattering were mainly via shearing of the lines of force caused by anisotropic solar plasma emission then it is equally unlikely that an analytic expression would exist for the scattering centre scale sizes and their radial dependence.

The features of the modulation can only be described in terms of the general conditions. Cosmic ray modulation in the latitude-sensitive region in the years 1962 and 1963 is better represented by a scattering mean free path $\lambda \propto P$ than by $\lambda \propto P^2$. A spectrum of scattering centre scale sizes must exist in any diffusion - convection model. If the scattering centres re sharp kinks as in the Dorman model then the range of scattering centre dimensions is at least 8.10^{10}cm to 10^{12}cm (scattering centre fields of 5γ). This observed form of the modulation is anticipated in the work of Quenby (1966b) and Gloeckler and Jokipii (1966).

As solar minimum conditions correspond to a generally smooth interplanetary magnetic field near the Earth's orbit, the modulating conditions will change towards the solar maximum period as the interplanetary field becomes more turbulent. The modulation process may then change from one in which waves and kinks in the field lines contribute equivalent amounts to a process which is dominated by scattering in magnetic kinks. Subsequent latitude surveys nearer to solar maximum may well observe a rigidity dependence to the modulation which differs from that appropriate to solar minimum conditions.

Appendix to Chapter 6.

The data obtained in the 12 surveys are plotted against the experimentally corrected cut-offs in the following figures 6.1.1 to 6.1.12.

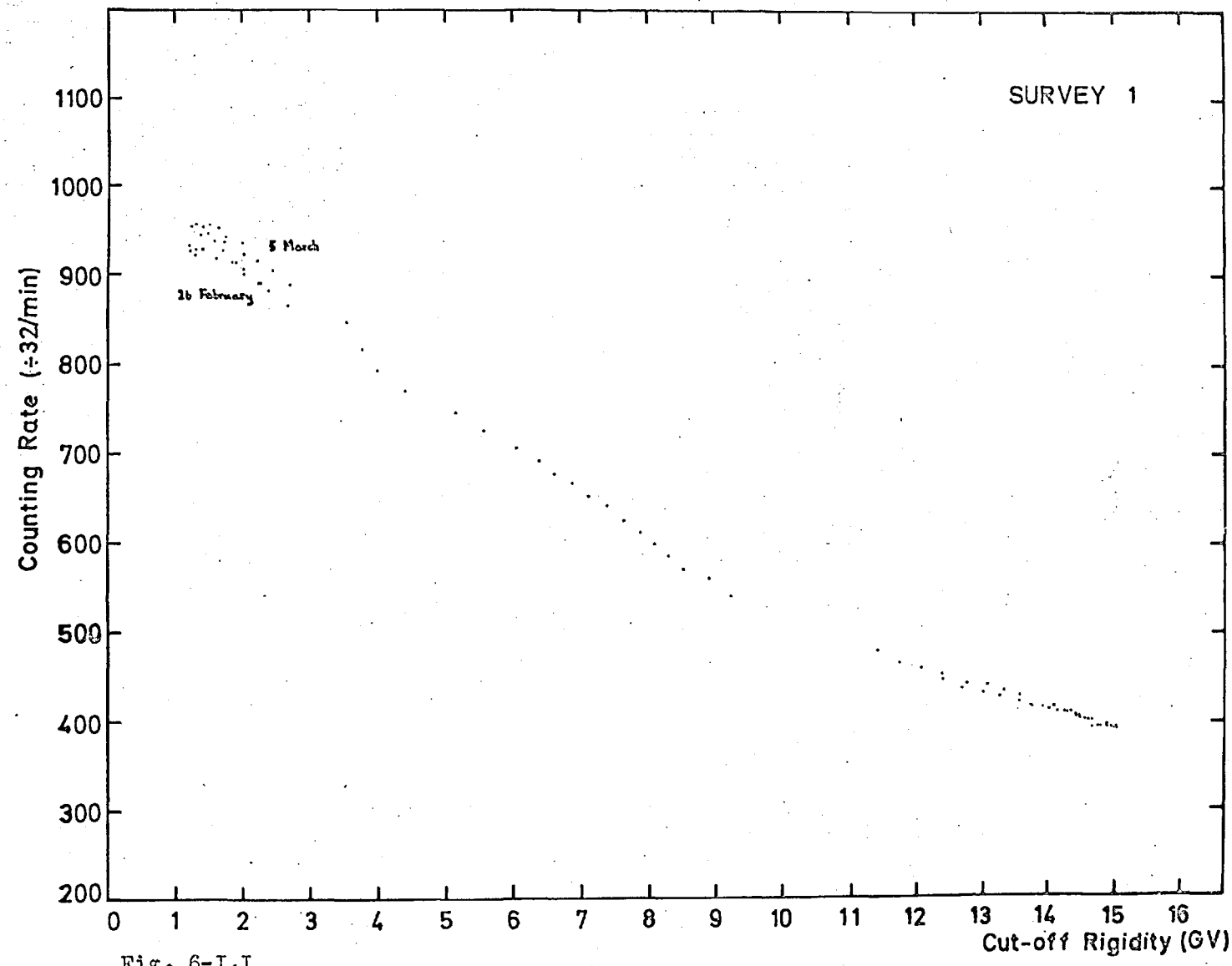

SURVEY 1
5 March
26 February
Counting Rate (÷32/min)
1100
1000
900
800
700
600
500
400
300
200
0
1
2
3
4
5
6
7
8
9
10
11
12
13
14
15
16
Cut-off Rigidity (GV)

Fig. 6-I.I

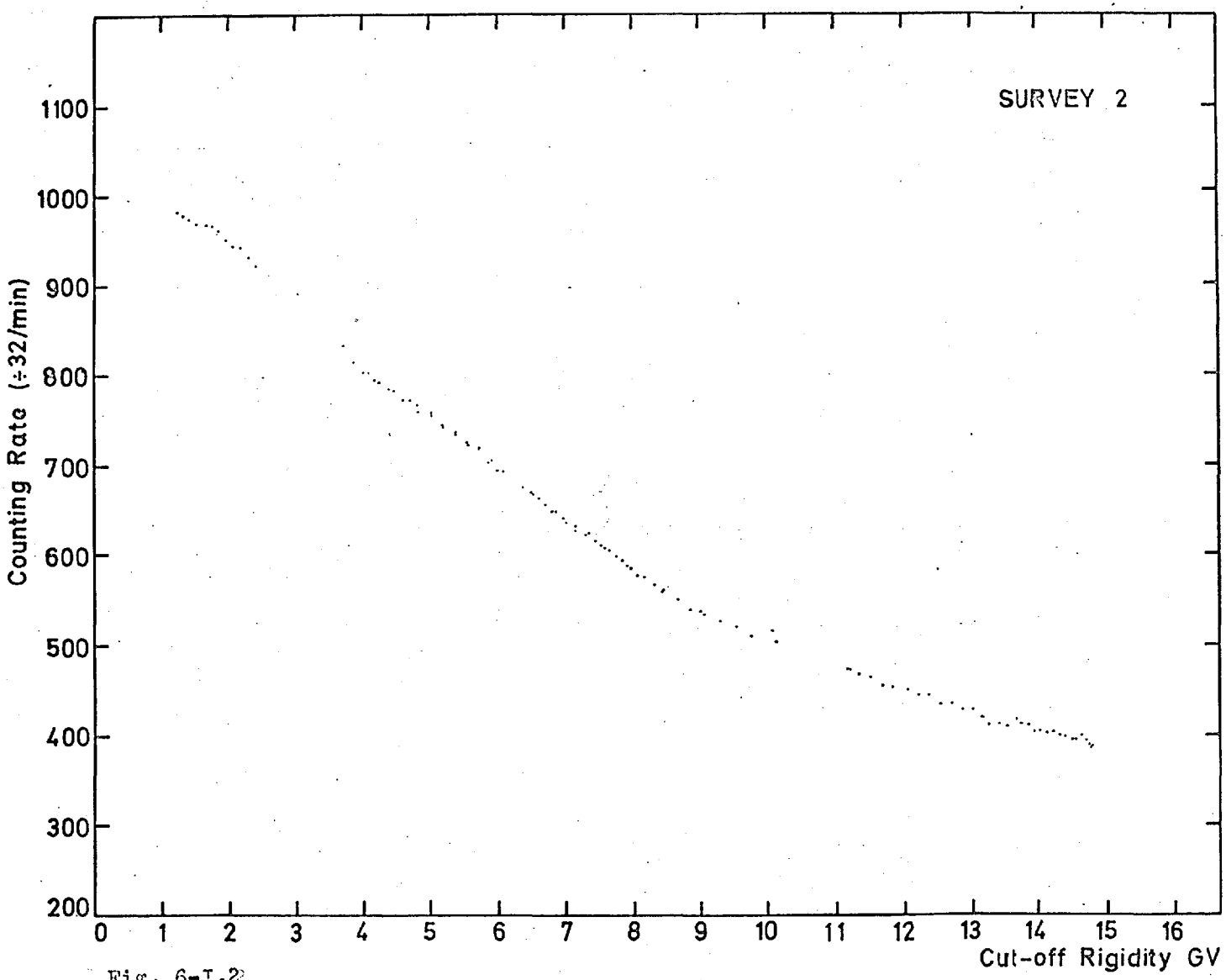

SURVEY 2
Counting Rate (÷32/min)
1100
1000
900
800
700
600
500
400
300
200
0
1
2
3
4
5
6
7
8
9
10
11
12
13
14
15
16
Cut-off Rigidity GV

Fig. 6-I.2

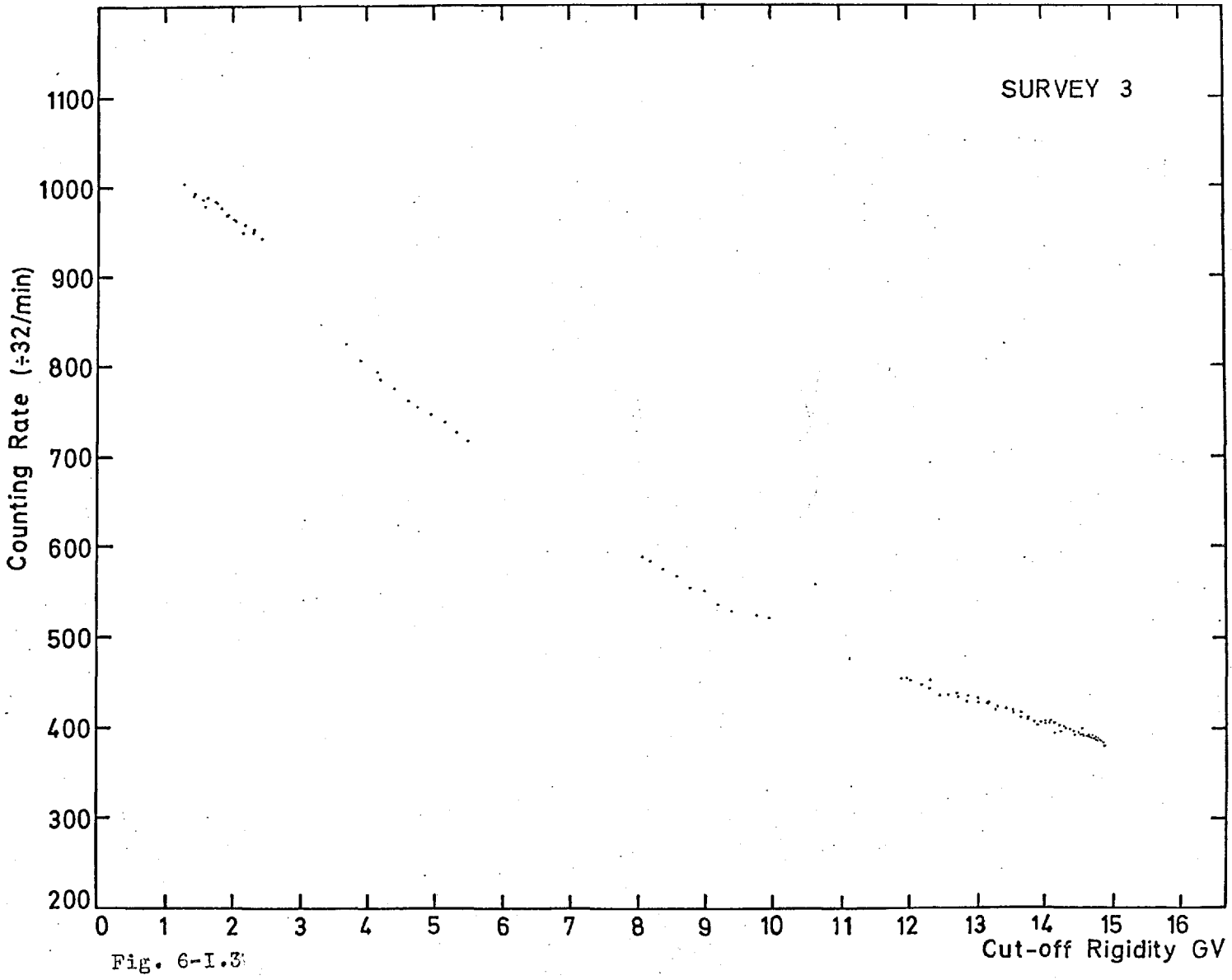

SURVEY 3
Counting Rate (÷32/min)
1100
1000
900
800
700
600
500
400
300
200
0
1
2
3
4
5
6
7
8
9
10
11
12
13
14
15
16
Cut-off Rigidity GV

Fig. 6-I.3

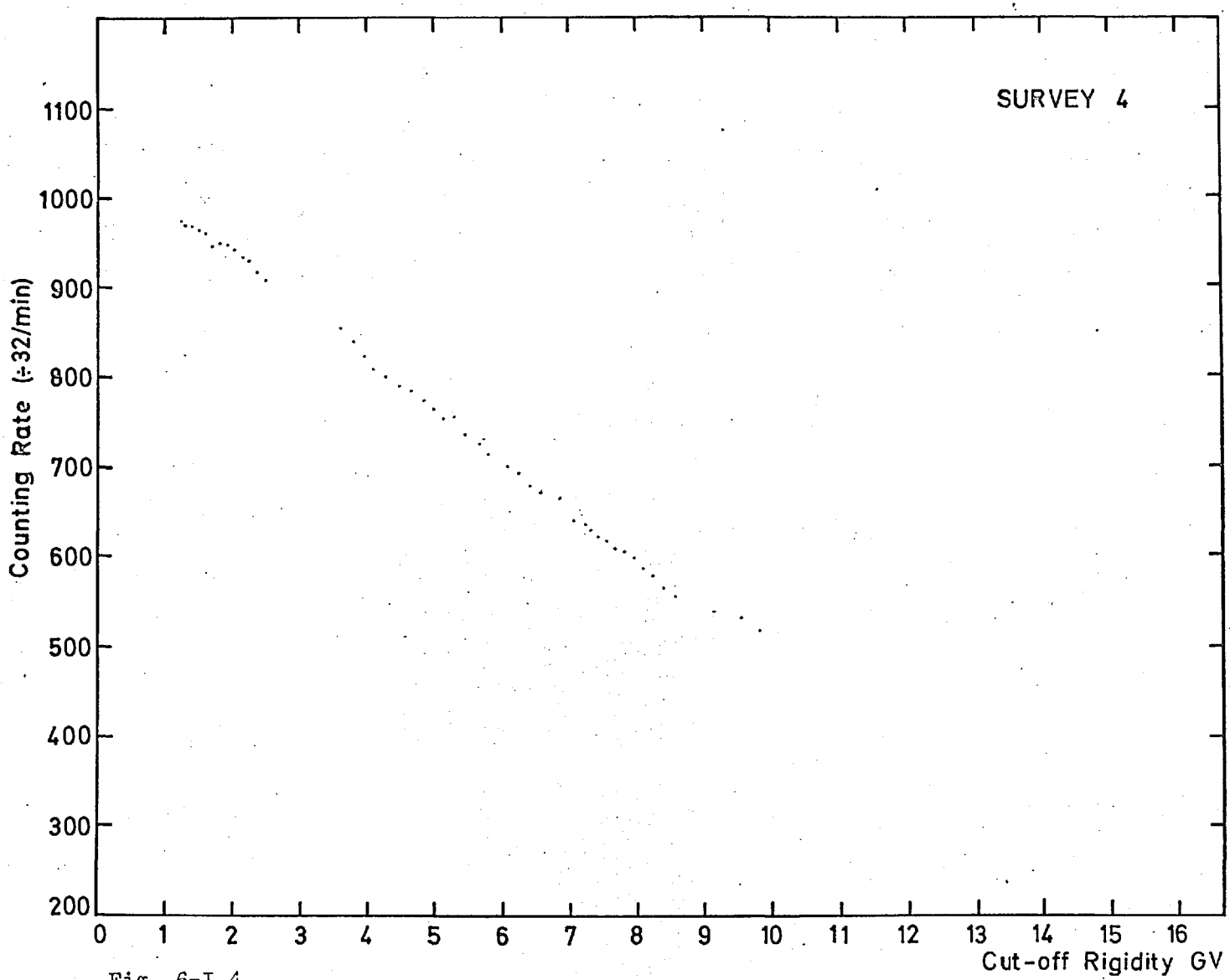

SURVEY 4
Counting Rate (÷32/min)
1100
1000
900
800
700
600
500
400
300
200
0
1
2
3
4
5
6
7
8
9
10
11
12
13
14
15
16
Cut-off Rigidity GV

Fig. 6-I.4

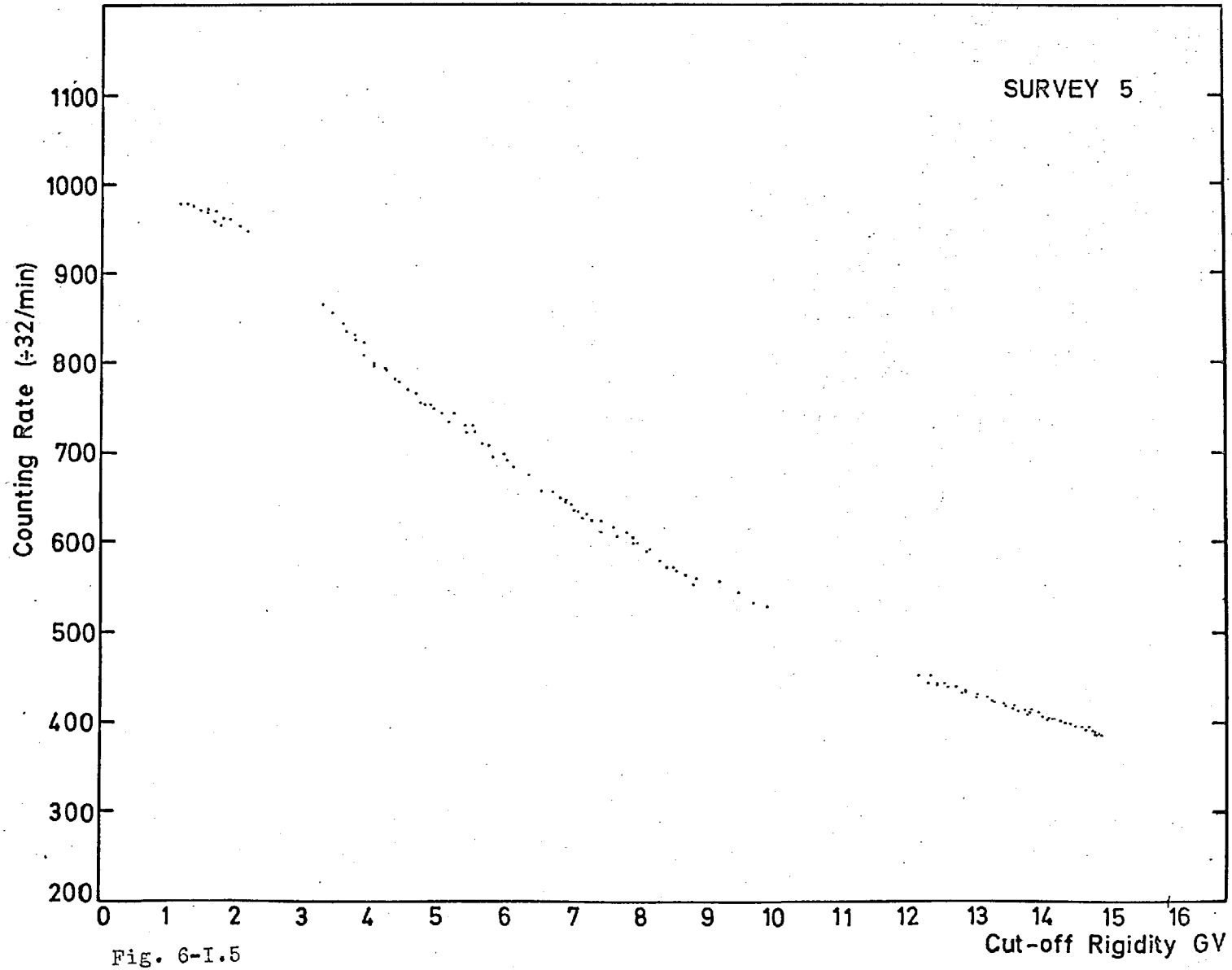

SURVEY 5
Counting Rate (÷32/min)
1100
1000
900
800
700
600
500
400
300
200
0
1
2
3
4
5
6
7
8
9
10
11
12
13
14
15
16
Cut-off Rigidity GV

Fig. 6-I.5

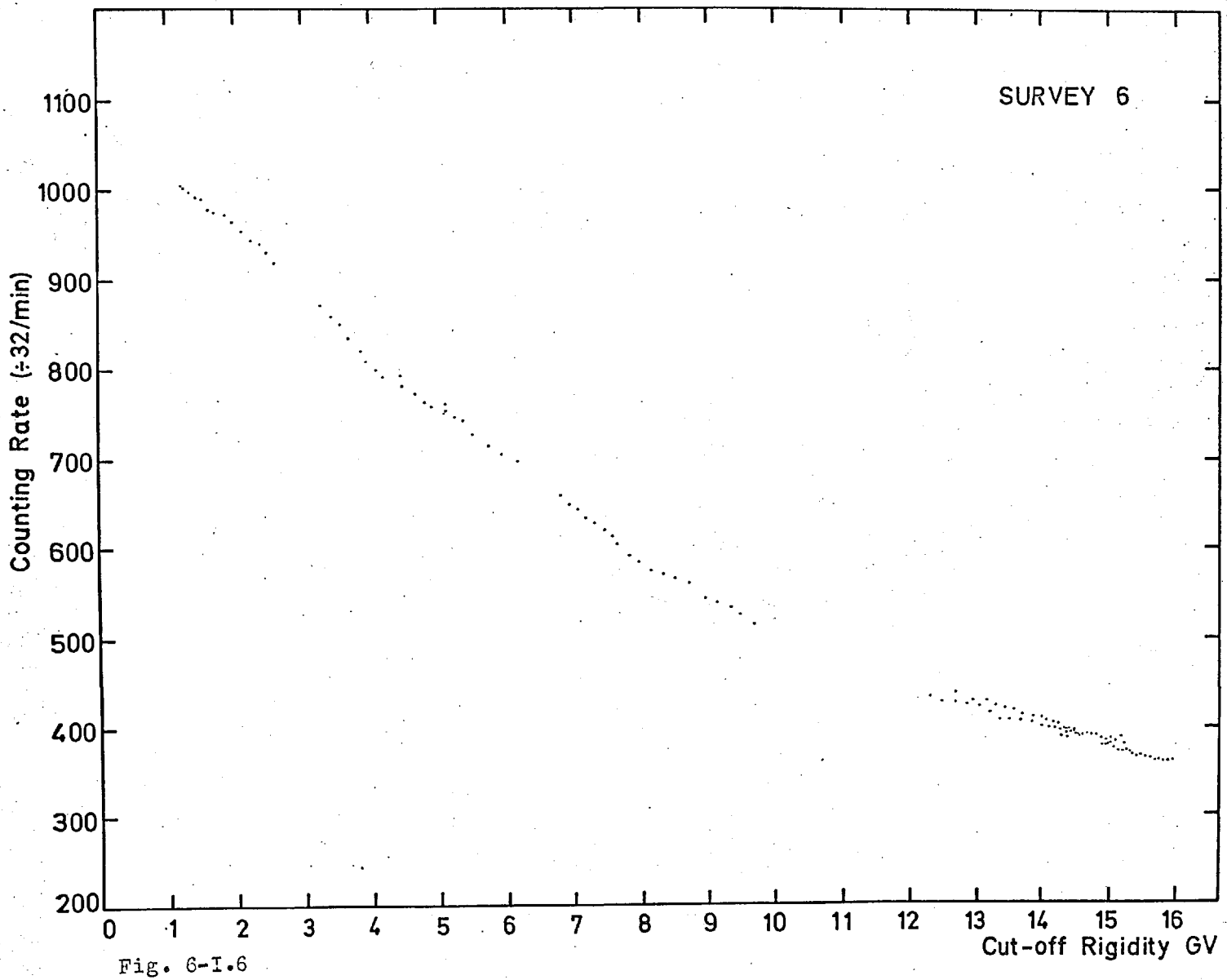

SURVEY 6
Counting Rate (÷32/min)
1100
1000
900
800
700
600
500
400
300
200
0
1
2
3
4
5
6
7
8
9
10
11
12
13
14
15
16
Cut-off Rigidity GV

Fig. 6-I.6

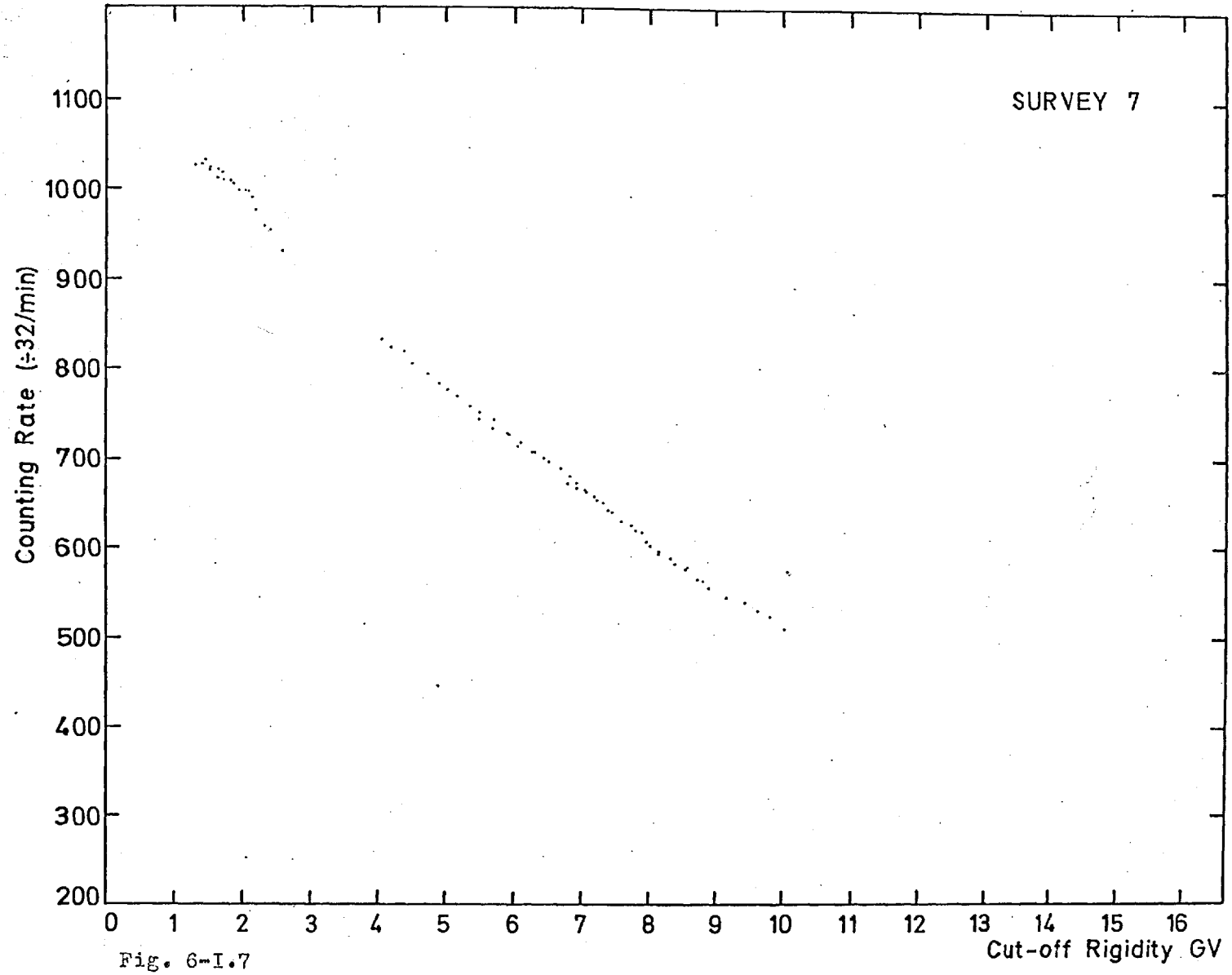

SURVEY 7
Counting Rate (÷32/min)
1100
1000
900
800
700
600
500
400
300
200
0
1
2
3
4
5
6
7
8
9
10
11
12
13
14
15
16
Cut-off Rigidity GV

Fig. 6-I.7

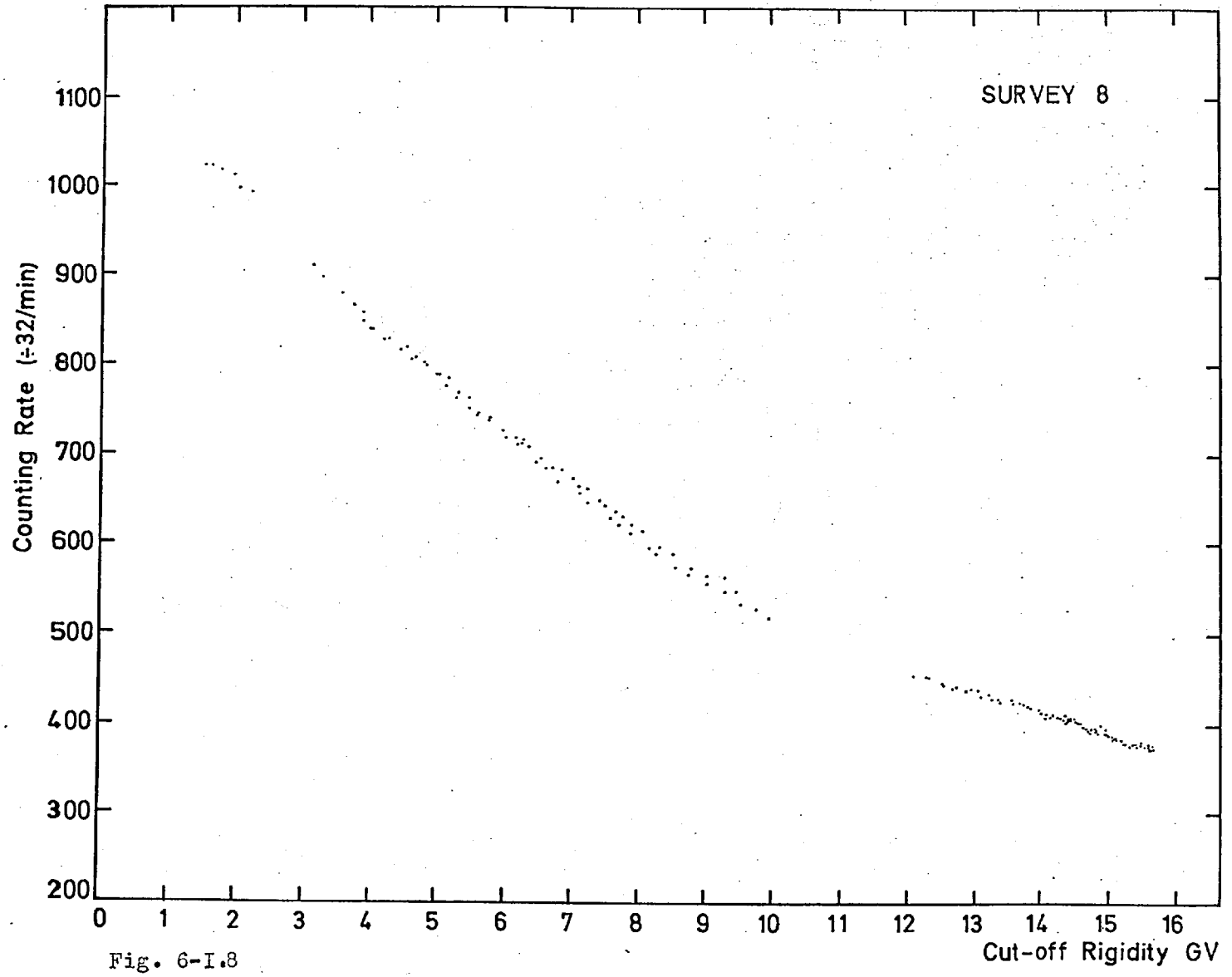

SURVEY 8
Counting Rate (÷32/min)
1100
1000
900
800
700
600
500
400
300
200
0
1
2
3
4
5
6
7
8
9
10
11
12
13
14
15
16
Cut-off Rigidity GV

Fig. 6-I.8

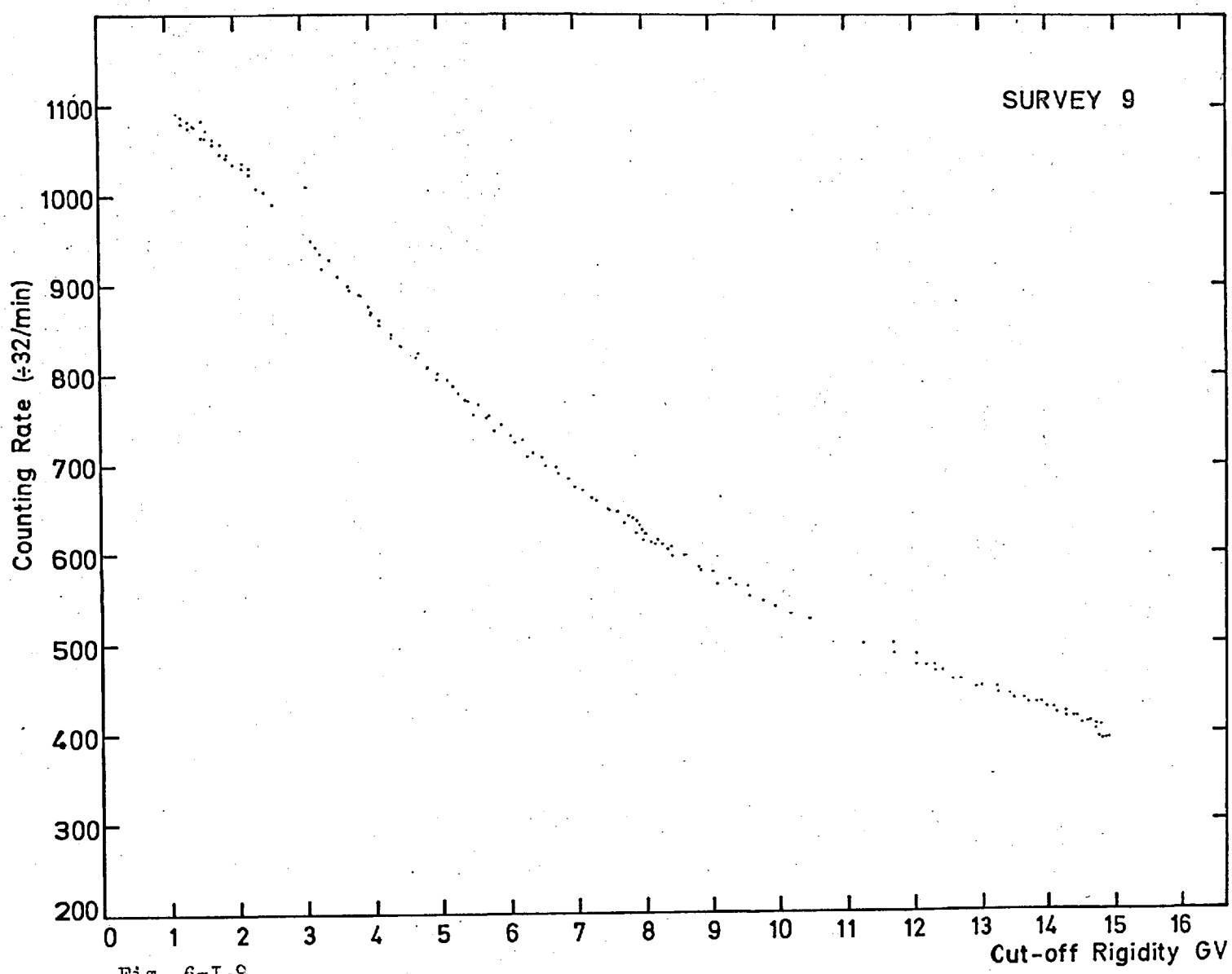

SURVEY 9
Counting Rate (÷32/min)
1100
1000
900
800
700
600
500
400
300
200
0
1
2
3
4
5
6
7
8
9
10
11
12
13
14
15
16
Cut-off Rigidity GV

Fig. 6-I.9

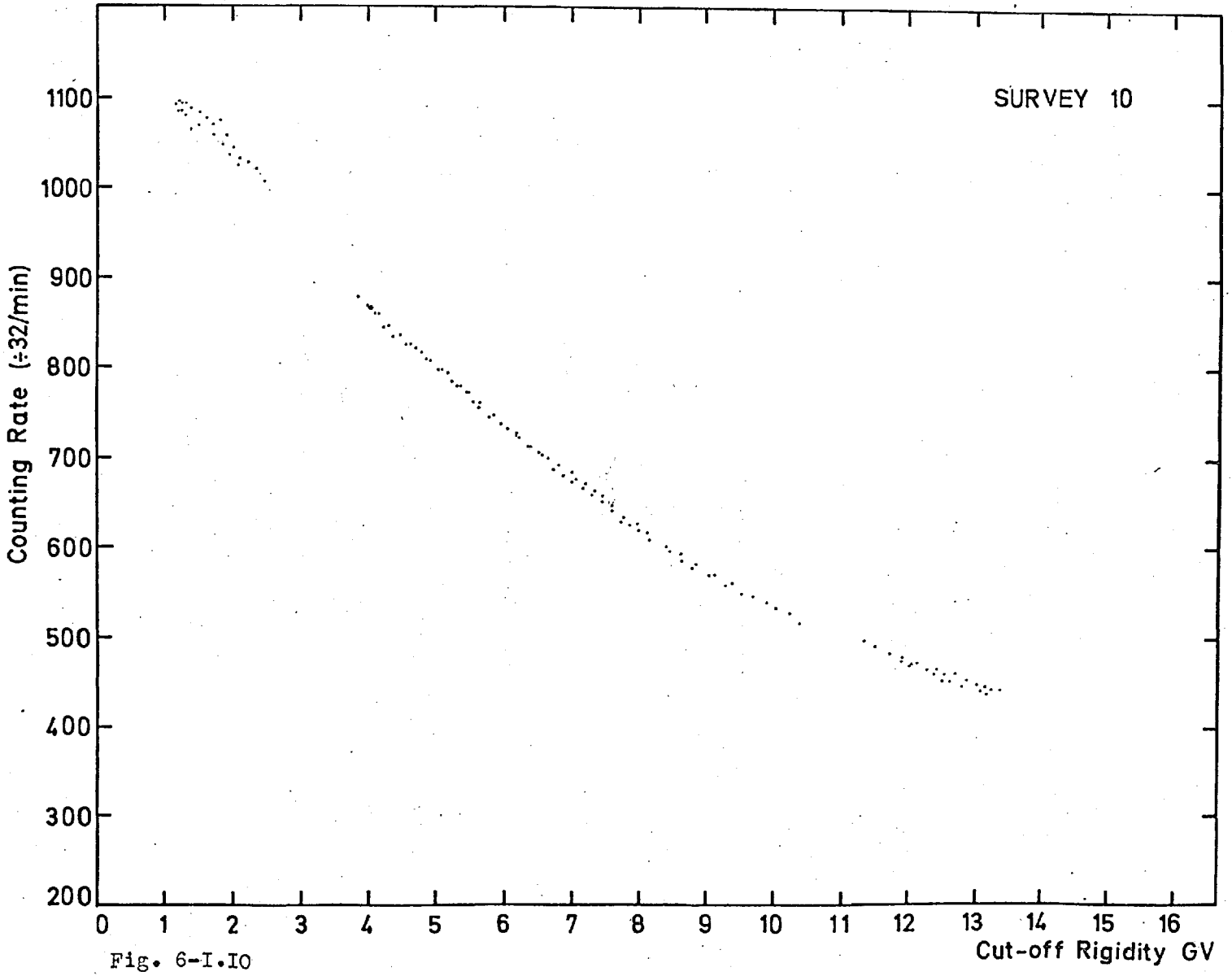

SURVEY 10
Counting Rate (±32/min)
1100
1000
900
800
700
600
500
400
300
200
0
1
2
3
4
5
6
7
8
9
10
11
12
13
14
15
16
Cut-off Rigidity GV

Fig. 6-I.IO

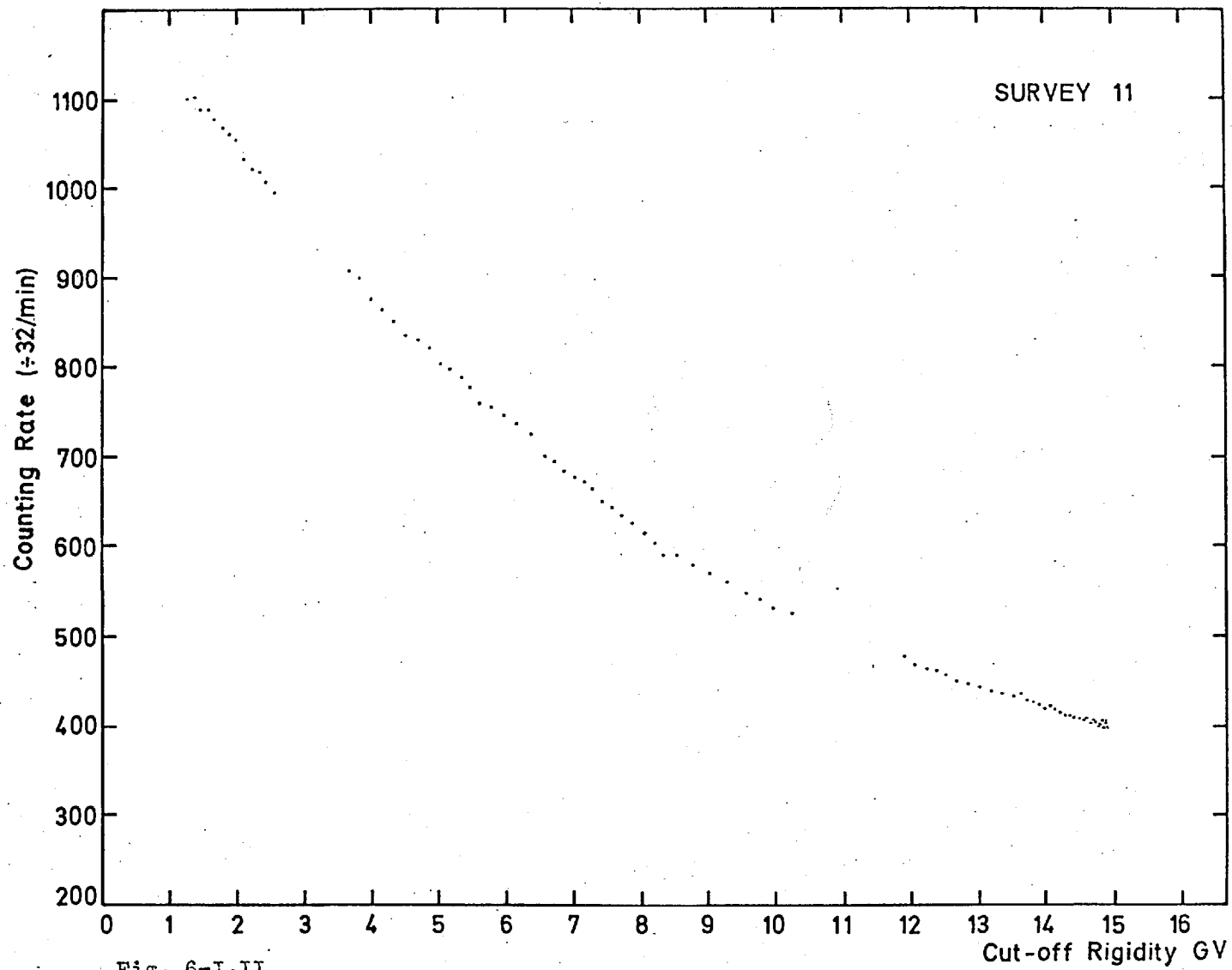

SURVEY 11
Counting Rate (÷32/min)
1100
1000
900
800
700
600
500
400
300
200
0
1
2
3
4
5
6
7
8
9
10
11
12
13
14
15
16
Cut-off Rigidity GV

Fig. 6-I.II

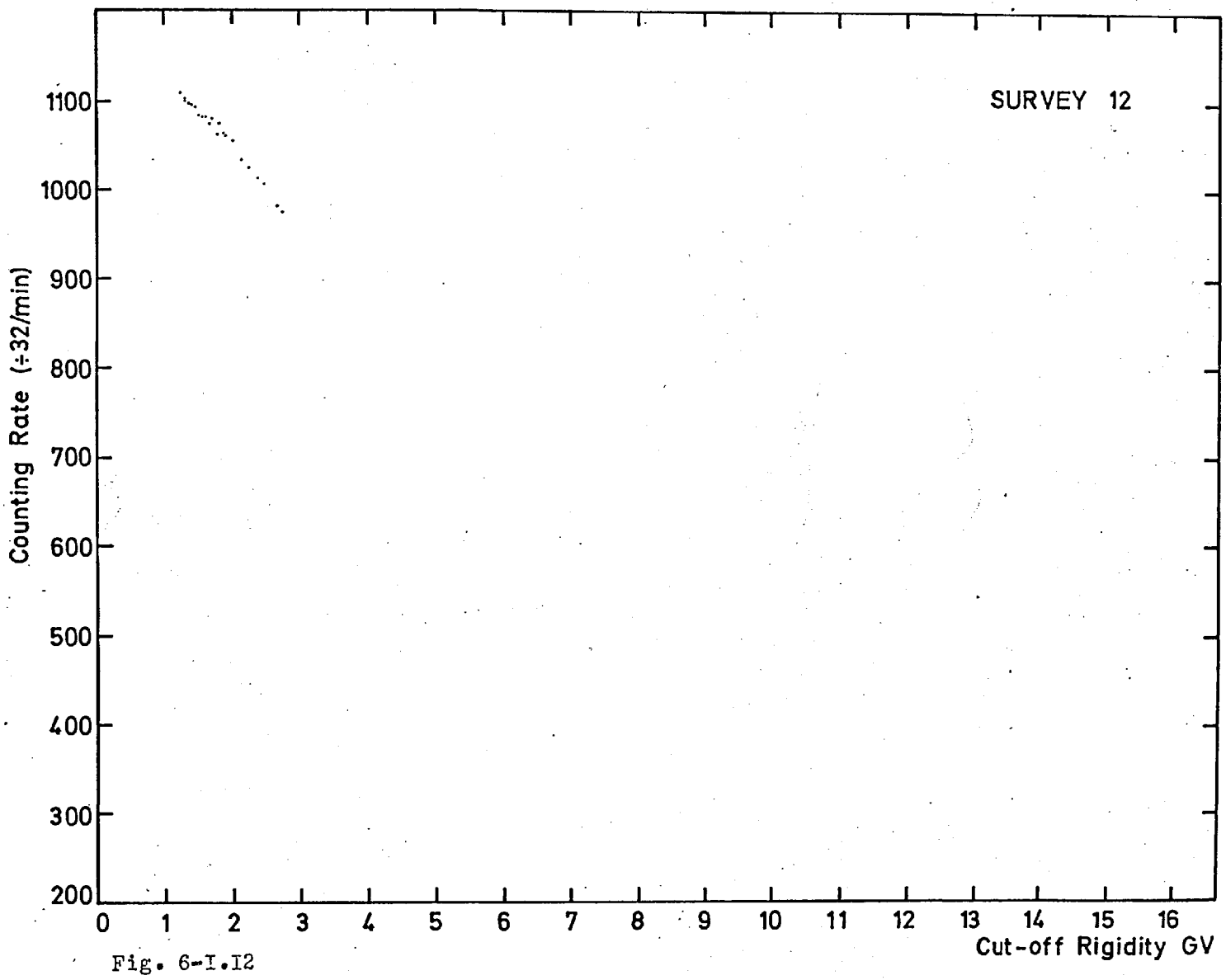

SURVEY 12
Counting Rate (÷32/min)
1100
1000
900
800
700
600
500
400
300
200
0
1
2
3
4
5
6
7
8
9
10
11
12
13
14
15
16
Cut-off Rigidity GV

Fig. 6-I.I2

ACKNOWLEDGEMENTS.

I am grateful to Professor P.M.S. Blackett and Professor C.C. Butler for the laboratory facilities provided to me.

I am also grateful to Professor H. Elliot and Dr. J.J. Quenby, my supervisor, for their continued interest and advice.

I would like to acknowledge the help and guidance given by Mr. A. Bewick, under whose supervision the early surveys were carried out.

It is a pleasure to record the cooperation of the staff and personnel of the Royal Aircraft Establishment, Farnborough, both in the flying of the recorder and the provision of flight information.

I would like to thank Dr. M.A. Shea and Dr. R.J. Hynds for their trajectory calculations.

Thanks are due to the members of the Cosmic Ray and Space Physics Group, Imperial College, for many fruitful discussions.

Finally, I would like to thank the Science Research Council for providing a maintenance grant during the period of this work.

REFERENCES

ALFVEN H., 1950, Cosmical Electrodynamics, (Clarendon Press, Oxford).

AKASOFU S.I. and W.C. LIN, 1963, J. Geophys. Res., 68, 873.

AKASOFU S.I., W.C. LIN, and J.A. VAN ALLEN, 1963, J. Geophys. Res., 68, 5327.

AXFORD W.I., 1965, Planet. and Spa. Sci., 13, 115.

BABCOCK H.D., 1959, Astrophys. J., 130, 364.

BABCOCK H.W., 1961, Astrophys. J. 133, 572.

BABCOCK H.W. and H.D. BABCOCK, 1955, Astrophys. J. 121,349.

BALASUBRAHMANYAN V.K. and F.B. McDONALD, 1964, J. Geophys. Res., 69, 3289.

BALASUBRAHMANYAN V.K., D.E. HAGGE, G.H. LUDWIG and F.B. McDONALD, 1966, Int. Conf. on Cosmic Rays, London (1965), 1, 427.

BARTLEY W.C., R.P. BUKATA, K.G. McCRACKEN and U.R. RAO, J. Geophys. Res., 71, 3297.

BEWICK A., 1963, Private Communication.

BIERMAN L., 1951, Z. Astrophys., 29, 274.

BRIDGE H.S., A. EGIDI, A. LAZARUS, E. LYON and L. JACOBSON, 1965, Space Research V, (North-Holland:Amsterdam), 969.

BRYANT D.A., T.L. CLINE, U.D. DESAI and F.B. McDONALD, 1965, Astrophys. J., 141, 478.

CAHILL L.J., 1966, J. Geophys. Res., 71, 4505.

CAHILL L.J. and P.G. AMAZEEN, 1963, J. Geophys. Res., 68, 1835.

CAHILL L.J. and D.H. FAIRFIELD, 1965, (Reported by J.W. Dungey (1966)).

CAIN J.C., 1966, Advanced Study Institute, Bergen, 1965, (Reidel Publishing Co.:Holland), 7.

CAIN J.C., W.E. DANIELS, S.J. HENDRICKS and D.C. JENSEN, 1965, J. Geophys. Res., 70, 3647.

CARMICHAEL M., M. BERCOVITCH, J.F. STELJES and M. MAGIDIN, 1966, Int. Conf. on Cosmic Rays, London (1965), 1, 553.

CHASSON R.L., 1954, Phys. Rev., 96, 1116.

CLAY J., 1927, Proc. Roy. Acad. Amst., 30, 1115.

COMPTON A.H., 1933, Phys. Rev., 43, 387.

COON J.H., 1966, Advanced Study Institute, Bergen 1965, (Reidel Publishing Co: Holland), 231.

COURTIER G.M. & A.D. LINNEY, 1966, Planet.and Spa. Sci. 14, 503.

DAVIS L.R. & J.M. WILLIAMSON, 1963, Space Res., 3, 365.

DESSLER A.J. & E.N. PARKER, 1959, J. Geophys. Res., 64, 223.

DORMAN L.I., 1957, Cosmic Ray Variations (State Publishing House, Moscow).

DORMAN L.I., 1963, Progress in Elementary Particles & Cosmic Ray Physics, VII, 133 (North-Holland Publishing Co., Amsterdam).

DUNGEY J.W., 1958, Cosmic Electrodynamics, (Cambridge University Press).

DUNGEY J.W., 1966, Advanced Study Institute, Bergen 1965, (Reidel Publishing Co., Holland), 389.

DUPERERIER A., 1949, Proc. Phys. Soc. A, 62, 684.

DURNEY A.C., H. ELLIOT, R.J. HYNDS & J.J. QUENBY, 1964, Proc. Roy. Soc. A, 281, 553.

DUTT J.C. & T. THAMBYAHPILLAI, 1965, J. Atmos. Terr. Phys., 27, 349.

EHMERT A., 1960, Proc. Int. Conf. on Cosmic Rays, Moscow (1959) 4, 142.

ELLIOT H. , 1960, Phil. Mag., 5, 601.

ELLIOT H., R.J. HYNDS, J.J. QUENBY & G.J. WENK, 1960, Proc. Int. Conf. on Cosmic Rays, Moscow (1959) 4, 319.

FAN C.Y., P. MEYER & J.A. SIMPSON, 1960a, Phys. Rev. Letters, 5, 269.

FAN C.Y., P. MEYER & J.A. SIMPSON, 1960b, Phys. Rev. Letters, 5, 272.

FAN C.Y., G. GLOECKLER & J.A. SIMPSON, 1966, Proc. Int. Conf. on Cosmic Rays, London (1965), 1, 380.

FERMI E., 1949, Phys. Rev., 75, 1169.

FICHTEL C.E., D.E. GUSS, D.A. KNIFFEN & K.A. NEELAKANTAN, 1964, J. Geophys. Res., 69, 3293.

FINCH H.P. & B.R. LEATON, 1957, Mon. Not. R. Astr. Soc., Geophys. Suppl., 1, 314.

FORBUSH S.E., 1954, J. Geophys. Res., 59, 525.

FRANK L.A., 1965, J. Geophys. Res., 70, 1593.

FRANK L.A., 1966, J. Geophys. Res., 71, 4631.

FREIER P.S., 1962, J. Geophys. Res., 67, 2617.

FREIER P.S. & C.J. WADDINGTON, 1964, Phys. Rev. Letters, 13, 108.

FREIER P.S. & C.J. WADDINGTON, 1965, Space Sci. Rev., 4, No.3, 313.

FREIER P.S., E.P. NEY & J.R. WINCKLER, 1959, J. Geophys. Res., 64, 685.

FREON A. & K.G. McCRACKEN, 1962, J. Geophys. Res., 67, 888.

GINZBURG V.L. & S.I. SYROVATSKY, 1964, The Origin of Cosmic Rays, (Pergamon Press).

GLOECKLER G. & J.R. JOKIPII, 1966, Phys. Rev. Letters, 17, 203.

HOFFMANN R.A. & P.A. BRACKEN, 1965, J. Geophys. Res., 70, 3541.

HULTQVIST B., 1958, Arkiv für Geofysik, 3, 63.

HYNDS R.J., 1965, Private Communication.

JANOSSY L., 1937, Zeit. f. Phys., 104, 430.

JENSEN D.C. & J.C. CAIN, 1962, J. Geophys. Res., 67, 3568.

JOHNSON T.H., 1938, Rev. Mod. Phys., 10, 194.

JOHNSON T.H. & J.C. STREET, 1933, Phys. Rev. 43, 381.

KATZ L.,P.,MEYER & J.A. SIMPSON, 1958, Nuovo Cim., 8, Suppl. 11, 277.

KELLOGG P.J., 1960, J. Geophys. Res., 65, 2701.

KELLOGG P.J. & J.R. WINCKLER, 1961, J. Geophys. Res., 66, 3991.

KODAMA M., 1964, Private Communication.

KODAMA M., 1965, Canad. J. Phys., 43, 836.

KODAMA M. & T. MATHEWS, 1964, J. Geophys. Res., 69, 4429.

KODAMA M. & Y. MIYAZAKI, 1957, Rept. of Ionosphere Res. in Japan, 11, 99.

KOMORI H.L., 1962, J. Phys. Soc. Japan, 17, 620.

KONDO I. & M. KODAMA, 1966, Proc. Int. Conf. on Cosmic Rays, London (1965), 1, 558.

KONDO I., M. KODAMA & T. MAKINO, 1963, Proc. Int. Conf. on Cosmic Rays, Jaipur, 2, 383.

LASTER H., A.M. LENCHECK & S.F. SINGER, 1963, J. Geophys. Res., 67, 2639.

LEINBACH H., 1961, Ark.f. Geofys. 3, 427.

LEINBACH H., VENKATESAN D. & R. PARTHASARATHY, 1965, Planet. Spa. Sci., 13, 1075.

LEMAITRE G. & M.S. VALLARTA, 1936, Phys. Rev., 50, 493.

LIN W.C., D. VENKATESAN & J.A. VAN ALLEN, 1963, J. Geophys. Res., 68, 4885.

LOCKWOOD J.A. & H. RAZDAN, 1963, J. Geophys. Res., 68, 1581.

McCRACKEN K.G., 1960, Phys. Rev., 117, 1570.

McCRACKEN K.G., 1962, J. Geophys. Res., 67, 447.

McCRACKEN K.G., U.R. RAO & M.A. SHEA, 1962, Mass. Inst. Tech. Rept., 77, August 1962.

McILWAIN C.E., 1961, J. Geophys. Res., 66, 3681.

MAEHLUM B. & B.J. O'BRIEN 1963, J. Geophys. Res., 68, 997.

MAKINO T., 1963, Rept. Ionosphere Spa. Res. Japan, 17, 173.

MAKINO T. & M. KODAMA, 1966, Proc. Int. Conf. on Cosmic Rays, London (1965) 1, 564.

MARSDEN P.L. & J.G. WILSON, 1958, Nuovo Cim., 8, Suppl. 11, 228.

MATHEWS T., 1963, Phil. Mag., 8, 387.

MEYER P. & J.A. SIMPSON, 1957, Phys. Rev., 106, 568.

MEYER P., E.N. PARKER & J.A. SIMPSON, 1956, Phys. Rev., 104, 768.

MILLIKAN R.A. & H.V. NEHER, 1936, Phys. Rev., 50, 15.

MORRISON P., 1956, Phys. Rev., 107, 1397.

NAGASHIMA K., 1953, J. of Geomag. & Geoelec. 5, 141.

NAGASHIMA K., S.P. DUGGAL & M.A. POMERANTZ, 1966, Planet. Spa. Sci., 14, 177.

NEHER H.V. & H.R. ANDERSON, 1964, J. Geophys. Res., 69, 1911.

NEHER H.V. & S.E. FORBUSH, 1958, Phys. Rev. Letters, 1, 173.

NESS N.F., 1965, J. Geophys. Res., 70, 2989.

NESS N.F. & J.M. WILCOX, 1965, Sci., 148, 1592.

O'BRIEN B.J., 1963, J. Geophys. Res., 68, 989.

ORMES J.F. & W.R. WEBBER, 1966, Proc. Int. Conf. on Cosmic Rays, London (1965), 1, 349.

PARKER E.N., 1958a, Electromagnetic Phenomena Cosm. Phys. (Cambridge University Press), 420.

PARKER E.N., 1958b, Astrophys. J., 123, 664.

PARKER E.N., 1963, Interplanetary Dynamical Processes, (Interscience Publishers: New York).

PARKER E.N., 1964, J. Geophys. Res., 69, 1755.

PARKER E.N. 1965a, Planet. Spa. Sci., 13, 9,

PARKER E.N., 1965b, University of Chicago, EFINS-65-92.

PFOTZER G., 1958, Nuovo Cim., 8, suppl. 11, 220.

PIEPER I.G.F., A.J. ZMUNDA, C.O. BOSTROM & B.J. O'BRIEN, J. Geophys. Res., 67, 4959.

POMERANTZ M.A., V.R. POTNIS & A.E. SANDSTROM, 1960, J. Geophys. Res., 65, 3539.

POMERANTZ M.A. & S.P. AGARWAL, 1962, Phil. Mag., 7, 1503.

PUPPI G., 1956, Progress in Elementary Particles and Cosmic Ray Physics, 3, 341 (North-Holland Publishing Co. : Amsterdam).

QUENBY J.J., 1964, Handb. d. Phys., 46, 2 (Springer-Verlag: Berlin).

QUENBY J.J., 1966a, Proc. Int. Conf. on Cosmic Rays, London (1965), 1,3.

QUENBY J.J., 1966b, Imperial College of Science & Technology Preprint. (to be published in Planet. and Spa. Sci).

QUENBY J.J. & W.R. WEBBER, 1959, Phil. Mag., 4, 90.

QUENBY J.J. & G.J. WENK, 1962, Phil. Mag., 7, 1457.

RAO U.R., K.G. McCRACKEN & D. VENKATESAN, J. Geophys. Res., 68, 345.

RAY E.C., 1963, Ann. of Phys., 24, 1.

REID G.C. & H.H. SAUER, 1966, Institute for Telecommunication Services and Aeronomy Preprint (Environmental Science Services Admin., Boulder, Colorado).

ROBERTS A.M., 1967, Private Communication.

ROSE D.C., K.B. FENTON, J. KATZMAN & J.A. SIMPSON, 1956, Canad.J.Phys., 34, 968.

ROTHWELL P., 1958, Phil. Mag., 3, 961.

ROTHWELL P. & J.J. QUENBY, 1958, Nuovo Cim., 8, Suppl. 11, 249.

SANDSTROM A.E., 1958, Nuovo Cim., 8, Suppl. 11, 263.

SANDSTROM A.E., M.A. POMERANTZ & B.O. GRÖNKVIST, 1963, Tellus, 15, 184.

SCHWARTZ M., 1959, Nuovo Cim., 11, Suppl 1, 27.

SHEA M.A., 1966, Private Communication.

SHEA M.A., & D.F. SMART, 1966, Reprint of Paper given at the Symposium on Recent Advances in Cosmic Ray Research, Douglas Advanced Research Labs., April 1966.

SHEA M.A., D.F. SMART & K.G. McCRACKEN, 1965, J. Geophys. Res., 70, 4117.

SHEA M.A., D.F. SMART & K.G. McCRACKEN 1966. Private Communication.

SILBERBERG R., 1966, Phys. Rev., 148, 1247.

SIMPSON J.A., F. JORY & M. Pyka, 1956, J. Geophys. Res., 61, 11.

SINGER S.F., 1957, Trans. Am. Geophys. Union, 38, 175.

SINGER S.F., 1958, Nuovo Cim., 8, Suppl. 11, 334.

SNYDER C.W. & M. NEUGEBAUER, 1964, Space Research, IV, (Amsterdam: North-Holland), 89.

SNYDER C.W., M. NEUGEBAUER & U.R. RAO, 1963, J. Geophys. Res., 68, 6361.

STONE E.C., 1964, J. Geophys. Res., 69, 3577.

STORMER C., 1907, Arch. Sci. Phys. Nat., 24, 317.

STORMER C., 1955, The Polar Aurora, (Clarendon Press: Oxford).

VAN ALLEN J.A., C.E. McILWAIN & G.H. LUDWIG, J. Geophys. Res., 64, 271.

VAN der WALT A.J., P.H. STOKER, J.P. MAREE & W.F. COETZEE, 1966, Int. Conf. on Cosmic Rays, London (1965), 1, 548.

WADDINGTON C.J., 1956, Nuovo Cim., 3, 930.

WEBBER W.R., 1962, Progress in Elementary Particles & Cosmic Ray Physics, VI, 75, (North-Holland Publishing Co: Amsterdam).

WEBBER W.R., 1964, Symposium on Solar Flares, NASA SP 50.

WEBBER W.R., 1966, Proc. Int. Conf. on Cosmic Rays, London (1965), 1, 403.

WEBBER W.R. & J.J. QUENBY, 1959, Phil. Mag. 4, 654.

WILLIAMS D.J. & W.F. PALMER, 1965, J. Geophys. Res., 70, 557.